



**UNIVERSITY
OF ICELAND**

Ph.D. Thesis

in Geology

**Effect of basaltic particles and iron-containing
minerals in wetland soils and reservoirs on
CO₂ drawdown**

An analogue for Enhanced Rock Weathering

Tobias Linke

September 2024

FACULTY OF EARTH SCIENCES

Effect of basaltic particles and iron-containing minerals in wetland soils and reservoirs on CO₂ drawdown: An analogue for Enhanced Rock Weathering

Tobias Linke

Dissertation submitted in partial fulfillment of a
Philosophiae Doctor degree in Geology

Ph.D. Committee
Sigurður Reynir Gíslason
Eric H. Oelkers
Knud Dideriksen
Bergur Sigfússon

Opponents
Heather L. Buss
Jens Hartmann

Faculty of Earth Sciences
School of Engineering and Natural Sciences
University of Iceland
Reykjavik, September 2024

Effect of basaltic particles and iron-containing minerals in wetland soils and reservoirs on
CO₂ drawdown: An analogue for Enhanced Rock Weathering
Dissertation submitted in partial fulfillment of a *Ph.D.* degree in Geology

Copyright © 2024 Tobias Linke
All rights reserved

Faculty of Earth Sciences
School of Engineering and Natural Sciences
University of Iceland
Askja, Sturlugata 7
102, Reykjavik
Iceland

Telephone: 525 4000

Bibliographic information:

Tobias Linke, 2024, *Effect of basaltic particles and iron-containing minerals in wetland soils and reservoirs on CO₂ drawdown: An analogue for Enhanced Rock Weathering*, Ph.D. dissertation, Faculty of Earth Sciences, University of Iceland, 162 pp.

ISBN 978-9935-9772-1-2

Abstract

Battling climate change and rising temperatures is a major task of this century. To achieve current climate goals the large-scale removal of carbon dioxide from the atmosphere is needed. Enhanced Rock Weathering ERW is one of the most promising methods to draw down carbon dioxide from the atmosphere at large scale, but it has been challenging to demonstrate. This work reports the soil water chemistry, mineralogy and carbon balance in an Icelandic Andosol that has received large quantities of basaltic dust over 3300 years, providing opportunity to quantify the rates and long-term consequences of Enhanced Rock Weathering. The continuous dust dissolution has been promoted by the precipitation of Al-Si-minerals, such as allophane, and organic anion ligands released from organic decay. Consequently, the water pH, alkalinity and the concentrations of most major elements have increased. Initially released toxic trace metals are scavenged at depth, likely by uptake through secondary minerals. Some carbon dioxide was stored in solid form as siderite FeCO_3 . Meanwhile, the alkalinity generation in these soil waters is more than ten-times higher than in equivalent basalt-dust-free soils.

This study shows that oxidation in these soil systems leads to the transformation of the dominant Al-rich allophane phases to Fe^{3+} -dominated nontronite and ferrihydrite. Simultaneously, soil water alkalinity is reduced. Potentially remobilized toxic trace metals are scavenged by newly formed minerals such as ferrihydrite. Even in surface waters, ferrihydrite is able to adsorb effectively high concentrations of naturally derived heavy metals, but also affects nutrients like phosphorus. These scavenged elements will potentially be released upon interaction with seawater.

After accounting for oxidation and degassing when the soil waters are exposed to the atmosphere, the annual CO_2 drawdown by alkalinity generation is estimated at $62 \text{ g CO}_2 \text{ m}^{-2} \text{ yr}^{-1}$. Therefore, this study validates the ability of soil amendments containing fine-grained mafic minerals to attenuate increasing atmospheric CO_2 by alkalinity export. If the results of our studied field site are representative, the removal of $1 \text{ Gt yr}^{-1} \text{ CO}_2$ from the atmosphere through alkalinity production alone would require a total of 16 million km^2 of surface. However, induced changes in soil organic carbon storage likely dominate the net CO_2 drawdown of Enhanced Rock Weathering efforts. At our Icelandic site the rate of organic carbon storage is estimated to be 1.5 to 3 times larger than that of alkalinity storage.

This measured specific alkalinity flux is of similar order as the fluxes observed in NE-Icelandic glacier meltwater-fed reservoirs loaded with suspended basaltic particles. Low CO_2 partial pressures in these waters, stemming from the water-rock interactions in the reservoirs and beneath the glacier, result in a direct CO_2 drawdown from the atmosphere. The annual CO_2 drawdown from Hálslón, one of the largest hydro power reservoirs in Iceland, was quantified at 5000 tons annually or $120 \text{ g CO}_2 \text{ m}^{-2} \text{ yr}^{-1}$ present during a six-month ice-free period. Simultaneously, the emissions from the downstream Lagarfljót reservoir decreased from $\sim 5300 \text{ t yr}^{-1}$ ($100 \text{ g CO}_2 \text{ m}^{-2} \text{ yr}^{-1}$) to $\sim 1700 \text{ t yr}^{-1}$ ($32 \text{ g CO}_2 \text{ m}^{-2} \text{ yr}^{-1}$), after receiving the redirected waters from the new Hálslón reservoir. While the partial pressure gradient between the atmosphere and the water bodies is the main driving force for the CO_2 fluxes, it is highly affected by wind speeds but less by temperature variations. Although detailed analyses are lacking, additions of mafic materials to large water bodies to draw down CO_2 should still be considered in the future.

Útdráttur

Glíman við loftslagsbreytingar og hækkandi hita er meðal höfuðverkefna þessarar aldar. Nauðsynlegt mun reynast að fjarlægja koltvíoxíð úr andrúmslofti í miklum mæli ef loftslagsmarkmið eiga að nást. Einhver vænlegasta aðferð til að nema koltvíoxíð brott úr andrúmslofti í stórum stíl er "aukin bergveðrun", sem svo kallast, en örðugt hefur reynst að sanna mátt hennar. Í þessu riti er fjallað um rannsókn á efnasamsetningu jarðvegsvatns, á steindasamsetningu og á kolefnisjafnvægi í íslenskri eldfjallajörð (andósól), sem orðið hefur fyrir miklu áfoki basaltryks á 3300 árum. Þannig hefur gefist tækifæri til að leggja mat á hraða aukinnar bergveðrunar og áhrif hennar til lengri tíma. Útfelling álkísilsteinda, eins og allófans, og lífrænar jónir, sem fallið hafa til við niðurbrot lífrænna efna, hafa ýtt undir stöðuga upplausn ryksins, en hún hefur hækkað pH-gildi vatnsins, basavirkni og styrk flestra helstu frumefna. Eitraðir snefilmálmur, sem leysast út í fyrstu, eru trúlega teknir upp af síðsteindum á nokkru dýpi. Uptaka koltvíoxíðs úr andrúmslofti af völdum útfellingar járnkarbónats, síderíts, virðist takmörkuð í þessum jarðvegi, þótt hún sé möguleg, en síderítið bindur koltvíoxíðið sem fast efni. Engu að síður er framleiðsla basavirkni í þessu jarðvatni liðlega tífalt meiri en í sambærilegum jarðvegi sem laus er við basaltryk.

Rannsóknin sýnir, að oxun í þessum jarðvegi umbreytir hinum ríkjandi álríku allófansteindum í nontrónít og ferríhýdrít, en í þeim er þrígilt járn ráðandi. Um leið minnkar basavirkni jarðvegsvatnsins. Nýmyndaðar steindir, eins og ferríhýdrít, taka upp eitraða snefilmálma, sem kunna að hafa leyst út. Ferríhýdrít getur aðsogað mikið af náttúrulega tilfallandi þungmálmum, jafnvel í yfirborðsvatni, en hefur einnig áhrif á næringarefni eins og fosfór. Sjóvatn gæti leyst þessi uppteknu efni út aftur.

Árleg upptaka koltvíoxíðs úr andrúmslofti af völdum framleiðslu basavirkni er metin sem 62 g koltvíoxíðs á fermetra á ári, að teknu tilliti til oxunar og afgösunar, sem verður þegar jarðvegsvatnið kemst undir bert loft. Þessi rannsókn staðfestir þannig, að jarðvegsbætur með finkorna basalti geta dregið úr aukningu koltvíoxíðs í andrúmslofti með flutningi basavirkni. Séu niðurstöður af þessu rannsóknarsvæði dæmigerðar, má ætla að alls þyrfti 16 milljónir ferkílómetra yfirborðs til að binda eitt gígatonn koltvíoxíðs úr andrúmslofti á ári með framleiðslu basavirkni einni saman. Líklegt er hins vegar, að breytingar á forða lífræns kolefnis í jarðvegi, sem verða í kjölfarið, séu ráðandi um bindingu koltvíoxíðs úr andrúmslofti með aukinni bergveðrun. Á íslenska rannsóknarreitnum er lífræn binding kolefnis metin á bilinu hálf önnur til þreföld binding basavirkinnar.

Þetta basavirkniflæði er álfka mikið og mælist í Háslóni, en í því er mikil basaltsvifaur. Hlutþrýstingur koltvíoxíðs í Háslóni er lágur vegna efnahvarfa milli vatns og bergs í lóninu og undir jökli, og veldur þessi lági þrýstingur beinni upptekt koltvíoxíðs úr andrúmslofti. Árleg upptaka koltvíoxíðs úr andrúmslofti í Háslón, eitt stærsta uppistöðulón á Íslandi, var metin sem 5000 tonn á ári, eða 120 g á fermetra á ári, á sex mánaða tímabili þegar lónið var íslaust. Á sama tíma minnkaði losun úr Leginum úr u.þ.b. 5300 tonnum koltvíoxíðs á ári (100 g á fermetra á ári) niður í um 1700 tonn á ári (32 g á fermetra á ári) eftir að vatni úr Háslóni var veitt þangað. Þó að mismunur hlutþrýstings koltvíoxíðs milli andrúmslofts og vatna sé það sem knýi flæði koltvíoxíðs, þá hefur vindhraði samt mikil áhrif á flæðið, en hiti minni. Þótt ítarlega greiningu vanti ennþá, er ástæða til að íhuga íbót basaltagna í stór vatnshlot þegar fram líða stundir, í því augnamiði að binda koltvíoxíð úr andrúmslofti.

Objective science for a better future

Table of Contents

| | |
|---|------------|
| Abstract | iii |
| Útdráttur | v |
| Abbreviations | xiv |
| Acknowledgements | xv |
| 1 Introduction | 1 |
| 1.1 Climate warming | 1 |
| 1.1.1 IPCC and the different paths of climate warming mitigation..... | 2 |
| 1.1.2 Importance of CO ₂ removal to achieve 1.5/2°C climate goal | 4 |
| 1.1.3 Potential of Enhanced Rock Weathering and its limitations | 4 |
| 1.2 Iceland – Geology, Volcanic activity and soils..... | 5 |
| 1.3 Field site | 6 |
| 1.4 General overview of the sampling methods..... | 8 |
| 1.5 Summary of scientific contributions | 8 |
| 1.6 References | 12 |
| 2 Paper I - The geochemical evolution of basalt Enhanced Rock Weathering systems quantified from a natural analogue | 19 |
| 3 Paper II - Direct evidence of CO₂ drawdown through enhanced weathering in soils analogue | 33 |
| 4 Paper III- Enhanced basaltic rock weathering: oxidative mineral transformation | 41 |
| 5 Paper IV - Stability of iron minerals in Icelandic peat areas and transport of heavy metals and nutrients across oxidation and salinity gradients – a modelling approach | 63 |
| 6 Paper V - Water-air-CO₂-flux changes after damming rivers loaded with suspended basaltic particles | 73 |
| Appendix | 97 |
| Appendix A: Supplementary Material Paper I | 97 |
| Appendix B: Supplementary Material Paper II | 107 |
| Appendix C: Supplementary Material Paper III..... | 123 |
| Appendix D: Supplementary Material Paper V..... | 141 |
| Appendix E: Unpublished Material | 155 |

List of Tables

| | |
|--|----|
| Table 2.1 Metal oxide composition of the ‘on-site’ basalt | 22 |
| Table 4.1 Mean particle size distributions of siderite inclusions before and after ultrasonic treatment | 55 |
| Table 5.1 pH, alkalinity and elemental concentrations used for modelling | 66 |
| Table 6.1 Mean monthly CO ₂ fluxes of Lagarfljót 1998-2003..... | 85 |
| Table 6.2 Mean monthly CO ₂ fluxes of Lagarfljót 2007-2013..... | 86 |
| Table 6.3 Mean monthly CO ₂ fluxes of Háslón | 88 |

List of Figures

| | |
|--|----|
| Figure 1.1 Atmospheric CO ₂ concentrations of the past 800,000 years..... | 2 |
| Figure 1.2 Projected mitigation strategies to limit global warming to 1.5°C..... | 3 |
| Figure 1.3 Map of dust deposition rates in Iceland. | 7 |
| Figure 2.1 Overview of the field site and schematic cross section | 21 |
| Figure 2.2 Representative Powder X-ray diffraction patterns and Pair distribution function of soil and siderite samples | 23 |
| Figure 2.3 Redox state, logarithm of the partial pressure of CO ₂ and dissolved inorganic carbon of soil water samples | 24 |
| Figure 2.4 Evolution of major dissolved constituents in sampled soil waters | 24 |
| Figure 2.5 Sulfur and trace metal concentrations in soil water samples | 25 |
| Figure 2.6 Eh-pH diagram with predominance fields of iron phases..... | 25 |
| Figure 2.7 Saturation indices of samples soil waters | 26 |
| Figure 2.8 Calculated volumes of minerals precipitated, and basalt dissolved per kg of soil solution..... | 26 |
| Figure 2.9 Ratio of selected element concentrations normalized to Ca in collected soil waters relative to the release from basalt..... | 28 |
| Figure 3.1 Photography and schematic view of the soil profile..... | 35 |
| Figure 3.2 Measured soil water concentrations..... | 36 |
| Figure 3.3 Comparison of pH and alkalinity of soil waters of this study with soil waters from volcanic dust-free soils..... | 37 |
| Figure 3.4 Schematic illustration of the processes drawing down CO ₂ at the field site | 37 |
| Figure 4.1 Overview of the outcrop and sampling locations | 47 |
| Figure 4.2 Images of siderite samples | 48 |
| Figure 4.3 Powder X-ray diffraction patterns and I(Q) of soil samples..... | 49 |
| Figure 4.4 Powder X-ray diffraction patterns and I(Q) of siderite samples..... | 50 |
| Figure 4.5 Pair distribution functions of soil and siderite samples | 51 |
| Figure 4.6 Schematic soil profile and relative proportions of the solid phases based on principle component analysis | 55 |

| | |
|---|----|
| Figure 4.7 Simulated reaction path during oxidation | 56 |
| Figure 4.8 Schematic illustration of the main processes in the soil outcrop with changing redox conditions..... | 56 |
| Figure 5.1 Predominance diagrams of the most stable iron phases at 500 and 50 Fe $\mu\text{mol/l}$ | 67 |
| Figure 5.2 Predominance diagrams of metastable iron phases under varying iron and carbonate concentrations | 68 |
| Figure 5.3 Modeled uptake and release of heavy metals and phosphate by ferrihydrite..... | 69 |
| Figure 6.1 Map of the study area..... | 77 |
| Figure 6.2 Temperature and wind speed distributions..... | 82 |
| Figure 6.3 Time evolution of partial pressure of CO_2 for different reservoirs | 83 |
| Figure 6.4 Time evolution of partial pressure of CO_2 for Háslón | 87 |
| Figure 6.5 Specific CO_2 flux as a function of $\Delta p\text{CO}_2$ | 90 |

List of Publications

Publications as first author:

Linke, T., Oelkers, E.H., Dideriksen, K. Möckel, S.C., Nilabh, S., Grandia, F., Gislason, S.R., 2024. The geochemical evolution of basalt Enhanced Rock Weathering systems quantified from a natural analogue, *Geochimica et Cosmochimica Acta* 370, 66-77.

Linke, T., Oelkers, E.H., Möckel, S.C., Gislason, S.R., 2024. Direct evidence of CO₂ drawdown through enhanced weathering in soils, *Geochemical Perspective Letters* v30, 7-12.

Linke, T., Dideriksen, K., Dietmann, K.M., Gislason, S.R., 2024. Enhanced basaltic rock weathering: oxidative mineral transformation, *to be submitted to Frontiers*.

Linke, T., Gislason, S.R., 2018. Stability of iron minerals in Icelandic peat areas and transport of heavy metals and nutrients across oxidation and salinity gradients – a modelling approach, *Energy Procedia* 146, 30-37.

Linke, T., Eiríksdóttir, E.S., Petersen, G.N., Gislason, S.R., 2024. Water-air-CO₂-flux changes after damming rivers loaded with suspended basaltic particles, *to be submitted to Water research*.

Publications as contributing author over the course of the Ph.D.:

Dietmann, K.M., **Linke, T.**, Trujillano, R., Rives, V., 2019. Effect of Chain Length and Functional Group of Organic Anions on the Retention Ability of MgAl- Layered Double Hydroxides for Chlorinated Organic solvents. *ChemEngineering*, 3, 89.

Dietmann, K.M., **Linke, T.**, del Nogal Sánchez, M., Pérez Pavón, J.L., Rives, V., 2020. Layered Double Hydroxides with Intercalated Permanganate and Peroxydisulphate Anions for Oxidative Removal of Chlorinated Organic Solvents Contaminated Water. *Minerals*, 10, 462.

Dietmann, K.M., **Linke, T.**, Reischer, M., Rives, V., 2020. Fluorescing Layered Double Hydroxides as Tracer Materials for Particle Injection during Subsurface Water Remediation. *ChemEngineering*, 4, 3, 53.

Reischer, M., Alonso-de-Linaje, V., Digiacomio, F., Dietmann, K.M., Füllenbach, L.C., **Linke, T.**, Mangayayam, M.C., Mulders, J.J.P.A., Rubio, S.N., Nilabh, S., Perez, J.P.H., Schiefler, A.A., Sun, W., Thomas, A., Christensen, A.G., Weber, K., Tobler, D.J., Dideriksen, K. - Injection and Transport of Sulfidized Nanoparticulate Zero Valent iron (S-nZVI) in Clastic Sediments: A Tank Experiment, *in preparation*

Abbreviations

| | |
|--------|---|
| a.s.l. | Above sea level |
| BECCS | Bioenergy with Carbon Capture and Storage |
| BP | Before present, referring to years before 1950 |
| CDR | Carbon dioxide removal |
| ERW | Enhanced Rock Weathering |
| IPPC | Intergovernmental Panel on Climate Change |
| NOAA | National Oceanic and Atmospheric Administration |
| ppm | Parts per million |
| yr | Year |

All chemical elements are named after the classification issued by the International Union of Pure and Applied Chemistry IUPAC.

All units are abbreviated following the International System of Units SI and are either provided as base units or derived units.

Acknowledgements

First of all, I would like to thank Siggi for the opportunity to come to Iceland and work on this topic. He is a great supervisor who encouraged me and provided me with all the support I could have asked for. I also want to thank him for the endless hours we spent together in meetings, looking at my “beautiful data” and all the life lessons and great moments. It was a long journey and I’m very grateful for it.

Thank you also to the other members of my Ph.D. committee. Special thanks to Eric for helping me with shortening and improving the manuscripts and finding new ways of interpretation. Knud, thank you so much for the nice conversations about all the iron minerals, the chance to work with you in Copenhagen and to analyze my samples at the synchrotron. Bergur, thanks for helping me initially to find a field site and discussing my project and the soil water sampling.

I want to thank all members of the Bambi group for the nice gatherings and talks about work, food and other fun topics, sharing your experience and encouraging me to keep going. Special thanks to Deirdre, for introducing me in the lab and taking me to the field, and for all the other things you helped with or organized for us. Thanks to Eydís, Iwona and Martin, who helped me with my samples, analysis and other small things.

To the many colleagues and friends in Askja, including the ones that only came for a visit, also the ones I worked with abroad that provided input to my work or simply showed interest, encouraging me or providing new ideas. Everyone that was so welcoming and helpful over the course of my Ph.D. Thanks, Jón Örn for discussing my work and helping me with some translations.

Special thanks to Ríkey, Steini and Susanne for assisting me in the field and in the lab, for designing coring equipment, helping with all the soil and discussing the practical parts. Also, to Egill and Guðrún, who’s unfortunately no longer with us, for the interesting discussions about soil and sampling.

Thanks to Kevin Burton for the insights into soil pore water sampling, the many discussions about work and soils and the visits to the different soil sections.

My colleagues in the Metal-Aid network, for the many nice discussions, sharing ideas and great moments over the course of the project and beyond. Thanks to the Metal-Aid organizers, especially Claire, for making this project and all the nice meetings abroad happen. Special thanks to Susan Stipp, Liane Benning, Vicente Rives and Fidel Grandia for having me at their institutes, providing great insight into their work and the chance to work in different environments.

Eirikur Benjaminson, who granted us access to his land, where my field site is located, without hesitation and who was always very open and supportive towards my work and the scientist installing weird samplers in his soil. Sorry to the sheep we might have disturbed.

My mom, for encouraging me to take this opportunity in Iceland and supporting me and my work from the first day until now, even though it was a big jump far away. I hope you're relieved that I made it this far.

Finally, Karen, who first pointed me to this project and with whom I started this journey. Thank you so much for your support throughout this long time, the help in Salamanca and the many hours we spent together.

This doctoral thesis is part of the project Metal-Aid, Metal oxide aided subsurface remediation: from invention, which was funded by the European Union's Horizon 2020 research and innovation programme under the Marie Skłodowska-Curie action with the grant agreement number 675219.

This work was also part partially funded by Landsvirkjun under the project number 2456, the Icelandic Center for Research (Rannís) on behalf of the Doctoral Student Fund of the Ministry for the Environment and Natural Resources under the grant No 218929-051, the Research Fund of the University of Iceland and the Travel grant for doctoral students at the University of Iceland, as well as from the research grant CRG9 2020 KAUST-UI provided by the KAUST University, Saudi Arabia.

1 Introduction

1.1 Climate warming

Each year, human activities release more carbon dioxide into the atmosphere than natural processes can remove, causing the amount of carbon dioxide in the atmosphere to increase. Atmospheric carbon dioxide is now 50 percent higher than before the Industrial Revolution, in the mid-1700's, when the atmospheric carbon dioxide concentration was less than 280 ppm (WMO 2024, NOAA 2024). Carbon dioxide is Earth's most important greenhouse gas, a gas that warms the earth by absorbing energy and radiating heat (Lacis et al. 2010, IPCC 2021).

By adding more carbon dioxide to the atmosphere, people are supercharging the natural greenhouse effect, causing global temperature to rise. According to observations by the NOAA Global Monitoring Laboratory in 2021, carbon dioxide alone was responsible for about two-thirds of the total heating influence of all human-produced greenhouse gases (NOAA Annual Greenhouse Gas Index). A large amount of CO₂ that is put into the atmosphere diffuses into the ocean (Ballantyne et al. 2012). Dissolving carbon dioxide in the ocean creates carbonic acid, thereby increasing the acidity of the water (IPCC 2005, Figuerola et al. 2021, Campbell et al. 2022). Since the start of the Industrial Revolution, the pH of the ocean's surface waters has dropped from 8.21 to 8.10, which is an increase by approximately 30 % in acidity (EEA 2024). This drop in pH is called ocean acidification, which has negative feedback on many marine organisms.

Based on paleoclimate evidence and paleo-atmospheric sampling on ice cores, the atmospheric carbon concentration of the past million years can be reconstructed (Fig. 1.1). The highest recorded CO₂ concentrations of the atmosphere, measured in various ice cores (Vostock and EPICA dome c) dating back to the onset of the Middle Pleistocene approximately 790,000 years before present, are around 300 ppm (Lüthi et al. 2008).

Monitoring stations all over the world such as on Mauna Loa, Hawaii, or the Westman Islands (Vestmannaeyjar), Iceland, were built to record the atmospheric CO₂ concentrations. By the time continuous observations began at Mauna Loa Volcanic Observatory in 1958, global atmospheric carbon dioxide was already at 315 ppm (Lan et al. 2024, Keeling and Keeling 2017). Carbon dioxide levels today are higher than at any point in human history. The latest "record" was measured on April 26, 2024, at the Mauna Loa Observatory reading 426.9 ppm (Lan et al. 2024). Carbon dioxide, besides other gases like ozone, methane and nitrous oxides have a large effect on the atmospheric composition and impact its role as a protection layer for the earth that directly regulates solar radiation. Increasing the concentration of any of these so called "greenhouse" gases leads to an increase in solar radiation which directly leads to an increase in global temperatures. Therefore, attempts are made to limit the emissions of these greenhouse gases as increasing global temperatures are providing negative feedback such as extreme events like droughts, tropical cyclones, extreme precipitation and compound extremes (IPCC 2023).

CARBON DIOXIDE OVER 800,000 YEARS

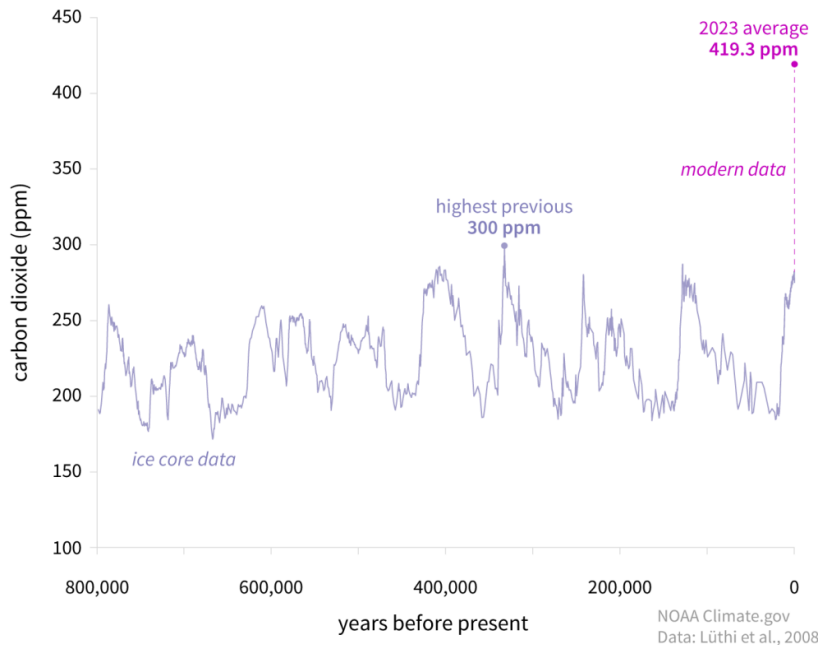


Figure 1.1 Atmospheric carbon dioxide (CO₂) in parts per million (ppm) for the past 800,000 years based on ice-core data (light purple line) compared to 2023 concentration (bright purple dot). The peaks and valleys in the line show ice ages (low CO₂) and warmer interglacials (higher CO₂). Throughout that time, CO₂ was never higher than 300 ppm (light purple dot, between 300,000 and 400,000 years ago). The increase over the last 60 years is 100 times faster than previous natural increases. (Graph by NOAA Climate.gov based on data from Lüthi et al. 2008, via NOAA NCEI Paleoclimatology Program)

1.1.1 IPCC and the different paths of climate warming mitigation

The Intergovernmental Panel on Climate Change (IPCC) was founded in 1988 by the World Meteorological Organization (WMO) and the United Nations Environment Programme (UNEP), with the goal to provide governments at all levels with scientific information that they can use to develop climate policies. The first assessment report published in 1990 led to the creation of the United Nations Framework Convention on Climate Change (UNFCCC), the key international treaty to reduce global warming and cope with the consequences of climate change. The fourth assessment report (AR4) published in 2007 was focused on limiting the global warming to 2°C above pre-industrial level until the end of the century 2100. (<https://www.ipcc.ch/about/history>)

Based on the work of the IPCC, the goal of the Paris agreement signed in 2015 is: to limit global warming to less than 2°C compared to preindustrial levels, preferably 1.5°C by the year 2100. To achieve this, it was proposed that global carbon dioxide emissions should

peak no later than 2020, and gross CO₂ emissions should be successively reduced to ~24 gigatons in 2030, ~14 gigatons in 2040 and ~5 gigatons in 2050 (Röckström et al. 2017, Rogelj et al. 2015). In addition, the cumulative CO₂ emissions of 700 Gt CO₂ since 2017 need to be decreased to below 200 Gt CO₂ by the end of the century, for the atmospheric CO₂ concentrations to return to 380 ppm by 2100 (Röckström et al. 2017). As not all greenhouse gas emissions can be fully mitigated (Royal Society and Royal Academy of Engineering 2018), technologies have to be developed to actively remove carbon dioxide from the atmosphere.

The IPCC reports and special reports provide insight into the causes and consequences of global climate warming as well as possible strategies towards the limitation and mitigation of climate warming. Special Report Global Warming of 1.5°C presents four different pathways on how to limit global warming to 1.5°C by various combinations of emission reduction from fossil fuel and industry, agriculture, forestry and other land use (AFOLU) and implementation of negative emission strategies including contributions from Bioenergy with Carbon Capture and Storage (BECCS) reducing the risk of global warming in a long term and providing more time for adaptation. While the first projection (Fig 1.2. P1) requires a drastic reduction in conventional fossil fuel usage to reduce annual CO₂ emissions, all other scenarios (Fig. 1.2 P2-P4) show a less pronounced reduction in CO₂ emissions from fossil fuels in the early years, but a more dominant role of Bioenergy with Carbon Capture and Storage at a later stage. As, by the present date in 2024, even an immediate shut down of all CO₂ emissions would still not be sufficient to reach the climate goal of 1.5°C, direct removal of CO₂ from the atmosphere will be needed to achieve this climate goal. This underlines the importance of research and development of possible carbon dioxide removal CDR technologies.

Breakdown of contributions to global net CO₂ emissions in four illustrative model pathways

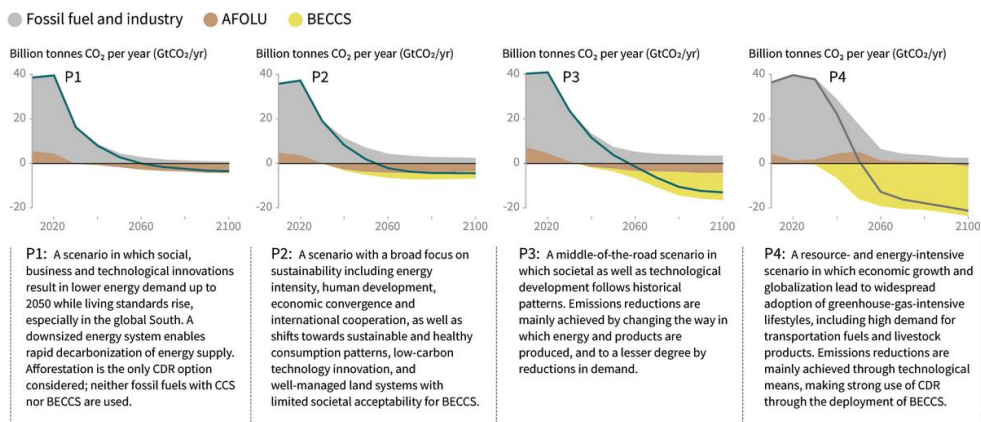


Figure 1.2 Different mitigation strategies can achieve the net emissions reductions that would be required to follow a pathway that limits global warming to 1.5°C with no or limited overshoot. All pathways use Carbon Dioxide Removal (CDR), but the amount varies across pathways, as do the relative contributions of Bioenergy with Carbon Capture and Storage (BECCS) and removals in the Agriculture, Forestry and Other Land Use (AFOLU) sector. This has implications for emissions and several other pathway characteristics. (IPCC 2018)

1.1.2 Importance of CO₂ removal to achieve 1.5/2°C climate goal

The IPCC special report on Global Warming of 1.5°C projects potential CO₂ emission scenarios during the continued usage of conventional fossil fuels. All projected mitigation pathways that would prevent exceeding the 1.5°C warming include CDR (IPCC 2018). In addition, CDR will be capable of counter balancing emissions that are technically difficult to eliminate, such as those from agriculture or aviation (Royal Society and Royal Academy of Engineering 2018). The IPCC defines carbon dioxide removal as “anthropogenic activities that remove CO₂ from the atmosphere and store it durably in geological, terrestrial, or ocean reservoirs, or in products” (IPCC 2021). Carbon dioxide removal does not include any methods reducing emissions or removing CO₂ from a point source (e.g. smokestack, coal power plant or cement factory) nor does it cover any natural occurring processes that are not influenced by human activity.

Carbon dioxide removal covers a wide range of physical or chemical treatments to remove carbon dioxide on a large scale from the atmosphere. Currently studied technologies include direct air capture (DAC) (Nikulshina et al. 2012, Sanz-Perez et al. 2016, Jiang et al. 2023, Zanatta et al. 2023), enhanced mineralization or Enhanced Rock Weathering (ERW) (Pronost et al. 2011, Alfredsson et al. 2013, Power et al. 2014, Harrison et al. 2013, Harrison et al. 2015, Hartmann et al. 2013, Zeyen et al. 2022, Haque et al., 2019, Taylor et al., 2016), Bioenergy with carbon capture and storage (BECCS) (Hanssen et al. 2020, Pour et al. 2018), ocean-based carbon dioxide removal technologies e.g., ocean fertilization or ocean alkalinity enhancement (Hartmann et al. 2023), afforestation or reforestation (Fennel et al. 2023, Siegel et al. 2021, Wu et al. 2023). In contrast to CDR, carbon capture and storage (CCS) does not reduce the amount of carbon dioxide that is already in the atmosphere. But it is often proposed to couple these techniques to provide long-term storage solutions e.g. CO₂ injection into depleted gas reservoirs, saline aquifers or mineralization. As of 2023, CDR is estimated to remove approximately 2 gigatons of CO₂ annually, mostly by afforestation, reforestation and management of existing forests (UNEP 2023). This is equivalent to about 4 % of the annual greenhouse gas emissions worldwide, emphasizing the need to further develop existing technologies. To achieve the 1.5°C climate goal, CDR needs to reach at least 10 Gt CO₂ annually by 2050 (UNEP 2023).

1.1.3 Potential of Enhanced Rock Weathering and its limitations

Even though a large variety of CDR methods is known, different limitations exist especially with respect to cost efficiency and logistical infrastructure (Fuss et al. 2018). Contrary, enhanced weathering or Enhanced Rock Weathering ERW, which aims to spread finely-ground silicate rocks on soils, usually agricultural land, has the potential to overcome these shortcomings (Beerling et al. 2018, Campbell et al. 2022, Hartmann et al. 2013, Kantola et al. 2017, Streifer et al. 2018). Therefore, it is feasible to rapidly introduce Enhanced Rock Weathering applications at large scale within decades (Beerling et al. 2020, Hartmann et al. 2013, Taylor et al. 2016). Enhanced Rock Weathering aims to increase the carbon uptake of soils, while potentially also increasing nutrient levels, improving crop yields and crop health (Haque et al. 2019, Hartmann et al. 2013). It combines direct removal of atmospheric carbon dioxide with long-term storage through conversion into aqueous alkalinity or carbonate minerals (Hartmann et al. 2013, Meysman and Montserrat 2017, Minx et al. 2018, Streifer et al. 2018). While carbon dioxide uptake

through weathering of silicates is the main regulator of atmospheric CO₂ concentrations over geological times scales (Gaillardet et al. 1999, Gislason et al. 2008, Gislason et al. 2009, White and Buss 2014), it is too slow to sufficiently counterbalance anthropogenic CO₂ emissions. Therefore, it has been widely suggested to enhance the natural weathering processes by spreading finely ground silicate materials as an alternative CDR strategy (Beerling et al. 2018, Beerling et al. 2020, Goll et al. 2021, Renforth 2019).

Enhanced Rock Weathering is projected to provide a carbon dioxide drawdown of 0.5-4 Gt CO₂ annually feasible on a global scale (Beerling et al. 2020, Fuss et al. 2018), while avoiding competition for land used in food production and potentially mitigating ocean acidification (Campbell et al. 2022, Hartmann et al. 2013, Meysman and Montserrat 2017, Moosdorf et al. 2014, Taylor et al. 2015). Co-application of ERW with feedstock crops for BECCS and biochar could further enhance the feasibility and carbon sequestration potential of these methods (Amann and Hartmann 2019, Beerling et al. 2018). This can further be enhanced by using ERW with soil organic carbon sequestration at large scale as suggested in decarbonization scenarios for 2050 (Rockström et al. 2017). In addition, ERW can potentially replace conventional fertilizers based on agriculture lime (Dietzen et al. 2018, Haque et al. 2019), which globally have a significant CO₂ footprint (IPCC 2014, West and McBride 2005).

CDR strategies have two major challenges, one is the capability to upscale the investigated processes in a cost-efficient way, while the second is to understand potential side effects. While upscaling of ERW seems to be feasible, especially as application areas and infrastructure exist and prices are comparable low (Renforth and Henderson 2017). The major challenge is to understand the interactions between introduced ERW materials and the natural system, including soil, water and biota, on short and long timescale. The main effect of ERW amendments is the pH increase, which is favorable for most agricultural applications (Edwards et al. 2017, Haque et al. 2019). While the wrong usage of materials can potentially release toxic metals, polluting soils and surface waters. In addition, changes in the hydrological soil properties and processes affecting the organically stored carbon and biota can result in positive or negative outcomes. As ERW models and laboratory experiments are not sufficient, and conducted field studies are rare and covering only very limited time spans, natural analogues can potentially provide very important information on the long-term effects of ERW and the interaction with the environment. Hence, the goal of the here presented Ph.D. work is to provide insights into ERW by studying natural processes in Iceland, gathering data on soil and surface waters and comparing these results with data from ERW experiments and modelling predictions.

1.2 Iceland – Geology, Volcanic activity and soils

Geologically, Iceland is a young volcanic island, mainly built from volcanic rocks with basaltic composition. Additionally, intermediate and silicic volcanics and clastic sediments of volcanic origin can be found (Saemundsson 1979). The oldest exposed rocks are about 15 Myr (McDougall et al. 1984). During the last glacial maximum, approximately 20,000 years before present, Iceland was fully covered with glaciers. Around 10,300 years before present, the ice sheet retreated close to where the present coastline is located. About 8,000 years before present the Icelandic glaciers were of similar or less extent than nowadays

(Norðdahl et al. 2008). As most of the soil was removed by the advancing ice sheet and started to form after its retreat, all present Icelandic soils are assumed to be of Holocene age, approximately 10,000 years, or younger (Arnalds 2008).

As Iceland is dominated by volcanic activity and has the most extensive sandy tephra areas on earth, most soils are characterized by input of volcanic material. Andosols are the most common soils in Iceland, they represent an intermediate soil type between organic-poor Vitrisols, the soils of the desert areas, and the organic-rich Histosols that are found in wetland areas (Arnalds 2008). Even though, Andosols are not common in Europe, they are widespread in the active volcanic areas of the world (Arnalds 2008). Icelandic soils are typically classified based on two main factors: the deposition of aeolian (volcanic) material and drainage (Arnalds 2004). Aeolian material, which is transported by wind, originates from the sandy desert areas located near active volcanic zones or from glaciofluvial outwash plains. After the settlement in Iceland, around 1076 yr BP, the extent of barren areas as a source of aeolian material significantly increased (Gísladóttir et al. 2008, Gísladóttir et al. 2011, Dugmore et al. 2009).

The basaltic tephra material and the steady aeolian input to the soil surface, together with numerous freeze-thaw cycles create distinct soil properties (Arnalds 2008). The observed soils show a variety of features stemming from the influence of andic (volcanic soil properties) and histic (organic) properties.

Andosols are common for Icelandic wetland areas that are covered by vegetation and that receive a substantial aeolian input, which lowers the relative organic content and increases drainage. Contrary, Histosols are organic-rich soils of wetlands with limited aeolian input. Following increasing drainage conditions and decreasing organic carbon content the soil types can be ranked in the following order: Histosols (>20 % C), Histic Andosols (12–20 % C), Gleyic Andosols (>1 to <12 % C, poorly drained), and Brown Andosols (>1 to <12 % C, freely drained) and Vitrisols with <1 % organic carbon (Arnalds 2008). Coincidentally, this order reflects the decreasing distance from volcanic zones and the input of aeolian material.

The transition between these soil types is fluent, and changes in drainage or aeolian input can lead to a change of the soil type. It is postulated that in absence of the volcanic influences, Icelandic wetland soils would largely be organic Histosols, typical of the arctic environments (Arnalds 2008 and 2015). Thus, deploying enhanced weathering methods that add fine-grained basaltic material to organic-rich Histosols should result in a transition towards a more mineral-rich soil, e.g., Andosols as found in the described study area.

1.3 Field site

The field site is located in the lowlands of South Iceland, 12 km NW from the town of Hella at the headwaters of the river Raudelaekur (“red creek”). During the last glaciation (10,000 years before present) the southern lowlands were covered with ice. The Holocene glacial retreat marked the onset of soil formation on the basaltic bedrock. Today, the lowlands are quite fertile and widely used for agriculture (Arnalds 2004, Arnalds 2015). By nature, the soils are commonly quite water-rich, limiting the use for agriculture and heavy machinery. Hence, large parts of the Icelandic soils were drained by excavating

ditches. The peak of ditch construction was reached in the 1960's, due to state compensation, leading to a total of 35,000 km of drainage ditches in 2010, affecting about 70 % of the wetland areas (Arnalds et al. 2016). As agriculture declined, large, drained areas are left unused, but only few ditches were filled up due to the extra cost. The area of the field site is confined by drainage ditches about 50-150 m away from the soil profile. It has not been used for agricultural purposes within the last 30 years. Therefore, no fertilizers are expected to be present in the soil or soil waters, making it a good natural analogue.

Soil thickness in this area can reach multiple meters, which is quite significant compared to soil heights observed elsewhere in Iceland. The studied soil profile was accessible to a depth of ~2.2 m with the oldest tephra layers dating back to 3300 years before present.

The field site is located in one of the dustiest places in Iceland. It is estimated to receive at least somewhere between 500 to 800 g of mostly basaltic dust annually (Fig. 1.3). The dust originates from the nearby volcanic systems, including material from the volcanoes Hekla, Katla and Grimsvötn (see Chapter 2 Paper I). Fine-grained dust is transported constantly from the highlands and the erosion areas of the volcanoes as well as from the glacier outwash plains. In addition, larger size fractions can be transported during heavy windstorms. Infrequent volcanic eruptions provide an additional source of basaltic material that form by deposition larger ash layers also called “tephra”. These tephra layers provide isochronous makers tephrocorrelating different soil profiles and providing age estimates in the soil profile.

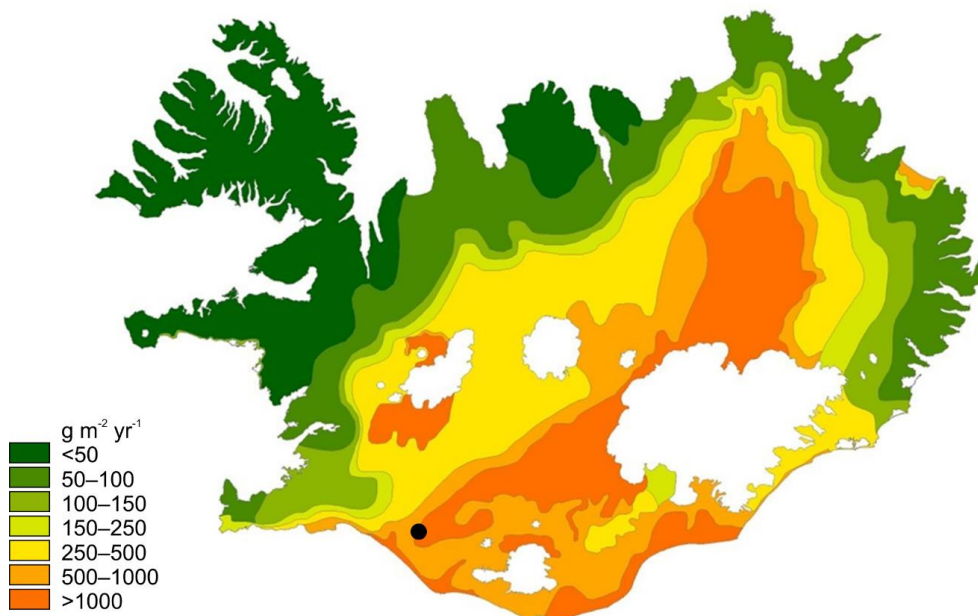


Figure 1.3 Map of dust deposition rates in Iceland, location of the study site marked with the black dot. (modified from Arnalds et al., 2023).

1.4 General overview of the sampling methods

To understand the occurring processes at the field site, various samples were collected including soil water samples, surface water samples and solid samples. Soil water down to a depth of ~2.6 m, was sampled using suction cup lysimeters (see chapter 2 and 3) and extracted using large (60 ml) syringes connected via Teflon tubes. Additionally, shallower samples along a vertical outcrop wall were taken using Rhizon samples (see chapter 4) that are extracting soil water with low under-pressure simulating the root system of plants. As the waters are very reactive, various measurements were done in closed containers directly on site or after stabilizing the samples, e.g. by acidification. Following the water flow from the outcrop wall and from small springs, along puddles to a nearby drainage channel and finally all the way down to the ocean, surface water samples were collected (Appendix 5). While soil water samples were challenging to preserve, the nearby surface water sources were very dependent on seasonal variations, frozen during winter and dried up during summer when no rain was present. In addition to the aforementioned water samples, solid samples from the same soil horizons or surface puddles were collected to provide insight into the mineralogy and chemical composition of accompanying solids (see chapter 4). All obtained data is presented in the following chapters, either as already published manuscripts or as work in preparation for publication.

1.5 Summary of scientific contributions

The effects of climate change, including increasing global temperatures that are ubiquitous present require joint efforts to secure the future of society. Following the directive of the Paris agreement and the Intergovernmental Panel on Climate Change to limit global warming to less than 2°C, global CO₂ emissions have to be limited to a minimum and additionally CO₂ has to be actively removed from the atmosphere within the next decades. Therefore, carbon dioxide removal technologies have to be further developed and brought to an economical feasible level. Enhanced Rock Weathering is suggested as one of the most promising techniques to remove CO₂ from the atmosphere on a large scale. It is based on the natural weathering of rocks like basalts, where naturally occurring chemical reactions slowly lead to the uptake of CO₂ and the formation of dissolved carbonate or carbonated rocks. But a deep understanding of the occurring processes and involved reactions is required before it can be used on a large scale at a much faster rate. As these natural processes are very slow adequate man-made experiments at small scale, e.g. in the laboratory or via modelling, do not provide sufficient insight. Therefore, information gained from natural analogues is very important.

The main part of this Ph.D. thesis focuses on understanding such a natural system, where a comparable fast weathering and soil formation occurs. A large data set comprised of soil water and mineral data, including aqueous soil and surface water samples and solid rock and soil samples, was collected over the course of this work. This data is used together with geochemical modelling to estimate the potential CO₂ uptake of this system and is then compared to natural environments elsewhere and proposed ERW projects and laboratory and small-scale field studies. The results of this Ph.D. study are presented in a set of

scientific articles that are partially peer reviewed and partially still in preparation for publication.

The first paper presented in chapter 2, “Direct evidence of CO₂ drawdown through enhanced weathering in soils” (Linke et al. 2024a, *Geochemical Perspective Letters* 30, 7-12), firstly describes the field site in South Iceland and the dominating processes that lead to the formation of the soil waters, namely basaltic dust dissolution, organic decay and precipitation of secondary minerals. The paper provides information about the soil water chemistry, mineral saturation states as well as the soil profile and further provides estimates on the alkalinity generation that is coupled to CO₂ uptake. The maximum carbon drawdown potential of the study site was quantified and compared to other natural sites without basaltic dust and to data on ERW. This work shows that basaltic dust is present throughout the soil profile and dissolves continuously, which can be recreated via simple geochemical models. Nevertheless, the natural rock dissolution seems to be much slower than estimates by laboratory experiments suggest, which needs to be taken into account for ERW applications. On the other side, potentially released toxic metals are suspected to be scavenged by secondary forming minerals, thus decreasing their mobility within the subsurface and limiting their negative impact on the environment.

The second paper, “The geochemical evolution of basalt Enhanced Rock Weathering systems quantified from a natural analogue” (Linke et al. 2024b, *Geochimica et Cosmochimica Acta* 370, 66–77) is looking at Iceland as a long-term ERW analogue, where the findings and implications of this doctoral study can have potential important implications on future ERW applications and show limitations. The paper investigates the chemical composition and mineral transformation in the soil and recreates their evolution by geochemical modelling. It details the estimate of the CO₂ drawdown potential of the soil system, predicting that approximately 0.17 t C per hectare are removed annually from the atmosphere by alkalinity generation. The alkalinity generation in the presence of basaltic dust is much larger (at least ten-times) than in equivalent dust-free soils elsewhere, but changes in the organic carbon stock of the soil can negate this positive effect. As the studied system has stabilized over several thousands of years, abrupt changes of the soil chemistry by amendment of basaltic rock powder to comparable dust-free soils can cause unknown, possibly negative results, potentially releasing CO₂. Additionally, the upscaling of this slow process might be challenging due to the large land requirements.

While the previous sections focused mainly on the dissolution and the processes occurring inside the soil, the third paper with the preliminary title “Enhanced basaltic rock weathering: oxidative mineral transformation” (Linke et al. 2024c – in preparation), covers mineral transformations that are occurring in the transition zones towards the atmosphere, e.g. in drainage channels. This paper covers critical points regarding the security of the engineered ERW systems with respect to environmental changes, including transitions in the redox environment, mineral transformations and potential release of toxic metals. This section provides proof of occurring mineral transformations, including results from X-ray diffractometry and synchrotron-based analysis, as well as for the formation of siderite, which is storing CO₂ in solid form. Notably, the formation of ferrihydrite in the oxic environment can scavenge potentially liberated toxic metals.

A fourth paper, “Stability of iron minerals in Icelandic peat areas and transport of heavy metals and nutrients across oxidation and salinity gradients – a modelling approach” (Linke et al. 2018, Energy Procedia 146, 30-37), provides insight into the stability of iron mineral phases using geochemical modelling. Predictions of the dominating iron phases and their effect on potential heavy metals when transported towards the ocean are included. Consequently, the most common metastable iron phase is ferrihydrite, which is in agreement with field observations (see chapter 2-4). Ferrihydrite's large reactive surface area has the capacity to adsorb large amounts of heavy metals and phosphate. This work provides first information on the fate of heavy metals and phosphate in the surface waters and estimates the mixing ratios with seawater for their release to the ocean.

Additionally to paper four, a large data set of surface water samples, from the source area along the river course to the ocean, was collected over the study period, including samples of associated mineral phases. The data is presented in the supplementary material (Appendix F: Unpublished Material) but has not yet been included in a scientific publication. This data provides information on the fluxes of major and trace elements, including measurements of alkalinity, redox potential and dissolved organic carbon.

The last chapter of the thesis includes a preliminary scientific manuscript on the CO₂ fluxes from Icelandic reservoirs and rivers, titled “Water-air-CO₂-flux changes after damming rivers loaded with suspended basaltic particles” (Linke et al. 2024d). This work evolved as a side project with Landsvirkjun and is mainly based on a large set of data on river and reservoir compositions that has been collected over the past decades provided by the co-authors and Landsvirkjun. In the following, the existing water analysis were used together with meteorological data on temperature, windspeed and ice cover to estimate the potential CO₂ fluxes from and into one of Iceland's major hydropower reservoirs and associated rivers. The results show that the glacier melt water streaming into the reservoir is highly undersaturated with respect to atmospheric CO₂ concentrations, leading to a total drawdown of ~5000 t CO₂ annually in the Hálslón reservoir. The change of the river course, as a result of damming, also lowered the CO₂ emissions from the downstream Lagarfljót reservoir. The work shows that the fluxes are mainly affected by wind speed and ice cover, and changes of these parameters can result in large changes of the fluxes. Overall, this study shows that water rock interactions underneath the glaciers can lead to significant CO₂ uptake similar to the Enhanced Rock Weathering in soils as described in the previous chapters.

Additionally to the data provided in the previous chapters, an extensive collection of data and additional information, including description of methods, calculations and definitions, is included in the supplementary material accompanying each described article.

Overall, this Ph.D. study and the associated scientific manuscripts show that natural weathering of basaltic material in Icelandic wetland soils lead to a clear increase of alkalinity in the soil waters compared to non-basaltic soil systems. Additionally, similar alkalinity generation is observed in glacier melt water that interacted with basaltic material. Nevertheless, the generated alkalinity is mainly decreased by iron oxidation, when in contact with the atmosphere, leading to a decrease of the carbon dioxide removal potential. Simultaneously, the forming iron phases are capable of scavenging and immobilizing potentially released toxic trace metals. Altogether, the study proves the applicability of

Enhanced Rock Weathering, but the potential carbon drawdown effect might be notable lower compared to proposed values in the literature due to various limitations shown in the presented papers. Additionally, the organic carbon stock of the soils is much larger than the annual alkalinity generation. Changes affecting this carbon pool can lead to adverse effects, resulting in a higher release of CO₂ than negated by the alkalinity production. This work provides a first insight into the potential of Enhanced Rock Weathering based on natural analogues. Nonetheless, the potential CO₂ release and the complexity of the studied soil system issues a warning that a deeper understanding is required before an employment of ERW on large scale should be attempted.

1.6 References

- Alfredsson, H.A., Oelkers, E.H., Hardarsson, B.S., Franzson, H., Gunnlaugsson, E. and Gislason, S.R. (2013) The geology and water chemistry of the Hellisheidi, SW-Iceland carbon storage site. *International Journal of Greenhouse Gas Control*, 12, 399-418
- Amann, T. and Hartmann, J. (2019) Ideas and perspectives: Synergies from co-deployment of negative emission technologies. *European Geosciences Union, Articles*, 16 (15), 2949-2960
- Arnalds, O. (2004) Volcanic soils of Iceland. *Catena*, 56, 3–20
- Arnalds, O. (2008) Soils of Iceland. *Jökull*, 58, 409–421
- Arnalds, O. (2015) *The Soils of Iceland*. World Soils Book Series, Springer, Dordrecht.
- Arnalds, O., Dagsson-Waldhauserova, P., Olafsson, H. (2016) The Icelandic volcanic aeolian environment: processes and impacts - A review. *Aeolian Research*, 20, 176–195
- Arnalds, O., Marteinsdottir, B., Brink, S.H., Orsson, J. (2023) A framework model for current land condition in Iceland, *PLoS ONE*, 18(7), e0287764, 18p.
- Ballantyne, A.P., Alden, C.B., Miller, J.B., Tans, P.P. and White, J.W.C. (2012) Increase in observed net carbon dioxide uptake by land and oceans during the last 50 years. *Nature*, 488, 70-72
- Beerling, D.J., Kantzas, E.P., Lomas, M.R., Wade, P., Eufrazio, R.M., Renforth, P., Sarkar, B., Andrews, M.G., James, R.H., Pearce, C.R., Mercure, J.F., Pollitt, H., Holden, P.B., Edwards, N.R., Khanna, M., Koh, L., Quegan, S., Pidgeon, N.F., Janssens, I.A., Hansen, J. and Banwart, S.A. (2020) Potential for large-scale CO₂ removal via enhanced rock weathering with croplands. *Nature*, 583, 242–248
- Beerling, D.J., Leake, J.R., Long, S.P., Scholes, J.D., Ton, J., Nelson, P.N., Bird, M., Kantzas, E., Taylor, L.L., Sarkar, B., Kelland, M., DeLucia, E., Kantola, I., Müller, C., Rau, G. and Hansen, J. (2018) Farming with crops and rocks to address global climate, food and soil security. *Nature Plants*, 4, 138–147
- Campbell J.S., Foteinis S., Furey V., Hawrot O., Pike D., Aeschlimann S., Maesano C.N., Reginato P.L., Goodwin D.R., Looger L.L., Boyden E.S. and Renforth P. (2022) Geochemical Negative Emissions Technologies: Part I. Review. *Frontiers in Climate*, 4:879133
- Dietzen, C., Harrison, R. and Michelsen-Correa, S. (2018) Effectiveness of enhanced mineral weathering as a carbon sequestration tool and alternative to agricultural lime: An incubation experiment. *International Journal of Greenhouse Gas Control*, 74, 251-258
- Dugmore, A.J., Gísladóttir, G., Simpson, I.A., Newton, A. (2009) Conceptual Models of 1200 Years of Icelandic Soil Erosion Reconstructed Using Tephrochronology. *Journal of the North Atlantic*, 2, 1–18

Edwards, D.P., Lim, F., James, R.H., Pearce, C.R., Scholes, J., Freckleton, R.P. and Beerling, D.J. (2017) Climate change mitigation: potential benefits and pitfalls of enhanced rock weathering in tropical agriculture. *Biology Letters*, 13

European Environment Agency. Ocean acidification, 29 May 2024. Web Archive. <https://www.eea.europa.eu/en/analysis/indicators/ocean-acidification> [last accessed: 02:06:2024 12:35]

Fennel, K., Long, M.C., Algar, C., Carter, B., Keller, D., Laurent, A., Mattern, J.P., Musgrave, R., Oschlies, A., Palter, J.B., Whitt, D.B. (2023) Modelling considerations for research on ocean alkalinity enhancement (OAE). *State of the Planet*, 2-oe2023, 9

Figuerola, B., Hancock, A.M., Bax, N., Cummings, V.J., Downey, R., Griffiths, H.J., Smith, J. and Stark, J.S. (2021) A Review and Meta-Analysis of Potential Impacts of Ocean Acidification on Marine Calcifiers From the Southern Ocean. *Frontiers in Marine Science*, 8:584445

Fuss, S., Lamb, W. F., Callaghan, M. W., Hilaire, J., Creutzig, F., Amann, T., Beringer, T., Garcia, W. D. O., Hartmann, J., Khanna, T., Luderer, G., Nemet, G. F., Rogelj, J., Smith, P., Vicente, J. L. V., Wilcox, J., Dominguez, M. D. M. Z., and Minx, J. C. (2018). Negative emissions-Part 2: Costs, potentials and side effects. *Environmental Research Letters*, 13 (6), 063002

Gaillardet, J., Dupré, B., Louvat, P. and Allègre, C.J. (1999) Global silicate weathering and CO₂ consumption rates deduced from the chemistry of large rivers. *Chemical Geology*, 159 (1-4), 3-30

Gísladóttir, G., Erlendsson, E., Lal, R., Bigham, J. (2008) Erosional effects on terrestrial resources over the last millennium in Reykjanes, southwest Iceland. *Quaternary Research* 73, 20–32.

Gísladóttir, G., Erlendsson, E. and Lal, R. (2011) Soil evidence for historical human-induced land degradation in West Iceland. *Applied Geochemistry*, 26, 2009–2012

Gislason, S.R., Oelkers, E.H., Eiriksdottir, E.S., Kardjilov, M.I., Gisladottir, G., Sigfusson, B., Snorrason, A., Elefsen, S., Hardardottir, J., Torssander, P., and Oskarsson, N. (2008) The feedback between climate and weathering, *Mineralogical Magazine*, 72(1). 317-320.

Gislason, S.R., Oelkers, E.H., Eiriksdottir, E.S., Kardjilov, M.I., Gisladottir, G., Sigfusson, B., Snorrason, A., Elefsen, S.O., Hardardottir, J., Torssander, P., Oskarsson, N. (2009). Direct evidence of the feedback between climate and weathering. *Earth and Planetary Science Letters*, 277, 213–222.

Goll, D.S, Ciais, P., Amann, T., Buermann, W., Chang, J., Eker, S., Hartmann, J., Janssens, I., Li, W., Obersteiner, M., Penuelas, J., Tanaka, K. and Vicca, S. (2021) Potential CO₂ removal from enhanced weathering by ecosystem responses to powdered rock. *Nature Geoscience*, 14, 545–549

Hanssen, S.V., Daioglou, V., Steinmann, Z.J.N., Doelman, J.C., Van Vuuren, D.P. and Huijbregts, M.A.J. (2020) The climate change mitigation potential of bioenergy with carbon capture and storage. *Nature Climate Change*, 10, 1023–1029

Haque, F., Santos, R. M., Dutta, A., Thimmanagari, M., and Chiang, Y. W. (2019) Co-Benefits of Wollastonite Weathering in Agriculture: CO₂ Sequestration and Promoted Plant Growth. *ACS omega*, 4(1), 1425–1433

Harrison, A., Power, I.M. and Dipple, G.M. (2013) Accelerated Carbonation of Brucite in Mine Tailings for Carbon Sequestration. *Environmental Science & Technology*, 47 (1), 126–134

Harrison, A.L., Dipple, G.M., Power, I.M. and Mayer, K.U. (2015) Influence of surface passivation and water content on mineral reactions in unsaturated porous media: Implications for brucite carbonation and CO₂ sequestration. *Geochimica et Cosmochimica Acta*, 148, 477-495, doi: 10.1016/j.gca.2014.10.020

Hartmann, J., Suitner, N., Lim, C., Schneider, J., Marín-Samper, L., Arístegui, J., Renforth, P., Taucher, J., Riebsell, U. (2023) Stability of alkalinity in ocean alkalinity enhancement (OAE) approaches-consequences for durability of CO₂ storage. *Biogeosciences* 20, 781–802

Hartmann, J., A. J. West, P. Renforth, P. Köhler, C. L. De La Rocha, D. A. Wolf-Gladrow, H. H. Dürr, and J. Scheffran (2013), Enhanced chemical weathering as a geoengineering strategy to reduce atmospheric carbon dioxide, supply nutrients, and mitigate ocean acidification. *Reviews of Geophysics*, 51, 113–149

Intergovernmental Panel on Climate Change (2005) IPCC Special Report on Carbon Dioxide Capture and Storage. Prepared by Working Group III of the Intergovernmental Panel on Climate Change [Metz, B., O. Davidson, H. C. de Coninck, M. Loos, and L. A. Meyer (eds.)]. Cambridge University Press, Cambridge, United Kingdom and New York, NY, USA, 442 pp., ISBN 978-0-521-86643-9

Intergovernmental Panel on Climate Change (2007) Climate Change 2007: Synthesis Report. Contribution of Working Groups I, II and III to the Fourth Assessment Report of the Intergovernmental Panel on Climate Change, Core Writing Team, Pachauri, R.K and Reisinger, A. (eds.). IPCC, Geneva, Switzerland, 104 pp.

Intergovernmental Panel on Climate Change (2018) Global Warming of 1.5°C. An IPCC Special Report on the impacts of global warming of 1.5°C above pre-industrial levels and related global greenhouse gas emission pathways, in the context of strengthening the global response to the threat of climate change, sustainable development, and efforts to eradicate poverty , Masson-Delmotte, V., P. Zhai, H.-O. Pörtner, D. Roberts, J. Skea, P.R. Shukla, A. Pirani, W. Moufouma-Okia, C. Péan, R. Pidcock, S. Connors, J.B.R. Matthews, Y. Chen, X. Zhou, M.I. Gomis, E. Lonnoy, T. Maycock, M. Tignor, and T. Waterfield (eds.). Cambridge University Press, Cambridge, UK and New York, NY, USA, 616 pp.

Intergovernmental Panel on Climate Change (2021) Climate Change 2021: The Physical Science Basis. Contribution of Working Group I to the Sixth Assessment Report of the Intergovernmental Panel on Climate Change, Masson-Delmotte, V., P. Zhai, A. Pirani, S.L. Connors, C. Péan, S. Berger, N. Caud, Y. Chen, L. Goldfarb, M.I. Gomis, M. Huang, K. Leitzell, E. Lonnoy, J.B.R. Matthews, T.K. Maycock, T. Waterfield, O. Yelekçi, R. Yu, and B. Zhou (eds.). Cambridge University Press, Cambridge, United Kingdom and New York, NY, USA, 2409 pp.

Intergovernmental Panel on Climate Change (2023) Climate Change 2023: Synthesis Report. Contribution of Working Groups I, II and III to the Sixth Assessment Report of the Intergovernmental Panel on Climate Change, Core Writing Team, H. Lee and J. Romero (eds.). IPCC, Geneva, Switzerland, 184 pp.

Intergovernmental Panel on Climate Change. History of the IPCC. Web Archive. <https://www.ipcc.ch/about/history/> [Accessed: 27:05:2024 12:08]

Jiang, L., Liu, W., Wang, R.Q., Gonzalez-Diaz, A., Rojas-Michaga, M.F., Michailos, S., Pourkashanian, M., Zhang, X.J. and Font-Palma, C. (2023) Sorption direct air capture with CO₂ utilization. *Progress in Energy and Combustion Science*, 95, 101069

Kantola, I.B., Masters, M.D., Beerling, D.J., Long, S.P. and DeLucia E.H. (2017) Potential of global croplands and bioenergy crops for climate change mitigation through deployment for enhanced weathering. *Biology Letters*, 13 (4), 20160714

Keeling, R.F.; Keeling, C.D. (2017) Atmospheric Monthly In Situ CO₂ Data - Mauna Loa Observatory, Hawaii (Archive 2024-01-08). In Scripps CO₂ Program Data. UC San Diego Library Digital Collections

Lacis, A.A., Schmidt, G.A., Rind, D., Ruedy, R.A. (2010) Atmospheric CO₂: Principal Control Knob Governing Earth's Temperature. *Science*, 330,356-359

Lan, X, National Oceanic and Atmospheric Administration Global Monitoring Lab. Trends in Atmospheric Carbon Dioxide. Web Archive, updated continuously (gml.noaa.gov/ccgg/trends/) [Accessed: 02:06:2024 14:45]

Lan, X., Tans, P. and K.W. Thoning: Trends in globally-averaged CO₂ determined from NOAA Global Monitoring Laboratory measurements. Version 2024-06

Lüthi, D., Le Floch, M., Bereiter, B., Blunier, B., Barnola, J.-M., Siegenthaler, U., Raynaud, D., Jouzel, J., Fischer, H., Kawamura, K. und Stocker, T.F. (2008) High-resolution carbon dioxide concentration record 650,000–800,000 years before present. *Nature*, 453, 379–382

McDougall, I., Kristjansson, L., Saemundsson, K. (1984) Magnetostratigraphy and Geochronology of Northwest Iceland. *Journal of Geophysical Research Solid, Earth* 89, 7029–7060

Meysman, F.J., and Montserrat, F. (2017). Negative CO₂ emissions via enhanced silicate weathering in coastal environments. *Biology Letters*, 13.

Minx, J. C., Lamb, W. F., Callaghan, M. W., Fuss, S., Hilaire, J., Creutzig, F., Amann, T., Beringer, T., Garcia, W. D. O., Hartmann, J., Khanna, T., Lenzi, D., Luderer, G., Nemet, G. F., Rogelj, J., Smith, P., Vicente, J. L. V., Wilcox, J., & Dominguez, M. D. M. Z. (2018). Negative emissions-Part 1: Research landscape and synthesis. *Environmental Research Letters*, 13 (6), 063001

Moosdorf, N., Renforth, P., Hartmann, J. (2014) Carbon dioxide efficiency of terrestrial enhanced weathering. *Environmental Science & Technology* 48, 4809–4816.

National Oceanic and Atmospheric Administration Global Monitoring Lab. No Sign of greenhouse gases increase in 2023, 5 April 2024. Web Archive. <https://research.noaa.gov/2024/04/05/no-sign-of-greenhouse-gases-increases-slowng-in-2023/> [Accessed: 28:05:2024 14:30]

National Oceanic and Atmospheric Administration's NOAA's Annual Greenhouse Gas Index (An Introduction). Earth System Research Laboratory, last updated 1 March 2024. Web Archive. <https://gml.noaa.gov/aggi/aggi.html> [Accessed: 28:05:2024 14:15]

Nikulshina, V., Ayesa, N., Gálvez, M. E. and Stainfeld, A. (2016) Feasibility of Na-Based Thermochemical Cycles for the Capture of CO₂ from air. Thermodynamic and Thermogravimetric Analyses. *Chemical Engineering Journal*, 140 (1–3), 62–70

Norðdahl, H., Ingólfsson, Ó., Pétursson, H.G., Hallsdóttir, M. (2008) Late Weichselian and Holocene environmental history of Iceland. *Jökull*, 58, 343–364

Pour, N., Webley, P.A. and Cook, P.J. (2018) Potential for using municipal solid waste as a resource for bioenergy with carbon capture and storage (BECCS). *International Journal of Greenhouse Gas Control*, 68, 1-15

Power, I.M., McCutcheon, J., Harrison, A.L., Wilson, S., Dipple, G.M., Kelly, S., Southam, C. and Southam, G. (2014) Strategizing Carbon-Neutral Mines: A Case for Pilot Projects. *Minerals*, 4, 399-436

Pronost, J., Beaudoin, G., Tremblay, J., Larachi, F., Duchesne, J., Hébert, R. and Constantin, M. (2011) Carbon Sequestration Kinetic and Storage Capacity of Ultramafic Mining Waste. *Environmental Science & Technology*, 45 (21), 9413-9420

Renforth, P. and Henderson, G. (2017) Assessing ocean alkalinity for carbon sequestration. *Reviews of Geophysics*, 55, 636–674

Renforth, P. (2019) The negative emission potential of alkaline materials. *Nature Communications*, 10, 1401

Röckström, J., Gaffney, O., Rogel, J., Meinshausen, M., Nakicenovic, N., Schnellhuber and H.J. (2017) A roadmap for rapid decarbonization. *Science*, 355,1269-1271

Rogel, J., Luderer, G., Pietzcker, R.C., Kriegler, E., Schaeffer, M., Krey, V. and Riahi, K. (2015) Energy system transformations for limiting end-of-century warming to below 1.5 °C. *Nature Climate Change*, 5, 519-527

Royal Society and Royal Academy of Engineering (2018) Green gas removal. Issued: September 2018 DES5563_1, ISBN 978-1-78252-349-9

Saemundsson, K. (1979) Outline of the geology of Iceland. *Jökull*, 29, 7–28

Sanz-Pérez, E.S., Murdock, C.R., Didas, S.A., Jones and C.W. (2016) Direct Capture of CO₂ from Ambient Air. *Chemical reviews*, 116 (19), 11840–11876

Siegel, D.A., DeVries, T., Doney, S.C., Bell, T. (2021) Assessing the sequestration time scales of some ocean-based carbon dioxide reduction strategies. *Environmental Research Letters*, 16 (10), 104003

Streffer, J., Amann, T., Bauer, N., Kriegler, E. and Hartmann, J. (2018) Potential and costs of carbon dioxide removal by enhanced weathering of rocks. *Environmental Research Letters*, 13, 034010

Taylor, L.L., Quirk, J., Thorley, R.M.S., Kharecha, P.A., Hansen, J., Ridgwell, A., Lomas, M.R., Banwart, S.A. and Beerling, D.J. (2016) Enhanced weathering strategies for stabilizing climate and averting ocean acidification. *Nature Climate Change*, 6, 402–406

United Nations Environment Programme (2023). *Emissions Gap Report 2023: Broken Record – Temperatures hit new highs, yet world fails to cut emissions (again)*. Nairobi

West, T.O. and McBride, A.C. (2005) The contribution of agricultural lime to carbon dioxide emissions in the United States: dissolution, transport, and net emissions. *Agriculture, Ecosystems & Environment*, 108 (2), 145-154

White, A. F., and Buss, H. L. (2014). Natural Weathering Rates of Silicate Minerals. In J. I. Drever (Ed.), *Treatise on Geochemistry: Surface and Ground Water, Weathering and Soils* (2nd ed., pp. 115-155). Amsterdam, Elsevier

World Meteorological Organization. Climate Change indicators reached record levels in 2023, 19 March 2024. Web Archive. <https://wmo.int/news/media-centre/climate-change-indicators-reached-record-levels-2023-wmo> [Accessed: 28:05:2024 13:45]

Wu, J., Keller, D.P., Oeschles, A. (2023) Carbon dioxide removal via macroalgae open-ocean mariculture and sinking: an Earth system modeling study. *Earth System Dynamics*, 14, 185-221

Zanatta, M., García-Verdugo, E. and Sans, V. (2023) Direct Air Capture and Integrated Conversion of Carbon Dioxide into Cyclic Carbonates with Basic Organic Salts. *ACS Sustainable Chemistry & Engineering*, 11 (26), 9613–9619

Zeyen, N., Wang, B., Wilson, S., Paulo, C., Stubbs, A.R., Power, I.M., Steele-MacInnis, M., Lanzirrotti, A., Newville, M., Paterson, D.J., Hamilton, J.L., Jones, T.R., Turvey, C.C., Dipple, G.M. and Southam, G. (2022) Cation Exchange in Smectites as a New Approach to Mineral Carbonation. *Frontiers in Climate*, 4:913632

2 Paper I - The geochemical evolution of basalt Enhanced Rock Weathering systems quantified from a natural analogue

Tobias Linke, Eric H. Oelkers, Knud Dideriksen, Susanne Claudia Möckel, Shikar Nilabh, Fidel Grandia, Sigurdur Reynir Gislason

Published in 2024 in Geochimica et Cosmochimica Acta 370, 66-77.

doi.org/10.1016/j.gca.2024.02.005



Contents lists available at ScienceDirect

Geochimica et Cosmochimica Acta

journal homepage: www.elsevier.com/locate/gca

The geochemical evolution of basalt Enhanced Rock Weathering systems quantified from a natural analogue

T. Linke^{a,*}, E.H. Oelkers^{a,b}, K. Dideriksen^{c,d}, S.C. Möckel^e, S. Nilabh^f, F. Grandia^f, S. R. Gislason^a

^a Institute of Earth Sciences, University of Iceland, Sturlugata 7, 102 Reykjavik, Iceland

^b Ali I. Al-Naimi Petroleum Engineering Research Center, KAUST, Saudi Arabia

^c Nano-Science Center, Department of Chemistry, University of Copenhagen, 2100 Copenhagen, Denmark

^d Geological Survey of Denmark & Greenland (GEUS), Øster Voldgade 10, 1350 Copenhagen, Denmark

^e Institute of Life and Environmental Sciences, University of Iceland, Sturlugata 7, 102 Reykjavik, Iceland

^f Amphos21, Carrer de Vençuela, 103, 08019 Barcelona, Spain

ARTICLE INFO

Associate editor: Alexis Navarre-Sitchler

Keywords:

CO₂ storage
Alkalinity production
Basalt weathering
Heavy-metal mobility
Soil degassing
Enhanced rock weathering

ABSTRACT

Substantial quantities of fine-grained basaltic dust have fallen on South Iceland soils over at least the past 3300 years, making this region an ideal natural analogue to define the long-term consequences of current Enhanced Rock Weathering efforts. A relatively pristine South Iceland Gleyic/Histic Andosol, 3 m in height, receiving approximately 1250 mm of rainfall annually was selected for this study. This soil receives an estimated 500–800 g m⁻² y⁻¹ of basaltic dust. The soil waters in this system were regularly sampled as a function of depth from May to November 2018. The fluid pH, alkalinity and the concentrations of most major elements increased with depth as the fluids became more reduced. In contrast, whereas numerous toxic trace metals are initially released to the fluid by the dissolution of the basalt near the surface they are scavenged at depth likely due to their uptake by secondary minerals. Equilibrium reaction path modelling suggests that 1) the added airborne basaltic dust dissolves throughout the soil column and 2) in total 0.26 cm³ of basalt dust dissolves per kg water in this soil–water system. Mass balance calculations indicate that the annual mass of basalt dissolved is less than 60 % of that added to the system, such that the mass of basaltic material in the soil column likely increases continuously over time. Basalt dissolution is maintained throughout the soil by the precipitation of Al-Si-minerals such as allophane, and organic anion ligands released from organic decay. These processes limit aqueous Al³⁺ activity and keep the soil waters undersaturated with respect to primary basaltic minerals and glass. The soil water pH is ~6 and has a higher alkalinity than that of both Icelandic surface waters and the ocean. In contrast, if no basalt was present, the pH of the soil solutions would be 4.4, with zero alkalinity, illustrating the role of added basalt in drawing CO₂ out of the atmosphere.

1. Introduction

Enhanced Rock Weathering (ERW) is currently being explored as a method to remove CO₂ directly from the atmosphere to limit future global warming (e.g., Schuiling and Krijgsman, 2006; Hartmann et al., 2013; Moosdorf et al., 2014; Edwards et al., 2017; Beerling et al., 2018; Dietzen et al., 2018, IPCC, 2018; Haque et al., 2021; Paulo et al., 2021; Kantzas et al., 2022; Baek et al., 2023; Deng et al., 2023; Reershemius et al., 2023). This process involves amending soils with crushed fast-reacting Ca-Mg-silicate rocks and minerals such as basalt (Haque et al., 2019a, 2020; Beerling et al., 2020). To date these studies have

been short-term, lasting for no more than 5 years (Haque et al., 2019a; Goll et al., 2021). Consequently, the long-term consequences of enhanced weathering efforts are poorly constrained. The present study was motivated to illuminate the longer-term consequences of Enhanced Rock Weathering efforts through a detailed characterization of the geochemistry of an analogue field site located in South Iceland.

The natural analogue considered in the present study in South Iceland is a Gleyic/Histic Andosol (Arnalds, 2015). Gleyic and Histic Andosols are soil classes and correspond to Aquands in Soil Taxonomy. Andosols are mineral soils derived from volcanic sediments and cover about 2 % of the Earth's terrestrial surface (Arnalds, 2015). Andosols

* Corresponding author.

E-mail address: tol5@hi.is (T. Linke).

<https://doi.org/10.1016/j.gca.2024.02.005>

Received 19 September 2023; Accepted 8 February 2024

Available online 16 February 2024

0016-7037/© 2024 The Author(s). Published by Elsevier Ltd. This is an open access article under the CC BY license (<http://creativecommons.org/licenses/by/4.0/>).

store about 5 % of the terrestrial carbon (Eswaran et al., 1993). The Andosols of South Iceland receive frequent basaltic dust fallout; the mass of basaltic dust added to these soils is estimated to be 500 to 800 g m⁻² y⁻¹ (Arnalds, 2010; Arnalds et al., 2014, 2016). In addition, less frequent and larger grained airborne volcanic material is transported during explosive volcanic eruptions in the form of glassy volcanic ash fallout referred to as *tephra*. The tephra forms distinct horizons that can be used to date the soil as a function of depth. In total it is estimated that up to 800 g m⁻² y⁻¹ of natural basaltic dust has been added to the soils in South Iceland for the past 3300 years. In contrast, enhanced rock weathering experiments to date have added up to 40 kg m⁻² of crushed Ca-Mg-silicate rocks to agricultural soils annually (Gillman et al., 2002; Cho et al., 2010; ten Berge et al., 2012; Amann et al., 2018; Haque et al., 2019b). Due to the long regular addition of natural basaltic dust to South Icelandic soils, these soils likely provide an insightful natural analogue to illuminate the long-term effect of adding ground basalt to soils as part of enhanced rock weathering efforts.

This is the first manuscript exploring the long-term efficiency and consequences of enhanced rock weathering efforts through the study of a South Iceland Gleyic/Histic Andosol. Future manuscripts will present an estimate of the rate of alkalinity generation and carbon drawdown due to the addition of basaltic dust to this Gleyic/Histic Andosol. In this article we report the composition of fluids and solids in our studied South Iceland soil as a function of depth and time over two field seasons. These observations were used together with geochemical modelling calculations to 1) quantify the saturation state of the primary and secondary mineral phases with respect to the soil solutions, 2) to determine the processes controlling the mobility of heavy metals, and 3) assess the rate at which basalt dissolved in the soils.

2. Methods

2.1. Field site description

The field site chosen for this study is located approximately 7 km north from the town of Hella, at the headwaters of the Rauðalækur river in South Iceland (Fig. 1A). This site was selected as an analog to understand the long-term behavior and consequences of current ERW efforts. There are a number of reasons why these soils provide an excellent natural analogue for ERW systems. First, due to annual dust fallout,

these soils have received over 16,500 t ha⁻¹ of basaltic dust over the past 3300 years. Second, the specific surface area of natural basaltic dust is likely substantially higher than that added to the soils in current ERW experiments due to its finer grain size. The grain size of the crushed rocks used in ERW-applications, if reported, is commonly less than 150 μm (Gillman et al., 2002; Haque et al., 2019b). In contrast, the average size of basaltic Icelandic dust ranges from 10 to 62 μm (Arnalds et al., 2014; Liu et al., 2014; Baldo et al., 2020).

The area upstream of the field site has not been used for agriculture nor fertilized during the past several decades and is therefore considered to be in a natural state. Some drainage channels have been cut in the region, the closest located around 150 m from the study site. The soil at this site is organic-rich and receives substantial and regular input of aeolian basaltic material. Tephra layers from past volcanic eruptions are visible in an outcrop wall located about 10 m downstream from the suction cup lysimeters used in this study (see Fig. 1B). These tephra layers can be used to date the soil profile.

2.2. Soil water, soil sampling and field measurements

Soil water samples were collected using suction cup lysimeters provided by Prenart Denmark. These lysimeters were installed 10 m upstream from a southwest facing outcrop wall and placed at depths of 76, 121, 173 and 260 cm from the surface. Collected fluid samples were analyzed for pH, temperature, dissolved H₂S concentration and redox potential in the field. The dissolved H₂S content was measured by precipitation titration immediately after sampling with an uncertainty of ±0.7 μmol kg_{water}⁻¹, using mercury acetate solution Hg(CH₃COO)₂ as described by Arnórrsson (2000). The redox potentials were measured using an Ag/AgCl micro redox electrode. Measured values were converted to equivalent potentials for a standard hydrogen electrode (E_{SHE}) using a value of +199 mV for the reference potential E⁰ of the Ag/AgCl electrode (Sawyer et al., 1995) via the Nernst equation. Additional fluid samples were filtered through 0.2 μm cellulose acetate in-line filters for major element and alkalinity measurements in the laboratory. For major element analysis, 10 ml of soil water collected from each level was transferred into acid washed polypropylene bottles and acidified to 0.5 % HNO₃ using concentrated Merck suprapure 65 % HNO₃. Samples for iron speciation determination were collected into acid washed polypropylene bottles and acidified to 0.5 % HCl using Merck suprapure HCl.

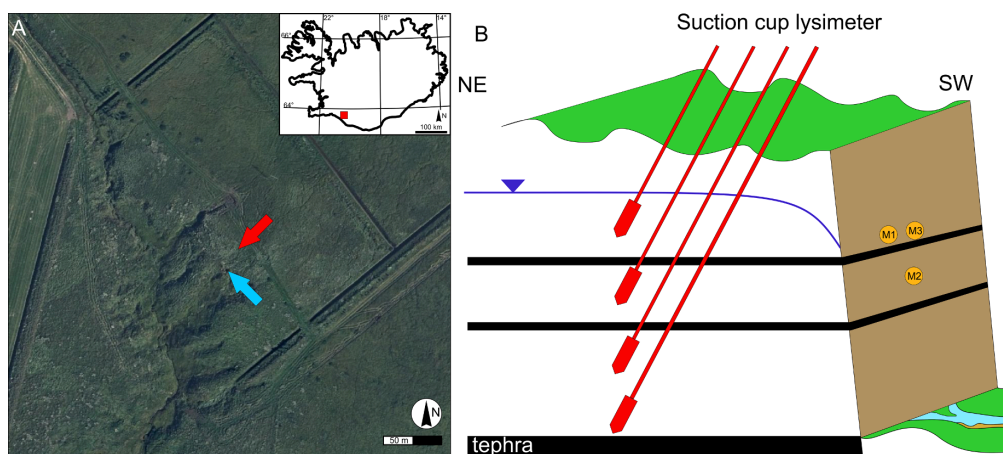
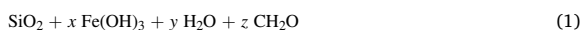


Fig. 1. A: Aerial photo of the studied field site and sampling locations, the red arrow shows the location of suction cup lysimeters and the orange arrow shows the location of the natural outcrop where solid samples were collected. Straight lineations on the photo are man-made drainage channels (aerial photo published with permission from Loftmyndir ehf). B: Schematic NE-SW cross section of the studied outcrop and the position of suction cup lysimeters (shown in red). The locations of soil core samples collected from horizons at 71–96 cm and 120 cm depths are shown as orange dots (labeled M1, M2 and M3). Black horizontal lines represent tephra layers, and the blue curve illustrates the estimated position of the groundwater table.

Samples for dissolved organic carbon (DOC) measurement were collected in 30 ml acid washed polycarbonate bottles and acidified with 0.5 M Merck suprapure HCl to 1:30 ratio. Alkalinity titrations were performed after returning to the laboratory by titrating fluid samples, while constant stirring to pH 3.3 using 0.1 M HCl. The alkalinity was then calculated via the Gran method (Gran, 1952) with an uncertainty of $\pm 5\%$ or less. A detailed description of the analysis methods is provided in section 2.3.

Solid soil samples were collected in May 2017 from the cleared face of the outcrop wall, located 10 m from the suction cup lysimeters (see Fig. 1B). Soil cores were obtained by pushing 7.5 cm diameter, 30 cm long PVC tubes horizontally into the outcrop, which were then sealed to prevent oxidation. The sample tubes were subsequently opened in the laboratory, inside a glove box under an anoxic atmosphere consisting of 97 % N₂ and 3 % H₂. Palladium catalysts were present in the glove box to remove traces of O₂ and minimize sample oxidation. Material from the inner parts of the cores was prepared for powder X-ray diffraction analysis (XRD) in a Bruker dome sample holder. The prepared samples were analyzed immediately after their preparation using a Bruker D8 Advance Plus X-ray diffractometer with 2 θ geometry equipped with a copper X-ray source ($\lambda = 0.15406$ nm) and a Ni-filter. The samples were measured over the 5–70° 2 θ range with a step size of 0.02° 2 θ and a counting time of 1.2 s per step. Additionally, some of the sample material was dried in the glove box and then analyzed by powder X-ray diffraction as described above.

Pair distribution function PDF analysis was performed on the soil samples to further characterize the structure of amorphous or cryptocrystalline phases. The samples were first dried and then loaded into Cole-Parmer polyimide capillaries. Measurements were performed as described by Dideriksen et al. (2015) at Beam line 11-ID-B of the Advanced Photon Source, Argonne National Laboratory using X-rays with an energy of 58.6 keV. To calibrate and convert data from 2D to 1D we used the program fit2D (Hammersley et al., 1996; Hammersley, 1997). Further data processing was performed using PDFgetX2 (Qiu et al., 2004). Pair distribution functions, G(r), were generated by Fourier transformation using a Q_{max} of 24 Å⁻¹ and are provided together with the X-ray scattering data I(Q). The PDFgetX2 data treatment requires definition of the chemical composition of the samples. To obtain these compositions, preliminary SEM/EDX analyses were performed. These showed a pronounced Fe and O signal with less pronounced Si and C signals. Based on these results, it was assumed that the soil samples had a composition consistent with:



The value of x in Equation (1) was estimated from the relative peak intensities at ~ 1.6 Å, corresponding to Si–O, and at ~ 2 Å for Fe(III)-O or ~ 2.1 Å for Fe(II)-O, taking into account the difference in electron density and expected coordination number of SiO₄ and FeO₆. The values of y and z in equation (1) were subsequently defined by trial and error to avoid high amplitude oscillations in the G(r) function at low r values. Tests of the procedure on the same samples yielded highly similar PDF fits at $r > 1$ Å with values of x varying within $\pm 30\%$.

2.3. Analytical Techniques

Major element concentrations were analyzed in duplicate using a Ciro Vision, Spectro Inductively Coupled Plasma Optical Emission Spectrometer (ICP-OES). The same subsamples were used to measure the trace element compositions of fluid samples using a Thermo iCAP Qc Inductive coupled plasma mass spectrometer (ICP-MS). Prior to the analysis the samples were diluted with milliQ water and spiked with internal Rh, Ir, and Ga standards to correct measurements for detector drift. For both ICP-OES and ICP-MS measurements, the uncertainties were below $\pm 5\%$ for all elements. Iron redox species were determined using a Dionex 3000 ion chromatography system using the method

described by Kaasalainen et al., (2016). DOC concentrations were determined by size exclusion chromatography using a Liquid Chromatography – Organic Carbon Detection system (LC-OCD) following the method of Huber et al. (2011). The limit of quantification (LOQ) for each element is presented in S1.

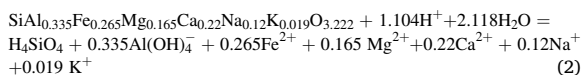
2.4. Geochemical Modelling

In-situ aqueous speciation, charge balance, mineral saturation states and equilibrium reaction paths were modelled using the PHREEQC interactive software version 3.4.0 (Parkhurst and Appelo, 1999). Calculations were performed using the minteq.v4.dat (Allison et al., 1991; U.S. Environmental Protection Agency, 1998) database after adding to it the thermodynamic data for minerals, aqueous species and glasses listed in electronic supplement S2.

Based on these calculations, predominance diagrams were plotted using PhreePlot (Kinniburgh and Cooper, 2004) as described in Linke and Gislason (2018). Hematite, magnetite, goethite, were not allowed to form making ferrihydrite and siderite the most stable Fe phases in the modelled system that form as a result of weathering process at the surface. These two minerals have been identified in the studied field site. Note that Baldo et al. (2020) identified hematite, goethite, and magnetite in Icelandic dust. Neither these minerals nor maghemite and lepidocrocite were observed to form in our field area nor the field observations reported by Arnalds (2004). Geochemical modelling was also used to assess the saturation state of the soil solutions with respect to atmospheric CO₂ and O₂, selected minerals and glasses.

2.4.1. Reaction path modelling

Equilibrium reaction path modelling was performed in the present study using PHREEQC. The initial fluid compositions entering the soil used in the modelling was set to the average composition of South Iceland rainwater as provided in Table S3 (Eiriksdóttir et al., 2014). The composition of the dissolving basalt was based on the chemical analysis of volcanic rocks located close to the study area (Harðardóttir, 2020) comprising the most likely source for the dust added into the studied soils (Arnalds et al., 2014, 2016). The composition of this basalt is provided in Table S2 and its metal oxide composition is provided in Table 1. The dissolution reaction of this ‘On-Site’ basalt can be written as:



Equilibrium reaction path models were used to calculate the fluid composition and mass of minerals precipitating from the fluid phase as this basalt dissolves into the fluid. Based on field observations, only the upper 70 cm of the soil column is assumed to be oxic with the uppermost part in equilibrium with atmospheric oxygen. No oxygen source is present deeper in the soil. The initial rainwater is set to be in equilibrium with atmospheric CO₂ and oxygen. As Fe²⁺ dominates the oxidation state of iron in the ‘On-Site’ basalt, all iron released from this basalt was assumed to be in this oxidation state. During the simulations, O₂ is

Table 1
Metal oxide composition of the ‘On-Site’ basalt used for data interpretation in this study. Note for simplicity all iron is shown as Fe²⁺.

| metal oxide | Mass-% |
|--------------------------------|--------|
| SiO ₂ | 50.15 |
| Al ₂ O ₃ | 14.26 |
| FeO | 15.89 |
| MgO | 5.55 |
| CaO | 10.3 |
| Na ₂ O | 3.1 |
| K ₂ O | 0.75 |

continuously removed from the system as Fe^{2+} is released from the dissolving basalt and oxidized. The partial pressure of CO_2 in the soil is set to 0.05 bar, which is the average of that measured in the soil water samples. The effect of the presence of DOC in the model calculations was taken into account by assuming that all DOC was present as aqueous oxalate. This choice was made because oxalate is representative of aqueous organic species and because of the availability of equilibrium constants for aqueous metal-oxalic complexes (Pettit and Powell, 2008).

The minerals allowed to precipitate in the reaction path models were restricted to include only those observed in andosols, namely ferrihydrite and allophane. In addition, a silica phase with thermodynamic properties of moganite was included. Under reduced conditions allophane, moganite, siderite and mackinawite were allowed to precipitate at local equilibrium if these phases became supersaturated. The mass of basalt dissolved was tuned to best fit the Ca and Mg concentration observed in the field. The model, however, does not include provision for bacterial activity or local compositional, physical, or mineralogical heterogeneities.

3. Results

3.1. Mineral and chemical composition of the collected solids

X-Ray diffraction (XRD) analysis and Pair Distribution Function (PDF) analysis were conducted to determine the mineralogical composition of the soil samples. The XRD pattern of the soil, as shown in Fig. 2A, exhibits a strong background at 10° to 20° 2θ caused by the dome sample holder used to protect the samples from oxidation and at 30° and 60° 2θ by the presence of amorphous and/or poorly crystalline material that cannot be identified by XRD. Additional minor amounts of crystalline feldspar and pyroxene are present. Material collected from a soil horizon between 71 and 96 cm in depth (Fig. 1B) contains crystalline siderite (Fig. 2B). No difference in the mineral composition or relative peak intensity was observed between the wet samples measured in the dome sample holders and corresponding material dried in the glove box. Red material collected from the same horizon as the siderite does not show distinct XRD peaks, but Pair Distribution Function analysis indicates that it contains a short range ordered ferrihydrite, indicated by peaks at e.g., 2.0 Å for Fe-O pairs, at 3.1 Å for edge sharing Fe-Fe pairs and at 3.4 Å for corner sharing Fe-Fe pairs (Fig. 2C and Fig. 2D).

3.2. Fluid Compositions

Soil water samples were analyzed for their major and trace metal composition as well as for redox sensitive elements and dissolved organic and inorganic carbon. All measured compositions are provided in Tables S1 and S4. These compositions were recalculated to the *in-situ* soil temperature of 7°C , the average soil temperature at 76–260 cm depth during the summer months (Petersen and Berber, 2018), using PHREEQC (Parkhurst and Appelo, 1999). These recalculated fluid compositions are shown as a function of depth in Figs. 3 and 4.

The redox potential (E_{hSHE}), the logarithmic partial pressure of the CO_2 , and the dissolved inorganic carbon (DIC) concentrations of the soil water samples are shown in Fig. 3. For comparison, the redox potential was also calculated based on measured concentrations of $\text{Fe}^{2+}/\text{Fe}^{3+}$ and of $\text{SO}_4^{2-}/\text{HS}^-$ using PHREEQC. These values are compared to the Eh measured in the field in Fig. S5 in the Electronic Supplement. In general, the closer the samples are to the atmosphere, the more oxic the soil water samples.

The redox potential of the soil water samples, E_{hSHE} , decreases with increasing depth and pH. There are significant variations in pH, E_{hSHE} and $p\text{CO}_2$ with time at each soil depth. Although no clear trend for temporal pH evolution is evident, the measured Eh increased in all soil water samples during October and November likely due to changes in bacterial activity. The alkalinity of the fluid samples increased during the summer months, peaking in mid-September, it declined thereafter (see Table S4).

The concentrations of DIC and Si are relatively high compared to other constituents, reflecting basalt dissolution and organic matter decomposition. Average DIC concentration increases with increasing depth but varies seasonally (see Fig. 3 and Fig. S1). The highest DIC concentration was found in samples collected during September, except for the deepest samples collected at 260 cm depth, where this concentration peaked later in the fall. DOC concentrations increased with time during the summer and fall and have the lowest concentrations at the greatest depths. The DOC concentrations are generally 7–21 times lower than the DIC concentrations. The variations in DIC and DOC over time are likely caused by the response of bacterial activity and organic decay to seasonal changes in temperature and environmental conditions. There are significant temporal variations in measured Si concentrations at depths of 76 cm and 121 cm. Deeper in the soil, the Si concentrations

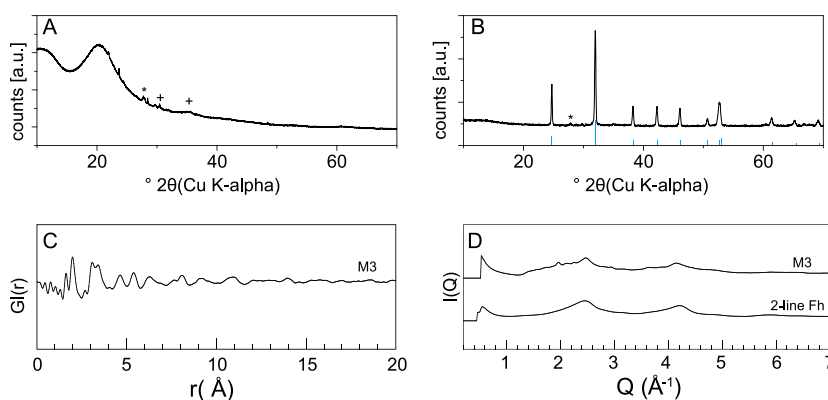


Fig. 2. A: Representative Powder X-ray Diffraction (XRD) pattern of a soil sample collected from ~ 120 cm in depth. The small peaks indicated by the * and + symbols are consistent with feldspar and pyroxene, the major crystalline phases in basalt. The high background is caused by the dome sample holder and the presence of amorphous and nanocrystalline material. B: Powder X-ray diffraction pattern of a dried nodule identified as siderite collected from ~ 80 cm in depth. All major peaks correspond to the siderite reference pattern; the siderite peaks shown with relative intensity as blue bars were reported by Effenberger et al. (1981). The additional peak indicated with a * at 27.9° 2θ corresponds to the main peak of Ca-rich feldspar. C: Pair Distribution function ($G(r)$) in real space of red solid material collected from the outcrop wall at ~ 80 cm depth. This is identified as a ferrihydrite-rich soil. The absence of larger peaks at >15 Å indicates the short order of the mineral phase. D: X-ray scattering data, $I(Q)$, of red material collected from the outcrop wall at ~ 80 cm in depth. Also shown is the $I(Q)$ of a 2-line ferrihydrite standard. The natural sample with minor impurities resembles closely the ferrihydrite standard material.

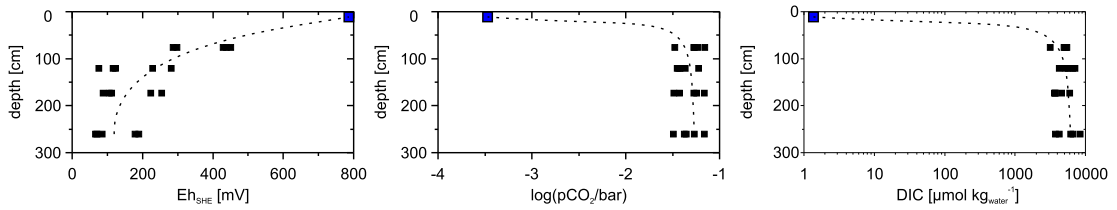


Fig. 3. The redox state, $E_{h_{SHE}}$, the logarithm of the partial pressure of CO_2 , $\log(pCO_2/\text{bar})$, and the dissolved inorganic carbon (DIC), in log scale, at each sampling depth for all collected fluid samples and for rainwater (plotted as a blue square). Dashed lines show the trend of the data with increasing soil depth.

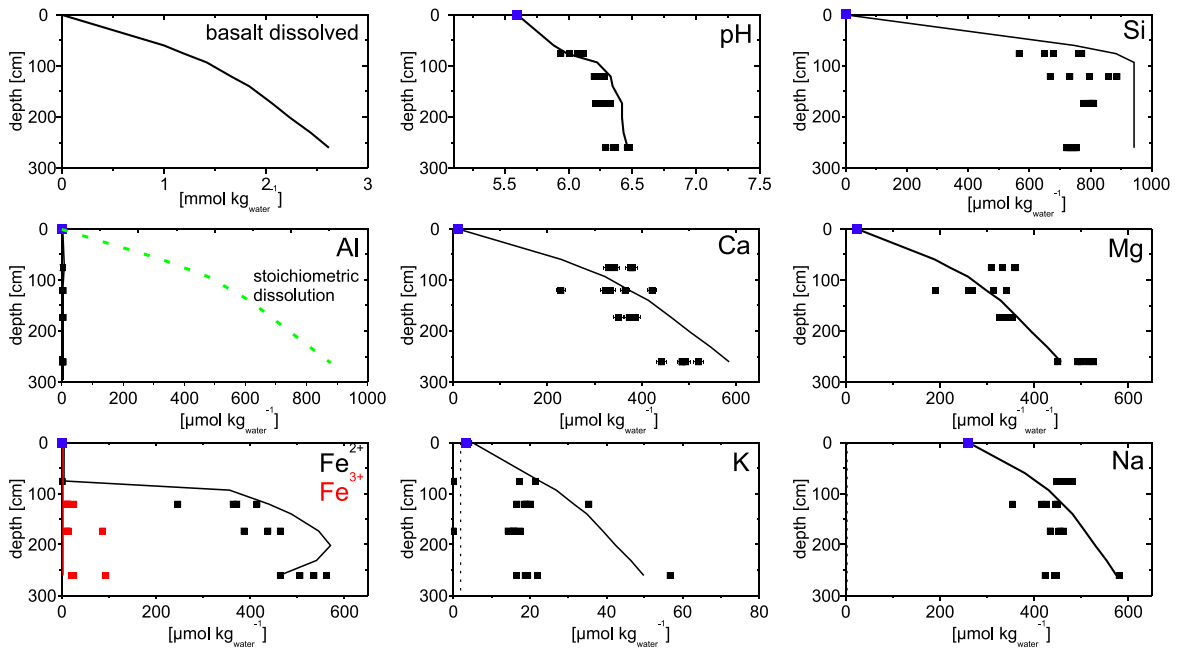


Fig. 4. Evolution of major dissolved constituents in sampled soil water as a function of depth. The black and red symbols correspond to measured soil water concentrations, the blue symbols represent the composition of rainwater, and the solid curves show the results of modelling calculations (see text). Note the different concentration scales for each constituent. Also shown as a green dashed curve are the calculated Al concentrations determined assuming stoichiometric dissolution of basalt in the absence of secondary mineral precipitation. The iron species are shown as red and black squares depending on the measured oxidation state of the iron. The iron concentration is close to the detection limits in the shallowest soil water samples at 76 cm depth, causing the symbols to appear as a single square, and the modelled concentrations of Fe^{3+} and Fe^{2+} at shallow levels are $\pm 0 \mu\text{mol kg}_{\text{water}}^{-1}$. Dashed lines represent limit of quantification, and uncertainties are within symbol size except for Ca.

vary less over time (Fig. 4).

The concentrations of all other elements are lower than those of Si. The Al concentrations, as shown in Fig. 4, range from below the $0.28 \mu\text{mol kg}_{\text{water}}^{-1}$ quantification limit to $3 \mu\text{mol kg}_{\text{water}}^{-1}$. This is ~ 200 times lower than the corresponding measured Si concentrations. The concentrations of Mg, Ca, Fe, Mn, Sr, and Ti generally increase with depth and their concentrations suggest the close to stoichiometric dissolution of the basalt in the soil. Only 10 to 20 % of the total dissolved iron is present as Fe^{3+} . At 76 cm depth, under oxidizing conditions, the concentrations of both Fe^{2+} and Fe^{3+} are close to the detection limit. Manganese concentrations exhibit the same trend as iron, being only present as reduced Mn^{2+} deeper in the soil, where anoxic conditions are present. The concentrations of Cl, Na and K do not correlate with depth, as these concentrations are largely controlled by their concentrations in the influent rainwater.

The soil water H_2S concentration increases with depth, while total S decreases (Fig. 5). The concentrations of the trace metals Cd, Co, Cu, Mo,

Ni, and Pb also decrease with depth (see Fig. 5 and Table S1). The similarity of these behaviors suggests consumption of these trace metals by secondary sulfide mineral precipitation (e.g., Charriau et al., 2011; Smieja-Król et al., 2015). The concentrations of other metals including As and Cd are close or below the detection limit in all collected water samples and Pb is only above the limit of quantification in one shallow soil water sample.

An Eh-pH diagram illustrating the stability of iron phases at the conditions of our field site is shown in Fig. 6. The pH of the soil water samples increases continuously with depth as the samples become more anoxic. At shallow levels the oxidized Fe^{3+} species are dominant, which lead to a supersaturation of the fluid phase with respect to ferrihydrite at these depths. Deeper in the soil Fe^{2+} dominates. The dissolved iron concentrations increase with depth and up to $\sim 500 \mu\text{mol kg}_{\text{water}}^{-1}$. As a consequence, the water approaches equilibrium with respect to siderite. The sulfur concentrations of the sampled soil waters at depth greater than 121 cm did not exceed $80 \mu\text{mol kg}_{\text{water}}^{-1}$. No sulfide minerals are

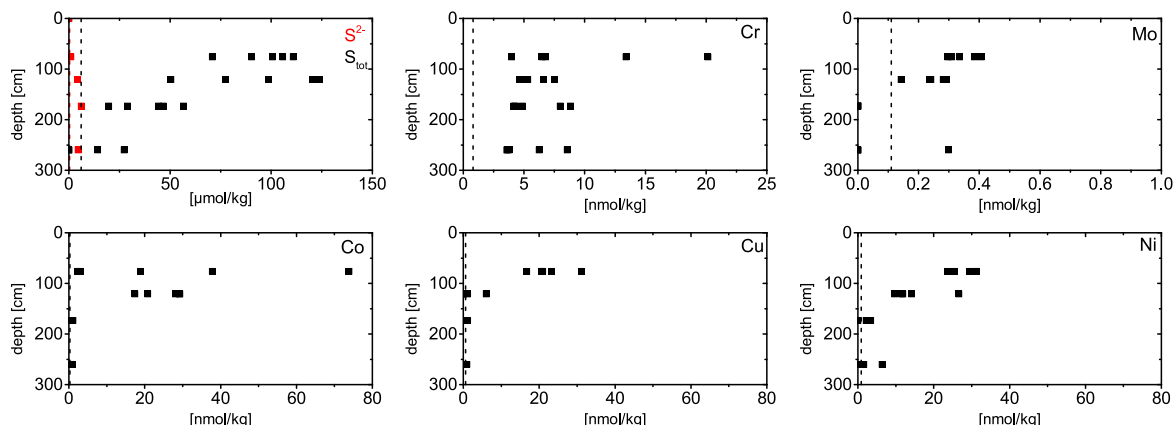


Fig. 5. Sulfur and trace metal concentrations in soil water samples versus depth. Note the different units and scales on the horizontal axes. Black dashed lines represent Limit of quantification. Uncertainties are within symbol size.

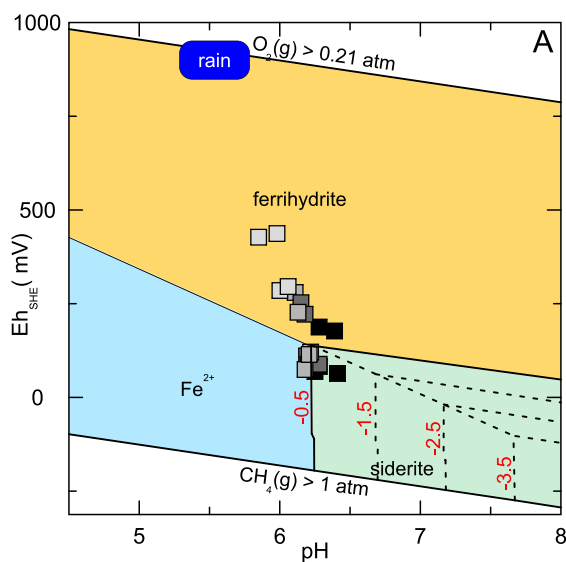


Fig. 6. Eh-pH diagram computed with PhreePlot illustrating the predominance fields of iron phases as at a temperature of 7 °C. The square symbols show the composition of collected soil water samples. The shading of the symbols indicates the depth of the water sample; the darker the shading, the deeper the sample. The black lines show the predominance field for a total Fe concentration of 500 μmol and a $\log(p\text{CO}_2/\text{bar})$ of -1.0 . The dashed black lines represent the ferrhydrite predominance field at the total Fe concentrations indicated in the figure. The dashed red lines illustrate the siderite predominance field at the $\log(p\text{CO}_2)$ values indicated by the red numbers in the plot at a Fe concentration of 500 μmol . The light orange field shows the extent of the predominance field of the $\text{Fe}(\text{OH})_2^+$ species at 10 and 1 $\mu\text{mol Fe}_{\text{tot}}$ concentrations. The average pH-Eh of rainwater, shown as a blue field labeled ‘rain’ was taken from Eiriksdottir et al. (2014).

found to be stable at these low sulfur concentrations and the pH-Eh of studied soil system.

3.3. Geochemical modelling

3.3.1. Mineral saturation states in the soil water samples

Calculated saturation indices of the sampled soil waters with respect to the ‘On-Site’ basaltic glass and common primary and secondary soil minerals at 7 °C are shown in Fig. 7. All the sampled soil solutions are saturated or supersaturated with respect to the SiO_2 polymorphs quartz and chalcedony, but undersaturated with respect to amorphous silica. Moganite is slightly undersaturated in all samples but closer to equilibrium than the other SiO_2 -phases.

The Al-Si-mineral allophane, the most common secondary mineral in Icelandic soils along with iron oxyhydroxides (Wada, 1989; Arnalds, 2004, 2015), is supersaturated at all depths, except for some of the samples collected at a depth of 76 cm. The silica-rich allophane, Al/Si1.26, is more supersaturated than the silica-poor allophanes. The Fe-Mg-rich smectite is undersaturated in all the shallow samples but close to saturation deeper in the soil (Fig. 7), while the Fe-Mg-poor smectite is only undersaturated at 76 cm and always supersaturated at deeper levels. The soil water samples are supersaturated with respect to ferrhydrite, except for some of the shallowest samples, which are undersaturated. Siderite (FeCO_3) and mackinawite (FeS) are undersaturated in the fluid samples at the shallowest depth, but close to saturation deeper in the soil. Amorphous FeS (not shown) and calcite are always undersaturated.

All fluid samples are undersaturated with respect to the main primary phases present in basalt, including ‘On-Site’ basaltic glass, which is consistent with the ongoing dissolution of the basaltic material throughout the soil column. The continuous undersaturation of the basaltic glass is due to the low concentrations of its dissolution products in the aqueous solution. The presence of organic acids also increases the degree of undersaturation of the Al-bearing primary minerals. In this way, the presence of DOC helps to accelerate the dissolution of the primary basaltic phases (Oelkers and Gislason, 2001).

3.3.2. Reaction path modelling

Reaction path models were run to 1) reproduce the soil water compositions measured in the field, 2) quantify the mass and volume of basalt dust dissolved, 3) predict the mass and volume of secondary phases, and 4) estimate the spatial variation in basalt dissolution and secondary mineral precipitation. The mass of basalt dissolved in the model calculation as a function of depth was determined by fitting the

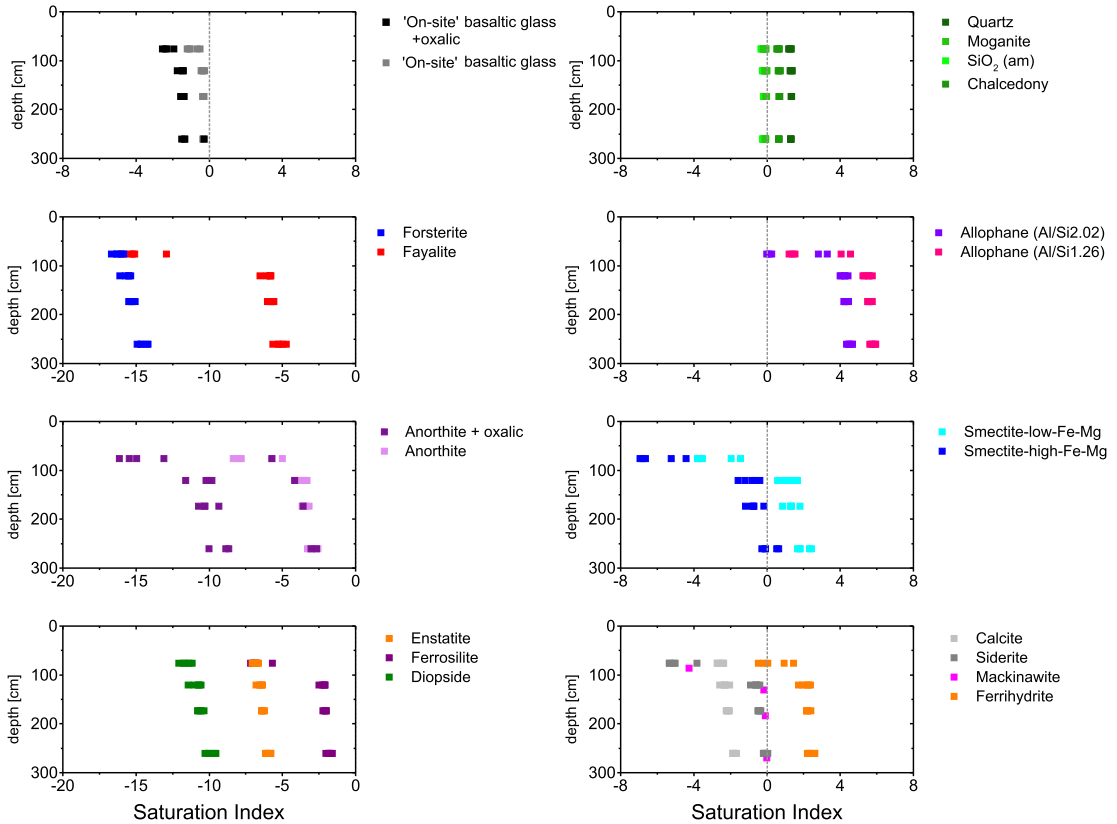


Fig. 7. Saturation indices of the sampled waters as a function of depth for primary basalt minerals on the left and for common secondary soil minerals on the right. The calculated saturation state of 'On-Site' basaltic class and anorthite in the presence and absence of aqueous oxalate are both shown. The dashed vertical lines are consistent with fluid mineral equilibrium. The redox state used in the calculations is based on the measured fluid Fe^{2+}/Fe^{3+} and H_2S/S_{TOT} ratios. Note the different scales on the various plots.

results of the calculation to the measured water compositions. The calculated soil water compositions as a function of depth obtained by this effort are illustrated as solid black curves in Fig. 4. A good agreement between the calculated curves and measured concentrations is evident.

As shown in the top left plot of Fig. 4, up to $260 \text{ mmol kg}_{\text{water}}^{-1}$, equal to $\sim 310 \text{ mg kg}_{\text{water}}^{-1}$, of basalt needs to dissolve to reproduce the measured soil water compositions. This is equal to 0.26 cm^3 of basaltic glass per kg soil water solution. The dissolution of this basalt induces the precipitation of allophane, ferrihydrite, siderite and the silica polymorph moganite. The volume of each of these secondary minerals

precipitated as a function of depth is illustrated in Fig. 8. The precipitation of these minerals has a complex influence on carbon uptake rates. Their precipitation maintains the aqueous fluid at undersaturated conditions with respect to the basaltic dust, promoting the dissolution of these solids. This precipitation can also alter fluid pH which can either increase or decrease the solubility of CO₂ in the aqueous phase.

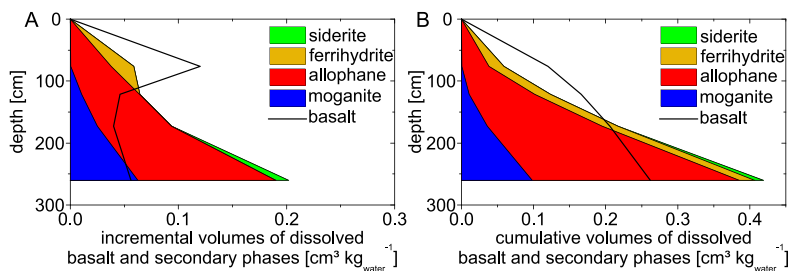


Fig. 8. Calculated volumes of minerals precipitated, and basalt dissolved per kg of soil solution A) incremental volume change and B) cumulative volume change from the top of the soil column to the indicated depth.

4. Discussion

4.1. Soil water chemistry and estimation of basalt dissolution rates

The measured soil waters are enriched in Si, Ca, Mg and Fe compared to rainwater. This confirms the dissolution of basalt in the soil. The breakdown of soil organic matter increases DOC and DIC concentration, as well as S and N, which are only present in low concentrations in the dissolving basalt. The pH of the water in this basalt-rich soil ranges from 5.8 to 6.7 and the alkalinity up to 3 meq kg⁻¹ water. In contrast, the alkalinity of water in corresponding organic-rich basaltic mineral-poor soils are commonly less than 0.3 meq kg⁻¹ water (Verry, 1975; Vitt et al., 1995). This comparison illustrates the ability of fine ground basalt dissolution to increase soil water alkalinity.

As the mass of sulfur in basalt is low (Wallace and Carmichael, 1992), it is likely that most of the S in the sampled soil water originated from the decomposition of organic material. Much of the sulfur in the organic material likely originated from sea spray, volcanic gas emissions, and global pollution. Organic decay occurs continuously with depth and organic matter decay releases sulfur (e.g., (Chen and Stevenson, 1986; Kirkby et al., 2011)). It might be expected, therefore, that the total sulfur concentration in the soil waters will also increase with depth. Nevertheless, as shown in Fig. 5, total dissolved sulfur concentrations in the soil water decrease with depth, suggesting that aqueous S is being consumed by one or more solid phases. Based on the fluid saturation states, the most likely precipitating sulfide mineral at depth in the anoxic zone is mackinawite. The formation of this (or perhaps another) sulfide mineral likely helps scavenge some potentially toxic metals from the soil solutions via co-precipitation or sorption (see below and Rickard and Luther (2007); Swanner et al. (2019)).

The variation of soil water compositions as a function of depth allows estimation of the geometric surface area normalized dissolution rate of the ‘On Site’ basaltic glass in our studied soil. The dissolution rate, r , of this glass can be estimated taking account of (Oelkers and Gislason, 2001; Gislason and Oelkers, 2003)

$$r = \frac{1}{A_{\text{geo}}} \left(\frac{dm_{\text{basalt}}}{dm_{\text{water}}} \right) \left(\frac{dm_{\text{water}}}{dt} \right) \quad (3)$$

where A_{geo} corresponds to the total geometric surface area of basalt in the soil column, $\left(\frac{dm_{\text{basalt}}}{dm_{\text{water}}} \right)$ designates the mass of basalt dissolved into each incremental mass of water, and $\left(\frac{dm_{\text{water}}}{dt} \right)$ represents the rate at which water is passing through the soil column. Reactive path calculations suggest that up to ~ 310 mg kg⁻¹ water or $\sim 2.6 \times 10^{-3}$ mol kg⁻¹ water of basaltic glass dissolved in our studied soil column. Correspondingly, the mass of water flowing through our soil system is estimated to be 925 ± 150 kg water m⁻² yr⁻¹.

The geometric surface area, A_{geo} in Eq. (3) is equal to the product of the specific surface area of the basaltic glass and its mass in the soil column. The specific geometric surface area, A'_{geo} can be estimated using (Brantley et al., 1999; Gautier et al., 2001).

$$A'_{\text{geo}} = \frac{6}{\rho \bullet d_{\text{eff}}} \quad (4)$$

where d_{eff} and ρ symbolize the effective grain diameter and the density of the basaltic glass, respectively. The effective particle size, d_{eff} can be determined from (Tester et al., 1994)

$$d_{\text{eff}} = \frac{d_{\text{max}} - d_{\text{min}}}{\ln \left(\frac{d_{\text{max}}}{d_{\text{min}}} \right)} \quad (5)$$

where d_{max} and d_{min} denote the maximum and minimum grain size of the basalt in the soil. A number of past studies concluded that most of the basaltic dust in Iceland is dominated by 10 to 62 μm size grains (Arnalds

et al., 2014; Liu et al., 2014; Baldo et al., 2020). Based on these values, the effective diameter of the basalt grains is 28.5 μm . Taking account of Eq. (4) and a basaltic glass density of 2.7 t m⁻³, the specific geometric surface area of the basaltic dust in our soil equals 78 m² kg⁻¹.

The mass of basalt in the soil column is somewhat challenging to estimate. The soil contains approximately at least 50 % pore space (Snæbjörnsson, 1982) and up to 20 % organic carbon based on field observations (Arnalds, 2015). If it is assumed that half of the remaining volume is occupied by basalt, 15 percent of the volume of the soil is basalt and the remainder secondary minerals, including allophane and ferrihydrite. This estimate is roughly consistent with the current rate of basaltic glass input versus dissolution in the soil column. As mentioned above, the mass of basaltic dust in South Iceland can be a maximum of 0.8 kg m² yr⁻¹. This flux is approximately 2.8 times the estimated rate of basalt dissolution in each m² of the soil column, which is estimated to be ~ 0.286 kg m² yr⁻¹ by taking account of the mass of basalt dissolved annually in the soil column and the mass of water passing through this soil column.

Assuming the soil column contains 15 % basaltic glass by mass, the total volume of basalt in each square cm of the soil column is 40.5 cm³, equal to 0.000045 m³. This volume of basalt has a mass of 0.109 kg, such that the total surface area of basalt in the soil column equals 8.53 m². Taking account of this surface area together with the mass of basalt dissolving into each kg of water and the mass of water passing through the system, an estimate of the rate of basalt dissolution can be determined using Eq. (3), yielding a rate of 9×10^{-20} mol m² s⁻¹. The uncertainty associated with this number is large owing to uncertainties in the mass and surface area of basalt in the soil column. Nevertheless, this field measured surface area normalized dissolution rate is approximately 2 orders of magnitude or more, slower than that measured in the laboratory at similar pH and temperature conditions, as reported by Oelkers and Gislason (2001) and Gislason and Oelkers (2003). Numerous past studies have reported that mineral reaction rates in the field are significantly slower than corresponding laboratory measured rates (Gislason and Arnórsson, 1993; White and Blum, 1995; White et al., 1996; White and Brantley, 2003; Molins et al., 2012). Numerous origins of this discrepancy have been proposed as summarized by White and Brantley (2003).

It should be emphasized that that both the large uncertainties in field-based weathering rates and large variations in annual environmental conditions including annual and seasonal temperature and rainfall patterns make it difficult to quantify carbon drawdown rates of proposed enhanced weathering efforts. Attempts to develop novel methods to overcome these limitations are currently ongoing (e.g., Kantola et al., 2023; Reershemis et al., 2023).

4.2. Toxic metal mobility

The mass of toxic metals released to the soil water in the study site by basalt dissolution can be estimated by taking account of the total mass of basalt dissolved in the system and the average composition of the dissolving basalt. To a first approximation the trace and toxic metal concentration of the basalt was taken to be equal to that of MORB as reported by Gale et al. (2013). The choice to use the composition of MORB in this instance is that it likely represents an average composition of the dust entering our system over time. Note because of annually and seasonally changes in wind direction, and of distinct volcanic eruptions, the trace element composition of dust arriving to our system is somewhat variable. The composition of MORB is also similar to that being considered for current enhanced rock weathering applications (Beerling et al., 2018). Taking this into account, the 0.31 g kgw⁻¹ basaltic glass dissolved into the soil water would release ~ 245 nmol kg⁻¹ water Co, ~ 1600 nmol kg⁻¹ water Cr, ~ 390 nmol kg⁻¹ water Cu, ~ 525 nmol kg⁻¹ water Ni, and ~ 1 nmol kg⁻¹ water Pb, respectively. The concentration of each of these trace metals in the deepest collected soil waters are, however, lower by a factor of at least 5–200 relative to these values. This comparison

suggests that these trace metals have been reincorporated into the solid phase following their liberation from dissolving basalt. Note that this reduction in toxic trace element reduction may be underestimated as it does not take into account the potential remobilization of these elements from the secondary minerals in the soil. It is likely that the trace elements in our studied soil were originally sourced from the earlier dissolution of basaltic dust input.

The degree of depletion of selected major, toxic and trace metals in the collected soil waters are depicted in Fig. 9 relative to that of Ca. It is assumed that Ca is not incorporated into secondary phases. This choice is made due to the relatively high concentration of this element in the dissolving basalt, its low concentration in the influent rainwater, and the low stability of Ca-bearing secondary minerals in the studied system. Copper is the most depleted trace metal relative to its concentration in MORB, and chromium, nickel and cobalt are also strongly depleted at depth. Numerous past studies reported the incorporation of trace and toxic metals into iron oxyhydroxide phases (Scheinost et al., 2001; Brinza et al., 2008; Moon and Peacock, 2012) and into sulfide minerals (Rickard and Luther, 2007; Swanner et al., 2019). Both of these phases are predicted and/or observed to have formed in our studied soil system. Ferrihydrate was observed to have formed near the surface of our soil column, where the fluids are oxic, whereas mackinawite is predicted to have formed deeper in the soil column at anoxic conditions. The efficiency of scavenging toxic trace metals by secondary minerals in our studied system suggests that similar processes might limit toxic metal release from the waters discharged from geoengineered enhanced weathering systems.

Total dissolved Al is depleted in the fluids at all depth. Note that dissolved Al is highly toxic (Roseland et al., 1992; Gensemer and Playle, 1999; Roy et al., 2000; Closset et al., 2021). Furthermore, the low concentration of Al^{3+} and potential complexation of this metal with aqueous organic species, ensures the continued dissolution of basaltic glass and plagioclase throughout the soil column. It can also be seen in Fig. 9 that Ca, Mg and Fe, dissolve near congruently at all depth, except for Fe at the shallowest level, which is at oxic conditions.

Due to secondary mineral scavenging, none of the soil water compositions contained metal concentrations that exceed the drinking water guidelines from the WHO, EPA or the Icelandic government, with the exception of Fe and Mn, (United States Environmental Protection Agency, 2009; Gunnarsdottir et al., 2016; World Health Organization, 2017). In all cases the trace and toxic metal concentrations were lower than the drinking water limits by at least a factor of 50. Nevertheless, the uptake of toxic trace elements by soils due to enhanced rock weathering

over time, eventually lead to soils accumulating metal contents that exceed environmental regulatory limits (Dupla et al., 2023).

4.3. Consequences for Enhanced Rock Weathering efforts

The results of this study have a number of implications for current enhanced weathering efforts. Notably, the enhanced weathering studies to date have added up to 400 t ha^{-1} (equal to $40,000 \text{ g m}^{-2}$) of ground basalt to soils (Gillman et al., 2002; Haque et al., 2019a). These efforts have only lasted for no more than several years. The present study, based on a natural analogue, provided insight into the long-term behavior of these efforts. Notably:

1. The basalt added annually to the soil of our study area does not totally dissolve each year. Only approximately half of the up to 800 g m^{-2} of basalt added annually to the soil is estimated to dissolve. Basalt and secondary minerals continue to accumulate in the soil over time. Results also suggest that basalt added up to 3300 years ago continues to dissolve in our studied soil system. Current ERW efforts typically add far more basalt annually than received by our study area, and the dust grains are also larger in size. It seems likely, therefore, that much of the basalt added in ERW efforts will persist long-term. Consequently, carbon drawdown by these efforts may not be as efficient as anticipated. Nevertheless, alkalinity production provoked by the addition of basalt to soils during ERW efforts will likely continue for significant time frames after the addition of the reactive material is terminated.
2. The dissolution of basaltic glass is observed to continue throughout the soil column. This observation favors the addition of reactive rock throughout the soil column, not just at the top of the soil. This continued dissolution is insured by the continued strong undersaturation of the soil waters with respect to primary basaltic minerals. This undersaturation is partially maintained by the decomposition of organic materials present in the soil column. This decomposition adds organic acid anions to the soil water, which helps maintain fluids at strongly undersaturated conditions.
3. The dissolution rates of basaltic glass are found to be approximately two orders of magnitude slower than corresponding laboratory rates. These slower field rates need to be taken into account when assessing the efficiency of enhanced weathering efforts.
4. Toxic and trace metals, likely released to the fluid phase by the dissolution of basaltic glass in our field area, are efficiently reincorporated into the soil column, likely by their coprecipitation and sorption into/to secondary minerals. Although this process assures that waters released from the soils into surface and groundwater systems will likely be non-toxic, these metals will build up in the soil profile. The degree to which the increasing content of trace and toxic metals in the soil column is detrimental to the local biota remains unclear.

5. Conclusions

This study focused on the fluid compositions and mineralogy of a natural soil that has received up to 800 g m^{-2} of basaltic dust annually for ~ 3300 years. Despite the dissolution of some of this basalt annually, it is estimated that more than half of the basalt added is still present in the studied soil column. The results of this field study, therefore, illuminate the potential and the limitations of ERW efforts. The precipitation of secondary minerals and the addition of organic acids maintains the soil waters undersaturated with respect to the primary minerals and glasses present in basalt. This assures the continued dissolution of basalt present in the soil system and suggests that the maximum total mass of basalt added to soil can be substantially greater than that of our studied soil system without slowing the specific dissolution rate of the basalt. Both this result and the observation that toxic metals are retained in the soil despite their likely release by dissolving basalts, encourages the

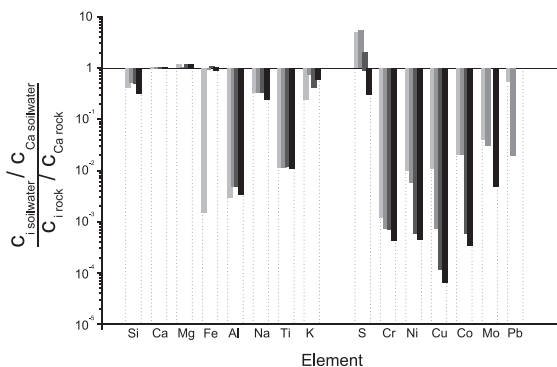


Fig. 9. The ratio of selected element concentrations normalized to Ca in the collected soil waters relative to the release from basalt assuming stoichiometric dissolution. All values have been corrected for seawater input. The shading of the columns indicates the depth of the water sample; the darker the shading, the deeper in the soil is the sample. The S concentration of MORB was taken from Wallace (2021) and trace metals from (Gale et al., 2013).

continued consideration of ERW for CO₂ drawdown from the atmosphere.

Nevertheless, this study also suggests some strong limitations to ERW efforts. Notably, basaltic glass dissolution rates are substantially lower than might be expected from laboratory experiments. This limits the near-term efficiency of such efforts. In addition, the long-term effect of the buildup of toxic and trace metals on soil ecosystems remains unresolved. Taken together these limitations compel new studies of natural analogue systems to further illuminate the long-term consequences of ERW efforts.

Funding

This project was funded by the European Union's Horizon 2020 research and innovation programme under the Marie Skłodowska-Curie grant agreement No 675219, from Landsvirkjun under the project number 2456, and the Icelandic Center for Research (Rannís) on behalf of the Doctoral Student Fund of the Ministry for the Environment and Natural Resources under the grant No 218929-051. This research used resources of the Advanced Photon Source, a U.S. Department of Energy (DOE) Office of Science User Facility operated for the DOE Office of Science by Argonne National Laboratory under Contract No. DE-AC02-06CH11357. This research was partly supported by research grant CRG9 2020 KAUST-UI.

Data availability

Data are available through Mendeley data at: <https://doi.org/10.17632/cnxs8ztzsk.1>.

Credit authorship contribution statement

T. Linke: Writing – review & editing, Writing – original draft, Visualization, Methodology, Investigation, Formal analysis, Data curation, Conceptualization. **E.H. Oelkers:** Writing – review & editing, Methodology, Conceptualization. **K. Dideriksen:** Methodology, Investigation. **S.C. Möckel:** Investigation. **S. Nilabh:** Investigation. **F. Grandia:** Investigation. **S.R. Gislason:** Writing – review & editing, Supervision, Project administration, Funding acquisition, Data curation, Conceptualization.

Declaration of competing interest

The authors declare that they have no known competing financial interests or personal relationships that could have appeared to influence the work reported in this paper.

Acknowledgement

We want to thank the Icelandic meteorological office (Veðurstofa Íslands) for providing rainwater data, Liane Benning and her team at the German research centre for Geosciences GFZ Potsdam for DOC measurements and Stephen Reid at the University of Leeds for ICP-MS analysis. Þorsteinn Jónsson for assistant in the field and design of various coring equipment and Egill Erlendsson and Guðrún Gísladóttir at University of Iceland for helping with the site selection. We would also like to thank Bryndís Róbertsdóttir at the National Energy Authority Iceland for her help with identifying the tephra layers and Eiríkur Benjaminsson for access to his property containing the studied field side. We would like to thank Susan Stipp and Dominique Tobler, the Metal-Aid coordinators, as well as the network members for their help and pleasant company during this study. SRG and EHO would like to thank Hussein Hoteit and Abdulkader M. Alafifi at KAUST University, Saudi Arabia for their hospitality and support.

Appendix A. Supplementary material

Chemical compositions of the soil water samples are provided together with a figure showing their temporal evolution, as well as the Eh measured and derived from different redox couples in the [supplementary material](#), as well as additions to the thermodynamic database and the rainwater composition used for the modeling and the calculations of the basalt dissolution rates. Supplementary material to this article can be found online at <https://doi.org/10.1016/j.gca.2024.02.005>.

References

- Allison, J.D., Brown, D.S., Novo-Gradac, K.J., 1991. *MINTEQA2/PRODEFA2—A geochemical assessment model for environmental systems—Version 3.0 user's manual*. Athens, Georgia 30605.
- Amann, T., Hartmann, J., Struyf, E., De Oliveira Garcia, W., Fischer, E.K., Janssens, I., Meire, P., Schoelynck, J., 2018. Constraints on Enhanced Weathering and related carbon sequestration—a cropland mesocosm approach. *Biogeosci. Discuss.* 1–21.
- Arnalds, O., 2004. Volcanic soils of Iceland. *Catena (Amst)* 56, 3–20.
- Arnalds, O., 2010. Dust sources and deposition of aeolian materials in Iceland. *Icel. Agric. Sci.* 23, 3–21.
- Arnalds, O., 2015. *The Soils of Iceland*. Springer, Netherlands, Dordrecht.
- Arnalds, O., Olafsson, H., Dagsson-Waldhauserova, P., 2014. Quantification of iron-rich volcanogenic dust emissions and deposition over the ocean from Icelandic dust sources. *Biogeosciences* 11, 6623–6632.
- Arnalds, O., Dagsson-Waldhauserova, P., Olafsson, H., 2016. The Icelandic volcanic aeolian environment: processes and impacts - A review. *Aeolian Res.* 20, 176–195.
- Arnórsson, S., 2000. Isotopic and Chemical Techniques in Geothermal Exploration, Development and Use. In: Arnórsson, S. (Eds.) *International Atomic Energy Agency, Vienna*.
- Baek, S.H., Kanzaki, Y., Lora, J.M., Planavsky, N., Reinhard, C.T., Zhang, S., 2023. Impact of climate on the global capacity for enhances rock weathering on croplands. *Earth's Future* 11, e2023EF003698.
- Baldo, C., Formenti, P., Nowak, S., Chevaillier, S., Cazaunau, M., Pangui, E., Di Biagio, C., Doussin, J.F., Ignatyev, K., Dagsson-Waldhauserova, P., Arnalds, O., Mackenzie, A.R., Shi, Z., 2020. Distinct chemical and mineralogical composition of Icelandic dust compared to northern African and Asian dust. *Atmos. Chem. Phys.* 20, 13521–13539.
- Beerling, D.J., Leake, J.R., Long, S.P., Scholes, J.D., Ton, J., Nelson, P.N., Bird, M., Kantzas, E., Taylor, L.L., Sarkar, B., Kelland, M., DeLucia, E., Kantola, I., Müller, C., Rau, G., Hansen, J., 2018. Farming with crops and rocks to address global climate, food and soil security. *Nat. Plants* 4, 138–147.
- Beerling, D.J., Kantzas, E.P., Lomas, M.R., Wade, P., Eufrazio, R.M., Renforth, P., Sarkar, B., Andrews, M.G., James, R.H., Pearce, C.R., Mercure, J.F., Pollitt, H., Holden, P.B., Edwards, N.R., Khanna, M., Koh, L., Quegan, S., Pidgeon, N.F., Janssens, I.A., Hansen, J., Banwart, S.A., 2020. Potential for large-scale CO₂ removal via enhanced rock weathering with croplands. *Nature* 583, 242–248.
- Brantley, S.L., White, A.F., Hodson, M., 1999. Surface Area of Primary Silicate Minerals. In: Jamtveit, B., Meakin, P. (Eds.), *Growth and Dissolution in Geosystems*. Kluwer Academic Publishers, Dordrecht, pp. 291–326.
- Brinza, L., Benning, L.G., Statham, P.J., 2008. Adsorption studies of Mo and V onto ferrihydrite. *Mineral. Mag.* 72, 385–388.
- Charriau, A., Lesven, L., Gao, Y., Leermakers, M., Baeyens, W., Ouddane, B., Billon, G., 2011. Trace metal behaviour in riverine sediments: role of organic matter and sulfides. *Appl. Geochem.* 26, 80–90.
- Chen, Y., Stevenson, F.J., 1986. Soil organic matter interactions with trace elements. In: Chen, Y., Avnimelech, Y. (Eds.), *The Role of Organic Matter in Modern Agriculture*. Springer, Dordrecht, pp. 73–116.
- Cho, Y., Driscoll, C.T., Johnson, C.E., Siccamo, T.G., 2010. Chemical changes in soil and soil solution after calcium silicate addition to a northern hardwood forest. *Biogeochemistry* 100, 3–20.
- Closset, M., Cailliau, K., Slaby, S., Marin, M., 2021. Effects of aluminum contamination on the nervous system of freshwater aquatic vertebrates: a review. *Int. J. Mol. Sci.* 23, 31.
- Deng, H., Sonnenthal, E., Arora, B., Breuning, H., Brodie, E., Kleber, M., Spycher, N., Nico, P., 2023. The environmental controls on efficiency of enhanced rock weathering. *Sci. Rep.* 13, 9765.
- Dideriksen, K., Frandsen, C., Bovet, N., Wallace, A.F., Sel, O., Arbour, T., Navrotsky, A., De Yoreo, J.J., Banfield, J.F., 2015. Formation and transformation of a short range ordered iron carbonate precursor. *Geochim. Cosmochim. Acta* 164, 94–109.
- Dietzen, C., Harrison, R., Michelsen-Correa, S., 2018. Effectiveness of enhanced mineral weathering as a carbon sequestration tool and alternative to agricultural lime: an incubation experiment. *Int. J. Greenhouse Gas Cont.* 74, 251–258.
- Dupla, X., Möller, B., Baveye, P.C., Grand, S., 2023. Potential accumulation of toxic trace elements in soils during enhanced rock weathering. *Eur. J. Soil Sci.* 74, e13343.
- Edwards, D.P., Lim, F., James, R.H., Pearce, C.R., Scholes, J., Freckleton, R.P., Beerling, D.J., 2017. Climate change mitigation: potential benefits and pitfalls of enhanced rock weathering in tropical agriculture. *Biol. Lett.* 13.
- Effenberg, H., Mereiter, K., Zemann, J., 1981. Crystal structure refinements of magnesite, calcite, rhodochrosite, siderite, smithsonite, and dolomite, with discussion

- of some aspects of the stereochemistry of calcite type carbonates. *Z Kristallogr. Cryst. Mater.* 156, 233–244.
- Eiríksdóttir, E.S., Sigurdsson, Á., Gíslason, S.R., Torssander, P., 2014. Chemical composition of precipitation and river water in southern Iceland: effects of Eyjafjallajökull volcanic eruptions and geothermal power plants. *Procedia Earth Planet. Sci.* 10, 358–364.
- Eswaran, H., van den Berg, E., Reich, P., 1993. Organic carbon in soils of the world. *Soil Sci. Soc. Am. J.* 57, 192–194.
- Gale, A., Dalton, C.A., Langmuir, C.H., Su, Y., Schilling, J.G., 2013. The mean composition of ocean ridge basalts. *Geochem. Geophys.* 14, 489–518.
- Gautier, J.M., Oelkers, E.H., Schott, J., 2001. Are quartz dissolution rates proportional to B.E.T. surface areas? *Geochim. Cosmochim. Acta* 65, 1059–1070.
- Gensemer, R.W., Playle, R.C., 1999. The bioavailability and toxicity of aluminum in aquatic environments. *Crit. Rev. Environ. Sci. Technol.* 29, 315–450.
- Gillman, G.P., Burkett, D.C., Coventry, R.J., 2002. Amending highly weathered soils with finely ground basalt rock. *Appl. Geochem.* 17, 987–1001.
- Gíslason, S.R., Arnórsson, S., 1993. Dissolution of primary basaltic minerals in natural waters: saturation state and kinetics. *Chem. Geol.* 105, 117–135.
- Gíslason, S.R., Oelkers, E.H., 2003. Mechanism, rates, and consequences of basaltic glass dissolution: II. An experimental study of the dissolution rates of basaltic glass as a function of pH and temperature. *Geochim. Cosmochim. Acta* 67, 3817–3832.
- Goll, D.S., Ciaisi, P., Amann, T., Buermann, W., Chang, J., Eker, S., Hartmann, J., Janssens, L., Li, W., Obersteiner, M., Penuelas, J., Tanaka, K., Vicca, S., 2021. Potential CO₂ removal from enhanced weathering by ecosystem responses to powdered rock. *Nat. Geosci.* 14, 545–549.
- Gran, G., 1952. Determination of the equivalence point in potentiometric Titrations. Part II. *Analyst* 77, 661–671.
- Gunnarsdóttir, M.J., Gardarsson, S.M., Jonsson, G.S., Bartram, J., 2016. Chemical quality and regulatory compliance of drinking water in Iceland. *Int. J. Hyg. Environ. Health* 219, 724–733.
- Hammersley, A.P., Svensson, S.O., Hanfland, M., Fitch, A.N., Häussermann, D., 1996. Two-dimensional detector software: from real detector to idealised image or two-theta scan. *High Press Res.* 14, 235–248.
- Hammersley, A.P., 1997. FIT2D: An Introduction and Overview., Grenoble, ESRF Internal Report, ESRF97HA02T.
- Haque, F., Chiang, Y., Santos, R., 2019a. Alkaline mineral soil amendment: a climate change 'stabilization wedge'? *Emerges* 12, 2299.
- Haque, F., Santos, R.M., Dutta, A., Thimmanagari, M., Chiang, Y.W., 2019b. Co-benefits of wollastonite weathering in agriculture: CO₂ sequestration and promoted plant growth. *ACS Omega* 4, 1425–1433.
- Haque, F., Santos, R.M., Chiang, Y.W., 2020. Optimizing inorganic carbon sequestration and crop yield with Wollastonite soil amendment in a microplot study. *Front. Plant Sci.* 11, 1012.
- Haque, F., Santos, R.M., Chiang, Y.W., 2021. Urban farming with enhanced rock weathering as a prospective climate stabilization wedge. *Cite This: Environ. Sci. Technol.* 55, 13575–13578.
- Harðardóttir, S., 2020. Spatial distribution and geochemical characterization of Icelandic mantle end-members. MSc Thesis, University of Iceland.
- Hartmann, J., West, A.J., Renforth, P., Köhler, P., De La Rocha, C.L., Wolf-Gladrow, D.A., Dürr, H.H., Scheffran, J., 2013. Enhanced chemical weathering as a geoengineering strategy to reduce atmospheric carbon dioxide, supply nutrients, and mitigate ocean acidification. *Rev. Geophys.* 51, 113–149.
- Huber, S.A., Balz, A., Abert, M., Pronk, W., 2011. Characterisation of aquatic humic and non-humic matter with size-exclusion chromatography - organic carbon detection - organic nitrogen detection (LC-OCD-OND). *Water Res.* 45, 879–885.
- IPCC (2018) *Global warming of 1.5°C An IPCC Special Report on the impacts of global warming of 1.5°C above pre-industrial levels and related global greenhouse gas emission pathways, in the context of strengthening the global response to the threat of climate change, sustainable development, and efforts to eradicate poverty.* Masson-Delmotte, V., Zhai, P., Pörtner, H.-O., Roberts, D., Skea, J., Shukla, P.R., Pirani, A., Moufouma-Okia, W., Péan, C., Pidcock, R., Connors, S., Matthews, J.B.R., Chen, Y., Zhou, X., Gomis, M.L., Lonnoy, E., Maycock, T., Tignor, M., Waterfield, T. (Eds.), Cambridge University Press, Cambridge, UK and New York, NY, USA, pp. 3–24.
- Kaasalainen, H., Stefánsson, A., Druschel, G.K., 2016. Determination of Fe(II), Fe(III) and Fetotal in thermal water by ion chromatography spectrophotometry (IC-Vis). *Int. J. Environ. Anal. Chem.* 96, 1074–1090.
- Kantola, I.B., Blanc-Benes, E., Master, M.D., Chang, E., Marklein, A., Moore, C.E., von Haden, A., Bernacchi, C.J., Wolf, A., Epifov, D.Z., Beerling, D.J., DeLucia, E.H., 2023. Improved net carbon budgets in the US Midwest through direct measured impacts of enhanced weathering. *Glob. Chang Biol.* 29, 7012–7028.
- Kantzas, E.P., Val Martin, M., Lomas, M.R., Eufrazio, R.M., Renforth, P., Lewis, A.L., Taylor, L.L., Mecure, J.F., Pollitt, H., Vercoleyen, P.V., Vakiliard, N., Holden, P.B., Edwards, N.R., Koh, L., Pidgeon, N.F., Banwart, S.A., Beerling, D.J., 2022. Substantial carbon drawdown potential from enhanced rock weathering in the United Kingdom. *Nat. Geosci.* 15, 382–389.
- Kinniburgh, D.G., Cooper, D.M., 2004. Predominance and mineral stability diagrams revisited. *Environ. Sci. Technol.* 38, 3641–3648.
- Kirkby, C.A., Kirkegaard, J.A., Richardson, A.E., Wade, L.J., Blanchard, C., Batten, G., 2011. Stable soil organic matter: A comparison of C:N:P ratios in Australian and other world soils. *Geoderma* 163, 197–208.
- Linke, T., Gíslason, S.R., 2018. Stability of iron minerals in Icelandic peat areas and transport of heavy metals and nutrients across oxidation and salinity gradients - A modelling approach. *Energy Procedia* 146, 30–37.
- Liu, E.J., Cashman, K.V., Beckett, F.M., Witham, C.S., Leadbetter, S.J., Hort, M.C., Guðmundsson, S., 2014. Ash mists and brown snow: Remobilization of volcanic ash from recent Icelandic eruptions. *J. Geophys. Res. Atmos.* 119, 9463–9480.
- Molins, S., Trebotich, D., Steefel, C.L., Shen, C., 2012. An investigation of the effect of pore scale flow on average geochemical reaction rates using direct numerical simulation. *Water Resour. Res.* 48, W03527.
- Moon, E.M., Peacock, C.L., 2012. Adsorption of Cu(II) to ferrihydrite and ferrihydrite-bacteria composites: Importance of the carboxyl group for Cu mobility in natural environments. *Geochim. Cosmochim. Acta* 92, 203–219.
- Moosdorf, N., Renforth, P., Hartmann, J., 2014. Carbon dioxide efficiency of terrestrial enhanced weathering. *Environ. Sci. Technol.* 48, 4809–4816.
- Oelkers, E.H., Gíslason, S.R., 2001. Mechanism, rates, and consequences of basaltic glass dissolution: I. An experimental study of the dissolution rates of basaltic glass as a function of aqueous Al, Si and oxalic acid concentration at 25°C and pH ? 3 and 11. *Geochim. Cosmochim. Acta* 67, 3817–3832.
- Parkhurst, D.L., Appelo, C.A.J., 1999. User's Guide to PHREEQC (Version 2)— A Computer Program for Speciation, Batch-Reaction, One-Dimensional Transport, and Inverse Geochemical Calculations., U.S. Geological Survey, Water Resources Investigations Report 99-4259, Washington DC.
- Paulo, C., Power, I.M., Stubbs, A.R., Wang, B., Zeyen, N., Wilson, S., 2021. Evaluating feedstocks for carbon dioxide removal by enhanced rock weathering and CO₂ mineralization. *App. Geochem.* 129, 104955.
- Petersen, G.N., Berber, D., 2018. Jarðvegshitamælingar á Íslandi. Staða núverandi kerfis og framtíðarsýn., VI 2018-009.
- Pettit, L.D., Powell, J.J., 2008. The IUPAC Stability Constants Database (SC-Database), current data version 4, Academic Software., Otley, UK.
- Qiu, X., Thompson, J.W., Billinge, S.J.L., 2004. PDFgetK2: a GUI-driven program to obtain the pair distribution function from X-ray powder diffraction data. *J. Appl. Cryst.* 37, 678.
- Reershemius, T., Kelland, M.E., Jordan, J.S., Davis, I.R., D'Ascanio, R., Kalderon-Asael, B., Asael, D., Suhroff, T.J., Epifov, D.Z., Beerling, D.J., Reinhard, C.T., Planavsky, N.J., 2023. Initial validation of a soil-based mass-balance approach for empirical monitoring of enhanced rock weathering rates. *Environ. Sci. Technol.* 57, 19497–19507.
- Rickard, D., Luther, G.W., 2007. Chemistry of Iron Sulfides. *Chem. Rev.* 107, 514–562.
- Rosseland, B.O., Blakar, I.A., Bulgar, A., Kroglund, F., Kvellstad, A., Lydersen, E., Oughton, D.H., Salbu, B., Staurnes, M., Vogt, R., 1992. The mixing zone between limed and acidic river waters: complex aluminium chemistry and extreme toxicity for salmonids. *Environ. Pollut.* 78, 3–8.
- Roy, R.L., Campbell, P.G.C., Prémont, S., Labrie, J., 2000. Geochemistry and toxicity of aluminum in the saguenay river, québec, Canada, in relation to discharges from an aluminum smelter. *Environ. Toxicol. Chem.* 19, 2457–2466.
- Sawyer, D.T., Roberts, J.L., Sobkowiak, A., 1995. *Electrochemistry for Chemists*, 2nd ed. Wiley, New York.
- Scheinost, A.C., Abend, S., Pandya, K.I., Sparks, D.L., 2001. Kinetic controls on Cu and Pb sorption by ferrihydrite. *Environ. Sci. Technol.* 35, 1090–1096.
- Schulling, R.D., Krijgsman, P., 2006. Enhanced weathering: an effective and cheap tool to sequester CO₂. *Clim. Change* 74, 349–354.
- Smieja-Król, B., Janeczek, J., Baurek, A., Thorseth, I.H., 2015. The role of authigenic sulfides in immobilization of potentially toxic metals in the Bagno Bory wetland, southern Poland. *Environ. Sci. Pollut. Res.* 22, 15495–15505.
- Snaebjörnsson, A., 1982. Um Vatnsleiðnismælingar í Jarðvegi á nokkrum stöðum í Borgarfirði. *Fjölrit* 45, 35.
- Swanner, E.D., Webb, S.M., Kappler, A., 2019. Fate of cobalt and nickel in mackinawite during diagenetic pyrite formation. *Am Min* 104, 917–928.
- ten Berge, H.F.M., van der Meer, H.G., Steenhuizen, J.W., Goedhart, P.W., Knops, P., Verhagen, J., 2012. Olivine weathering in soil, and its effects on growth and nutrient uptake in ryegrass (*Lolium perenne* L.): a pot experiment. *PLoS One*. 7.
- Tester, J.W., Worley, W.G., Robinson, B.A., Grigsby, C.O., Feerer, J.L., 1994. Correlating quartz dissolution kinetics in pure water from 25 to 625°C. *Geochim. Cosmochim. Acta* 58, 2407–2420.
- U.S. Environmental Protection Agency, 1998. MINTEQA2/PRODEFA2, A Geochemical Assessment Model for Environmental Systems: User Manual Supplement for Version 4.0., Athens, Georgia.
- United States Environmental Protection Agency, 2009. National Primary Drinking Water Guidelines. *Epa 816-F-09-004 1*, United States Environmental Protection Agency. 7p.
- Verry, E., 1975. Streamflow chemistry and nutrient yields from upland-peatland watersheds in Minnesota. *Ecology* 56, 1149–1157.
- Vitt, D.H., Bayley, S.E., Jin, T.-L., 1995. Seasonal variation in water chemistry over a bog-rich fen gradient in Continental Western Canada. *Can. J. Fish Aquat.* 52, 587–606.
- Wada, K., 1989. Allophane and Imogolite. In: Dixon, J.B., Weed, S.B. (Eds.), *Minerals in Soil Environments*, second ed. Soil Science Society of America, Madison, pp. 1051–1087.
- Wallace, P., Carmichael, I.S.E., 1992. Sulfur in basaltic magmas. *Geochim. Cosmochim. Acta* 56, 1863–1874.
- Wallace, P.J., 2021. Magmatic Volatiles. In: *Encyclopedia of Geology*. Elsevier. pp. 301–312.
- White, A.F., Blum, A.E., 1995. Effects of climate on chemical, weathering in watersheds. *Geoch Cosmochim Acta* 59, 1729–1747.
- White, A.F., Blum, A.E., Schulz, S., Bullen, T.D., Harden, J.W., Peterson, M.L., 1996. Chemical weathering rates of a soil chronosequence on granitic alluvium: I. Quantification of mineralogical and surface area changes and calculation of primary silicate reaction rates. *Geochim. Cosmochim. Acta* 60, 2533–2550.
- White, A.F., Brantley, S.L., 2003. The effect of time on the weathering of silicate minerals: why do weathering rates differ in the laboratory and field? *Chem. Geol.* 202, 479–506.
- World Health Organization, 2017. *Guidelines for Drinking-water Quality: fourth edition incorporating the first addendum*, Licence: CC BY-NC-SA 3.0 IGO., Icelandic

Meteorological Office, Climatological data, annual averages of precipitation.
<http://www.en.vedur.is/climatology/data> (accessed 15 Oct. 2021).

3 Paper II - Direct evidence of CO₂ drawdown through enhanced weathering in soils

Tobias Linke, Eric H. Oelkers, Susanne Claudia Möckel, Sigurdur Reynir Gislason

Published in 2024 in Geochemical Perspective Letters v30, 7-12.

doi.org/10.7185/geochemlet.2415

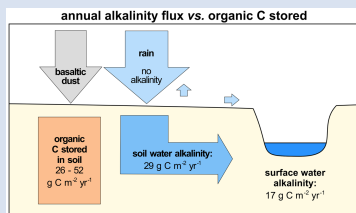
Direct evidence of CO₂ drawdown through enhanced weathering in soils

T. Linke^{1*}, E.H. Oelkers^{1,2}, S.C. Möckel³, S.R. Gislason¹



<https://doi.org/10.7185/geochemlet.2415>

Abstract



The ability of engineered enhanced weathering to impact atmospheric CO₂ has been challenging to demonstrate due to the many processes occurring in soils and the short time span of current projects. Here we report the carbon balance in an Icelandic Histic/Gleyic Andosol that has received large quantities of basaltic dust over 3300 years, providing opportunity to quantify the rates and long term consequences of enhanced weathering. The added basaltic dust has dissolved continuously since its deposition. The alkalinity of the soil waters is more than 10 times higher than in equivalent basalt dust-free soils. After accounting for oxidation and degassing when the soil waters are exposed to the atmosphere, the annual CO₂ drawdown due to alkalinity generation is 0.17 t C ha⁻¹ yr⁻¹. This study validates the ability of fine grained mafic mineral addition to soils to attenuate increasing atmospheric CO₂ by alkalinity export. Induced changes in soil organic carbon storage, however, likely dominate the net CO₂ drawdown of enhanced weathering efforts.

Received 25 October 2023 | Accepted 17 March 2024 | Published 30 April 2024

Introduction

The natural weathering of basaltic and ultramafic rocks has been demonstrated to have a relatively large role in the drawdown of CO₂ from the atmosphere (Dessert *et al.*, 2003; Gislason *et al.*, 2009; Taylor *et al.*, 2021). Such observations have motivated several proposals to use these rocks to remove CO₂ directly from the atmosphere through a process called Enhanced Weathering (EW) (Moosdorf *et al.*, 2014; IPCC, 2018; Beerling *et al.*, 2020). Enhanced weathering involves amending soils with crushed fine grained, fast reacting Ca-Mg silicate rocks and minerals such as basalts and peridotites (Strefler *et al.*, 2018). To date, enhanced weathering field experiments have demonstrated improved crop vigour, organic and inorganic carbon storage and decreased N₂O degassing (Haque *et al.*, 2019a, 2020; Beerling *et al.*, 2020). One of the goals of EW is to increase the alkalinity export of waters that drain from soils and enter rivers and streams. The quantification of carbon drawdown by enhanced weathering has been challenging to identify or quantify due to the large number of processes that occur in soils and the short duration of existing field studies.

One approach to investigate the long term behaviour and consequences of EW is *via* natural analogues. Enhanced weathering experiments to date have tested the addition of up to 400 t ha⁻¹ yr⁻¹ of crushed Ca-Mg silicate rocks to agricultural soils (Gillman *et al.*, 2002; Amann *et al.*, 2018; Haque *et al.*, 2019b). This crushed rock flux is orders of magnitude higher than the average global desert dust deposition on Earth, which is estimated to be 0.5 t ha⁻¹ yr⁻¹ (Mahowald *et al.*, 2005). In the vicinity

of the dust “hot spots”, such as South Iceland, however, the mass of deposited fine grained basaltic dust can be as high as 8 t ha⁻¹ yr⁻¹ (Arnalds, 2010; Arnalds *et al.*, 2014, 2016). Although this natural mass flux of basalt is less than that of current EW efforts, 1) this basaltic dust flux has been added continuously to the soil of this region over at least the past 3300 years, such that in total over 16,500 t ha⁻¹ of basaltic dust has been added over this time, and 2) the specific surface area of natural basaltic dust is likely higher than that added to soils in current EW experiments due to its finer grain size. The grain size of the crushed rocks used in EW applications, if reported, is commonly less than 150 μm (Haque *et al.*, 2019a; Gillman *et al.*, 2002). In contrast, the average size of basaltic Icelandic dust ranges from 10 to 62 μm (Arnalds *et al.*, 2014; Liu *et al.*, 2014). For these reasons, the mineral rich Histic/Gleyic Andosols (Arnalds, 2015) considered in this study located in South Iceland provide an insightful natural analogue to illuminate the long term effect of EW applications performed under similar climate, vegetation, and soil conditions. The studied soil receives large amounts of air borne volcanic material during 1) explosive volcanic eruptions in the form of glassy volcanic ash fallout, and 2) dust storms (Shoji *et al.*, 1995; Arnalds *et al.*, 2016). Explosive eruptions lead to evident tephra horizons that can be used to date these soils. The more frequently deposited windblown dust is finer grained than the tephra and intermingled with the soil organic carbon (see “Soil classification and soil evolution in Iceland” in Supplementary Information). Based on palaeoecologic research (Gísladóttir *et al.*, 2008; Arnalds, 2015; Möckel *et al.*, 2017), in the absence of volcanic dust input, the Histic/Gleyic Andosols of

1. Institute of Earth Sciences, University of Iceland, Sturlugata 7, 102 Reykjavik, Iceland
 2. Ali I. Al-Naimi Petroleum Engineering Research Center, KAUST, Saudi Arabia
 3. Institute of Life and Environmental Sciences, University of Iceland, Sturlugata 7, 102 Reykjavik, Iceland
 * Corresponding author (email: tol5@hi.is)



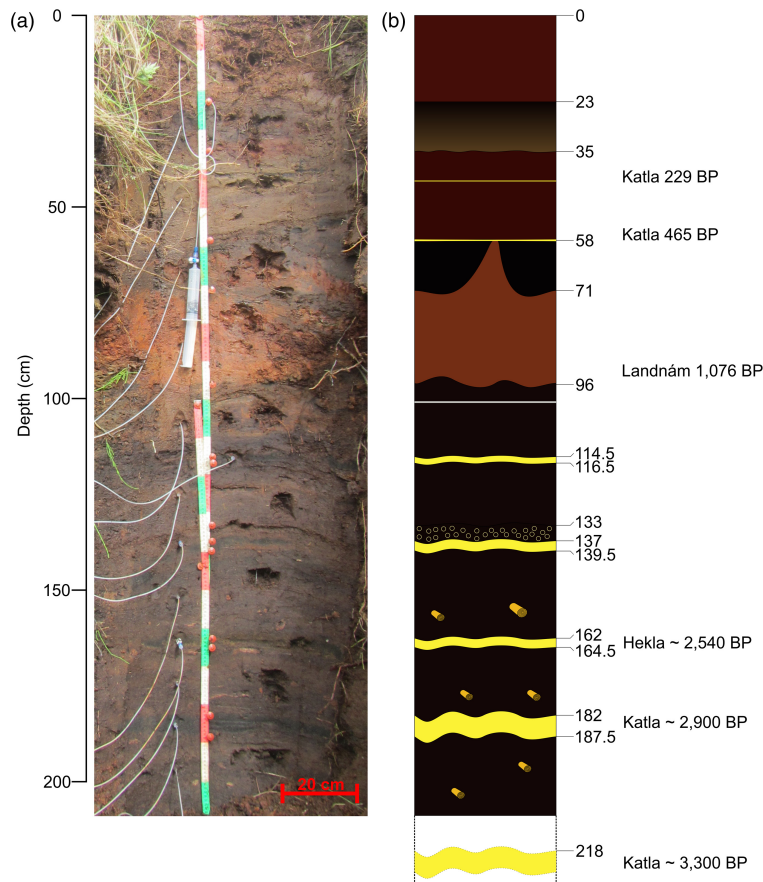


Figure 1 (a) Photograph of the studied soil system. The dark layers correspond to tephra originating from historic volcanic eruptions. (b) Schematic illustration of the soil profile with depths and ages (in years before present) of identified tephra layers shown in yellow for better visibility, the Landnám Layer that occurred around the time of the Icelandic settlement could not be clearly identified because of alteration. Plant remnants are visible in the lower part of the profile, indicating high organic content.

Southern Iceland would have developed into Histosols (Arnalds, 2008). Consequently, the comparison of the behaviour of South Icelandic Histic/Gleyic Andosols with that of volcanic dust-free Histosols, located in similar climatic zones provides insight into the consequences of adding fine grained basaltic material to soils as part of enhanced weathering efforts.

One of our motivations to focus on the addition of volcanic material to Histosols/peat soils to drawdown CO_2 from the atmosphere stems from the role of these soils in the global carbon cycle. Although peatlands cover only about 3 % of the continents (Xu *et al.*, 2018), they store ~ 10 % of all non-glacial freshwater and roughly 30 % of the land-based organic carbon (Mitra *et al.*, 2005; Bragazza *et al.*, 2013). Man made drainage and burning of peat areas worldwide releases 0.5–0.8 Gt C yr^{-1} , which is equivalent to 5–8 % of global anthropogenic carbon emissions (Hooijer *et al.*, 2006; Parish *et al.*, 2008). Carbon dioxide emission from the drainage of peat areas is estimated to be the largest anthropogenic source of CO_2 emissions in Iceland (Keller *et al.*, 2020). The addition of reactive silicate rock dust to peat soils might help increase carbon storage being otherwise lost due to peatland draining.

This manuscript is one of two exploring the long term efficiency and consequences of enhanced rock weathering efforts

through the study of a South Iceland Gleyic/Histic Andosol. The first manuscript (Linke *et al.*, 2024) reports the composition of fluids and solids collected over two field seasons to 1) quantify the saturation state of the primary and secondary mineral phases with respect to the soil solutions, 2) determine the processes controlling the mobility of heavy metals, and 3) assess the rate at which basalt dissolved in the soils. In this manuscript we present a comparison of the alkalinity export from this soil with corresponding results from volcanic dust-free Histosols to quantify the ability of enhanced weathering efforts to drawdown CO_2 from the atmosphere. Results are then used to estimate the efficiency of enhanced weathering at a larger scale. The purpose of this paper is to present the results of this study and use the results to gain insight into the consequences of current and future enhanced weathering efforts.

Field Site Description

The field site is located above the source of the Rauðalækur (“Red creek”) river at 63° 53' 42.5" N, 20° 21' 15.9" W, which is approximately 7 km north of the town of Hella in South Iceland. This site consists of an upper Gleyic Andosol and a lower Histic Andosol (see Supplementary Information for further

details). The study site receives an annual aeolian dust flux of $5\text{--}8\text{ t ha}^{-1}\text{ yr}^{-1}$, consisting of mostly basaltic glass (Arnalds *et al.*, 2016). Additional basaltic material is added during irregular volcanic events. During the past several decades, drainage trenches have been cut into the nearby soils; the closest drainage ditch is located more than 150 metres from the study site. The studied soil contains several prominent horizontal tephra layers, with thicknesses ranging from a few mm to few cm and deposited during the past 3300 years. An image and schematic illustration of the system is provided in Figure 1 and a detailed description of the field site is provided in the Supplementary Information and Table S-1 therein.

Results

Fluid compositions. Soil fluid samples were collected using suction cup samplers from May to November 2018. The compositions of all fluid samples are provided in Table S-2 (Supplementary Information) and selected dissolved constituents are shown as a function of depth in Figure 2. The pH of the samples was recalculated using PHREEQC (Parkhurst and Appelo, 1999) to the *in situ* soil temperature of $7\text{ }^{\circ}\text{C}$. This is the average soil temperature at $76\text{--}260\text{ cm}$ depth during the summer months (Petersen and Gerber, 2018). The concentrations of major elements increase continuously with depth suggesting the continuous dissolution of the basaltic dust in the soil. The soil waters become increasingly anoxic with depth as indicated by the Eh values shown in Figure 2b.

The alkalinity of the soil waters increases from 0 to 3 meq kg^{-1} with depth. Once these waters exit the soils, they will equilibrate with the O_2 and CO_2 in the atmosphere. PHREEQC calculations indicate that the alkalinity of the soil waters will decrease on average to $1.53 \pm 0.2\text{ meq kg}^{-1}$ due to iron oxidation/precipitation reactions when they come in contact with the atmosphere as they flow into local rivers (further details of this calculation are provided in the Supplementary Information).

The alkalinity of soil waters in our studied dust-rich soil are compared to the corresponding alkalinities of basalt

dust-free Histosols located in non-carbonate terrains in Figure 3. Our field site, mostly fed by rainwater, shows considerably higher alkalinity and pH values than observed in corresponding basalt dust-free Histosols. Histosols located in carbonate terrains are not included in this comparison as the presence of carbonate minerals leads to a pH and alkalinity increase due to carbonate dissolution, a process which has no long term net effect on atmospheric carbon drawdown. The comparison in Figure 3 shows that the addition of volcanic dust to our soil increased substantially the alkalinity in its soil waters, most notably deep in the soil column. This observation confirms the ability of enhanced weathering by the addition of basaltic dust to soils to drawdown CO_2 from the atmosphere.

A noteworthy observation is that the basaltic dust in the studied soil column persists and is reactive throughout the soil column, despite the fact that some of this dust has been present in the soil for 3300 years. This observation is consistent with mass balance estimates of the import and export of metals to the soil column. The study site receives an average annual dust flux of $500\text{--}800\text{ g m}^{-2}\text{ yr}^{-1}$. This basalt flux adds $0.96\text{--}1.54\text{ mol Ca}$ and $0.72\text{--}1.16\text{ mol Mg per m}^2\text{ yr}^{-1}$ to the soil. In contrast, the average Ca and Mg concentration of the deep soil water is 5×10^{-4} and $4 \times 10^{-4}\text{ mol kg}^{-1}$ for Ca and Mg, respectively. Taking account of the estimated $925 \pm 150\text{ kg m}^{-2}\text{ yr}^{-1}$ of water that flows through, and is exported annually by our studied soil (see Supplementary Information for details of this water flow estimate), we estimate that 0.47 ± 0.07 and $0.37 \pm 0.06\text{ mol yr}^{-1}$ of Ca and Mg, respectively, are removed from the soil per square metre of soil surface area at present. The input of Ca and Mg by volcanic dust addition is, therefore, approximately 2–3 times more than that removed by soil water export. The results of this comparison are consistent with the persistence of the reactive dust throughout the soil column and suggest the long term viability of enhanced weathering efforts.

Carbon Storage via alkalinity export by the addition of basaltic material to soils. The rate of carbon drawdown due to alkalinity export by enhanced weathering in our studied field site can be estimated by combining the annual water flux through the soil and the measured alkalinity, as demonstrated in

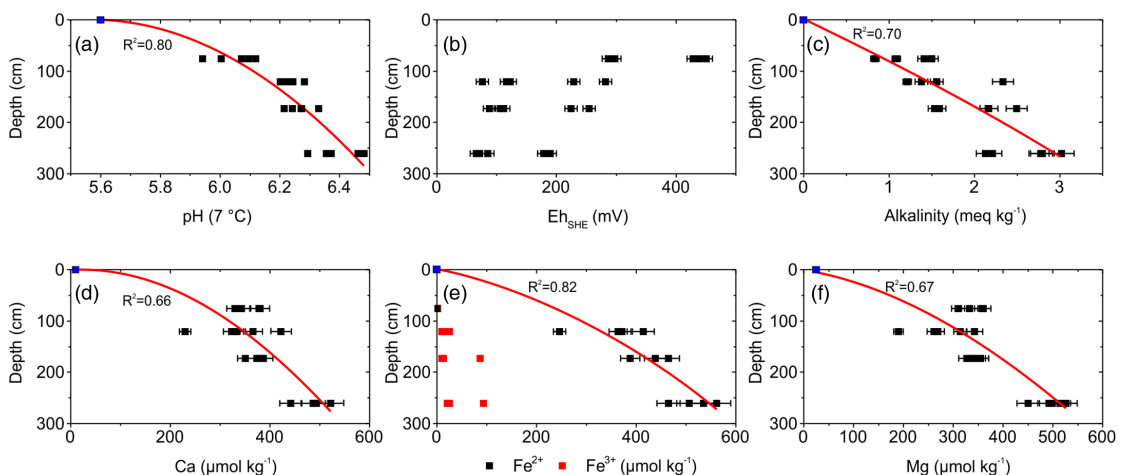


Figure 2 Measured soil water concentrations determined in the present study in all samples collected from May to November 2018, as a function of depth. The pH values are normalised to a $7\text{ }^{\circ}\text{C}$ reference temperature and Eh values to a Standard Hydrogen Electrode. The black squares represent measured water concentrations, whereas the blue squares show the composition of rainwater. The error bars correspond to a $\pm 5\%$ uncertainty on the measured concentrations; error bars do not appear if the uncertainty is smaller than the symbol size. The red curves in the figure show 2nd order polynomial fits of all the measured concentrations with the corresponding R^2 values next to each curve.



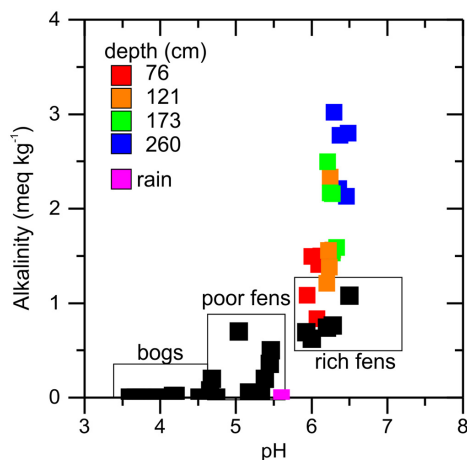


Figure 3 Comparison of pH and alkalinity of soil waters collected from our studied soil with similarly composed, but volcanic dust-free soils reported in other studies. The black symbols correspond to alkalinity values reported in the literature for Histosols from bogs, poor or rich fens located in non-volcanic regions and in the absence of carbonate bedrock. The black boxes around the black symbols represent the commonly reported pH-alkalinity ranges of bogs and fens respectively. The red, orange, green and blue symbols represent soil water samples measured in the present study at the depths indicated in the figure. The purple symbol shows the composition of rainwater at our field site. The sources and location of the literature data are provided in Table S-3 of the Supplementary Information.

Figure 4. By taking account of the rainfall, evaporation, and surface runoff it is estimated that $925 \pm 150 \text{ kg m}^{-2} \text{ yr}^{-1}$ of water pass through and are exported from the studied soil annually. Multiplying this number by the $1.53 \pm 0.2 \text{ meq kg}^{-1}$ average alkalinity of the deepest water samples of our study area, after its equilibration with the atmosphere, yields an estimated alkalinity export from our soils of $1.43 \pm 0.3 \text{ meq m}^{-2} \text{ yr}^{-1}$. Multiplying this number by the atomic weight of carbon yields an annual carbon addition to our river water of $17 \pm 3.6 \text{ g m}^{-2} \text{ yr}^{-1}$, which equals $0.17 \pm 0.036 \text{ t ha}^{-1} \text{ yr}^{-1}$ of C. The degree to which this carbon drawdown rate is influenced by the rate of basalt input to the soil and its surface area has yet to be quantified. Although, dissolution rates are commonly thought to be proportional to the fluid-mineral surface area, these rates are also influenced by fluid compositions, including approach to equilibrium and fluid flow paths in the soil column (Schott *et al.* 2009; Linke *et al.*, 2024).

It is insightful to extrapolate this annual rate of carbon drawdown to a larger scale. If the results of our studied field site are representative, the removal of $1 \text{ Gt yr}^{-1} \text{ CO}_2$ from the atmosphere through alkalinity production would require a total of 16 million km^2 of surface. This is larger than the total surface area of the United States. Moreover, the mass of basaltic dust required to provoke this rate of carbon removal may be unrealistically large. The average annual flux of basaltic dust into the studied South Iceland soils is $5\text{--}8 \text{ t ha}^{-1} \text{ yr}^{-1}$. Adding this mass of basalt over 16 million km^2 of surface would require 8 to 13 Gt of finely ground basalt annually. This mass of ground basalt is larger than the world's annual cement production of 4.3 Gt in 2020 (<https://iea.org/reports/cement>). This conclusion, based on the alkalinity export from our studied soil, which contains more organic matter (12 % to >20 % C) than most soils globally (<5 % C; e.g., Stockmann *et al.*, 2015), is nevertheless supported

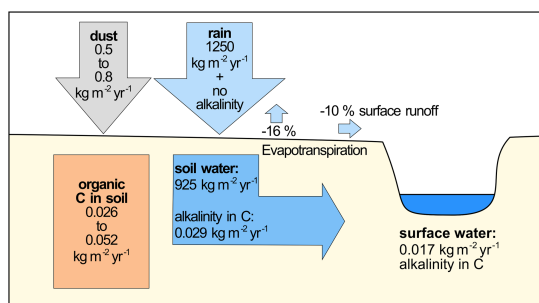


Figure 4 Schematic illustration of the processes drawing down CO_2 at our field site. The site receives $\sim 1250 \pm 200 \text{ kg m}^{-2} \text{ yr}^{-1}$ of rainfall. Of this rainfall 16 % is estimated to evaporate and 10 % is estimated to be lost to surface runoff. As the remaining $925 \pm 150 \text{ kg m}^{-2} \text{ yr}^{-1}$ of water passes through the soil, its alkalinity increases on average from 0 to $2.59 \pm 0.34 \text{ meq kg}^{-1}$ at depth. Once these waters equilibrate with the atmosphere, this fluid oxidises and some CO_2 is released such that the alkalinity decreases to $1.53 \pm 0.2 \text{ meq kg}^{-1}$ resulting in an annual export of $17 \pm 3.6 \text{ g C per m}^2$ soil surface area. At the same time $26\text{--}52 \text{ g m}^{-2} \text{ yr}^{-1}$ of C is drawn down from the atmosphere by organic carbon production and stored in the soil.

by other recent enhanced rock weathering studies. Our result of $0.17 \pm 0.036 \text{ t ha}^{-1} \text{ yr}^{-1}$ of carbon drawdown from alkalinity export by enhanced rock weathering is within the range of the handful of large scale cropland EW studies of 0.0005– $0.5 \text{ t C ha}^{-1} \text{ yr}^{-1}$ (Haque *et al.*, 2020; Taylor *et al.*, 2021; Larkin *et al.*, 2022). It should be noted, however, that the alkalinity generated in our studied Histic/Gleyic Andosol was the consequence of the dissolution of the basalt added to this soil annually over the past 3300 years. This annual addition has led to a buildup of basaltic material over time. The results shown in Figure 2 indicate that the presence of older basaltic dust, located deep in the soil profile is an important contributor to alkalinity production. As such, it seems likely that substantially more than $5\text{--}8 \text{ t ha}^{-1} \text{ yr}^{-1}$ would need to be added to soils near-term as part of enhanced weathering efforts to provoke a similar rate of alkalinity production as observed in our study area.

Carbon drawdown by alkalinity production versus soil organic carbon. The total mass of organic carbon in our studied soil is estimated to be $86\text{--}172 \text{ kg C m}^{-2}$ with average net annual rate of carbon drawdown estimated to be $26\text{--}52 \text{ g C m}^{-2} \text{ yr}^{-1}$ (see Supplementary Information). This rate of CO_2 drawdown is substantially larger than the corresponding $17 \pm 3.6 \text{ g C m}^{-2} \text{ yr}^{-1}$ drawdown due to alkalinity export in our studied soils. These estimates are in agreement with previous studies (Taylor *et al.*, 2021). These estimates also suggest that the amount of CO_2 removed by the addition of basaltic dust to the soil in one year by alkalinity export is more than 3 orders of magnitude less than the total CO_2 stored as organic carbon in the soil. This latter observation should serve as a warning to those attempting atmospheric CO_2 drawdown by enhanced weathering in soils. If the addition of basaltic dust to soil leads to the accelerated decomposition of organic material in soils, the latter process could readily dominate leading to a net increase of CO_2 released to the atmosphere due to enhanced weathering efforts.

Conclusions

The results of this study confirm the ability of fine grained basaltic rock added to soils to enhance CO_2 drawdown directly from the atmosphere due to alkalinity production. It is estimated

that $17 \pm 3.6 \text{ g C m}^{-2} \text{ yr}^{-1}$ is currently drawn down and added to rivers by alkalinity production from our South Iceland field site. The enhanced alkalinity production of our soils was produced by the addition of approximately $1.7\text{--}2.6 \text{ t m}^{-2}$ of basaltic dust to this soil over 3300 years. Upscaling of this process to address even a small fraction of the mass of anthropogenic CO_2 emissions to the atmosphere, however, may be challenging because 1) this enhanced weathering process is slow and would require more land than is available for a sizeable drawdown of CO_2 through alkalinity production, and 2) the currently unquantified effect of adding basalt powder to soils on soil organic matter. So, although this study demonstrates the potential of enhanced weathering efforts to contribute to attenuating atmospheric CO_2 concentrations, the degree to which this approach will prove successful at a larger scale remains unclear.

Acknowledgements

The authors thank Knud Dideriksen for his comments and discussions during the field work. We thank the Icelandic meteorological office (Veðurstofa Íslands) for providing rainwater data, Liane Benning and the interface geochemistry group at the Geological research centre GFZ Potsdam for the DOC measurements, Þorsteinn Jónsson for assisting in the field and designing coring equipment and Egill Erlendsson and Guðrún Gísladóttir at University of Iceland for helping with site selection. We thank Bryndís Róbertsdóttir at the National Energy Authority Iceland for her help with identifying the tephra layers and Eiríkur Benjaminsson for access to his property. We thank Susan Stipp and Dominique Tobler, the Metal-Aid coordinators, as well as the network members for their pleasant company during this study. This project was funded by the European Union's Horizon 2020 research and innovation programme under the Marie Skłodowska-Curie grant agreement No 675219, from Landsvirkjun under the project number 2456, and the Icelandic Center for Research (Rannís) on behalf of the Doctoral Student Fund of the Ministry for the Environment and Natural Resources under the grant No 218929-051. Additional financial support was received from the Research Fund of the University of Iceland and the Travel grant for doctoral students at the University of Iceland. This research was partly supported by research grant CRG9 2020 KAUST-UI. SRG and EHO would like to thank Hussein Hoteit and Abdulkader M. Alafifi at KAUST University, Saudi Arabia for their hospitality and support.

Editor: Satish Myneni

Additional Information

Supplementary Information accompanies this letter at <https://www.geochemicalperspectivesletters.org/article2415>.



© 2024 The Authors. This work is distributed under the Creative Commons Attribution 4.0 License, which permits unrestricted use,

distribution, and reproduction in any medium, provided the original author and source are credited. Additional information is available at <http://www.geochemicalperspectivesletters.org/copyright-and-permissions>.

Cite this letter as: Linke, T., Oelkers, E.H., Möckel, S.C., Gíslason, S.R. (2024) Direct evidence of CO_2 drawdown through enhanced weathering in soils. *Geochem. Persp. Let.* 30, 7–12. <https://doi.org/10.7185/geochemlet.2415>

References

- AMANN, T., HARTMANN, J., STRUVE, E., DE OLIVEIRA GARCIA, W., FISCHER, E.K., JANSSENS, I., MEIRE, P., SCHOELYNCK, J. (2018) Constraints on Enhanced Weathering and related carbon sequestration – a cropland mesocosm approach. *Biogeosciences Discussions* 1–21. <https://doi.org/10.5194/bg-2018-398>
- ARNALDS, O. (2008) Soils of Iceland. *Jökull* 58, 409–421. <https://doi.org/10.33799/jokull2008.58.409>
- ARNALDS, O. (2010) Dust sources and deposition of aeolian materials in Iceland. *Icelandic Agricultural Sciences* 23, 3–21.
- ARNALDS, O. (2015) *The Soils of Iceland*. World Soils Book Series, Springer, Dordrecht. <https://doi.org/10.1007/978-94-017-9621-7>
- ARNALDS, O., OLAFSSON, H., DAGSSON-WALDHAUSEROVA, P. (2014) Quantification of iron-rich volcanogenic dust emissions and deposition over the ocean from Icelandic dust sources. *Biogeosciences* 11, 6623–6632. <https://doi.org/10.5194/bg-11-6623-2014>
- ARNALDS, O., DAGSSON-WALDHAUSEROVA, P., OLAFSSON, H. (2016) The Icelandic volcanic aeolian environment: Processes and impacts — A review. *Aeolian Research* 20, 176–195. <https://doi.org/10.1016/j.aeolia.2016.01.004>
- BEERLING, D.J., KANTZAS, E.P., LOMAS, M.R., WADE, P., EUFRASIO, R.M., RENFORTH, P., SARKAR, B., ANDREWS, M.G., JAMES, R.H., PEARCE, C.R., MERCURE, J.-F., POLLITT, H., HOLDEN, P.B., EDWARDS, N.R., KHANNA, M., KOH, L., QUEGAN, S., PIDGEON, N.F., JANSSENS, I.A., HANSEN, J., BANWART, S.A. (2020) Potential for large-scale CO_2 removal via enhanced rock weathering with croplands. *Nature* 583, 242–248. <https://doi.org/10.1038/s41586-020-2448-9>
- BRAGAZZA, L., PARISOD, J., BUTTLER, A., BARDGETT, R.D. (2013) Biogeochemical plant-soil microbe feedback in response to climate warming in peatlands. *Nature Climate Change* 3, 273–277. <https://doi.org/10.1038/nclimate1781>
- DESSERT, C., DUPRÉ, B., GAILLARDET, J., FRANÇOIS, L.M., ALLÈGRE, C.J. (2003) Basalt weathering laws and the impact of basalt weathering on the global carbon cycle. *Chemical Geology* 202, 257–273. <https://doi.org/10.1016/j.chemgeo.2002.10.001>
- GILLMAN, G.P., BURKETT, D.C., COVENTRY, R.J. (2002) Amending highly weathered soils with finely ground basalt rock. *Applied Geochemistry* 17, 987–1001. [https://doi.org/10.1016/S0883-2927\(02\)00078-1](https://doi.org/10.1016/S0883-2927(02)00078-1)
- GÍSLADÓTTIR, G., ERLENDSSON, E., LAL, R., BIGHAM, J. (2008) Erosional Effects on Terrestrial Resources over the last Millennium in Reykjanes, Southwest Iceland. *Quaternary Research* 73, 20–32. <https://doi.org/10.1016/j.yqres.2009.09.007>
- GÍSLASON, S.R., OELKERS, E.H., EIRIKSDÓTTIR, E.S., KARDJLOV, M.I., GÍSLADÓTTIR, G., SIGFUSSON, B., SNORRASON, A., EILESEN, S., HARDARDÓTTIR, J., TORSSANDER, P., OSKARSSON, N. (2009) Direct evidence of the feedback between climate and weathering. *Earth and Planetary Science Letters* 277, 213–222. <https://doi.org/10.1016/j.epsl.2008.10.018>
- HAQUE, F., SANTOS, R.M., DUTTA, A., THIMMANAGARI, M., CHIANG, Y.W. (2019a) Co-Benefits of Wollastonite Weathering in Agriculture: CO_2 Sequestration and Promoted Plant Growth. *ACS Omega* 4, 1425–1433. <https://doi.org/10.1021/acsomega.8b02477>
- HAQUE, F., CHIANG, Y., SANTOS, R. (2019b) Alkaline Mineral Soil Amendment: A Climate Change ‘Stabilization Wedge’? *Energies* 12, 2299. <https://doi.org/10.3390/en12122299>
- HAQUE, F., SANTOS, R.M., CHIANG, Y.W. (2020) CO_2 sequestration by wollastonite-amended agricultural soils – An Ontario field study. *International Journal of Greenhouse Gas Control* 97, 103017. <https://doi.org/10.1016/j.ijggc.2020.103017>
- HOOIJER, A., SILVIUS, M., WÖSTEN, H., PAGE, S. (2006) PEAT- CO_2 , Assessment of CO_2 emissions from drained peatlands in SE Asia. *Delft Hydraulic Report* Q3943.
- IPCC (2018) *Global warming of 1.5°C. An IPCC Special Report on the impacts of global warming of 1.5°C above pre-industrial levels and related global greenhouse gas emission pathways, in the context of strengthening the global response to the threat of climate change, sustainable development, and efforts to eradicate poverty*. MASSON-DELMOTTE, V., ZHAI, P., PORTNER, H.O., ROBERTS, D., SKEA, J., SHUKLA, P.R., PIRANI, A., MOUFUOMA-OKIA, W., PEAN, C., PIDCOCK, R., CONNORS, S., MATTHEWS, J.B.R., CHEN, Y., ZHOU, X., GOMIS, M.I., LONNOY, E., MAYCOCK, T., TIGNOR, M., WATERFIELD, T. (Eds.) World Meteorological Organization, Geneva, Switzerland. https://www.ipcc.ch/site/assets/uploads/sites/2/2019/06/SR15_Full_Report_High_Res.pdf
- KELLER, N., STEFANI, M., EINARSDÓTTIR, S., HELGADÓTTIR, A., GUDMUNDSSON, J., SNORRASON, A., THORSSON, J., TINGANELLI, L. (2020) *National Inventory Report - Emissions of greenhouse gases in Iceland from 1990 to 2018*. The Environment Agency of Iceland, Reykjavík.



- LARKIN, C.S., ANDREWS, M.G., PEARCE, C.R., YEONG, K.L., BEERLING, D.J., BELLAMY, J., BENEDICK, S., FRECKLETON, R.P., GORING-HARFORD, H., SADEKAR, S., JAMES, R.H. (2022) Quantification of CO₂ removal in a large-scale enhanced weathering field trial on an oil palm plantation in Sabah, Malaysia. *Frontiers in Climate* 4, 959229. <https://doi.org/10.3389/fclim.2022.959229>
- LINKE, T., OELKERS, E.H., DIDERIKSEN, K., MÖCKEL, S.C., NILABH, S., GRANDIA, F., GISLASON, S.R. (2024) The geochemical evolution of basalt Enhanced Rock Weathering systems quantified from a natural analogue. *Geochimica et Cosmochimica Acta* 370, 66–77. <https://doi.org/10.1016/j.gca.2024.02.005>
- LIU, E.J., CASHMAN, K.V., BECKETT, F.M., WITHAM, C.S., LEADBETTER, S.J., HORT, M.C., GUDMUNDSSON, S. (2014) Ash mists and brown snow: Remobilization of volcanic ash from recent Icelandic eruptions. *Journal of Geophysical Research: Atmospheres* 119, 9463–9480. <https://doi.org/10.1002/2014JD021598>
- MAHOWALD, N.M., BAKER, A.R., BERGAMETTI, G., BROOKS, N., DUCE, R.A., JICKELLS, T.D., KUBILAY, N., PROSPERO, J.M., TEGEN, I. (2005) Atmospheric global dust cycle and iron inputs to the ocean. *Global Biogeochemical Cycles* 19, GB4025. <https://doi.org/10.1029/2004GB002402>
- MITRA, S., WASSMANN, R., VLEK, P.L.G. (2005) An appraisal of global wetland area and its organic carbon stock. *Current Science* 88, 25–35. <http://www.jstor.org/stable/24110090>
- MÖCKEL, S.C., ERENDSOHN, E., GISLADÓTTIR, G. (2017) Holocene environmental change and development of the nutrient budget of histosols in North Iceland. *Plant and Soil* 418, 437–457. <https://doi.org/10.1007/s11104-017-3305-y>
- MOOSDORF, N., RENFORTH, P., HARTMANN, J. (2014) Carbon dioxide efficiency of terrestrial enhanced weathering. *Environmental Science & Technology* 48, 4809–4816. <https://doi.org/10.1021/es4052022>
- PARISH, F., SIRIN, A., CHARMAN, D., JOOSTEN, H., MINAYEVA, T., SILVIUS, M., STRINGER, L. (2008) *Assessment on Peatlands, Biodiversity and Climate Change: Main Report*. Global Environment Centre, Kuala Lumpur and Wetlands International, Wageningen.
- PARKHURST, D.L., APPELO, C.A.J. (1999) *User's guide to PHREEQC (Version 2): A computer program for speciation, batch-reaction, one-dimensional transport, and inverse geochemical calculations*. Water-Resources Investigations Report 99-4259, US Geological Survey, Denver. <https://doi.org/10.3133/wri994259>
- PETERSEN, G.N., BERBER, D. (2018) Soil temperature measurements in Iceland, status and future outlook vision (in Icelandic: *Jarðvegshitamælingar á Íslandi. Staða núverandi kerfis og framtíðarsýn*). Report of the Icelandic Meteorological Office (Skýrsla Væðurstofu Íslands), VI 2018-009, Reykjavík, Iceland. https://www.vedur.is/media/vedurstofan-utgafa-2018/VI_2018_009_rs.pdf
- SCHOTT, J., POKROVSKY, O.S., OELKERS, E.H. (2009) The link between mineral dissolution/precipitation kinetics and solution chemistry. *Reviews in Mineralogy* 70, 207–258. <https://doi.org/10.2138/rmg.2009.70.6>
- SHOJI, S., NANZYO, M., DAHLGREN, R. (1995) *Volcanic Ash Soils: Genesis, Properties and Utilization*. Developments in Soil Science, Elsevier, Amsterdam.
- STOCKMANN, U., PADARIAN, J., MCBRATNEY, A., MINASNY, B., DE BROGNEZ, D., MONTANARELLA, L., HONG, S.Y., RAWLINS, B.G., FIELD, D.J. (2015) Global soil organic carbon assessment. *Global Food Security* 6, 9–16 <https://doi.org/10.1016/j.gfs.2015.07.001>
- STREFLER, J., AMANN, T., BAUER, N., KRIEGLER, E., HARTMANN, J. (2018) Potential and costs of carbon dioxide removal by enhanced weathering of rocks. *Environmental Research Letters* 13, 034010. <https://doi.org/10.1088/1748-9326/aaa9c4>
- TAYLOR, L.L., DRISCOLL, C.T., GROFFMAN, P.M., RAU, G.H., BLUM, J.D., BEERLING, D.J. (2021) Increased carbon capture by a silicate-treated forested watershed affected by acid deposition. *Biogeosciences* 18, 169–188. <https://doi.org/10.5194/bg-18-169-2021>
- XU, J., MORRIS, P.J., LIU, J., HOLDEN, J. (2018) PEATMAP: Refining estimates of global peatland distribution based on a meta-analysis. *Catena* 160, 134–140. <https://doi.org/10.1016/j.catena.2017.09.010>

4 Paper III- Enhanced basaltic rock weathering: oxidative mineral transformations

Tobias Linke, Knud Dideriksen, Karen Maria Dietmann, Sigurður Reynir Gíslason

To be submitted to Frontiers.

Enhanced basaltic rock weathering: oxidative mineral transformations

T. Linke¹, K. Dideriksen^{2,3}, K.M. Dietmann^{4,5}, S.C. Möckel⁶, S.R. Gislason¹

¹ Institute of Earth Sciences, University of Iceland, Sturlugata 7, 102 Reykjavik, Iceland

(*correspondence: tol5@hi.is)

² Nano-Science Center, Department of Chemistry, University of Copenhagen, 2100 Copenhagen, Denmark

³ Geological Survey of Denmark & Greenland (GEUS), Øster Voldgade 10, 1350 Copenhagen, Denmark

⁴ Grupo de Investigación Reconocido-Química del Estado Sólido, Materiales y Catálisis Heterogénea (GIR-QUESCAT), Departamento de Química Inorgánica, Universidad de Salamanca, 37008 Salamanca; Spain

⁵ Landesamt für Umwelt, Naturschutz und Geologie Mecklenburg-Vorpommern, Goldberger Straße 12b, 18273 Güstrow, Germany

⁶ Institute of Life and Environmental Sciences, University of Iceland, Sturlugata 7, 102 Reykjavik, Iceland

Abstract

Enhanced Rock weathering is widely discussed to be deployed globally on large-scale to remove carbon dioxide from the atmosphere. The stability of these engineered systems with respect to environmental changes is of importance. Here we report the changes in mineralogy and soil water chemistry and their effect on toxic trace metals and alkalinity in a natural setting experiencing redox gradients. Additionally, we quantitatively identified minerals in these soils that form as a result of natural weathering of basaltic material. The formation of siderite FeCO_3 , which stores carbon dioxide in solid form, seems to be very limited within these soil systems, making it a minor carbon sink. Using reaction path modelling we were able to recreate observed changes in the soil mineralogy under changing redox conditions, indicating the transformation of the dominant Al-bearing allophane phases to Fe^{3+} -dominated nontronite and ferrihydrite and affecting the alkalinity of the soil waters. Potentially liberated toxic trace metals are scavenged by the newly formed ferrihydrite. The additional formation of siderite as a carbon sink and the immobilization of toxic metals by reaction products of basalt dissolution encourage the use of enhanced rock weathering to increase ocean alkalinity and carbon dioxide removal.

Introduction

Enhanced rock weathering is widely discussed as a carbon dioxide removal technique to combat climate warming (Hartmann et al., 2013; Moosdorf et al., 2014; Edwards et al., 2017;

Beerling et al., 2018; Dietzen et al., 2018, IPCC, 2018; Haque et al., 2021; Deng et al., 2023; Reershemius et al., 2023). As field studies are scarce, only limited information about interactions of the suggested rock amendments with soils and biota is available (Angst et al., 2018, Haque et al., 2019a; Goll et al., 2021, Larkin et al., 2022, Vicca et al., 2022). The formation and reactivity of secondary minerals or interactions with organic compounds is unclear. Possibly introduced heavy metals, commonly found in mafic and ultra mafic rocks, are of concern as their release to the soil and ground water could negate any gains from carbon dioxide removal (Beerling et al., 2020, Dupla et al., 2023). Therefore, naturally occurring reactions could be helpful to provide insights into interactions of basaltic materials and their weathering products with their surrounding soil and soil waters. Additionally, the formation of carbonate minerals, e.g. siderite, as a possible carbon dioxide sink resulting from precipitation reactions after basalt rock amendments has been discussed.

Siderite is a ferrous iron carbonate FeCO_3 , which can occur in different geological settings. It has been found in hydrothermal deposits (Damyranov and Ratiev, 1994; Martin et al., 2017; Morton and Nebel, 1984), peat areas (Mcmillan and Schwertmann, 1998; Postma, 1980) and as secondary alterations (Eshaghpour, 2003). It is also predicted to form as a mineralization product of carbon capture and storage by injection of dissolved CO_2 into basaltic rocks (Snæbjörnsdóttir et al., 2018). Despite the fact that large parts of Iceland are covered by wetland soils, which have been intensively drained for agricultural use (Arnalds, 2015), there is only one report about siderite published (Gudmundsson, 1978). Gudmundsson (1978) reports siderite lenses in peat soil in West Iceland, which potentially formed by inorganic transformation of buried ferric Fe^{3+} lenses as bog iron. Information on the occurrence of siderite as well as goethite and pyrite in Icelandic soils are therefore very limited. As described by (Arnalds, 2015), the most common soil minerals in Iceland are allophane, ferrihydrite and imogolite. Since siderite seems to be a quite unusual mineral in Iceland, it is also not considered for the calculation of the carbon stock in the soil. We provided proof of siderite mineralization in Icelandic Andosols (Linke et al. 2024a), which is further investigated in this study.

Methods

Field site

The study site is located in Southern Iceland ($63^\circ53'42.5''\text{N}$ $20^\circ21'15.9''\text{W}$) at the headwaters of the river Rauðelækur, 7 km NNE from the town Hella. Rauðelækur means “red brook”, named after the reddish color of the water. The field site is situated in a former wetland area, which is drained and used for hay farming and grazing. Nevertheless, the direct vicinity (~200 m) of the sampled spot has not been used in the past 10 years, therefore man-made impact is expected to be negligible.

A natural cliff of about 2 m height is exposing a vertical soil cross section, which is the transition of a mainly waterlogged wetland area to surface runoff pools mixing with drainage channels forming the river Rauðelækur ("red creek"). The cross section has been cleaned up by removing the outermost ~10 cm. Afterwards the profile was pedological described and a time correlation was done using tephra layers (see Linke et al. 2024a and b).

Analytical techniques

For the mineralogical characterization, spot samples were collected from the soil profile by pushing PVC tubes (2 cm Ø and 8 cm length) into the cleared soil. Sample material was then dried in a desiccator flushed with N₂ over silica gel. Additionally, soil cores were taken by hammering 50 cm PVC tubes (75 mm Ø) horizontally into the section, which were closed right after the extraction. The cores were opened in a glove box under anoxic atmosphere (97 % N₂ + 3 % H₂, with palladium catalysts to react any traces of O₂ with the H₂ to water) to avoid any oxidation. Material from the inner parts of the cores was prepared for PXRD analysis using dome sample holders and measured right afterwards with a D8 diffractometer (Bruker). PXRD measurements on dried samples were additionally carried out with either a D8 Advance Plus X-ray diffractometer (Bruker) or a D5000 X-ray diffractometer (Bruker) both with 2 Θ geometry and equipped with a copper X-ray source ($\lambda=0.15406$ nm) and a Ni-filter. The samples were continuously measured in the range of 5-70 °2 Θ with a step size of 0.02 °2 Θ to 0.05 °2 Θ and a counting time of 1.2 s to 1.5 s per step depending on the instrument.

Scanning electron microscopy was conducted using a Quanta™ 3D FEG (FEI) SEM with an accelerating voltage of 20 kV. Samples were sputtered beforehand with a ~10 nm gold layer using a LEICA EDC 550. EDX spot measurements were conducted simultaneously for a range of elements including Fe, Si, O and C.

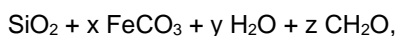
For pair distribution function (PDF) analysis samples were first dried and then loaded in Polyimide capillaries (Cole-Parmer). For a few samples, the preparation was performed in a glovebox and the material was loaded into glass capillaries (Mark-Röhrchen) and sealed with paraffin prior to transport. Based on previous tests, this procedure adequately protects highly oxygen sensitive, amorphous iron carbonate from oxidation (Dideriksen et al., 2015).

Measurements were conducted at Beam line 11-ID-B, Advanced Photon Source, Argonne National Laboratory, USA using monochromatic X-rays with an energy of 58.6 keV, a more detailed description can be found in Dideriksen et al. (2015). Scattered X-rays were detected with a 40 by 40 cm² Perkin Elmer XRD1621 amorphous silicon detector placed ~16 cm from the sample. Calibration of the measurement geometry was conducted with a CeO₂ standard and the program fit2D (Hammersley et al., 1996, Hammersley, 1997). This software was also used to polarization correct the 2D data and convert them to 1D. From the 1D data, the pair

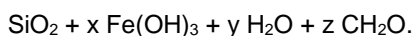
distribution function was obtained using the software PDFgetX2 (Qiu, et al., 2004), using standard procedures such as background correction using an empty capillary, normalization to the average scattering cross section of the sample, and correction for incoherent scattering and non-linear detector efficiency at different angles. The pair distribution functions, $G(r)$, were generated by Fourier transformation using a Q_{\max} of 24 \AA^{-1} .

Obtained pair distribution functions were fitted with the program PDFGui (Qiu et al., 2004). First, data from an $\alpha\text{-Al}_2\text{O}_3$ standard material was used to fit the instrumental damping (Q_{damp}) and broadening (Q_{broad}) parameters based on the structure from Smrčok et al. (2006). The $G(r)$ obtained for siderite were fitted with the structure for siderite from Effenberger et al. (1981), adjusting the structural parameters to minimize the discrepancy between measured and calculated pattern.

The data treatment requires definition of the chemical composition, which for many samples is unknown. While errors in the chemical composition to some extent is mitigated by the correction for non-linear angular detector efficiency, larger errors will be clearly visible, manifested as a high amplitude oscillation in the PDF at $r < 1 \text{ \AA}$. To define the chemical composition, preliminary SEM/EDX were conducted. The analyses showed a pronounced signal from primarily Fe, Si and O, and smaller signal for C, for which SEM/EDX is less sensitive. Based on these results, samples with $I(Q)$ showing pronounced peaks of siderite were assumed to be composed of:



whereas the composition of the remaining samples was calculated based on an assemblage of:



In the definition of composition, the value of x was estimated from the relative peak intensities at $\sim 1.6 \text{ \AA}$ (corresponding to Si-O) and $\sim 2 \text{ \AA}$ (Fe(III)-O) or $\sim 2.1 \text{ \AA}$ (Fe(II)-O), taking into account the difference in electron density and expected coordination number (SiO_4 and FeO_6). The values of y and z were then defined through trial and error to avoid high amplitude oscillations at low r values. Tests of the procedure on the same samples yielded highly similar PDF at $r > 1 \text{ \AA}$ for variation of x within $\pm 30\%$.

Fourier transform infrared spectroscopy (FTIR) analysis were carried out using a Perkin Elmer Spectrum Two FT-IR Spectrometer with Spectrum software. For each measurement 2 mg of sample was mixed with 300 mg of Potassium bromide KBr and then pressed to a pellet. Measurements were carried out in a range of $4000\text{-}400 \text{ cm}^{-1}$ with a resolution of 4 cm^{-1} , averaging 20 scans to improve the signal-to-noise ratio.

The specific surface area of the samples was determined from the nitrogen adsorption-desorption isotherms at -196 °C in a Micromeritics Gemini VII 2390t apparatus. The samples were pre-treated at 110 °C for 2 h under nitrogen flow (~30 mL min⁻¹) in a micromeritics FlowPrep 060 sample degas system in order to remove adsorbed species. The specific surface area was determined by the BET method (Brunauer et al., 1938).

The particle size distribution (PSD) of the samples was determined by laser diffraction (Low Angle Laser Light Scattering) using a Malvern Mastersizer 2000 equipment with a He-Ne gas laser ($\lambda=0.63 \mu\text{m}$), with software provided by the manufacturer. The samples were dispersed in water, stirred at 800 rpm, and pumped (2050 rpm) to the measuring unit. Deagglomeration of the particles was attained by in situ ultrasonic treatment for 5, 10 or 15 min. Measurements were conducted at a laser obscuration of 6.8-10.

Thermogravimetric analysis (TG) and Differential Scanning Calorimetry (DSC) curves were simultaneously recorded in a SDT Q600 TA instrument, using $\alpha\text{-Al}_2\text{O}_3$ (Fluka) previously calcined overnight at 1200 °C, as a reference material for the DSC measurements. All samples were heated up to 900 °C at a heating rate of 5 K min⁻¹ under O₂ flow (50 ml min⁻¹). Released gases during the heating process were simultaneously analyzed using a coupled mass spectrometer (MS, Pfeiffer Vacuum ThermoStar GSD 301 T2).

For chemical analysis 130-160 mg dried sample material was weighted and ashed in ceramic crucibles overnight in a furnace at 550 °C. Afterwards each sample was transferred to Teflon beakers and rinsed by addition of 5x 1 ml of conc. suprapure HNO₃. Then 2 ml hydrofluoric acid HF and 2-3 drops of perchloric acid were added to each sample and the Teflon beakers were heated overnight at ~70 °C. After evaporation of HF 2 ml of boric acid H₃BO₃ was added and then evaporated overnight at ~70 °C. The dry samples were cooled down and dissolved by addition of 5x 1 ml of conc. suprapure HNO₃ while heated up to ~70 °C. These solutions were transferred to volumetric flasks and mixed with milliQ water.

Analysis of the major elements were carried out using an inductively coupled plasma optical emission spectrometer (ICP-OES, Spectro, Ciros Vision) equipped with a semiconductor detector (CCD). The instrument was calibrated with in-house standards referenced to commercial standard material. All used standards and measured samples were acidified to 0.5 % HNO₃.

For trace element analysis, the sample solutions from the HF dissolution were diluted with milliQ water and spiked with internal standards (Rh, Ir, Ga). All samples were then measured using an inductive coupled plasma mass spectrometer (Thermo iCAP Qc ICP-MS). Detector drift was corrected with the added internal standards. Blank solutions were measured every 5 samples.

Reaction paths of predicted soil minerals and soil waters under changing redox conditions were simulated using PHREEQC interactive software version 3.4.0 (Parkhurst and Appelo, 1999). Calculations were performed using the minteq.v4.dat (Allison et al., 1991; U.S. Environmental Protection Agency, 1998) database.

Results

Soil profile description

The soil profile was divided into 14 sections, based on the pedological classification scheme from the Schoeneberger et al (2012). Interposed tephra layers were used for detailed subdivision. A detailed description can be found in Linke et al. (2024a).

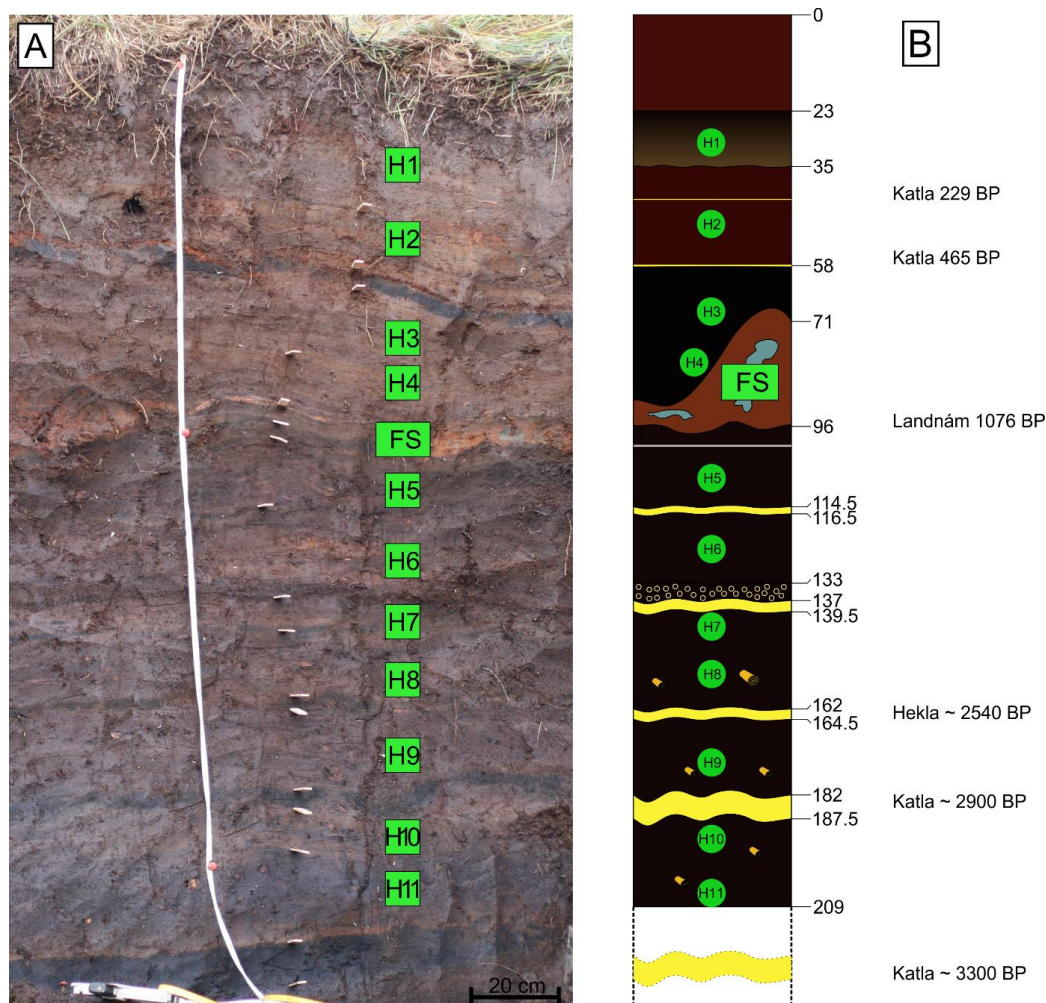


Figure 1A: Overview of the outcrop with the different horizons and sampling locations (green). **B:** schematic profile with identified soil horizons and tephra layers with names of the volcanoes and ages on the right side, modified after Linke et al. (2024a). Note: the siderite containing red horizon locally extends up to 40 cm thickness (not shown in A)

As seen in figure 1A and B, a large reddish horizon occurs at a depth of 60 to 95 cm, irregularly extending over 10 to 25 cm height, locally up to 40 cm thick. The soil depth of the red horizon coincided with the typical depth of the settlement layer “Landnám”. This horizon contains frequently irregular shaped greyish inclusions of 0.5 to 30 cm size (diameter) with sharp boundaries to the surrounding red material. Spot samples (samples H1 to H11) from the major horizons were collected and analyzed regarding their mineral and chemical composition. Multiple samples were taken from the greyish material (Fig. 2A) in the red horizon (samples FS). Distinct tephra layers were used to cross correlate the studied profile with nearby soil profiles and provide age estimates based on tephrochronology. The entire soil profile extends over ~220 cm and circa 3,300 years.

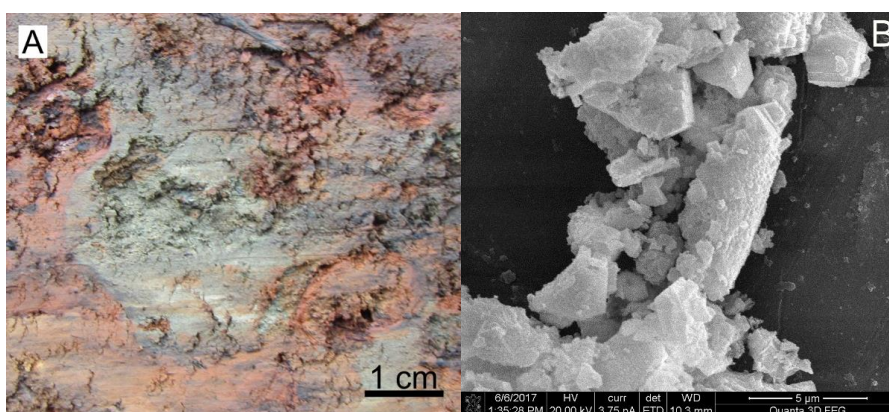


Figure 2A: Detailed view of blue/green/greyish nodules within the red horizon around 60-95 cm soil depth identified as siderite aggregations. **B:** SEM image of greyish sample material identified as siderite via EDX and XRD/PDF

Mineral phase characterisation

Powder X-ray diffraction and pair distribution function analyses of the dried soil samples (H1 to H11) from the different horizons show that the samples do not contain high amounts of well crystalline material (Fig. 3A and B). The few observed peaks in the XRD pattern between 20 and 40 °2 θ were attributed to feldspar and pyroxene phases that could not be identified any further. Feldspar and pyroxene were also identified in the PDF data and are indicated by black asterisk (*) in Figure 3B. Additionally, in the XRD data from sample H7 siderite could be identified and is indicated by the asterisks in Figure 3A and the blue lines in Figure 3B for the PDF analysis. In addition to the crystalline phases, peaks most likely corresponding to a nontronite phase were observed in the PDF data (see Fig. 3B green dashed lines). No other clay mineral phases such as allophane could be identified in any of the recorded PDF or XRD data.

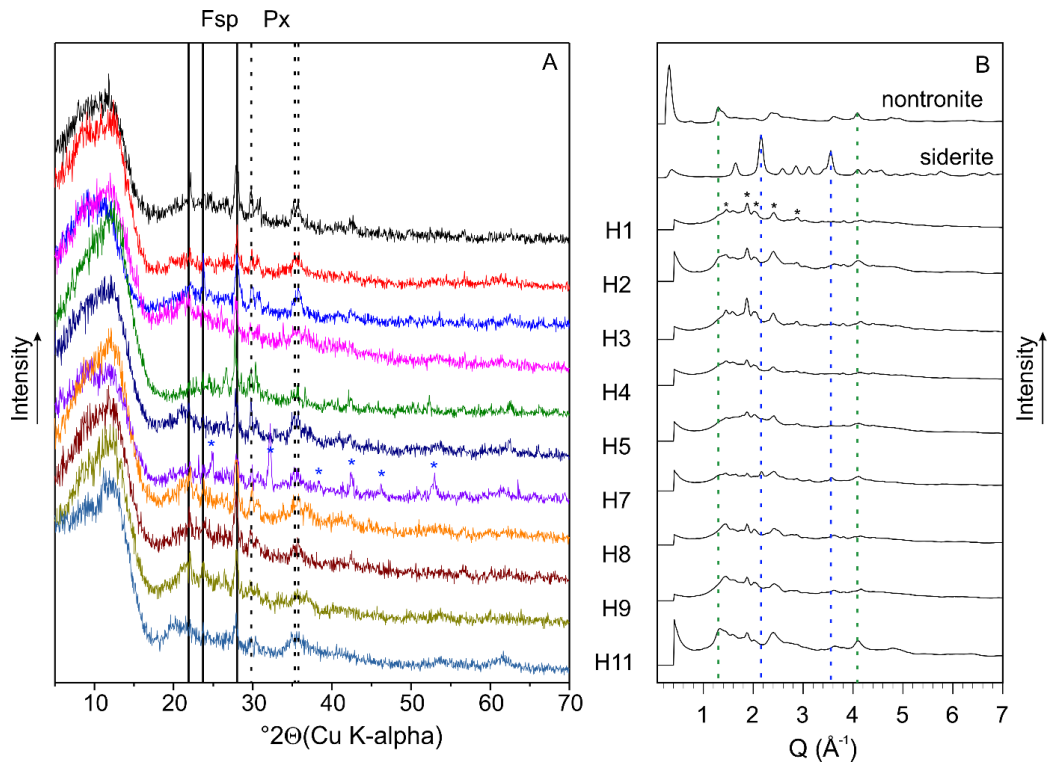


Figure 3A: XRD of the samples. Peaks for feldspar are indicated by black lines, for pyroxene by black dashed lines, and siderite by blue asterisks. **B** The $I(Q)$ of samples and standards (at the top). Peaks for siderite are indicated by blue dashed lines, for nontronite by green dashed lines, and for feldspar and pyroxene by black asterisks. Data for siderite from Dideriksen et al., 2015. Fig.

The greyish material in the FS samples (see Fig. 1 and Fig. 3) from the red horizon could be identified as siderite FeCO_3 using powder X-ray diffraction (Effenberger et al. 1981) showing a main peak at $31.9^\circ 2\theta$ (Fig. 4B). The XRD pattern shows a quite pure sample with an additional peak at $27.9^\circ 2\theta$, most likely caused by the main peak of a calcium-rich feldspar phase, which is commonly found in basalt (Barth 1936). The sharp PXRD peaks and the long-range order in the PDF data show a very high crystallinity of the siderite compared to the other minerals identified in the soil samples. The maximum crystallite size based on the PDF data is estimated to be around 40-50 nm, which matches with the calculated crystallite size of 44 nm based on the Scherrer equation (Scherrer 1918) for the main peak at $31.9^\circ 2\theta$ and the observations published by (McMillan and Schwertmann, 1998) for siderite found in low moor peat samples. SEM imaging reveals large subhedral crystals, partially up to a few micrometers (Fig. 2B).

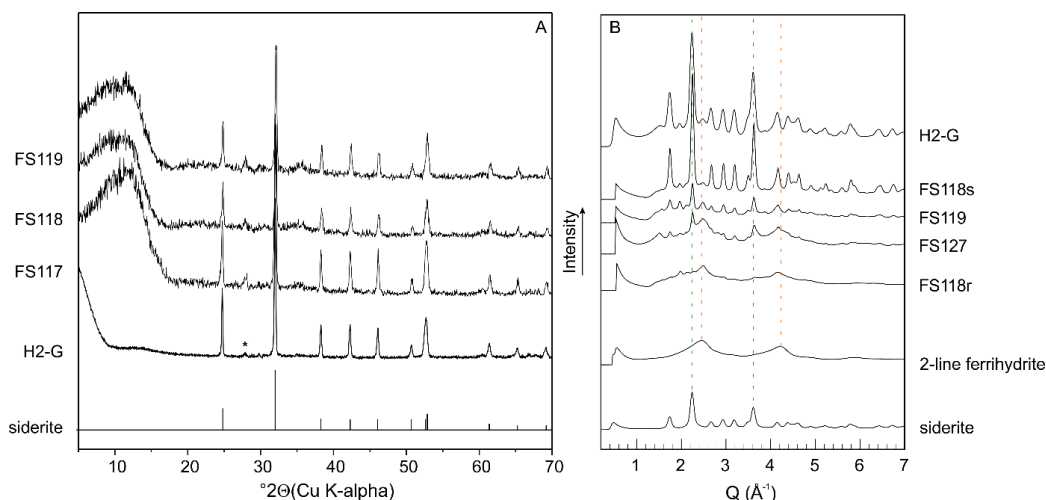


Figure 4A: XRD pattern of dried material from the greyish inclusions, all major peaks correspond to reference pattern for siderite (bottom) as described by Effenberger et al. (1997), an additional peak is observed at $28.0^\circ 2\theta$ (*) that agrees with the main peak observed in feldspars. **B:** The $I(Q)$ of samples and standards (bottom) of the grey nodules and proximity. Peaks for siderite are indicated by green dashed lines, and for ferrihydrite by orange dashed lines. Data for siderite from Dideriksen et al., 2015.

No siderite could be identified in the red material (e.g. samples FS118r) surrounding the grey inclusions. The PDF data of these samples largely matches the peaks observed for 2-line ferrihydrite, indicating a possible transformation between siderite and ferrihydrite. Analysis of the grey-red color boundary with SEM/EDX did not show any difference in appearance/morphology or chemical composition within a scale of 1-2 mm.

Pair distribution function analysis and principal component analysis

Principal component analysis (PCA) was conducted in the range $1 \leq r < 60 \text{ \AA}$. The PCA results in five principal components (PCs) accounting for 96 % of the variance in the analysis (see supplementary Fig. ES1). Based on the determined chemical composition, XRD and $I(Q)$, we surmise that these PCs could reflect the presence of siderite, short range ordered silicates and Fe-oxides, and silicates with longer range ordering. To derive patterns for real phases through recombination of the PCs, the top five PCs were selected for deconvolution based on the procedure used in Eiby et al. (in preparation). The recombination is based on the assumption that a target pattern can be properly described by a weighted sum of the PCs. This recombination was carried out in steps by fitting the weighing factors to minimize the sum of the squared residual between the calculated pattern and the target pattern(s):

1. Combined, the chemical analysis and $I(Q)$ indicate the presence of a short range ordered Fe-oxide, presumably a ferrihydrite like phase. To probe how the PDF for this material might look, a sample of Fe-oxides was taken from the nearby ditch. The PDF of this material is shown

in supplementary figure ES2. This pattern greatly resembles the PDFs measured for natural ferrihydrite (Cismasu et al., 2011). In the second step, it was tested if the PCs could be recombined to yield the measured PDF. Supplementary Figure ES2 shows good agreement between the measured and calculated PDF, which was assigned as PC1'.

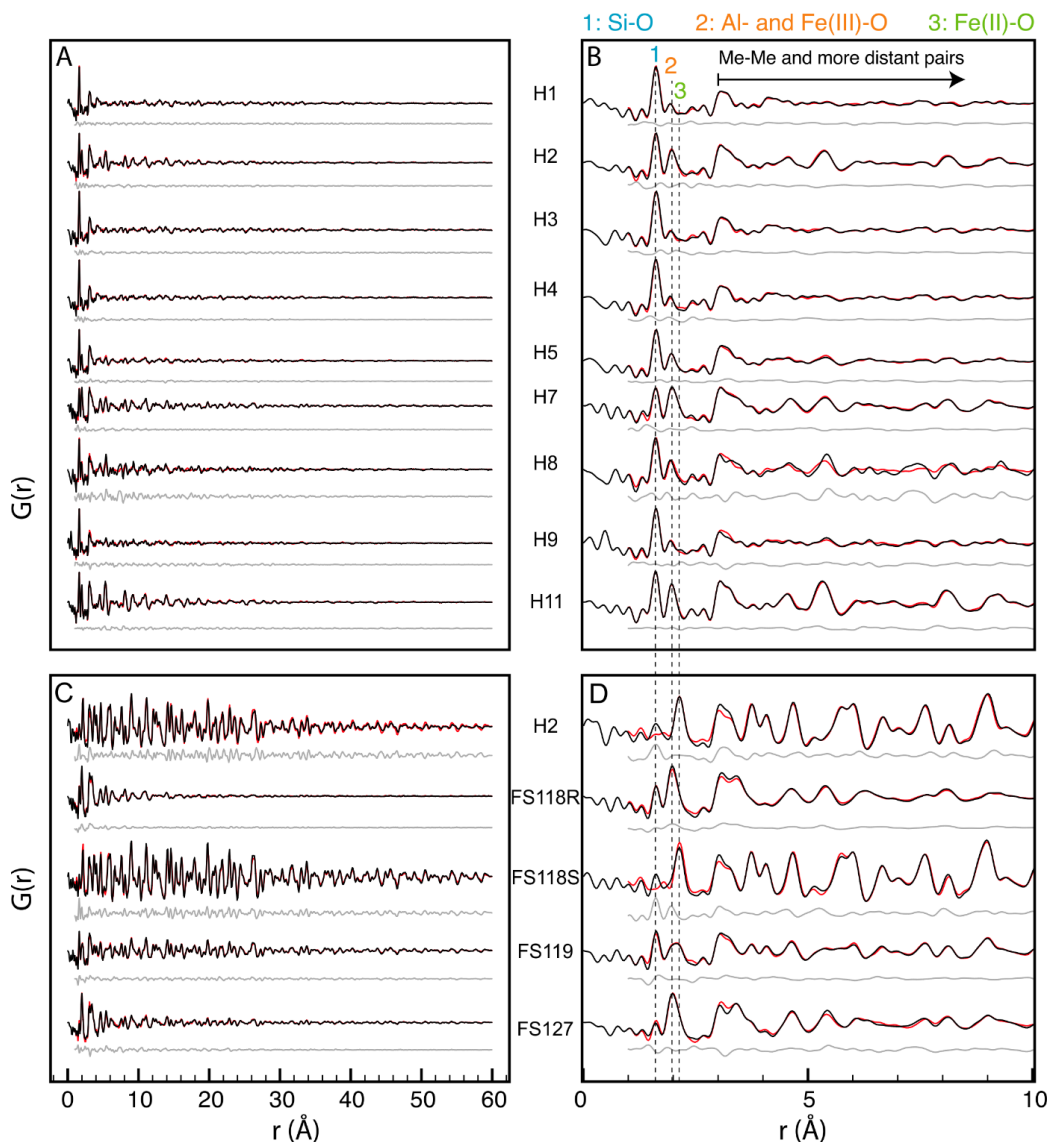


Figure 5: The PDFs of the samples showing A) and C) overview and B) and D) zoom of the range 0-20 Å from the soil horizons and the greyish horizon respectively. The measured patterns are given in black, the calculated patterns from the deconvolution of principal components in red, and the difference between the two in grey. Pattern for siderite has been reproduced using $Q_{max} = 24$ from the data in Dideriksen et al., 2015. The data from the different soil horizon is showing in the upper part and the data from the siderite containing horizon in the lower section.

2. Given that the XRD and $I(Q)$ show the presence of siderite, a measured PDF reprocessed from the data of Dideriksen et al. (2015) to have $Q_{\max} = 24 \text{ \AA}^{-1}$ was used as the target pattern to derive the first recombined principal component (PC2'). The measured PDF and PC2' is shown in Figure ES2.

3. Given that our data also indicate the presence of short and longer range ordered silicates, a final step was performed where two PC's were derived simultaneously using the measured PDFs for the samples as target patterns. In this fitting, PC1' and PC2' were included and a scaling factor for their contribution to the measured patterns for samples were fitted. To stimulate the development of a short range ordered PC', one of the calculated patterns was assigned a penalty for intensities at $r > 20 \text{ \AA}$. This meant that the sum of the squared residuals included contributions from both the mismatch between measured and calculated patterns for the samples as well as for one PC', the difference from zero for intensities with $r > 20 \text{ \AA}$, which was given additional weight by a factor of 5. In this fitting it was finally imposed that the sum of the scaling factors for the PC' should equal 1. After this fitting, a total of four PC's had been derived (see ES1 and ES2). However, the intensities varied widely. To normalize for variation in intensities, the PC's were scaled to have equal intensity for the major Si-O or Fe-O peak at $\sim 1.6 \text{ \AA}$ and $\sim 2 \text{ \AA}$. The scaling factor for their contribution to the samples was then refitted, again imposing a total of scaling factors of 1 for each sample.

The derived PC's for the two silicate components are shown in the supplementary Figure ES2. The short range ordered PC' most likely represents basaltic glass, where it shows good agreement with. Surprisingly the longer range ordered PC' agrees well with the pattern measured for the nontronite standard, NAU-1, in particular at lower r values. Given the nature of the PDFs, where peak intensities depend on both, the electron densities of the atom pairs and the coordination number, the scaling factors cannot be readily recast into absolute abundance. However, variation in scaling represents variation in abundance. Based on these abundances, relative phase proportions were simulated.

Fourier-transform infrared spectroscopy

Adsorption bands within the retrieved spectra were assigned vibrational frequencies in order to determine the mineral composition of the characterized samples. Additionally, detailed assigned vibrational frequencies for selected samples, namely FS117, H1, H9, H10, H11, are given in the Appendix in tables 1-5.

Vibrational frequencies indicative for moganite and different aluminum silicate clay minerals, here allophane and imogolite, were found within the spectra of all samples within the 1200 to 400 cm^{-1} range, attributed to lattice vibrations within the clay minerals. Common Si-O stretching vibrations, asymmetrical at 1160 cm^{-1} and symmetrical at 790 cm^{-1} , and anti-symmetrical bending at 460 cm^{-1} , could be assigned and are in agreement with literature

(Lippincott et al. 1958, Saikia et al. 2008, Viana et al. 2012). Within the spectra of the samples FS117, H10 and H11 adsorption bands could be attributed to siderite, an iron (II) carbonate. Characteristic bands include the asymmetric stretching vibration within the carbonate group between 1420 to 1410 cm^{-1} and out-of-plane bending vibrations at 861 cm^{-1} (Dubrawski et al. 1989). A sharp adsorption band at 737 cm^{-1} confirms the presence of a crystalline carbonate phase via in-plane bending vibrations (Dubrawski et al. 1989). Bands from water are visible at 1627 cm^{-1} and $\sim 3400 \text{ cm}^{-1}$. Small features occurring at 2925 and 2854 cm^{-1} were interpreted as vibrations from methyl and O-CH₂ groups respectively.

Thermal analysis

Thermal analysis of the siderite samples up to 800 °C show a mass loss in 3 steps attributed to the loss of water, CO₂ and minor amounts of NO₂. Water is desorbed up to 100 °C. Decarbonization occurs in 2 steps, with maximum CO₂ release around 270 °C and 400 °C respectively. The same maxima are observed for the release of NO₂. No mass loss is measured after 450 °C. The theoretical mass loss that would occur during the transformation of FeCO₃ to Fe₂O₃ in the presence of O₂ is $\sim 31.5 \%$, whereas the average mass loss of the samples, normalized to the mass at 100 °C, between 100 °C and 450 °C is 27.6 %. The difference can be explained by accessory phases like feldspar and amorphous basaltic glass that do not show a mass loss upon heating. No sulfur gases are observed during heating, indicating the absence of accessory sulfide or sulfate minerals or organic material with noticeable sulfur content.

Particle size and surface area

Particle size characterization of the dried samples show a monomodal distribution with d(0.5) values mostly around 100-160 μm and d(0.9) of 500-790 μm (see table 1 and supplementary figure ES12). After ultrasonic treatment the d(0.5) and d(0.9) values decrease significantly to 20-28 μm and 110-150 μm respectively, indicating particle aggregates disperse. Some samples show a smaller d(0.5) value around 10 μm even before the ultrasonic treatment, and nearly no decrease in the particle size afterwards, indicating less aggregates. BET surface area calculations using N₂ infiltration reveal a surface area of 120-150 $\text{m}^2 \text{ g}^{-1}$. All samples show sorption isotherms (Thommes et al. 2015) typical for platy materials. This is in agreement with the observed crystals of the siderite in the SEM images (see Fig. 2B).

Table 1: Mean particle size distributions of siderite inclusions before and after 15 min ultrasonic treatment (US) respectively

| Sample | d(0.5) | d(0.9) | d(0.5) 15US | d(0.9) 15US |
|-----------|--------|--------|-------------|-------------|
| Peat soil | 110 | 790 | 20 | 112 |
| FS112 | 319 | 1064 | 9 | 32 |
| FS114 | 12 | 55 | 7.5 | 25 |
| FS117 | 97 | 517 | 25 | 112 |
| FS118 | 161 | 782 | 28 | 152 |
| FS124 | 10.7 | 173 | 6.5 | 32 |

Discussion

Chemical analysis and PXRD results show that the greyish inclusions found inside the red horizon in the outcrop are made off well-crystalline siderite. Lovley and Phillips (1988) and Sparks et al. (1990) have shown that siderite can form as a product of microbial iron reduction in a carbonate buffered systems. In addition, feldspar and pyroxene could be identified, which are commonly found in basalt (bed rock) or as accessory minerals in basaltic glass (tephra). Thermal analysis and FT-IR spectra give evidence for the presence of organic compounds, most likely soil organic matter. The decomposition of these organics leads to the release additional CO₂. Chemical analyses of the bulk material show elevated concentrations of elements (Ca, Mg, Al, Ti) commonly found in basaltic glass. Especially Ca and Mg can be incorporated into siderite forming a solid solution but could also be derived from dissolution of admixed basaltic material. From the total digestion method, no values for Si in the solid material are available. Nevertheless, vibration bands for Si are present in the FT-IR spectra. Si can be found in basaltic material, as well as in common secondary soil minerals like allophane as well as Al-humic complexes (Arnalds 2008).

Besides the crystalline siderite additional short range ordered phases could be identified in the soil horizons via pair distribution function analysis a principal component analysis. The results were used to provide a semi-quantitative overview of the solid phases throughout the soil profile (see Fig. 6). Most of the soil profile is dominated by basaltic glass, ferrihydrite and nontronite can be found with varying amounts throughout the soil profile. The highest nontronite concentration can be found at depth in sample H11. Siderite was only found in small quantities in one soil sample H7, but in high quantities in most of the grey inclusions as indicated by XRD. Allophane was not identified in any of the samples despite its predicted abundance in the soils (Linke et al. 2024b, Arnalds 2015).

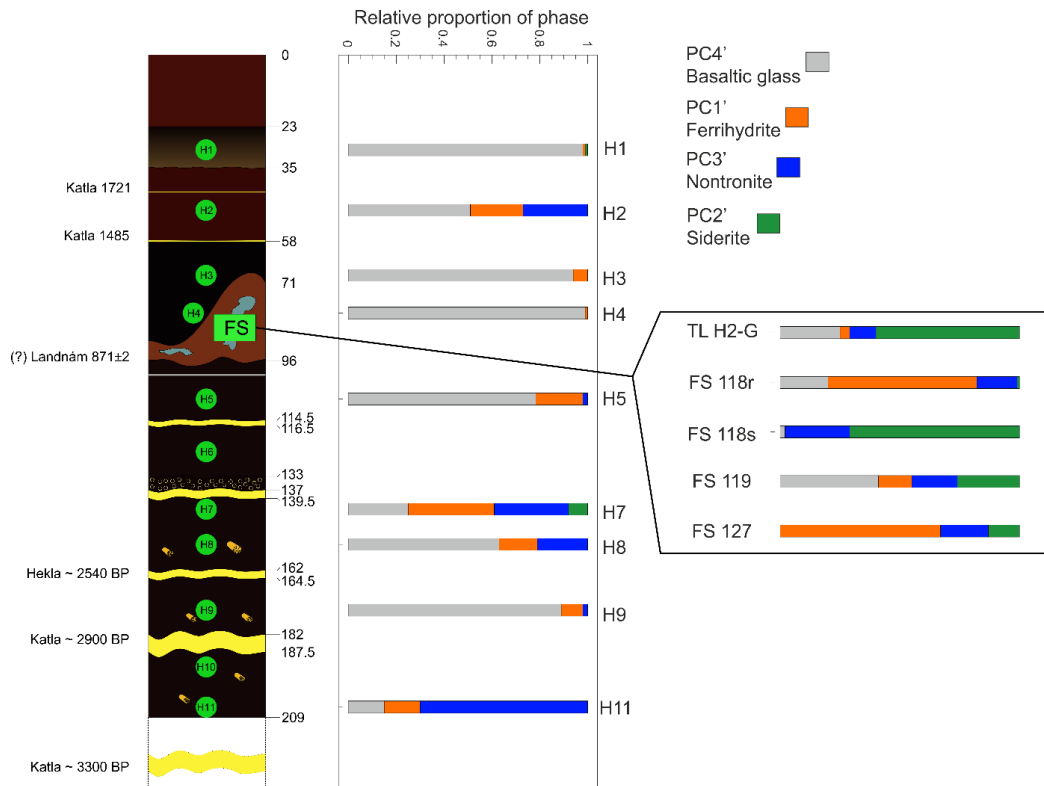


Figure 6: Left: Schematic soil profile with soil horizons and identified tephra layers on the left side and soil depth on the right side, sampling spots marked by green circles, Right: The relative proportion of the PC' derived from the deconvolution of the PC with depth offset. Spot samples from the grey material inside the box. PC1' represents ferrihydrite, PC2', siderite, PC3', nontronite, and PC4', basaltic glass

PHREEQC reaction path modelling was used to recreate the possible evolution of iron-rich, reduced soil waters that are the product of basalt-water interactions. The models suggest in agreement with the synchrotron analysis that allophane is dissolved and a new iron-rich aluminum silicate phase, nontronite, forms (Fig. 7 and Fig. ES6). Aluminum seems to be the limiting element for nontronite in this system. Therefore, excessive iron is precipitated as ferrihydrite upon oxidation. In sum these processes result in a decrease of pH and alkalinity.

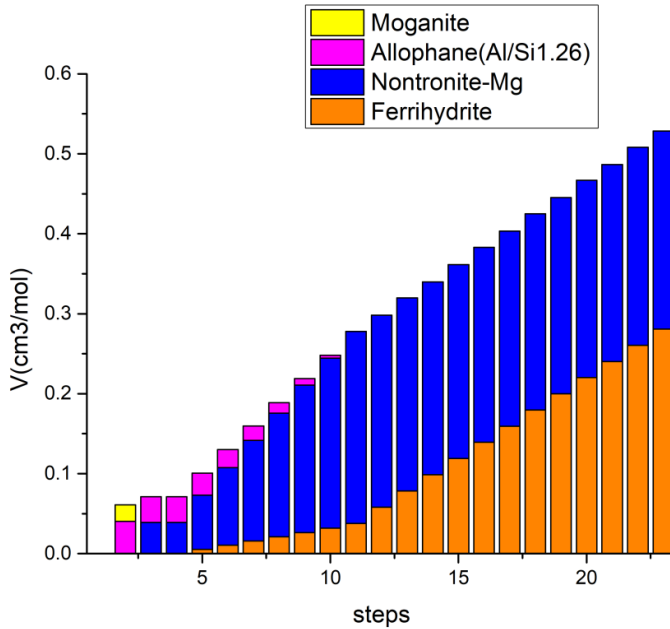


Figure 7: Simulated reaction path outcome when reacting anoxic allophane-rich soil water solutions in the presence of oxygen, Moganite and Allophane are initially transformed into Nontronite and Ferrihydrite until fully consumed, steps show that different mineral compositions are possible in the soil based on reaction progress as observed in Fig. 6

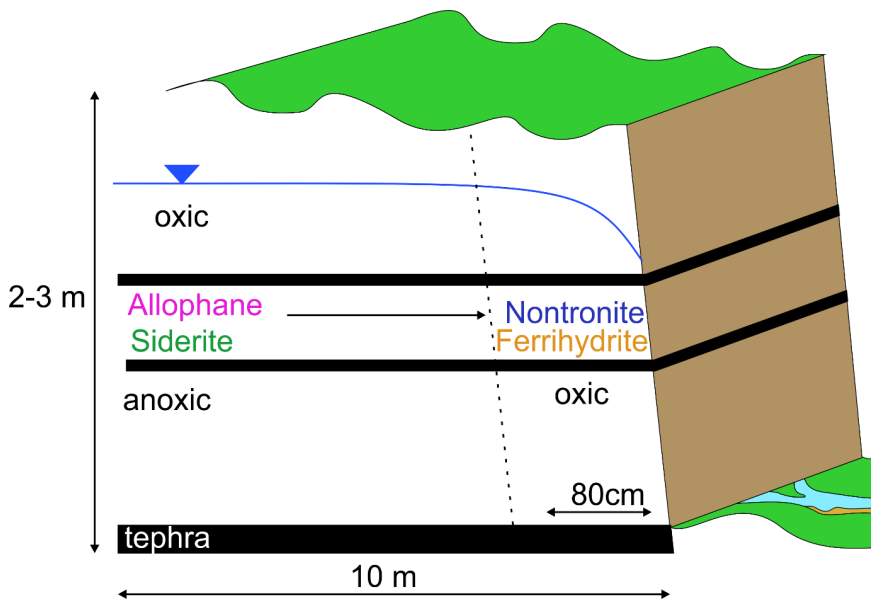


Figure 8: Schematic illustration of the main processes in the soil outcrop with changing redox conditions, upper blue line marks the water table,

The results of Linke et al. (2024b) show in agreement with other literature (Arnalds 2015) that nanocrystalline phases like allophane and ferrihydrite, in oxic environments, are the prevalent forming soil minerals in the studied Andosol. These phases form as products of the weathering of basaltic material. Our results show that allophane as well as possibly present moganite and siderite are transformed to nontronite and ferrihydrite upon oxidation (see Fig. 8 and Fig. ES6). Nontronite precipitation keeps aluminum concentrations in the soil solutions at a minimum, which is in agreement with the measured field data. Once, any aluminum sources are depleted, ferrihydrite precipitation will be prevalent. Ferrihydrite is known to have a high affinity to take up various heavy metals as well as phosphorus (Linke et al. 2018). Our soil water data shows that heavy metal concentrations and phosphorus in the soil water are overall low, mostly below the detection limits. Simultaneously, the oxidation of Fe^{2+} and the precipitation of ferrihydrite decrease the alkalinity. Therefore, future enhanced rock weathering projects should take the iron content of the applied material into account to optimize the alkalinity production while providing enough iron to immobilize all potential toxic trace metals via ferrihydrite precipitation and adsorption.

Acknowledgment

Additionally, the authors want to thank Stephen Reid at the University of Leeds for the ICP-MS analysis and Karina Chapman, Peter Chupas, Rick Spence and Kevin A. Beyer at the APS beam line 11 ID-B. The use of the Advanced Photon Source was supported by the U. S. Department of Energy, Office of Science, Office of Basic Energy Sciences, under Contract No. DE-AC02-06CH11357.

Funding

This project has received funding from the European Union's Horizon 2020 research and innovation programme under the Marie Skłodowska-Curie grant agreement No 675219 and from Landsvirkjun under the project number 2456.

References

- Allison, J.D., Brown, D.S., Novo-Gradac, K.J. (1991) MINTEQA2/PRODEFA2—A geochemical assessment model for environmental systems—Version 3.0 user's manual., Athens, Georgia 30605.
- Angst, G., Messinger, J., Greiner, M., Häusler, W., Hertel, D., Kirfel, K., Kögel-Knabner, I., Leuschner, C., Rethemeyer, J., Mueller, C.W. (2018) Soil organic carbon stocks in topsoil and subsoil controlled by parent material, carbon input in the rhizosphere, and microbial-derived compounds. *Soil Biology and Biochemistry* 122, 19–30.
- Arnalds, O. (2008) Soils of Iceland. *Jökull*, 58, 409–421
- Arnalds, O. (2015) The Soils of Iceland. World Soils Book Series, Springer, Dordrecht.

- Barth, T. (1936) The crystallization Process of Basalt, *American Journal of Science*, 5 (31), 321-351
- Beerling, D.J., Kantzas, E.P., Lomas, M.R., Wade, P., Eufrazio, R.M., Renforth, P., Sarkar, B., Andrews, M.G., James, R.H., Pearce, C.R., Mercure, J.F., Pollitt, H., Holden, P.B., Edwards, N.R., Khanna, M., Koh, L., Quegan, S., Pidgeon, N.F., Janssens, I.A., Hansen, J., Banwart, S.A. (2020) Potential for large-scale CO₂ removal via enhanced rock weathering with croplands. *Nature* 583, 242–248.
- Beerling, D.J., Leake, J.R., Long, S.P., Scholes, J.D., Ton, J., Nelson, P.N., Bird, M., Kantzas, E., Taylor, L.L., Sarkar, B., Kelland, M., DeLucia, E., Kantola, I., Müller, C., Rau, G., Hansen, J. (2018) Farming with crops and rocks to address global climate, food and soil security. *Nat Plants* 4, 138–147.
- Brunauer, S., Emmett, P. H., Teller E. (1938) Adsorption of Gases in Multimolecular Layers, *Journal of the American Chemical Society*, 60 (2), 309-319
- Cismasu, A.C., Michel, F.M., Tcaciuc, A.P., Tyliczszak, T., Brown Jr., G.E. (2011) Composition and structural aspects of naturally occurring ferrihydrite, *C. R. Geosci.*, 343, pp. 210-218
- Damyantov, Z., Ratiev, L. (1994) Mineralogical-genetic types of siderite from Kremikovci deposit, *Geologica Balc.*, 24, 2, 71-82.
- Deng, H., Sonnenthal, E., Arora, B., Breuning, H., Brodie, E., Kleber, M., Spycher, N., Nico, P. (2023) The environmental controls on efficiency of enhanced rock weathering. *Sci. Rep* 13, 9765.
- Dideriksen, K., Frandsen, C., Bovet, N., Wallace, A. F., Sel, O., Arbour, T., Navrotsky, A., De Yoreo, J. J., Banfield, J. F. (2015) Formation and transformation of a short range ordered iron carbonate precursor. *Geochim. Cosmochim. Acta*, 654, 53– 70.
- Dideriksen, K., Frandsen, C., Bovet, N., Wallace, A.F., Sel, O., Arbour, T., Navrotsky, A., De Yoreo, J.J., Banfield, J.F. (2015) Formation and transformation of a short range ordered iron carbonate precursor. *Geochim Cosmochim Acta* 164, 94–109.
- Dietzen, C., Harrison, R., Michelsen-Correa, S. (2018) Effectiveness of enhanced mineral weathering as a carbon sequestration tool and alternative to agricultural lime: An incubation experiment. *Int.J. Greenhouse Gas Cont.* 74, 251-258.
- Dubrawski, J.V., Channon, A.L., Warne, S.S.J. (1989) Examination of the siderite-magnesite mineral series by Fourier transform infrared spectroscopy. *American Mineralogist*, 74 (1-2): 187–190.
- Dupla, X., Möller, B., Baveye, C., Grand, S. (2023) Potential accumulation of toxic trace elements in soils during enhanced rock weathering, *Eur. J. Soil Sci.*, 74(1), e13343
- Edwards, D.P., Lim, F., James, R.H., Pearce, C.R., Scholes, J., Freckleton, R.P., Beerling, D.J. (2017) Climate change mitigation: Potential benefits and pitfalls of enhanced rock weathering in tropical agriculture. *Biol Lett* 13.
- Effenberger, H., Mereiter, K., Zemann, J. (1981) Crystal structure refinements of magnesite, calcite, rhodochrosite, siderite, smithonite, and dolomite, with discussion of some aspects of the stereochemistry of calcite type carbonates. *Z Kristallogr Cryst Mater* 156, 233–244.

- Eshaghpour, M. (2003) Borehole Geology and alteration mineralogy of Well HE-9 in Hellisheidi Geothermal Field, SW-Iceland, Report No. 8, Geothermal Training Programme
- Goll, D.S., Ciais, P., Amann, T., Buermann, W., Chang, J., Eker, S., Hartmann, J., Janssens, I., Li, W., Obersteiner, M., Penuelas, J., Tanaka, K., Vicca, S. (2021) Potential CO₂ removal from enhanced weathering by ecosystem responses to powdered rock. *Nat Geosci* 14, 545–549.
- Gudmundsson, Th. (1978). Pedological studies of Icelandic peat soils. Ph.D. Thesis, University of Aberdeen, Scotland.
- Hammersley A. P. (1997) FIT2D: An Introduction and Overview. ESRF Internal Report, ESRF97HA02T. Available at http://www.esrf.eu/computing/scientific/FIT2D/FIT2D_INTRO/fit2d.html.
- Hammersley, A. P., Svenson, S. O., Hanfland, M., Hauserman, D. (1996) Two-dimensional detector software: From real detector to idealised image or two-theta scan, *High Pressure Res.* (4-6), 235–248.
- Haque, F., Chiang, Y., Santos, R. (2019) Alkaline Mineral Soil Amendment: A Climate Change ‘Stabilization Wedge’? *Energies* 12, 2299.
- Haque, F., Santos, R.M., Chiang, Y. W. (2021) Urban Farming with Enhanced Rock Weathering As a Prospective Climate Stabilization Wedge. *Cite This: Environ. Sci. Technol* 55, 13575–13578.
- Hartmann, J., West, A.J., Renforth, P. Köhler, P., De La Rocha, C.L., Wolf-Gladrow, D.A., Dürr, H.H. Scheffran, J. (2013) Enhanced chemical weathering as a geoengineering strategy to reduce atmospheric carbon dioxide, supply nutrients, and mitigate ocean acidification, *Rev. Geophys.* 51, 113–149.
- Larkin, C.S., Andrews, M.G., Pearce, C.R., Yeong, K.L., Beerling, D.J., Bellamy, J., Benedick, S., Freckleton, R.P., Goring-Harford, H., Sadekar, S., James, R.H. (2022) Quantification of CO₂ removal in a large-scale enhanced weathering field trial on an oil palm plantation in Sabah, Malaysia. *Front. Clim.* 4:959229.
- IPCC (2018) Global warming of 1.5°C An IPCC Special Report on the impacts of global warming of 1.5°C above pre-industrial levels and related global greenhouse gas emission pathways, in the context of strengthening the global response to the threat of climate change, sustainable development, and efforts to eradicate poverty. Masson-Delmotte, V., Zhai, P., Pörtner, H.-O., Roberts, D., Skea, J., Shukla, P.R., Pirani, A., Moufouma-Okia, W., Péan, C., Pidcock, R., Connors, S., Matthews, J.B.R., Chen, Y., Zhou, X., Gomis, M.I., Lonnoy, E., Maycock, T., Tignor, M., Waterfield, T. (Eds.), Cambridge University Press, Cambridge, UK and New York, NY, USA, pp. 3-24,
- Linke, T., Gislason, S.R. (2018) Stability of iron minerals in Icelandic peat areas and transport of heavy metals and nutrients across oxidation and salinity gradients – a modelling approach, *Energy Procedia*, 146, 30-37.
- Linke, T., Oelkers, E.H., Dideriksen, K. Möckel, S.C., Nilabh, S., Grandia, F., Gislason, S.R. (2024a) The geochemical evolution of basalt Enhanced Rock Weathering systems quantified from a natural analogue, *Geochimica et Cosmochimica Acta* 370, 66-77.

- Linke, T., Oelkers, E.H., Möckel, S.C., Gislason, S.R. (2024b) Direct evidence of CO₂ drawdown through enhanced weathering in soils, *Geochemical Perspective Letters* v30, 7-12.
- Lippincott, E.R., Van Valkenburg, A., Weir, C.E. and Bunting, E.N. (1958) Infrared Studies on Polymorphs of Silicon Dioxide and Germanium Dioxide. *Journal of Research of the National Bureau of Standards*, 61 (1), 2885
- Lovley DR, Phillips EJP (1988) Novel mode of microbial energy metabolism: organic carbon oxidation coupled to dissimilatory reduction of iron or manganese. *Appl Environ Microbiol* 54:1472-1480
- Martin, S., Toffolo, L., Moroni, M., Montorfano, C., Secco, L., Agnini, C., Nimis, P., Tumiati, S. (2017) Siderite deposits in northern Italy: Early Permian to Early Triassic hydrothermalism in the Southern Alps. *Lithos* 284–285, 276–295.
- McMillan, S.G., Schwertmann, U. (1998) Morphological and genetic relations between siderite, calcite and goethite in a Low Moor Peat from southern Germany. *European Journal of Soil Science*, 49: 283-293.
- Moosdorf, N., Renforth, P., Hartmann, J. (2014) Carbon dioxide efficiency of terrestrial enhanced weathering. *Environ Sci Technol* 48, 4809–4816.
- Morton, R.L., Nebel, M.L. (1984) Hydrothermal alteration of felsic volcanic rocks at the Helen siderite deposit, Wawa, Ontario. *Econ. Geol.* 79, 1319–1333.
- Parkhurst, D.L., Appelo, C.A.J. (1999) User's Guide to PHREEQC (Version 2)— A Computer Program for Speciation, Batch-Reaction, One-Dimensional Transport, and Inverse Geochemical Calculations., U.S. Geological Survey, Water Resources Investigations Report 99-4259, Washington DC.
- Postma, D. (1980) Formation of siderite and vivianite and the pore-water composition of a Recent bog sediment in Denmark. *Chem. Geol.* 31, 225–244.
- Qiu, X., Thompson, J.W., Billinge, S.J.L. (2004) PDFgetX2: a GUI-driven program to obtain the pair distribution function from X-ray powder diffraction data. *J. Appl. Cryst.* 37, 678.
- Reershemius, T., Kelland, M.E., Jordan, J.S., Davis, I.R., D'Ascanio, R., Kalderon-Asael, B., Asael, D., Suhrhoff, T.J., Epihov, D.Z., Beerling, D.J., Reinhard, C.T., Planavsky, N.J. (2023) Initial validation of a soil-based mass-balance approach for empirical monitoring of enhanced rock weathering rates. *Environ. Sci. Technol.* 57, 19497-19507.
- Saikia, B.J., Parthasarathy, G. and Sarmah, N.C. (2008) Fourier transform infrared spectroscopic estimation of crystallinity in SiO₂ based rocks. *Bulletin of Materials Science*, 31, 775-779
- Scherrer, P. (1918) Bestimmung der Größe und der inneren Struktur von Kolloidteilchen mittels Röntgenstrahlen, *Nachrichten von der Gesellschaft der Wissenschaften zu Göttingen, Mathematisch-Physikalische Klasse*, Volume 1918, 98-100
- Schoeneberger, P.J., D.A. Wysocki, E.C. Benham, and Soil Survey Staff (2012) Field book for describing and sampling soils, Version 3.0. Natural Resources Conservation Service, National Soil Survey Center, Lincoln, NE.

Smrčok, L., Langer, V., Krestan, J. (2006) γ -Alumina: a single-crystal X-ray diffraction study, *Acta Crystallographica*, C62, i83-i84

Snæbjörnsdóttir, S.O. Gislason, S.R., Galeczka, I.M., Oelkers, E.H. (2018) Reaction path modelling of in-situ mineralisation of CO₂ at the CarbFix site at Hellisheidi, SW-Iceland, *Geochimica et Cosmochimica Acta* 220, 348-366

Sparks, N.H.C., Mann, S., Bazylinski, D.A., Lovley, D.R., Jannasch, H.W., Frankel, R.B. (1990) Structure and morphology of magnetite anaerobically-produced by a marine magnetotactic bacterium and a dissimilatory iron-reducing bacterium. *Earth Planet Sci Lett* 98:14-22.

Thommes, M., Keneko, K., Neimark, A.V., Olivier, J.P., Rodriguez-Reinoso, F., Rouquerol, J., Sing, K.S.W. Physisorption of Gases, with special reference to the evaluation of surface area and pore size distribution (IUPAC Technical Report). *Pure Appl. Chem.* 2015, 87, 1051–1069, doi:10.1515/pac-2014-1117.

U.S. Environmental Protection Agency, 1998. MINTEQA2/PRODEFA2, A Geochemical Assessment Model for Environmental Systems: User Manual Supplement for Version 4.0., Athens, Georgia.

Viana, R.B., da Silva, A.B.F. Pimentel, A.S. (2012): Infrared Spectroscopy of Anionic, Cationic, and Zwitterionic Surfactants, *Advances in Physical Chemistry*, Vol. 2012, 14p.

Vicca, S., Goll, D.S., Hagens, M., Hartmann, J., Janssens, I.A., Neubeck, A., Peñuelas, J., Poblador, S., Rijnders, J., Sardans, J., Struyf, E., Swoboda, P., van Groenigen, J.W., Vienne, A., Verbruggen, E. (2022) Is the climate change mitigation effect of enhanced silicate weathering governed by biological processes? *Global Change Biology* 28, 711–726.

5 Paper IV - Stability of iron minerals in Icelandic peat areas and transport of heavy metals and nutrients across oxidation and salinity gradients – a modelling approach

Tobias Linke, Sigurður Reynir Gíslason

Published 2018 in Energy Procedia 146, 30-37.

doi.org/10.1016/j.egypro.2018.07.005



International Carbon Conference 2018, ICC 2018, 10–14 September 2018, Reykjavik, Iceland

Stability of iron minerals in Icelandic peat areas and transport of heavy metals and nutrients across oxidation and salinity gradients – a modelling approach

Tobias Linke^{a,*}, Sigurður Reynir Gíslason^a

^aUniversity of Iceland, Sturlugata 7, 101 Reykjavik, Iceland

Abstract

The storage of carbon, metals and nutrients in peat lands at high latitude is sensitive to climate- and land usage changes. This work shows that the thermodynamically most stable iron phases in Icelandic peat areas, like hematite or magnetite do not form, but rather the metastable ferrihydrite, which forms in abundance. Model calculations suggest that this ferrihydrite is able to adsorb high concentrations of natural derived heavy metals (Pb, As, Cr, Cu) and nutrients (P). If this ferrihydrite comes in contact with the oceans, these elements will be released through ferrihydrite-seawater interaction. This process may have significant effects to the chemistry of the near shore environments if ferrihydrite transport to the oceans increase due to future increased flooding and sea level rise.

Copyright © 2018 Elsevier Ltd. All rights reserved.

Selection and peer-review under responsibility of the publication committee of the International Carbon Conference 2018.

Keywords: Iron oxides; ferrihydrite; metal transport; peat; Iceland

1. Introduction

Peat lands cover huge areas in the sub-polar region and store vast amounts of organic carbon [1]. Their soil waters are reduced and rich in dissolved carbon, metals and nutrients [2,3]. Peat lands buffer natural floods as well as metal- and nutrient-fluxes to the oceans [2]. These fluxes are probably affected by climate change and man-made drainage channels. The overall objective of this project is to define the *in situ* mineralogy and soil water composition in Icelandic peat under conditions of high dust fluxes and their evolution along oxidation, pH and salinity gradients. The

* Corresponding author. Tel.: +354-525-5414

E-mail address: tol5@hi.is

dust is mostly composed of basaltic glass and is the main source of the dissolved metals, and tends to increase the pH and alkalinity of the soil solutions when it dissolves [4, 5]. Icelandic soils are reported to contain up to 8 wt. % ferrihydrite ($\text{Fe}_{10}\text{O}_{14}(\text{OH})_2$), typically estimated with ammonium oxalate extraction methods [6], whereas other thermodynamically more stable secondary iron phases are absent [7]. However, most of the Icelandic rivers are of drinking water quality; the concentrations of toxic metals are in most cases below the drinking water quality guidelines published by the World Health Organization [8].

Some rivers and soil waters have high dissolved and particulate iron content, as evidenced by chemical analysis and commonly observed as red precipitates. The importance of these widely observed iron phases and their role in heavy metals and nutrients transport from within the soil until reaching the ocean, across oxygen, pH and salinity gradients, is not yet fully understood. Through geochemical modelling, we attempt to get insight into this process.

Here we present: 1) the predominant fields of the metastable iron phases along pH, Eh, alkalinity and dissolved Fe gradients and 2) a model of the adsorption and desorption of metals and nutrients on ferrihydrite surfaces along an Eh and salinity gradient. The modelling was constrained by reported chemistry of soil waters under reduced conditions within Icelandic peat [9]. The adsorption-desorption modelling mimics the mechanical transport of ferrihydrite surfaces saturated with adsorbed metals and nutrients to the ocean and its eventual interaction with ocean waters.

To understand these adsorption-desorption processes and transport along various gradients, the identification and characterization of the mineral phases in the soil as well as the precipitates in the drainage channels is required. This will be the focus of future studies.

2. Methods

2.1. Geochemical modelling

The stability of various iron mineral phases and dissolved species were predicted using PHREEQC Interactive 3.3.8.11728 [10] together with its minteq.v4 database [11] after adding data for green rust carbonate taken from Drissi et al. [12]. The calculations include the chemical analysis of different soil water samples from West-Iceland containing major and trace elements, alkalinity, pH as well as the reference temperature during the pH measurements [9].

In addition to PHREEQC and the databases described above, the graphical output program PhreePlot [13] was used to illustrate the stability relations between the iron phases to predict the dominant solid phase or aqueous species as a function of pH and Eh at 25 °C. Results are achieved by a simple looping feature, which can either calculate each single point in the diagram by a 'grid' approach or track internal boundaries via a 'hunt and track' approach. While the 'hunt and track' approach is faster, it also makes the assumption that all fields can be delineated by tracking the boundaries starting from a domain boundary. In contrast, the 'grid' approach calculates the dominating phase for each defined point. [13]

The diagrams in Fig. 1 and 2 are calculated for a pH range from 4 to 10 covering the most common pH range in natural waters [14]. All calculations are limited by the stability of water under oxidized conditions ($p\text{O}_2 > 0.21$ atm) and methane ($p\text{CH}_4 > 1$ atm) under reduced conditions (the lower part of the diagrams). The predominance diagrams were not extended to the lower stability line of water ($p\text{H}_2 > 1$ atm), which lies below the methane stability field, because this would require an open system where the methane could degas from solution to keep the partial pressure below 1 atm.

For the study of transport across Eh, pH and salinity gradients, the soil solution is specified (Table 1) and then equilibrated with O_2 at atmospheric pressure to simulate the oxidation of the soil solution when in contact with the atmosphere. In addition, ferrihydrite is allowed to precipitate and then used as a surface for adsorption and desorption. The concentration of weak and strong adsorption sites are maintained as the default values of PHREEQC: 0.2 mol weak sites per mol ferrihydrite with a surface area of 5.33×10^4 m²/mol and 0.5×10^{-2} mol of strong sites per mol ferrihydrite. It is then assumed that the adsorption-desorption process on ferrihydrite surfaces attained equilibrium at 25 °C and atmospheric O_2 pressure.

The oxidized solution and the precipitated ferrihydrite, as a surface adsorbent, are mixed with seawater during a second reaction step using the composition published by Stefánsdóttir et al. [15] for North Atlantic seawater. The mixing ratio of the oxidized soil solution and the seawater is varied from 3:1 to 1:100.000 in the models to simulate

the effect of increasing fluid mixing. All element concentrations are then corrected for the dilution during mixing and the final values are normalized to 100 % for each element compared to the original soil solution as shown in Fig. 3.

2.2. Soil water sampling and analysis

The soil solution used for calculations in this study (Table 1) was collected in the peat area in Hvammsendi on the eastern shore of Hvalfjörður in western Iceland [9]. The sample 98-JA086 was collected on the 8th of September 1998 [9]. This samples was collected from a hole made using a stainless steel auger with 2.5 cm diameter at 45 ° to a depth of 50 cm. A soil solution sampler used was made of PTFE (Teflon) and quartz (Prenart, Denmark) was installed as reported in detail by Sigfusson et al. [3]. The soil solution was analyzed for pH, alkalinity (by titration with 0.1 M HCl), major anions and cations (by ion chromatography and inductively coupled plasma atomic emission spectrometry), trace elements (by High Resolution Inductively Coupled Plasma Mass Spectrometry) and nutrients (by autoanalyzer) as described by Sigfusson et al. [5] and Gislason et al. [9]. The composition of this soil solution is given in Table 1. This sample represents a typical soil water composition from natural peat areas in western Iceland.

Table 1: pH, alkalinity and concentrations of nutrients, major and trace elements of soil solution 98-JA086, used for the geochemical model

| Major constituents | Concentration per liter | Nutrients | Concentration nmol/l | Trace elements | Concentration nmol/l | Trace elements | Concentration nmol/l |
|--------------------|-------------------------|-----------------|----------------------|----------------|----------------------|----------------|----------------------|
| pH | 6.39 | NH ₄ | 0.746 | Al | 634 | Hg | 0.02 |
| alkalinity | 1.170 meq | NO ₂ | 0.086 | As | 3.08 | Mn | 7010 |
| Ca | 350 μmol | NO ₃ | 0.145 | Ba | 20.5 | Mo | 1.21 |
| Cl | 810 μmol | PO ₄ | 0.127 | Cd | 0.09 | Ni | 44.0 |
| F | 2.82 μmol | | | Co | 60.6 | Pb | 0.12 |
| Mg | 320 μmol | | | Cr | 2.25 | Sr | 188 |
| Na | 900 μmol | | | Cu | 4.78 | Ti | 3.46 |
| SiO ₂ | 480 μmol | | | Fe | 138000 | Zn | 42.1 |
| SO ₄ | 240 μmol | | | | | | |

3. Results

Based on the soil water composition shown in Table 1, predominance diagrams for the most stable iron phases were calculated (Fig. 1). The iron concentrations in Fig. 1 were set at 50 and 500 μmol/l Fe to cover variations in the measured soil water samples reported in Gislason et al. [9]. The most thermodynamically stable iron minerals are hematite (α -Fe₂O₃) and magnetite (Fe₃O₄). At low pH and at high reducing conditions the aqueous Fe²⁺ specie dominates the predominance diagram. By decreasing the iron concentration to 50 μmol/l pyrite (FeS₂) becomes present (Fig. 1, right) in a narrow field covering most of the pH range at very reduced conditions right above the stability line for methane (pCH₄ > 1 atm). These results are in agreement with the findings of Rickard and Luther [16] for seawater conditions.

Despite these results, soil waters and associated minerals do not reach an equilibrium state under natural conditions [17]. The reaction rates are the limiting factors for the formation of iron oxides like hematite and magnetite from solution. Precipitation of ferrihydrite from Fe²⁺/Fe³⁺ bearing solutions is favored over the formation of goethite (FeO(OH) or hematite [18]. A wide range of literature shows that ferrihydrite is the most common iron phase in natural soils, soil water and surface water [7, 16,18].

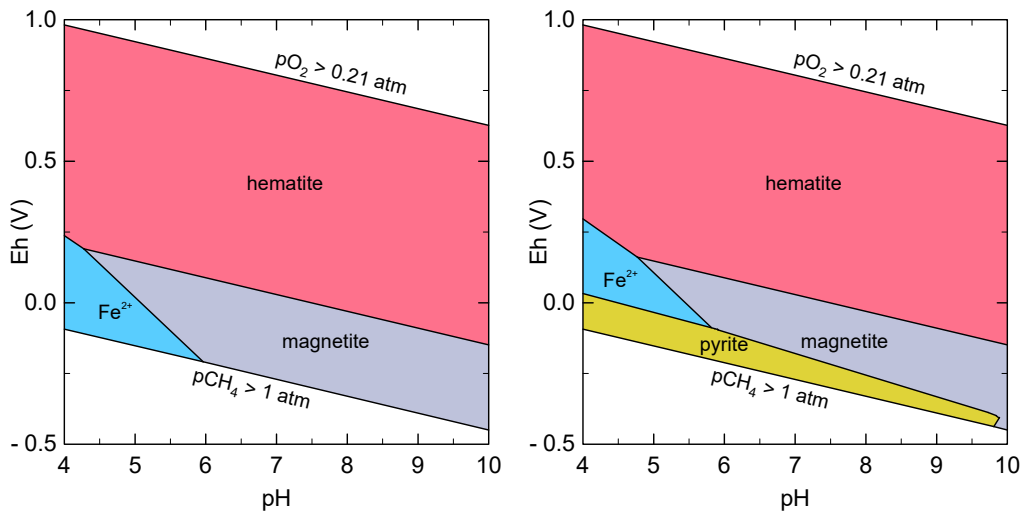


Fig. 1: Predominance diagram of the most stable iron phases in natural soil waters with 500 $\mu\text{mol/l}$ Fe (left) and 50 $\mu\text{mol/l}$ Fe (right), calculated with PHREEQC assuming equilibrium state (see text).

Ferrihydrite transforms slowly into goethite and is therefore the most common but metastable iron phase [19, 20]. Hence, the pH Eh diagram showing hematite and magnetite as the dominant iron phases cannot be used as a guide for natural processes, especially at low temperature in the sub-polar region.

By prohibiting the kinetically hindered mineral phases - hematite, magnetite, goethite and maghemite ($\gamma\text{-Fe}_2\text{O}_3$) - to form in the model, we constructed a new predominance diagram showing the metastable but natural occurring iron phases. The robustness of the model was tested by varying the total dissolved iron and alkalinity concentrations within reasonable range based on chemical analysis of soil water in western Iceland [9]. As shown in Fig. 2, all pH Eh diagrams are dominated by the presence of ferrihydrite over the whole pH range at oxidizing and moderate reducing conditions. In addition, iron carbonates can form at $\text{pH} > 7.5$ at very reduced conditions. They are represented by siderite (FeCO_3) and green rust carbonate (GR), a mixed $\text{Fe}^{2+} \text{Fe}^{3+}$ metal hydroxide phase with intercalated carbonate anions ($\text{Fe}_6(\text{OH})_{12}\text{CO}_3$). It is reported that green rust phases were found in soils and sediments under suboxic and anoxic conditions [21, 22, 23]. While the variation of alkalinity shows little effect on the dominant phases, a decrease in the iron concentration leads to the formation of pyrite under most reducing conditions. Our predominance diagrams are in good agreement with published data [16, 19].

The superimposed data for peat bogs (shaded area in the upper left diagram, Fig. 2) from Baas Becking et al. [14] show, that the pH-Eh conditions in peats can vary substantially and cover nearly the whole predominance diagram. Therefore, the formation of all shown phases could be possible under natural conditions. Natural peat bogs can also exhibit very low reducing conditions reaching down below CH_4 degassing pressure ($\text{pCH}_4 > 1 \text{ atm}$). Presently, there is very limited data about the occurrence of siderite in Icelandic soils [24]. As described by the author, siderite was found only in very small amounts and with probably negligible importance [24]. To our knowledge, to date there is no published data about any green rust phases in Icelandic soils. The pyrite predominance field disappears when decreasing the dissolved sulfur concentration by a factor of 5 or more in the modeled solution. At alkaline pH, siderite takes predominance over pyrite, whereas at lower pH aqueous Fe^{2+} dominates, similar to what can be observed at higher iron concentrations (Fig. 2, left side). The predominance fields of green rust and ferrihydrite are not affected by these changes. The models show that the pyrite stability is mostly effected by the Fe:S ratio, whereas alkalinity has less effect on the predominance field of pyrite in the pH-Eh diagrams. A change of the Fe and S concentrations while keeping the total dissolved Fe : S ratio constant does not affect the extent of the pyrite field.

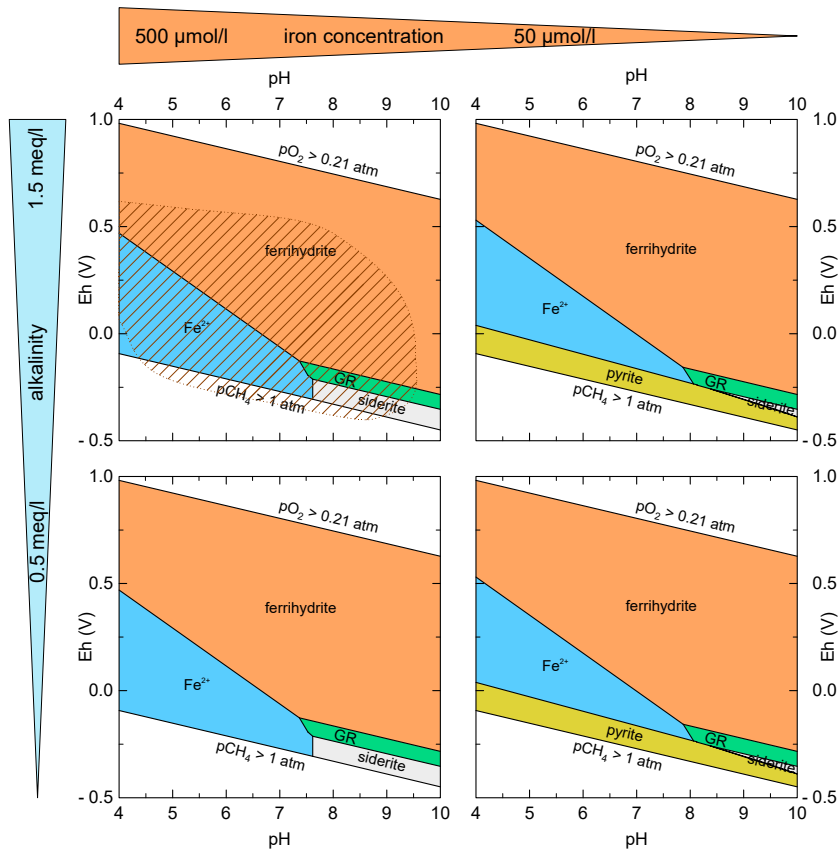


Fig. 2. Predominance diagrams for metastable iron phases under varying iron and carbonate concentrations, shaded field in the upper left diagram represents common pH Eh conditions in peat bogs (data from Baas Beeking et al. [14]).

Based on the observation that ferrihydrite covers most of the predominance diagram, as shown in Fig. 2, and is abundant in Icelandic peat areas [7], we modeled the oxidation of the soil solution in Table 2 to ferrihydrite and its effect on other dissolved species. Furthermore, the stepwise mixing of the newly formed ferrihydrite and its oxidized soil water with seawater simulates the transport of the ferrihydrite by water to the ocean and a subsequent mixing in coastal waters across a salinity gradient. Our model shows that oxidation of a Fe^{2+} rich soil water leads to the formation of ferrihydrite, which then acts as a surface for adsorption processes. The initial oxidation of the fluid leads to a decrease of the fluid concentration of (Fig. 3, circles): Ni by 4.1 %, Cd by 5.0%, Zn by 15.7 %, Cu by 92.8 %, Cr by 95.9%, P by 99.7 %, Pb by 99.8 %, and As by 99.8 %. Elements whose concentration changes less than 1 % during the simulations are not shown in the diagram. After the equilibration of the reduced soil solution (Table 1) with atmospheric O_2 ($p\text{O}_2 = 0.21 \text{ atm}$), the mixing of this fluid with seawater was simulated in 41 steps covering oxidized soil water to seawater ratios from 3:1 to 1:100,000 – see Fig. 3.

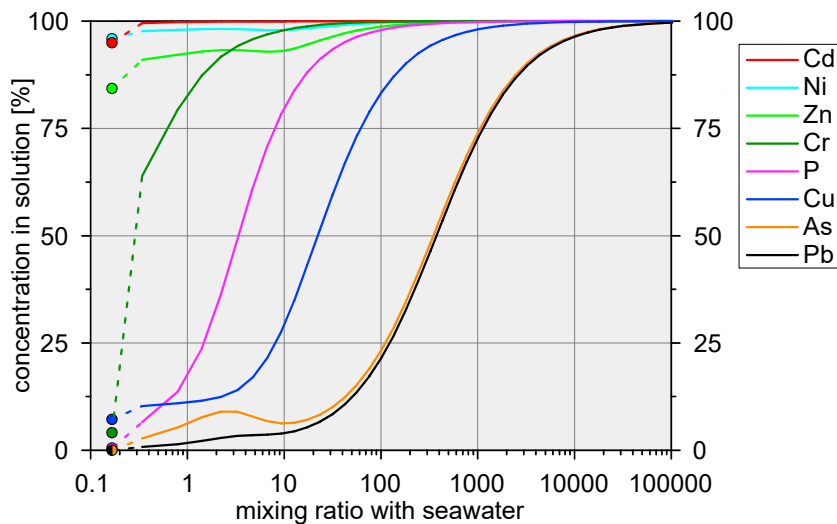


Fig. 3. Modeled decrease in the dissolved concentration of heavy metals and phosphate in oxidized soil solution in the presence of ferrihydrite (initial values as circles) and during its mixing with seawater (solid lines).

By mixing the oxidized peat water with seawater, the different adsorbed constituents are released from the ferrihydrite. Cadmium is fully released during the first mixing step, followed by Ni, Zn, Cr and P at a ratio of 1:100, whereas Cr and P was initially nearly completely adsorbed. Copper is fully desorbed at a ratio of 1:5'000, the release during the first steps is relatively low. Arsenic and lead release requires the greatest quantity of seawater, 25 % of each element is released at a ratio of 1:100 and 75 % at 1:1000. At a mixing ratio of 1:100,000 As and Pb are fully desorbed, whereas ferrihydrite is still supersaturated with respect to the aqueous solution. Based on calculations from Jones et al. [25] this mixing ratio could occur within the first 10 to 15 km from the river inlet into the ocean.

4. Discussion and conclusions

Based on geochemical modelling, we gained insight into the predominance of iron phases within Icelandic peat soils and their effect on heavy metal and nutrient retention upon oxidation and a subsequent release in costal water. Note that our models assume equilibrium between the solid phases and aqueous solutions, which may not be attained under natural conditions [16, 17]. Also, the interaction of other phases, especially natural organic matter, are not considered in our models. Models for adsorption of metals to humic and fulvic substances suggest strong Cu adsorption onto these compounds. Therefore, the Cu concentration in aqueous solution might be lower than in our model calculations. Additionally, the model is only capable of simulating the adsorption to pure ferrihydrite. Incorporation of heavy metals by coprecipitation cannot be simulated or any modification of the adsorption behavior of ferrihydrite by its interaction with other natural occurring phases or bacteria.

Our results indicating the high retention of phosphate, arsenate and lead by ferrihydrite are in good agreement with published data [26, 27, 28]. Poorly crystalline ferrihydrite, which has a high surface area, shows high retention capacity, but also so too do soils with high ferrihydrite content [29]. Therefore, the release of the adsorbed phases directly from the soil should be investigated.

The work of Hawley et al. [30] proposed that the export of iron(oxy)hydroxides with surface adsorbed constituents and their transport to the ocean is negligible in non-glacial Icelandic rivers. This conclusion is in contrast to the calculations presented in this report. Nevertheless, even if the transport and release of heavy metals to the ocean is limited at present, this process might become more important due to future flooding events or sea level rise.

Acknowledgements

This project has received funding from the European Union's Horizon 2020 research and innovation programme under the Marie Skłodowska-Curie grant agreement No 675219.

The authors thank Eydís S. Eiríksdóttir and Matthildur B. Stefánsdóttir for sampling as well as Norurál hf. and Íslenska járnblendifélagið hf. for providing the soil water data used in this work as well as the publication committee of the International Carbon Conference 2018 for reviewing this article.

References

- [1] Joosten H., and J. Couwenberg. "Peatlands and carbon" in: Parish F., A. Sirin, D. Charman, H. Joosten, T. Minayeva, and M. Silvius. (eds). "Assessment on peatlands, biodiversity and climate change: Main Report" Global Environment Centre, Kuala Lumpur and Wetlands International Wageningen (2008).
- [2] Barthelmes A., J. Couwenberg, M. Risager, C. Tegetmeyer, and H. Joosten. "Peatlands and Climate in a Ramsar context - A Nordic-Baltic Perspective" Nordic Council of Ministers, TemaNord 2015:544 (2015), doi: 10.6027/TN2015-544.
- [3] Sigfússon B., G.I. Paton, and S.R. Gislason. "The impact of sampling techniques on soil pore water carbon measurements of an Icelandic Histic Andosol" *Science of the Total Environment* 369 (2006): 203-219, doi: 10.1016/j.scitotenv.2006.01.012.
- [4] Stefánsson A., and S.R. Gislason. "Chemical weathering of basalts, southwest Iceland: Effect of rock crystallinity and secondary minerals on chemical fluxes to the ocean" *American Journal of Science* 301 (2001): 513-556, doi: 10.2475/ajs.301.6.513.
- [5] Sigfússon B., S.R. Gislason, and G.I. Paton. "Pedogenesis and weathering rates of a Histic Andosol in Iceland: Field and experimental soil solution study" *Geoderma* 144 (2008): 572-592, doi: 10.1016/j.geoderma.2008.01.014.
- [6] Parfitt R.L., and C.W. Childs. "Estimation of forms of Fe and Al: A review, and analysis of contrasting soils by dissolution and Moessbauer methods" *Australian Journal of Soil Research* 26 (1988): 121–144, doi: 10.1071/SR9880121.
- [7] Arnalds O. "Volcanic soils of Iceland" *Catena* 56 (2004): 3-20, doi: 10.1016/j.catena.2003.10.002.
- [8] World Health Organization. "Guidelines for drinking-water quality, fourth edition, incorporating the first addendum" Geneva (2017), Licence: CC BY-NC-SA 3.0 IGO.
- [9] Gislason S.R., E.S. Eiríksdóttir, M.B. Stefánsdóttir, and A. Stefánsson. "Vatnsrannsóknir í nágrenni iðnaðarsvæðisins á Grundartanga og í Kjós" (Chemistry of surface and soil waters in the vicinity of the industrial center at Grundartangi, SW Iceland), Final report in Icelandic (1999).
- [10] Parkhurst D.L., and C.A.J. Appelo. "Description of input and examples for PHREEQC version 3—A computer program for speciation, batch-reaction, one-dimensional transport, and inverse geochemical calculations" in U.S. Geological Survey techniques and methods, modeling techniques, groundwater, Denver, Colorado, U.S. Geological Survey (2013), available online at <https://pubs.usgs.gov/tm/06/a43/>.
- [11] U.S. Environmental Protection Agency. "MINTEQA2/PRODEFA2. A geochemical assessment model for environmental systems: User manual supplement for version 4.0" Athens, Georgia, National Exposure Research Laboratory, Ecosystems Research Division (1998), Revised September 1999.
- [12] Drissi S.H., P. Refait, M. Abdelmoula, and J.M.R. Génin. "The preparation and thermodynamic properties of Fe(II)-Fe(III) hydroxide-carbonate (green rust 1); Pourbaix diagram of iron in carbonate containing aqueous media" *Corrosion Science* 37 (1995): 2025-2041, doi: 10.1016/0010-938X(95)00096-3.
- [13] Kinniburgh D.G., and D.M. Cooper. "PhreePlot – Creating graphical output with PHREEQC" available at <http://www.phreeplot.org/>, original date June 2011, last updated November 1, (2016).
- [14] Baas Becking L.G.M., I.R. Kaplan, and D. Moore. "Limits of the natural environment in terms of pH and oxidation-reduction potential" *Journal of Geology* 68 (1960): 243-284.
- [15] Stefánsdóttir M.B., and S.R. Gislason. "The erosion and suspended matter/seawater interaction during and after the 1996 outburst flood from the Vatnajökull Glacier, Iceland" *Earth and Planetary Science Letters* 237 (2005): 433–452, doi: 10.1016/j.epsl.2005.07.002.
- [16] Rickard D., and W.L. Luther. "Chemistry of iron sulfides" *Chemical Reviews* 107(2) (2007): 514-562, doi: 10.1021/cr0503658.
- [17] Stefánsson A., S. Arnórsson, and A.E. Sveinbjörnsdóttir. "Redox reactions and potentials in natural waters at disequilibrium" *Chemical Geology* 221 (2005): 389-311, doi: 10.1016/j.chemgeo.2005.06.003.
- [18] Legrand L., L. Mazerolles, and A. Chaussé. "The oxidation of carbonate green rust into ferric phases: solid-state reaction or transformation via solution" *Geochimica et Cosmochimica Acta* 68 (2004): 3497-3507, doi: 10.1016/j.gca.2004.02.019.
- [19] Schwertmann U., and R.M. Cornell. "Iron oxides in the Laboratory: Preparation and Characterization" VCH Publishers, New York (1991) doi: 10.1002/9783527613229.
- [20] Jambor J.L., and J.E. Dutrizac. "Occurrence and constitution of natural and synthetic ferrihydrite, a widespread iron oxyhydroxide" *Chemical Reviews* 98 (1998): 2549-2585, doi: 10.1021/cr970105t.
- [21] Génin J.M.R., P. Refait, L. Simon, and S.H. Drissi. "Preparation and Eh-pH diagrams of Fe(II)-Fe(III) green rust compounds; hyperfine interaction characteristics and stoichiometry of hydroxy-chloride, -sulphate and -carbonate" *Hyperfine Interactions* 111 (1998): 313-318, doi: 10.1023/A:1012638724990.

- [22] Trolard F., J.M.R. Génin, M. Abdelmoula, G. Bourrié, B. Humbert, and A. Herbillon. "Identification of a green rust mineral in a reductomorphic soil by Mössbauer and Raman spectroscopies" *Geochimica et Cosmochimica Acta* 61 (1997): 1107–1111, doi: 10.1016/S0016-7037(96)00381-X.
- [23] Bearcock J.M., W.T. Perkins, E. Dinelli, and S.C. Wade. "Fe(II)/Fe(III) 'green rust' developed within ochreous coal mine drainage sediment in South Wales, UK" *Mineralogical Magazine* 70 (2006): 731–741, doi: 10.1180/0026461067060360.
- [24] Gudmundsson T. "Pedological Studies of Icelandic Peat Soils" PhD thesis, Department of Soil Science, University of Aberdeen, United Kingdom (1978).
- [25] Jones M.T., S.R. Gislason, K.W. Burton, C.R. Pearce, V. Mavromatis, P.A.E. Pogge von Strandmann, and E.H. Oelkers. "Quantifying the impact of riverine particulate dissolution in seawater on ocean chemistry" *Earth and Planetary Science Letters* 395 (2014): 91–100, doi: 10.1016/j.epsl.2014.03.039.
- [26] Rout K., M. Mohapatra, and S. Anand. "2-Line ferrihydrite: synthesis, characterization and its adsorption behaviour for removal of Pb(II), Cd(II), Cu(II) and Zn(II) from aqueous solutions" *Dalton Transactions* 41 (2012): 3302-3312, doi: 10.1039/C2DT11651K
- [27] Al Mamun A., M. Morita, M. Matsuoka, and C. Tokoro. "Sorption mechanisms of chromate with coprecipitated ferrihydrite in aqueous solution" *Journal of Hazardous Materials* 334 (2017): 142–149, doi: 10.1016/j.jhazmat.2017.03.058.
- [28] Alarcón R., J. Gáviria, and B. Dold. "Liberation of Adsorbed and Co-Precipitated Arsenic from Jarosite, Schwertmannite, Ferrihydrite, and Goethite in Seawater" *Minerals* 4 (2014): 603-620, doi: 10.3390/min4030603.
- [29] Nanzyo M., S. Shoji, and R. Dahlgren. "Physical characteristics of volcanic ash soils" in: Shoji S., M. Nanzyo, and R.A. Dahlgren (eds.). "Volcanic ash soils. Genesis, properties and utilization" *Developments in Soil Science*. Elsevier, Amsterdam (1993): 189–207.
- [30] Hawley S.M., P.A.E. Pogge von Strandmann, K.W. Burton, H.M. Williams, and S.R. Gislason. "Continental weathering and terrestrial (oxyhydr)oxide export: Comparing glacial and non-glacial catchments in Iceland" *Chemical Geology* 462 (2017): 55-66, doi: 10.1016/j.chemgeo.2017.04.026.

6 Paper V - Water-air-CO₂-flux changes after damming rivers loaded with suspended basaltic particles

Tobias Linke, Eydís Salóme Eiríksdóttir, Guðrún Nína Petersen, Sigurður Reynir Gíslason

To be submitted to Water research.

Water-air-CO₂-flux changes after damming rivers loaded with suspended basaltic particles

Linke^{1*}, T., Eiriksdottir², E.S., Petersen³, G.N., Gislason¹, S.R.

¹ Institute of Earth Sciences, University of Iceland, Sturlugata 7, 102 Reykjavik, Iceland

² Hafrannsóknastofnun, Marine & Freshwater Research Institute, Fornubudir 5, 220 Hafnarfjordur, Iceland

³ Veðurstofa Íslands, Icelandic Meteorological Office, Bústaðavegi 7- 9, 105 Reykjavík, Iceland

*corresponding author: tol5@hi.is

To be submitted to "Water Research"

Highlights

- Dissolution of basalt in glacier melt waters leads to direct CO₂ uptake from the atmosphere
- The rate of surface normalized CO₂ uptake was governed by the CO₂ gradient across the water-air-interphase and windspeed
- Sub-zero temperature can result in ice cover, terminating water-air interactions
- Atmospheric CO₂ concentration puts an upper limit on the rate of CO₂ influx at fixed wind speed

Abstract:

The contribution of CO₂ emissions from reservoirs to the atmosphere is continuously increasing with rising energy demand. Therefore, it is important to quantify the emissions and define the rate determining mechanism for degassing or uptake of CO₂ in man-made reservoirs. Here we present results from two reservoirs in Iceland over a total time span of 16 years. The partial pressure of CO₂ within the Háslón reservoir, fed by meltwater loaded with suspended basaltic particles at the northern edge of the Vatnajökull glacier NE-Iceland, was considerably less than the CO₂ pressure of the atmosphere during the years 2008-2013. The calculated specific direct uptake of CO₂ from the atmosphere into Háslón was $121 \pm 67.9 \text{ gCO}_2 \text{ m}^{-2} \text{ yr}$ during the ice-free period of 6 months and resulted in more than 5000 tonnes of CO₂ transferred from the atmosphere annually. The rate of uptake was governed by

the CO₂ gradient across the water-air-interphase and windspeed but less by temperature. However, temperature will affect water-rock interactions within the water body and sub-zero temperature can result in ice cover, terminating water-air interactions. Atmospheric CO₂ concentration dictates the upper limit of the CO₂ influx rate at fixed wind speed.

The mixing of Háslón reservoir water with the CO₂ emitting Lagarfljót reservoir downstream resulted in a decrease of the CO₂ emission from Lagarfljót, with 5335 t CO₂ yr⁻¹ before and 1670 t CO₂ yr⁻¹ after the damming and mixing. These annual CO₂ emissions from Lagarfljót reservoir were equal to 28 % of the total annual dissolved inorganic carbon (DIC) flux to the ocean but decreased to 4.9 % after the damming. The direct CO₂ uptake by the Háslón reservoir, as a percentage of the Lagarfljót DIC flux, was equal to 15 % for the years 2008-2013. This study shows that dissolution of basalt in glacier melt waters leads to direct CO₂ uptake from the atmosphere, which can potentially be utilised for future carbon removal from the atmosphere.

1. Introduction

The present 8 Gt CO₂ yr⁻¹ release of CO₂ from Earth's terrestrial surface waters to the atmosphere is a major contributor to the short-term carbon cycle (Raymond et al., 2013). This flux from surface waters is much larger than the 2 Gt CO₂ yr⁻¹ degassing from the Earth's crust and the 0.5 Gt CO₂ yr⁻¹ combined CO₂ drawdown from the atmosphere by weathering of silicates and carbonates on the continents (Gaillardet et al. 2019; Hartmann et al. 2009). According to Raymond and coworkers (2013), the majority of the CO₂ release from terrestrial surface waters is from wetlands. Furthermore, man-made drainage and burning of peat areas world-wide releases 2 to 3 Gt CO₂ yr⁻¹ to the atmosphere (Hooijer et al. 2006; Crump, 2017; Parish et al., 2008). Hence, a large fraction of the CO₂ degassing from terrestrial surface waters originates from organic matter decomposition in wetlands, and most likely due to draining of wetland soils worldwide. The contribution from lakes and reservoirs is estimated at 1.1 Gt CO₂ yr⁻¹ (Raymond et al. 2013).

Within the present study we quantify the water-air-CO₂ exchange through the surface of the Háslón reservoir constructed in 2003-2007, located at the northeastern edge of the Vatnajökull glacier, Iceland, and the water-air-CO₂ exchange before and after the modified downstream Lagarfljót reservoir (Fig. 1). This field site in NE-Iceland represents the extreme case where the reservoir waters are poor in suspended particulate organic matter but loaded

with reactive basaltic particles, capable of lowering the partial pressure of CO₂ in these waters via water-rock interactions, resulting in direct uptake of CO₂ from the atmosphere.

Here we report on, 1) the water chemistry and suspended material composition of the new Háslón reservoir in NE-Iceland, the outflow from the associated Kárahnjúkar power plant, and the down-stream Lagarfljót reservoir waters before and after mixing with the Háslón reservoir waters, 2) the measured air temperature and wind speed distribution at the Kárahnjúkar dam and the Lagarfljót reservoir at Egilsstaðir, before and after commission of the Kárahnjúkar dam, 3) the calculated in situ CO₂ partial pressure of the reservoir waters in comparison to the measured daily average CO₂ concentration in the atmosphere at the National Oceanic and Atmospheric Administration (NOAA) Stórhöfði South Iceland monitoring station, 4) the calculated CO₂-fluxes between these reservoir waters and the atmosphere during the sampling periods 1998-2003, and 2008-2013, and finally 5) a comparison of the water-air-fluxes with the combined dissolved inorganic carbon (DIC) river fluxes from these reservoirs to the ocean.

The chemistry of the river waters and their suspended material before the construction of the Kárahnjúkar dam and the Háslón reservoir during 2003 – 2007, were described in detail by Gislason et al. 2006; 2009; Eiriksdóttir et al., 2008; 2013, 2014; 2015; and Louvat et al. 2008 and furthermore by Eiriksdóttir et al., 2014; 2017 after the commission of the Kárahnjúkar power plant in November 2007, showing a doubling of the river discharge through the Lagarfljót reservoir at the Lagarfoss dam. Here we used this existing data to quantify the CO₂ water-air fluxes using additional climatological data and established modelling approaches to quantify the direct water-air-CO₂ fluxes, and to illuminate the rate regulating factors.

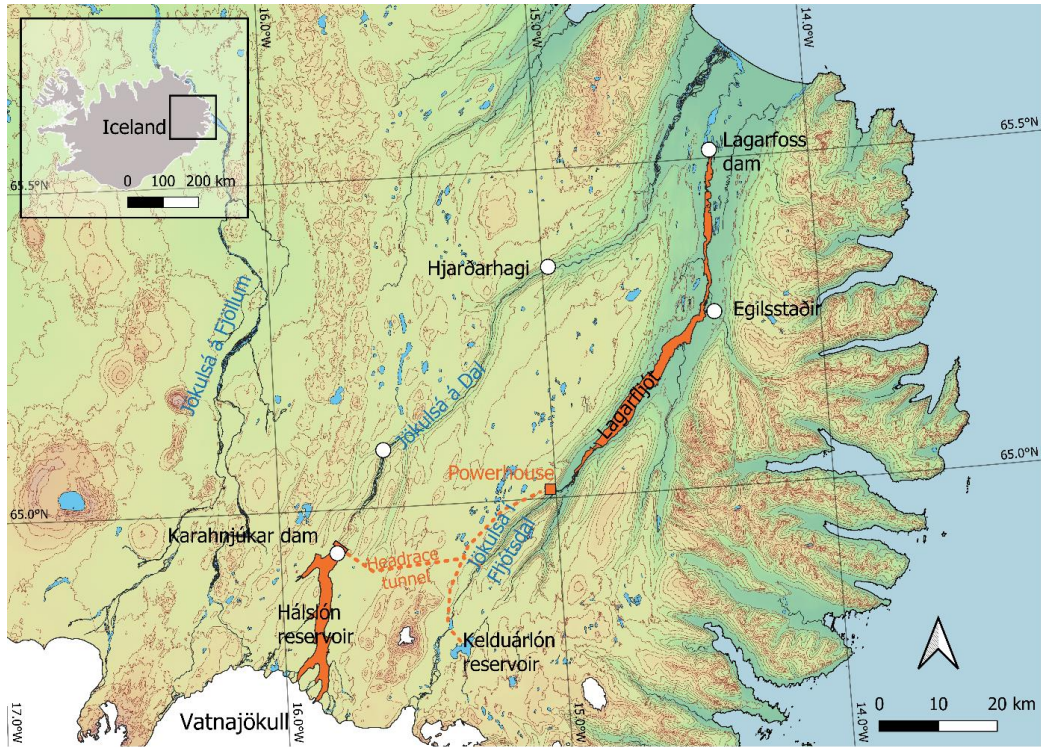


Fig. 1. Map showing the location of the two river catchments affected by the damming of the Jökulsá á Dal glacial river in Eastern Iceland, the location of the sampling sites (white filled circles), the Háslón reservoir (orange) created by the dam, the headrace tunnels (orange dashed curves), the Powerhouse (orange square), and the Lagarfljót reservoir downstream from the Powerhouse extending all the way down to the Lagarfoss dam. The Vatnajökull glacier is shown in white in the lower left corner. Weather stations are close to the Kárahnjúkar dam and Egilsstaðir (white circles). Map data from the National Land Survey of Iceland and Landsvirkjun, National Power Company of Iceland.

2. Methods

2.1. Field site

The location of the studied field site, which is affected by the damming of the Jökulsá á Dal glacial river in Eastern Iceland, is shown in Fig. 1. Accompanying the power plant construction in 2003-2007, the rivers have been monitored from 1998 to 2003, and after the damming from 2008 to 2013. Officially, the Kárahnjúkar power plant started commercial operation November 2nd, 2007. The Kárahnjúkar dam (Fig. 1) is the largest of its kind in Europe, 198 m high and 700 m long and the geographic surface area of the reservoir can reach up to 58.3 km² resulting in a total volume of 2.2 km³ (Leifsson et al., 2009). The reservoir is within 25 km of the northern edge of the Vatnajökull glacier (Leifsson et al., 2009;

Gunnarsson et al., 2014). The reservoirs maximum operational level is at 625 m above sea level (a.s.l.) (Leifsson et al. 2009). When exceeding this, the reservoir overflows into the old Jökulsá á Dal river channel, around 40 days each year during August to September (Fig. 1 and Fig. A1 in Appendix 1). The practical minimum operational water level is at 570 m a.s.l., reached in May each year (Fig. A1), when the reservoir becomes ice-free and the surface area is about 17 km² (Leifsson et al., 2009). If the Háslón reservoir reaches its minimum operational level, the power plant uses water from two other reservoirs, Kelduralón (Fig. 1) and Ufsarlón, situated in the catchment of the Jökulsá í Fljótssdal river.

The reservoir water is diverted from the Jökulsá á Dal river catchment into the Lagarfljót reservoir via a headrace tunnel to the Powerhouse (see Fig. 1), creating a 600 m vertical drop as the water flows through the Kárahnjúkar power plant. This water is then released into the Jökulsá í Fljótssdal river (normal water level ~25 m a.s.l., Leifsson et al. 2009) and eventually into the Lagarfljót reservoir. Its average water level at the Lagarfoss dam was at 19.9 m a.s.l. before the operation of the Kárahnjúkar dam (Axelsson 2012). The Lagarfljót reservoir is a 35 km long lake with a geographic surface area of 53 km², a maximum depth of 112 m, and a volume of 2.7 km³ (Hallgrímsson, 2005). The average discharge through the Kárahnjúkar headrace tunnel is 110 m³ s⁻¹ (Landsvirkjun, 2009), causing the average discharge from the Lagarfljót at Lagarfoss to double after the commissioning of the Kárahnjúkar power plant, November 2nd, 2007. Consequently, the water residence time in the Lagarfljót reservoir was halved, from one year to six months (Tómasson and Hardardóttir, 2001). The water level of the Lagarfljót reservoir rose by about 30 cm at the inlet of the reservoir and northward towards the town of Egilsstaðir (Fig. 1). North of the town the water level drops gradually and at the outlet at Lagarfoss the water level is 36 cm lower compared to the year 2004 due to modifications at the Lagarfoss outlet (Axelsson 2007).

These river catchments are partially glaciated, with glaciers covering 43 % and 6 %, respectively, of the catchments at Jökulsá á Dal and Lagarfljót above the monitoring sites in Hjarðarhagi and Lagarfoss (Fig. 1) before the installation of the Kárahnjúkar dam (Kardjilov, 2008). The glacier cover of the Háslón reservoir catchment is 78 % (Leifson et al. 2009). Every year after the Háslón reservoir fills up during late summer, and overflows via a spillway into the Jökulsá á Dal river channel for a few weeks, it dramatically changes the river discharge and the riverine concentration of suspended and dissolved material downstream of the reservoir (Eiriksdóttir et al., 2017).

2.2. Water sampling and analysis

The collection and analysis of samples was previously described by Eiriksdottir et al. (2013, 2014; 2015; 2017). Samples were collected throughout the year to account for seasonal changes on the chemical compositions of the rivers and the outlet from the power plant (Tables A1-5 and A7). Additionally, 21 samples, given in Tab. A6, were collected from the Háslón reservoir closest to its maximum depth at 64°56'24.24"N 15°47'32.46"W, at various depths in May 2008 through 80 cm thick ice (Fig. A3-4, Tab. A6) and by boat in August 2008 (Fig. A5). Again, in August 2009 from 5 m depth, and later that year in September as surface sample pulled in from the shore. One more surface sample was taken in August 2010. After that, samples were taken from a boat at various depths above the maximum depth of the reservoir at 64°56'29.28"N 15°47'40.56"W when water was overflowing the dam via the spillway in 2011, 2012 and 2013 (Fig A5). All these reservoir samples were collected with a Niskin sampler and treated in similar fashion as the river samples. Simultaneously, detailed temperature profiles from the surface and down to about 130-160 m depth were measured in 2008, 2011, 2012 and 2013 (Fig. A5 and Tab. A6 in the Appendix). A more detailed sampling description can be found in the supplementary material and the above cited literature.

2.3. Chemical speciation and CO₂ flux calculations

The flux F ($\text{mol m}^{-2} \text{s}^{-1}$) of slightly soluble nonreactive gases such as CO₂ across the air-water interface can be defined as the product of the gas transfer velocity k (m s^{-1}) and the concentration difference between the top and bottom of the liquid boundary layer (Wanninkof 2009).

$$F_{\text{CO}_2} = k (C_w - C_0) \quad (\text{eq.1})$$

where C_0 is the CO₂ concentration at the water surface and C_w is the CO₂ concentration of the well-mixed bulk fluid below (mol m^{-3}). Assuming a chemical equilibrium between the atmosphere and the water phase boundary, C_0 can be expressed as the product of the CO₂ concentration in air and the dimensionless Ostwald solubility coefficient α resulting in:

$$F_{\text{CO}_2} = k (C_w - \alpha C_{\text{atm}}), \quad (\text{eq.2})$$

F_{CO_2} is negative for a gas flux from the atmosphere to the water. Expressing equation 2 in terms of partial pressure of the gas in air and water results in:

$$F_{\text{CO}_2} = k K_{\text{H}}(p\text{CO}_{2\text{w}} - p\text{CO}_{2\text{atm}}) \quad (\text{eq.3})$$

where the *in situ* $p\text{CO}_{2w}$ and $p\text{CO}_{2atm}$ are the partial pressures (atm) of CO_2 in the well mixed bulk fluid, calculated with PHREEQC interactive software version 3.4.0 (Parkhurst and Appelo, 1999) using the minteq.v4.dat database (Allison et al., 1991; U.S. Environmental Protection Agency, 1998) and in the water surface film that is in equilibrium with the atmosphere, respectively (e.g., Alin et al., 2011). K_H is the temperature and salinity dependent CO_2 gas solubility constant, sometimes referred to as the Henry's law constant ($\text{mol m}^{-3} \text{atm}^{-1}$). Assuming CO_2 behaves as an ideal gas, K_H is related to α by $K_H = \alpha (R T_w)^{-1}$, where R ($\text{m}^3 \text{Pa K}^{-1} \text{mol}^{-1}$) is the ideal gas constant and T_w is the water temperature in Kelvin.

The transfer velocity k can be estimated using the approach by Wanninkhof (1992), where k is parameterized to the temperature-dependent nondimensional Schmidt's number Sc , which is the ratio of the kinematic viscosity of water ν and the molecular diffusivity D , and is equal to 600 for CO_2 at 20°C in fresh water (Jähne et al., 1987).

$$k = k_{600} (Sc_{\text{CO}_2} / 600)^n \quad (\text{eq. 4})$$

Where k_{600} is the gas transfer velocity normalized to Sc of CO_2 at 20°C with $n = 2/3$ for wind speeds U less than 3.6 m s^{-1} and $n = 1/2$ for wind speeds above 3.6 m s^{-1} (Jähne et al., 1987).

The Schmidt's number Sc_{CO_2} can be extrapolated to other water temperatures using the following equation (Roehm et al, 2009, Wanninkhof et al., 1992):

$$Sc_{\text{CO}_2} = 1911.1 - 118.11 * T_w + 3.4527 * T_w^2 - 0.041320 * T_w^3 \quad (\text{eq. 5})$$

with the water temperature T_w in $^\circ\text{C}$. In the calculations of the present study monthly median air temperatures from nearby meteorological stations measured at 2 m above ground level (a.g.l.) were used. For all calculations all temperatures at or below 0°C were set to 0.1°C , to avoid numerical problems.

Multiple studies have attempted to parameterize k_{600} , in this study the equation proposed by Cole and Caraco (1998) was used:

$$k_{600} = 2.07 + 0.215 * U_{10}^{1.7} \quad (\text{eq. 10})$$

together with the wind speeds measured at 10 m height from nearby meteorological stations.

2.4 Wind speed and air temperature

The wind speed and air temperature data are received from the data base of the Icelandic Meteorological Office (IMO) with a temporal resolution of 1 hour. Data is obtained from two stations, Kárahnjúkar (No. 5933, 64°56'49.6"N 15°47'34.5"W, 639 m a.s.l.) by the Háslón reservoir and Egilsstaðir airport (No. 4271, 65°16'29.0"N 14°24'23.3"W, 23.5 m a.s.l.) by the Lagarfljót reservoir (see Fig. 1). The wind velocity was measured by standard Young anemometers, with an accuracy of $\pm 0.3 \text{ m s}^{-1}$ at 10 m a.g.l. and the air temperature by Logan platinum resistance thermometers, with an accuracy of $\pm 0.1 \text{ K}$ at 2 m a.g.l. Data was retrieved from the Kárahnjúkar station for the time period of June 2008 to September 2013, including the duration of the water monitoring period of the Háslón and the Lagarfljót reservoirs, and from the Egilsstaðir airport weather station from November 1998 to November 2003 (before the deviation of the Jökulsá á Dal river into Lagarfljót) and from November 2007 to December 2013 (after the deviation).

2.5 Estimation of Ice cover

The determination of the ice cover of the reservoirs is done by visual assessment through web cameras owned by the Landsvirkjun power company. In rare cases the reservoirs are inspected on site. During spring and autumn when changes in the ice conditions are expected, web cameras are regularly examined and the conditions of the reservoirs are noted. Low visibility during weather events (snow/fog) can affect the estimation of the dates, leading to some additional uncertainty if the web cameras cannot capture the entire lagoon. A lake is considered ice-free when there is little or no ice cover on the lake. Estimation of ice formation is more precise as the reservoirs usually freeze over all at once. The freezing and melting dates have an uncertainty of up to one week.

3. Results

3.1. Temperature and wind speed.

The wind speed and temperature distribution measured at Kárahnjúkar and Egilsstaðir airport for each calendar month are shown in Fig. 2 as boxplots and the underlying data are provided in Table A8 in the Appendix. Generally, the highest wind speeds are observed during the winter months, while the lower wind speeds are present during summer when higher temperatures occur. During storm events, the wind speeds can exceed 30 m s^{-1} , but typically only lasting for a few hours. Wind speeds above 13 m s^{-1} were typically not observed for more than 24 consecutive hours. Therefore, this time span was used to estimate maximum

fluxes from high wind speed events. The wind speeds measured at the Kárahnjúkar weather station are higher than that at the weather station at the Egilsstaðir airport, while the Kárahnjúkar temperatures are lower, due to the higher elevation. The air temperatures are similar during the two monitoring periods at the Egilsstaðir airport, but the wind speeds have declined slightly with time.

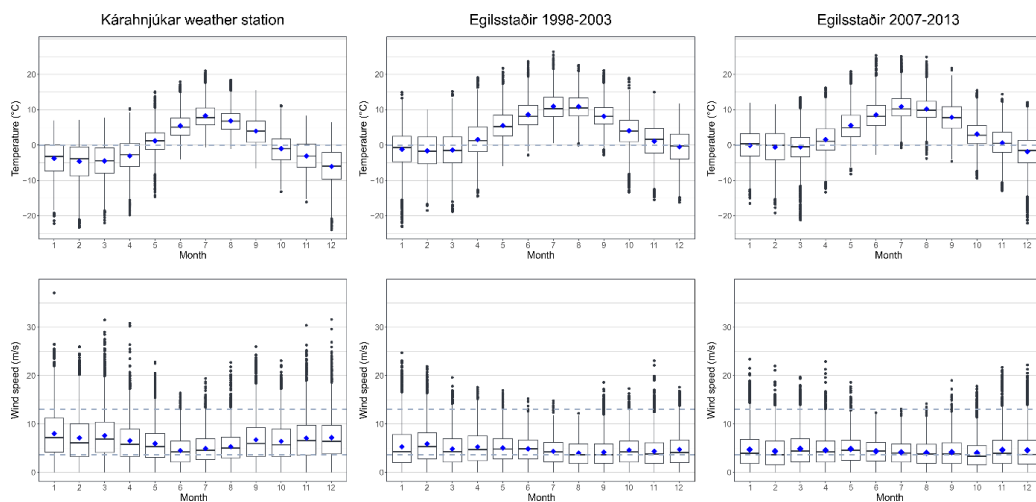


Fig. 2. The distribution of air temperature ($^{\circ}\text{C}$) at 2 m a.g.l. in the top row with the dashed grey line representing 0°C , and wind speed (m s^{-1}) at 10 m a.g.l. in the bottom row with dashed grey reference lines for 3.6 m s^{-1} and 13 m s^{-1} , for each calendar month. At the Kárahnjúkar weather station, by the Kárahnjúkar dam (Fig. 1), from beginning of June 2008 to end of September 2013 (left). At the Egilsstaðir airport weather station (Fig. 1) from November 1998 to November 2003 (middle), and November 2007 to December 2013 (right). The box plot shows the monthly median (horizontal line) and the lower and upper quartiles (25 % and 75 %) as well as the hourly outliers. The whiskers extend to the lowest/largest value no further than 1.5 inter-quartile range from the lower/upper quartile. The blue diamonds show the monthly mean values. Calculations are based on hourly measurements.

Water temperature profiles within the Háslón reservoir water body were measured from a boat in August 2008 at the deepest part of the reservoir shown by the white filled circle in the Háslón reservoir in Fig. 1, and again at the same location in September when the water level had reached the spillway at more than 625 m a.s.l. and yet again in 2011, 2012 and 2013 (Eiríksdóttir et al., 2014; Fig. A5). The air temperature was higher during the August campaign than during those in September, and strong wind prevailed before and during the 2011, 2012 and 2013 campaigns. The water temperature from the surface down to ~ 50 m water depth was higher in August 2008 ($\sim 6^{\circ}\text{C}$) than during September of the following years (only $3\text{-}4^{\circ}\text{C}$, Tab. A5).

Additional temperature profiles were measured in Hálslón six times per year, from June to November, 2009 to 2012, by the Landsvirkjun Power Company (Böðvarsdóttir and Axelsson, 2014). The highest measured temperatures are in late July to early August (6° to 8°C), the lowest temperatures are present in early June and late November (1°C to 2.5°C). The shallowest measurements reported were at 1 m depth in 2009-2011 and at 10 m depth in 2012. Hence, the temperature span of all the shallow waters (0-10 m depth, Figs. A4-A5) during the ice-free period, ranges from an average temperature of $4.5 \pm 4^\circ\text{C}$. This is in good agreement with the monthly median air temperature in Fig. 2 from the Kárahnjúkar weather station during the ice-free period. In the following, monthly mean air temperatures and wind speeds were used to calculate the monthly mean gas transfer.

3.2. Ice cover

The monthly median, the lower and upper quartiles for the air temperature at the Kárahnjúkar weather station are at or below zero from November to March, and most of April (Fig. 2). Field observations show that the Hálslón reservoir was fully covered with ice from mid to end of November during the water monitoring period from 2009 to 2013. The average and median air temperature at Hálslón was above zero degrees Celsius in May, but not the lower quartiles. The June median, average and the lower quartile were well above zero (Fig. 2). Ice was fully melted by 1st to 12th of June during 2009 to 2012. No ice cover data is available for the Hálslón reservoir for the year 2008, but the reservoir was fully covered with ice May 19th, 2008, when the temperature profile was measured (Fig. A3-4) The reservoir was ice-free for about half a year in 2014-2019, from June to November-December (average 179 days).

3.3. Chemical composition of water samples

The chemical compositions of the studied rivers before and after the damming and the associated reservoirs are presented in Appendix 2. Much of this data has been previously reported by Eiriksdóttir et al., 2015, 2017. Here we have added the composition of the Lagarfljót reservoir waters and particles before the installation of the Kárahnjúkar dam (Tab. A4). Furthermore, to all tables we have added the mass percent of organic carbon in the suspended organic and inorganic particle, the molar percent of dissolved organic carbon (DOC) in the total dissolved carbon (TDC = DIC + DOC) in each sample, the C/N molar ratio of the organic particles, the *in situ* pH, the *in situ* pCO_{2w} and CO_{2(aq)} the *in situ* concentration of dissolved CO₂ in the water. *In situ* refers to the calculated value at the measured water temperature at the time of sampling.

3.3.1 Lagarfljót reservoir

The calculated $p\text{CO}_{2w}$ for the Lagarfljót reservoir are shown in Fig. 3 and in the Appendixes in Table A4 and A5. Before the damming (1998-2003) the average $p\text{CO}_{2w}$ was **507 μatm** . The $p\text{CO}_{2w}$ values were mostly at or above the partial pressure of the atmosphere, $p\text{CO}_{2\text{atm}}$, at the time of sampling (avg. 367 μatm). After the construction of the Kárahnjúkar power plant in 2007 and the ensuing change in the Lagarfljót reservoir's inflow, the $p\text{CO}_{2w}$ values decrease to an average of **444 μatm** , while the atmospheric $p\text{CO}_{2\text{atm}}$ values increased due to continuous rise in man-made global CO_2 emissions (avg. 397 μatm). Overall, the partial pressure values were above the atmospheric reference in both cases, indicating a CO_2 flux from the reservoir to the atmosphere, but the difference ($p\text{CO}_{2w}-p\text{CO}_{2\text{atm}}$) became smaller decreasing the CO_2 flux to the atmosphere after the construction of the Kárahnjúkar power plant (see Fig. 3, Tab. 1 and 2).

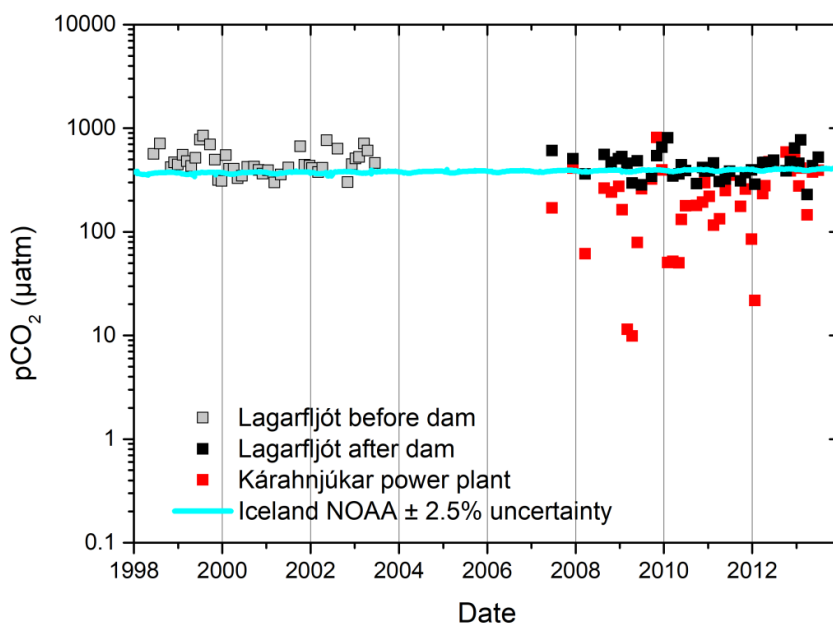


Fig. 3. Time evolution, before (grey filled squares) and after the erection of the Kárahnjúkar dam (black filled squares), of the in situ partial pressure of CO_2 in the Lagarfljót reservoir water at the Lagarfoss dam and in the outlet from the Kárahnjúkar power plant (red filled squares) sampled close to the powerhouse (Fig. 1). The light blue graph represents the partial pressure CO_2 concentration in the atmosphere at the NOAA Stórhöfði south Iceland CO_2 monitoring station (Lan et al. 2023).

The CO₂ fluxes from the Lagarfljót reservoir before (1998-2003) and after the damming of the Háslón reservoir (2007-2013) were calculated from the difference of pCO_{2atm} and pCO_{2w}, using the pCO_{2atm} derived from the average pCO₂ values (367 μatm and 392 μatm) over the measuring period from the NOAA station and the average pCO_{2w} of all measured water samples before (507 μatm) and after the damming (444 μatm) respectively. Flux calculations were done for each month, using median monthly air temperatures and median monthly wind speeds, and a constant surface area of 53 km². Error estimates were done using the upper and lower quartile of the median monthly temperatures and wind speeds. Additionally, we estimated potential high fluxes during short time (24 h) high wind speed events based on the highest hourly outliers of wind speed measured for each month. The average annual flux was calculated as a sum of the monthly fluxes, with additional information from the error estimates. The ice cover during the winter is assumed to prevent any gas exchange of the reservoir, reducing potential fluxes during these months. But as the Lagarfljót reservoir was not reported to fully freeze during the winter months, no ice cover has been assumed, therefore the fluxes represent maximum values without any effects of blockage by ice.

Table 1: Mean monthly CO₂ fluxes (tonne CO₂) of the Lagarfljót reservoir in 1998-2003 before the construction of the power plant, their estimated errors based on mean monthly temperature and wind speed variations and the effect of high wind speed events over 24 h as well as the estimated annual flux for the observation period.

| Month | Mean CO₂ flux (t) | Error (t) | Max flux at high wind speed (t/24h) |
|--------------|-------------------------------------|------------------|--|
| January | 459 | 227 | 166 |
| February | 511 | 241 | 161 |
| March | 459 | 227 | 111 |
| April | 510 | 311 | 93 |
| May | 509 | 242 | 89 |
| June | 509 | 242 | 93 |
| July | 410 | 212 | 73 |
| August | 367 | 197 | 55 |
| September | 367 | 198 | 102 |
| October | 410 | 213 | 93 |
| November | 411 | 213 | 145 |
| December | 412 | 212 | 93 |
| | | | |
| sum | +5335 | ±2736 | |

The annual CO₂ evasion from the Lagarfljót reservoir was estimated to be around **5335±2736 t** before the construction of Kárahnjúkar power plant. The annual flux was less

than one third, 1670 ± 2741 t, for the observation period of 2007-2013. While changes in temperature throughout the year are substantial, their effect on the flux is negligible. As the surface area of the reservoir is assumed to be constant, the main change of the mean monthly fluxes is caused by variations in wind speed. As shown by the calculated fluxes at the highest hourly measured wind speeds (up to 25 m s^{-1} , see Fig. 2) over a period of 24 hours, the mean monthly CO_2 flux can be increased by up to 50 %. The period of full ice cover is uncertain, but assuming a coverage of 3 months during winter would decrease the fluxes by around 25 %.

Table 2: Mean monthly CO_2 fluxes of the Lagarfljót reservoir in 2007-2013, after the construction of the Kárahnjúkar power plant, their estimated errors based on mean monthly temperature and wind speed variations and the effect of high wind speed events over 24 h as well as the estimated annual flux for the observation period 2007-2013.

| Month | Mean CO_2 flux (t) | Error (t) | Max flux at high wind speed (t/24h) |
|------------|-----------------------------|------------------------------|-------------------------------------|
| January | 153 | 232 | 54 |
| February | 113 | 210 | 50 |
| March | 171 | 255 | 43 |
| April | 153 | 255 | 54 |
| May | 170 | 255 | 36 |
| June | 170 | 255 | 21 |
| July | 152 | 231 | 22 |
| August | 124 | 209 | 24 |
| September | 122 | 210 | 39 |
| October | 116 | 210 | 36 |
| November | 113 | 210 | 50 |
| December | 113 | 210 | 54 |
| | | | |
| sum | +1670 | ± 2741 | |

3.3.2 Háslón reservoir

The data from the Háslón reservoir show clearly that the pCO_2w values are always at or below the atmospheric pCO_2atm pressure (Fig. 4 and Tab. A6). All but the first two samples were sampled in August and September each year. Some samples are at less than $10 \mu\text{atm}$. The measured depth profiles overall show a decrease of pCO_2 with increasing depth. Caution must be taken, as the sample dates and methods were not uniform as described in the method and introduction sections. This is observed by very low pCO_2w values for one 5 m deep sample. The average pCO_2w of all the samples from the Háslón reservoir was **$174 \mu\text{atm}$**

(median: 138 μatm), while the corresponding average $\text{pCO}_{2\text{atm}}$ during the study period of 2007-2013 was 392 μatm .

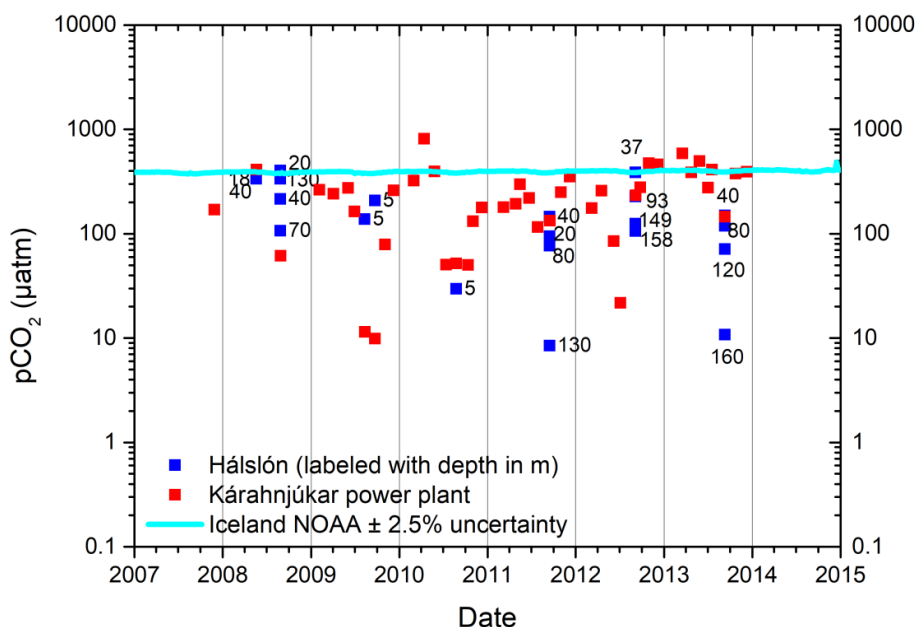


Fig. 4. Time evolution of the in situ partial pressure of CO_2 in the Hálslón reservoir water (blue filled squares) and in the outlet from the Kárahnjúkar Powerhouse (red filled squares). The sample numbers refer to the Hálslón water depth at which the samples were taken. The light blue graph represents the partial pressure CO_2 concentration in the atmosphere at the NOAA Stórhöfði south Iceland CO_2 monitoring station (Lan et al. 2023).

The samples collected from the Kárahnjúkar Powerhouse outflow channel are mostly at or below atmospheric pCO_2 values as depicted by the red filled squares in Fig. 3 and 4 (Tab. A7). The highest measured value is at 814 μatm , approximately double the atmospheric pCO_2 value, some values are as low as the deepest samples from the Hálslón reservoir at ~ 10 μatm . Data interpretation of the outlet waters has to be done with caution, as the Kárahnjúkar hydropower station is fed by two additional reservoirs, that are partially mixing in the headrace tunnels with each other or with water from the Hálslón reservoirs in May to July each year.

Monthly mean fluxes for the Hálslón reservoir were calculated as described for Lagarfljót but multiplied with the average surface area (Tab. A9) for each month derived from the reservoir

water level (see Fig. A1 and A2) and added up over the entire ice-free period in correspondence with table A10. The reservoir is often frozen till end of May and then fully ice covered around the last week of November. As the surface area in May is quite small, the flux is very small too, while the water fill level of the reservoir in November is nearly at its peak. This induces some additional uncertainty as the ice cover affects the gas flux. Therefore, the annual flux of the reservoir has been estimated by adding the values from June to November. Potential fluxes for May are provided in table 3 but are not included in the annual flux.

CO₂ flux from the Háslón reservoir is estimated to be **-5131 to -5515 t** over the entire ice-free period from June to November for each year with an error of ± 3011 to ± 3188 t. This value has a high uncertainty, as the average pCO_{2w} value of 174 μatm likely does not represent the overall reservoir. Changes in pCO_{2w} throughout the reservoir waterbody, as well as with seasons and over the years are large. Changes in the reservoir surface area contributed to water usage and precipitation increase the error. High wind speed events (Fig. 2 and Tab. A8) can lead to increased flux rates but are limited by ice cover and by the short event durations but can still be as large as 30 %.

Table 3: Mean monthly CO₂ fluxes (tonne) from the Háslón reservoir, potential fluxes in May in brackets, their estimated errors based on monthly median temperature and wind speed variations and the effect of high wind speed events over 24 h as well as the estimated annual flux calculated for June to late November.

| Month | mean CO ₂ flux (t) | Error (t) | Max flux at high wind speed (t/24h) |
|------------|-------------------------------|---|-------------------------------------|
| May | (-255) | (121) | (-72) |
| June | -316 to -382 | 159 to 192 | -60 to -72 |
| July | -399 to -619 | 196 to 305 | -94 to -146 |
| August | -673 to -868 | 320 to 412 | -198 to -255 |
| September | -1169 | 756 | -301 |
| October | -1172 | 755 | -256 |
| November | -1306 to -1402 | 767 to 824 | -382 |
| Sum | -5131 to -5515 | ± 3011 to ± 3188 | |

4. Discussion

The highest calculated in situ partial pressure of CO₂ (pCO_{2w}) in the waters of the present study was ~ 850 μatm from the Lagarfljót reservoir before the construction of the Kárahnjúkar dam March 1st, 1999. This was more than twice the atmospheric pCO_{2atm} at the time of sampling. Hence, CO₂ was then released from the water and to the atmosphere (Fig. 3 and Tab. A7). Nevertheless, this is a relatively low maximum pCO_{2w} as values as high as

100,000 μatm are observed in organic-rich wetland soil waters before their exposure to the atmosphere (Linke et al. 2024a and 2024b). The lowest $p\text{CO}_{2w}$ was about 10 μatm at 130-160 m depth within the Háslón reservoir and comparable to the lowest value in the outlet from Kárahnjúkar powerhouse in late summer of 2009 (Figs. 4 and 5 and Tab. A6 and A7). The lowest reported $p\text{CO}_{2w}$ in Iceland is around 0.32 μatm , measured in spring water emerging from glassy basaltic rocks at pH 10.10 and 2°C (Gislason et al. 1996).

The annual CO_2 flux from the Lagarfljót reservoir to the atmosphere was estimated to be around **5335±2736 t** before the construction of Kárahnjúkar power plant. The annual flux decreased to one third, **1670±2741 t**, for the observation period of 2007-2013. A 3-month ice cover during wintertime would decrease these fluxes further by ~25%. The CO_2 fluxes of the Háslón reservoir are negative, from the atmosphere into the reservoir water, -5131 t to -5515 t over the entire ice-free period of around 6 months per year with an error of ±3011 t to ±3188 t, making it a CO_2 sink.

The fluxes are mainly affected by variation in ice cover, changes in total water surface area as a function of reservoir fill level and wind speed. High wind speed events that lasted for only 24 hours can affect the monthly mean flux by up to 30 %, but often occur during winter when the Háslón reservoir is ice-covered. Apart from causing ice formation, temperature variations are less important, this can be seen in Lagarfljót over the months where the temperature varies by up to 10°C but the wind speeds are relative constant, resulting in fluxes that are nearly equal throughout the year. Temperature changes of around 10°C affect the fluxes within a few percentages, while as the increase of wind speed from 5 to 10 m s^{-1} results in more than doubling of the flux, and even more at higher wind speeds as the gas transfer velocity k_w becomes much larger with wind speed depending on the approach (see Fig. 2 and eqs. 5-10).

While the specific emission of water bodies to the atmosphere can be large, such as those waters emerging from organic-rich wetland soils in southern Iceland (Linke et al., 2024a and b), the potential uptake via negative fluxes is limited by $\Delta p\text{CO}_2$ (~400 μatm) as shown in Fig. 5. Assuming an atmospheric partial pressure $p\text{CO}_{2\text{atm}}$ of roughly 400 μatm , the maximum uptake of CO_2 from the atmosphere at a $p\text{CO}_{2w}$ value of zero is equal to ~800 $\text{t km}^{-2} \text{yr}^{-1}$ at 10°C and 10 m s^{-1} wind speed as shown in Fig. 5. Meanwhile, any positive $\Delta p\text{CO}_2$ values that are greater than approximately 400 μatm result in CO_2 emissions that are larger than any potential uptake under the before mentioned parameters, e.g. 2100 and 7800 $\text{t km}^{-2} \text{yr}^{-1}$ for 3 m s^{-1} and 10 m s^{-1} respectively at a $\Delta p\text{CO}_{2w}$ value that is 10-times higher (4000 μatm).

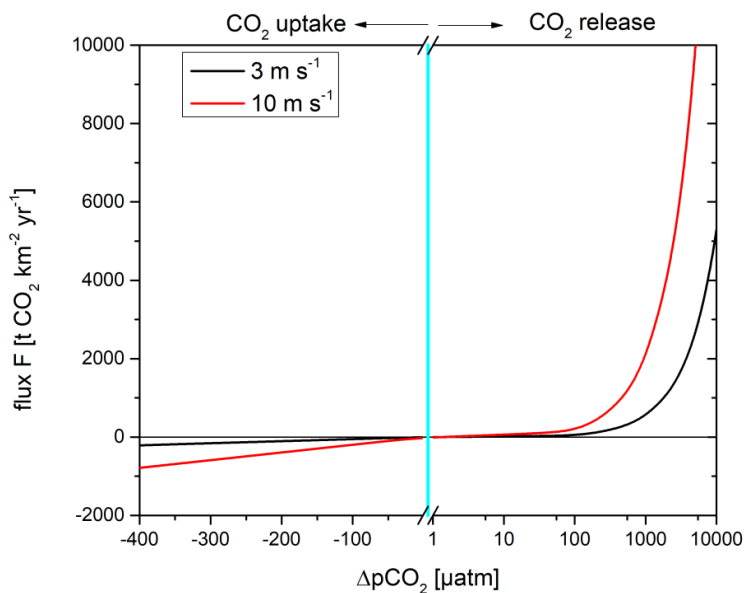


Fig. 5. The specific CO₂ flux F at 10°C as a function of $\Delta p\text{CO}_2$ ($p\text{CO}_{2w} - p\text{CO}_{2atm}$), assuming fixed wind velocities at 3.0 m s⁻¹ and 10 m s⁻¹, the blue line at $\Delta p\text{CO}_2 = 0$ indicates the equilibrium between CO₂ partial pressure of the atmosphere and the water phase. Note that CO₂ uptake at values below 0 is displayed in linear scale, while emissions are displayed in logarithmic scale to cover a larger scale.

Eiriksdottir et al. (2017) calculated an increase of the dissolved inorganic carbon (DIC) flux from 19,016 t yr⁻¹ to 34,048 t yr⁻¹ for Lagarfljót at Lagarfoss and a decrease from 21,558 t yr⁻¹ to 11,618 t yr⁻¹ for Jökulsá á Dal at Hjardarhagi for the time periods 1998-2003 and 2008-2013 respectively, with a total increase of these DIC fluxes to the ocean by 13 %. These changes are attributed to the change of the river course following the damming of Jökulsá á Dal and the construction of the Kárahnjúkar power plant, and about 10% climate induced increase in runoff during this period (Eiriksdottir et al. 2017). Compared to these river fluxes, the here presented potential CO₂ emissions from the Lagarfljót reservoir of 5335 t before and 1670 t after damming decreased by a factor of 3. Before the damming the annual CO₂ emissions from the Lagarfljót reservoir to the atmosphere were equal to 28 % of the riverine DIC fluxes to the ocean but decreased to 4.9 % after the damming. The CO₂ uptake by the Háslón reservoir as a percentage of the Lagarfljót DIC flux is equal to 15 % for the time span 2008-2013.

Carbon to nitrogen (C:N) ratios of the river suspended organic particulate matter in most river samples are around 20 to 23 indicating a terrestrial plant source, while lower ratios (C:N =

6.6) typically indicate algae or phytoplankton (Redfield 1934). The C:N ratio of mineral soils is reported with a ratio of 10.9 (Batjes 2009). The Jökulsá á Dal river at Hjardartangi shows a maximum C:N ratio of 29, which might indicate the influence of the surrounding peat areas that are known to reach very high C:N ratios of 60 and above (Loisel et al. 2014).

The Háslón reservoir's average soil thickness before dam construction was 2.2 m and the carbon content was low: 10 % in the top part, 1.5 – 2.5 % in the middle and 3.8 – 4.8 % in the lower part of the soil sections (Arnalds and Gísladóttir, 2001). The bedrock consists of basaltic rocks that are relatively young, about 1 Myr (Gislason et al. 2009). The river suspended basaltic particles in Jökulsá á Dal, before damming, were reactive Mg-rich basalt (Eiriksdóttir 2008, Gislason et al. 2006), and as can be seen in Table A3, the average concentration of suspended particulate organic carbon particles was only 0.38 weight-% of the total river suspended inorganic particle concentration. Similarly, the average concentration of suspended organic carbon particles from the outlet of the Kárahnjúkar power plant was only 0.22 weight-% of the total concentration of suspended inorganic and organic particles in the river. Concentrations in Háslón at various depths were 0.24 weight-%, highlighting the dominating effect of water rock interactions rather than organic processes such as photosynthesis and respiration, and break down of river transported organic matter.

The specific median flux of CO₂ to the atmosphere from the Lagarfljót reservoir over the entire year was estimated to be $100.7 \pm 51.6 \text{ gCO}_2 \text{ m}^{-2} \text{ yr}^{-1}$ (units equal to $\text{t km}^{-2} \text{ yr}^{-1}$) and $31.5 \pm 51.7 \text{ gCO}_2 \text{ m}^{-2} \text{ yr}^{-1}$ before and after the damming respectively. These fluxes are relatively low compared to the specific fluxes from temperate reservoirs of $511 \text{ gCO}_2 \text{ m}^{-2} \text{ yr}^{-1}$ (21 reservoirs, Louis et al. 2000 and references therein) or German reservoirs of $611 \text{ gCO}_2 \text{ m}^{-2} \text{ yr}^{-1}$ (39 reservoirs, Saidi and Koschorreck, 2017), while data from tropical reservoirs typically show a higher average flux (e.g. $1277 \text{ gCO}_2 \text{ m}^{-2} \text{ yr}^{-1}$ in Louis et al. 2000). This is caused by much higher median pCO_{2w} values in tropical freshwater lakes $1910 \mu\text{atm}$ compared to non-tropical freshwater lakes $1120 \mu\text{atm}$ (Raymond et al. 2013). The specific median flux of CO₂ from the atmosphere into the Háslón reservoir, which was constantly undersaturated with respect to atmospheric pCO_{2atm}, was estimated to be $-121.4 \pm 67.9 \text{ gCO}_2 \text{ m}^{-2}$ during the ice-free period of 6 months. If no ice cover was present the flux would be approximately $-208 \text{ gCO}_2 \text{ m}^{-2} \text{ yr}^{-1}$, with a large uncertainty caused by the varying geographical reservoir surface area and very high wind speeds observed during winter. The Háslón reservoir shows much higher specific fluxes than the Lagarfljót reservoir despite having similar total fluxes. This is caused by the large surface area variation of the Háslón reservoir

over the year, and the presence of higher wind speeds at higher altitude compared to those at the protected Lagarfljót reservoir. The here observed fluxes are of the same order of magnitude as the estimated CO₂ drawdown by alkalinity export (~62 g_{CO2} m⁻² yr⁻¹) from soil waters emerging from organic-rich soils in South Iceland or the average net annual carbon accumulation rate of corresponding soils (95-190 g_{CO2} m⁻² yr⁻¹) (Linke et al. 2024b). Overall, the CO₂ sink effect that is observed in the Háslón reservoir is small, which agrees with data from Barros et al. (2011) that observed on average only up to 4-times smaller influxes compared to reservoir emissions (see average emission values above). Additionally, CO₂ emissions from “young reservoirs” are often elevated in the first 15 to 20 years after their construction (Raymond et al. 2013), which is caused by the flooding and decomposition of organic material in soils. It is noteworthy that the soil present in the area of the Háslón reservoir had a low carbon content (Gísladóttir et al. 2014), hence flooding of this soil did not lead to large emissions. Despite the overall positive effect with respect to the decrease/negative CO₂ emissions of the study area, it has to be noted that degassing of wetlands, that were drained due to the diversion of the river course, is not accounted for in this study. In addition, it must be emphasized that the observed CO₂ drawdown is caused by natural processes, as a result of mechanical and chemical weathering of the rocks at the base of the glaciers and airborne dust (Gíslason et al. 1996, Eiríksdóttir et al. 2013, Raiswell and Thomas 1984) mostly under the glaciers before reaching the reservoirs. The dissolution of highly reactive basaltic particles creates alkalinity and raises the pH, resulting in CO₂ drawdown when in contact with the atmosphere (Gíslason and Eugster 1987a and b). The chemical weathering of the glacier fed rivers is highly affected by temperature and runoff (Gíslason et al. 2009; Eiríksdóttir et al. 2013) and will rise with increasing temperature and runoff and will be affected by changes in the river courses by damming.

5. Conclusions

Our work suggests that the diversion of water from one catchment to another caused by the construction of the Kárahnjúkar power plant led to a decrease in CO₂ emissions from the Lagarfljót reservoir over the study period. In comparison to the riverine DIC fluxes reported by Eiríksdóttir et al. (2017), the CO₂ emissions to the atmosphere were only 28 % and 5 % of the total riverine DIC fluxes before and after the diversion of the rivers, respectively. The CO₂ uptake from the atmosphere of feeding reservoir Háslón is about 5000 t CO₂ annually. But the rate of CO₂ uptake is limited by the CO₂ concentration in the atmosphere. The main factors affecting the total CO₂ fluxes are, the concentration difference between the water and the atmosphere, wind speed and total geographic surface area. Meanwhile, the temperature

has less of an effect on the flux across the water-air interface but will affect the water-rock interactions within the water body.

The observed water rock interactions of glacier meltwater with basaltic bedrock, river suspended reactive material, and reactive dust provide a considerable source of alkalinity that leads to the uptake of CO₂. These natural processes known for Icelandic glacier waters (e.g. Gislason et al. 1996) are similar to currently investigated enhanced rock weathering methods for CO₂ draw down from the atmosphere and can be considered as natural analogues, which can provide further insight (Linke et al. 2024a and b).

Declaration of competing interest

The authors declare that they have no known competing financial interests or personal relationships that could have appeared to influence the work reported in this paper.

Data availability

All data are provided either in the manuscript or the associated supplementary information.

Acknowledgments

This research was funded by the Landsvirkjun power company under the project number 2456. Additionally, the authors want to thank Hákon Aðalsteinsson, Ásrún Elmarsdóttir, Sveinn Kári Valdimarsson, Ragnheiður Ólafsdóttir and Árni Jóhann Óðinsson for their help over the course of this study.

Supplementary materials

Supplementary material associated with this article can be found in the online version. The Appendix 1 contains additional explanations of the flux calculations and surface area estimates of the reservoirs, as well as associated tables and figures. The Appendix 2 contains the underlying data tables of this work.

References

- Alin, S.R., Ramera, M.F.F.L., Salimon, C.I. Richey, J.E. Holtgrieve, G.W. Krusche, A.V., Snidvongs, A., 2011. Physical controls on carbon dioxide transfer velocity and flux in low-gradient river systems and implications for regional carbon budgets, *J. Geophys. Res.*, 116, G01009, doi:10.1029/2010JG001398.
- Allison, J.D., Brown, D.S., Novo-Gradac, K.J., 1991. MINTEQA2/PRODEFA2, A geochemical assessment model for environmental systems: version 3.0 user's manual. Environmental Research Laboratory Office of Research and Development U.S. Environmental Protection Agency, Athens, Georgia 30605
- Arnalds, O., Gísladóttir, F.O., 2001. Háslón, jarðvegur og jarðvegsrof. *Rannsóknastofnun landbúnaðarins*, 70p.

- Axelsson, E., 2012. Áhrif Kárahnjúkavirkjunar á vatnsborð og grunnvatn á láglendi á Héraði. Skýrsla VÍ 2012-007 ISSN 1670-8261, 24 pp (in Icelandic).
- Barros, N., Cole, J.J., Tranvik, L.J., Prairie, Y.T., Bastviken, D., Huszar, V.L.M., del Giorgio, P., Roland, F., 2011. Carbon emission from hydroelectric reservoirs linked to reservoir age and latitude, *Nature Geosci.* 4, 593–596.
- Batjes NH., 2019. Harmonized soil profile data for applications at global and continental scales: updates to the WISE database. *Soil Use and Management.* 25, 124–127.
- Bödvarsdóttir, E.B., Axelsson, E., 2014. Hiti í Háslóni og frárennsli Fljótsdalsstöðvar 2009-2012. report by Landsvirkjun LV-2014-075, 15p (in Icelandic).
- Cole, J.J., Caraco, N.F., 1998. Atmospheric exchange of carbon dioxide in a low-wind oligotrophic lake measured by the addition of SF₆, *Limnol. Oceanogr.* 43(4), 647-656.
- Crump, J., 2017. *Smoke on Water: Countering Global Threats from Peatland Loss and Degradation.* UN Environment, GRID-Arendal.
- Eiríksdóttir, E.S., Louvat, P., Gislason, S.R., Óskarsson, N., Hardardóttir, J., 2008. Temporal variation of chemical and mechanical weathering in NE Iceland: Evaluation of a steady-state model of erosion. *Earth and Planetary Science Letters*, 272, 78–88.
- Eiríksdóttir, E.S., Louvat, P., Gislason, S.R., Óskarsson, N., Hardardóttir, J., 2008. Temporal variation of the chemical and mechanical weathering in NE-Iceland, evaluation of a steady state model of erosion. *Earth and Planetary Science Letters* 272, 78-88.
- Eiríksdóttir, E.S., Gislason, S.R., Oelkers, E.H., 2013. Does temperature or runoff control the feedback between chemical denudation and climate? Insights from NE Iceland. *Geochimica et Cosmochimica Acta* 107, 65-81.
- Eiríksdóttir, E.S., Gislason, S.R., Snorrason, A., Harðardóttir, J., Thorláksdóttir, S.B., Sveinbjörnsdóttir, A.E., Neely, R.A., 2014. Efnasamsetning, rennsli og aurburður straumvatna á Austurlandi XI. Gagnagrunnur Jarðvísindastofnunar og Veðurstofunnar. Raunvísindastofnun Háskólans, Reykjavík, RH-05-2014, 126 bls.
- Eiríksdóttir, E.S., Gislason, S.R., Oelkers, E.H., 2015. Direct evidence of the feedback between climate and nutrient, major, and trace element transport to the oceans. *Geochimica et Cosmochimica Acta* 166, 249-266.
- Eiríksdóttir, E.S., Oelkers, E.H., Hardardóttir, J., Gislason, S.R., 2017. The impact of damming on riverine fluxes to the ocean: A case study from Eastern Iceland. *Water Research* 113, 124-138.
- Gaillardet, J., Dupre, B., Louvat, P., Allègre, C.J., 1999. Global silicate weathering and CO₂ consumption rates deduced from the chemistry of large rivers. *Chemical Geology* 159, 3-30.

Gisladdottir, G., Mankasingh, U., Þórsson J., 2014. Physical and chemical soil properties of different land cover types, related to soil carbon, at Sporðöldulón. RH-06-2014. Report Institute of Live and Environmental Sciences, University of Iceland. 27 pp.

Gislason, S.R. and Eugster, H.P., 1987. Meteoric water-basalt interactions. I: A laboratory study, *Geochim. Cosmo. Acta* 51, 2827-2840.

Gislason, S. R., Arnórsson, S., Ármannsson H., 1996. Chemical weathering of basalt as deduced from the composition of precipitation, rivers, and rocks in SW Iceland. *Am. J. Sci.* 296, 837-907.

Gislason, S.R., Oelkers, E.H., Snorrason, A., 2006. Role of river suspended material in the global carbon cycle. *Geology* 34, 49-52.

Gislason S.R., Oelkers, E.H., Eiríksdóttir, E.S., Kardjilov, M.I., Gisladdottir, G., Sigfusson, B., Snorrason, A., Elefsen, S., Hardardóttir, J., Torssander, P., Oskarsson, N., 2009. Direct evidence of the feedback between climate and weathering. *Earth and Planetary Science Letters* 277, 213-222.

Gunnarsson, A., Theodorsson, T., Thorhallson, R., Xuyi, J.B., Jonsson, G.T., 2014. Sniðmælingar Háslóns sumarið 2013 (Profile measurements in Háslón summer 2013). LV-2014-050, report in Icelandic, 20 p. https://www.sjalbbaerni.is/static/research/files/2.2.3-lv_2014_050_snidmaelingarhalsloni2013.pdf

Hartmann, J., Jansen, N., Dürr, H.H., Kempe S., Köhler, P., 2009. Global CO₂-consumption by chemical weathering: What is the contribution of highly active weathering regions? *Global and Planetary Change* 69, 185-194.

Hallgrímsson, H., 2005. Lagarfljót. Mesta vatnsfall Íslands ISBN 9979-772-43-3

Hooijer, A., Silvius, M., Wösten, H., Page, S., 2006. PEAT-CO₂, Assessment of CO₂ emissions from drained peatlands in SE Asia. Delft Hydraulic Report Q3943.

Kardjilov, M.I., 2008. Riverine and Terrestrial Carbon fluxes in Iceland. Doctoral Thesis from the Department of Geography and Tourism. University of Iceland, Reykjavik, p. 83 pp.

Lan, X., Mund, J.W., Crotwell, A.M., Crotwell, M.J., Moglia, E. Madronich, M., Neff, D., Thoning, K.W., 2023. Atmospheric Carbon Dioxide Dry Air Mole Fractions from the NOAA GML Carbon Cycle Cooperative Global Air Sampling Network, 1968-2022, Version: 2023-08-28.

Landsvirkjun, 2009. Karahnjúka Power Plant and Fljótsdalsstöð. Power Station in numbers. <http://www.landsvirkjun.is/Fyrirtaekid/Fjolmidlateg/Frettir/Frett/857/>.

Leifsson, Th.S., Kaelin, J., Baumann, B., 2009. Kárahnúkar Hydroelectric Project, Waterways Operation Manual, Revision 1. Landsvirkjun Report No. LV-2009/014, February 2009, 211 pages plus Appendixes.

- Linke, T., Oelkers, E.H., Dideriksen, K., Möckel, S.C., Nilabh, S., Grandia, F., Gislason, S. R., 2024a. The geochemical evolution of basalt Enhanced Rock Weathering systems quantified from a natural analogue. *Geochimica Cosmochimica Acta* 370, 66-77.
- Linke, T., Oelkers, E.H., Möckel, S.C., Gislason, S.R., 2024b. Direct evidence of CO₂ drawdown through enhanced weathering in soils. *Geochem. Persp. Let.* 30, 7-12.
- Loisel, J., Yu, Z., Beilman, D. W., Camill, P., Alm, J., Amesbury, M. J., Anderson, D., Andersson, S., Bochicchio, C., Barber, K., Belyea, L. R., Bunbury, J., Chambers, F. M., Charman, D. J., De Vleeschouwer, F., Fiałkiewicz-Kozieł, B., Finkelstein, S. A., Gałka, M., Garneau, M., ... Zhou, W., 2014. A database and synthesis of northern peatland soil properties and Holocene carbon and nitrogen accumulation. *The Holocene*, 24(9), 1028-1042.
- Louis, V.L.St., Kelly, C.A., Duchemin, E., Rudd, J.W.M., Rosenberg, D.M., 2000. Reservoir Surfaces as Sources of Greenhouse Gases to the Atmosphere: A Global Estimate. *BioScience* 50 (9), 766–775.
- Marty, B., Tolstikhin, I.N., 1998. CO₂ fluxes from mid-ocean ridges, arcs and plumes. *Chemical Geology* 145, 233-248.
- Olafur, A., Gísladóttir, F.O., 2001. Hálslón, jarðvegur og jarðvegsrof. *Rannsóknastofnun landbúnaðarins*, 70p.
- Parkhurst, D.L., Appelo, C.A.J., 1999. User's guide to PHREEQC (Version 2): A computer program for speciation, batch-reaction, one-dimensional transport, and inverse geochemical calculations. *Water-Resources Investigations Report*, US Geological Survey. <https://doi.org/10.3133/wri994259>
- Parish, F., Sirin, A., Charman, D., Joosten, H., Minayeva, T., Silvius, M., Stringer, L., 2008. Assessment on Peatlands, Biodiversity and Climate Change: Main Report. Global Environment Centre, Kuala Lumpur and Wetlands International, Wageningen, 179pp.
- Raiswell, R., Thomas, A.G. 1984. Solute acquisition in glacial melt waters: I. Fjallsjökull (South-East Iceland): bulk melt waters with closed-system characteristics, *J. Glaciol.*, 30, pp. 35-43
- Raymond, P.A., Hartmann, J., Lauerwald, R., Sobek, S., McDonald, C., Hoover, M., Butman, D., Striegl, R., Mayorga, E., Humborg, C., Kortelainen, P., Dürr, H., Meybeck, M., Ciais, P., Guth, P., 2013. Global carbon dioxide emissions from inland waters. *Nature*, 503, 355-359.
- Wanninkhof, R., 1992. Relationship between wind speed and gas exchange over the ocean. *Journal of Geophysical Research*, 97, 7373-7382.
- Wanninkhof, R., Asher, W.E., Ho, D.T., Sweeney, C., McGillis, W.R., 2009. Advances in quantifying air-sea gas exchange and environmental forcing. *Annu. Rev. Mar. Sci.*, 1, 213–44.

Appendix

Appendix A: Supplementary Material Paper I

Supplementary Material

The geochemical evolution of basalt Enhanced Rock Weathering systems quantified from a natural analogue

T. Linke, E. H. Oelkers, K. Dideriksen, S. Möckel, S. Nilabh, F. Grandia, and S.R. Gislason

The dataset includes the following: 1) measured soil water chemistry, 2) additions to the thermodynamic database and 3) the chemical composition of the rainwater used for the modelling, 4) temporal evolution of the soil water chemistry, 5) the redox values different redox couples in comparison to the measured data, 6) the calculations of the surface normalized dissolution rate of basalt.

Table S1: Soil water compositions measured in the present study.

| sample | date | depth cm | T °C | pH | E _h _{SHE} mV | Alk meq kg ⁻¹ | DIC µmol kg ⁻¹ | DOC µmol kg ⁻¹ | Charge Balance % | Major element concentrations [µmol kg _{water} ⁻¹] | | | | | | | | | |
|------------------|----------|-------------|---------|------|-------------------------------------|-----------------------------|------------------------------|------------------------------|---------------------|--|-----|------|-----|-----|--------|------------------|-----|-----|--|
| | | | | | | | | | | Si | Na | K | Ca | Mg | S(tot) | H ₂ S | Cl | | |
| LOQ ¹ | | | | | | | | | | 4.0 | 11 | 3.0 | 1.0 | 0.2 | 6.0 | 0.4 | 0.4 | 28 | |
| 1* | 23.05.18 | 76 | 9 | 5.84 | 233 | 1.48 | | | | 678 | 449 | 7 | 420 | 402 | 97 | <LOQ | | 402 | |
| 2* | | 121 | 9 | 6.27 | -9 | | | | | 716 | 395 | 13 | 427 | 379 | 102 | 3.5 | | 357 | |
| 3* | | 173 | 8.9 | 6.35 | -8 | | | | | 717 | 390 | 14 | 293 | 233 | 79 | 4.8 | | 350 | |
| 4* | | 260 | 10.1 | 6.37 | -57 | 2.3 | | | | 644 | 441 | 20 | 513 | 535 | 7 | 4.5 | | 284 | |
| 1a | 21.06.18 | 76 | 19.7 | 6.02 | 451 | 1.41 | 4452 | 247 | -1.27 | 678 | 464 | <LOQ | 380 | 359 | 90 | | | 404 | |
| 2a | | 121 | 19 | 6.21 | 116 | 1.56 | 3720 | 252 | 9.57 | 797 | 427 | 17 | 334 | 261 | 99 | | | 287 | |
| 3a | | 173 | 19.2 | 6.2 | 106 | 1.53 | 3675 | 344 | 20.7 | 778 | 435 | <LOQ | 384 | 340 | 47 | | | 322 | |
| 4a | | 260 | 24.8 | 6.25 | 71 | 2.21 | 4748 | 233 | 21.4 | 722 | 448 | 16 | 522 | 527 | <LOQ | | | 295 | |
| 1b | 14.08.18 | 76 | 16.8 | 6.06 | 298 | 1.5 | 4566 | 381 | 0.49 | 761 | 471 | 0 | 381 | 361 | 71 | | | 300 | |
| 2b | | 121 | 15.9 | 6.18 | 76 | 1.38 | 3503 | 258 | 19.84 | 860 | 446 | 19 | 365 | 314 | 120 | | | 255 | |
| 3b | | 173 | 15.2 | 6.28 | 88 | 1.59 | 3549 | 265 | 20.78 | 802 | 456 | 16 | 374 | 341 | 29 | | | 280 | |
| 4b | | 260 | 15.4 | 6.41 | 66 | 2.13 | 4049 | | 18.5 | 740 | 581 | 57 | 486 | 515 | 27 | | | 462 | |
| 1c | 18.09.18 | 76 | 7.6 | 6 | 287 | 1.5 | 5475 | 418 | 0.87 | 772 | 482 | <LOQ | 378 | 358 | 111 | 1.0 | | 206 | |
| 2c | | 121 | 8.9 | 6.22 | 123 | 2.34 | 5849 | 339 | 2.85 | 887 | 450 | 19 | 422 | 342 | 124 | 4.2 | | 254 | |
| 3c | | 173 | 8.2 | 6.19 | 112 | 2.5 | 6533 | 344 | 1.59 | 810 | 463 | 16 | 387 | 348 | 20 | 6.0 | | 293 | |
| 4c | | 260 | 7.5 | 6.28 | 85 | 3.02 | 7038 | 331 | 3.62 | 747 | 446 | 22 | 487 | 493 | <LOQ | 4.6 | | 282 | |
| 1d | 29.10.18 | 76 | 22.5 | 5.98 | 439 | 0.83 | 2731 | 382 | 4.37 | 566 | 449 | 22 | 330 | 310 | 101 | | | 583 | |
| 2d | | 121 | 22.5 | 6.13 | 229 | 1.56 | 4044 | 488 | 5.00 | 732 | 416 | 20 | 323 | 269 | 77 | | | 492 | |
| 3d | | 173 | 22.5 | 6.18 | 224 | 2.16 | 5204 | 329 | 7.03 | 807 | 453 | 14 | 383 | 354 | 57 | | | 332 | |
| 4d | | 260 | 22.5 | 6.39 | 179 | 2.8 | 5205 | 366 | 7.62 | 755 | 444 | 19 | 494 | 499 | 14 | | | 328 | |
| 1e | 21.11.18 | 76 | 22.6 | 5.85 | 429 | 1.08 | 4937 | | 2.93 | 650 | 450 | 17 | 343 | 333 | 106 | | | 446 | |
| 2e | | 121 | 22.6 | 6.11 | 282 | 1.21 | 3245 | | 3.15 | 668 | 354 | 36 | 229 | 190 | 50 | | | 368 | |
| 3e | | 173 | 22.6 | 6.15 | 255 | 2.17 | 5450 | | 3.69 | 794 | 435 | 17 | 351 | 327 | 44 | | | 349 | |
| 4e | | 260 | 22.6 | 6.28 | 190 | 2.78 | 5869 | | 4.54 | 730 | 423 | 20 | 442 | 451 | <LOQ | | | 309 | |

¹ LOQ = Limit of Quantification

*sample not used for modelling due to missing analysis

Table. S1 (continued)

| sample | major element concentrations [$\mu\text{mol kg}^{-1}$] | | | | | | | trace element concentrations [nmol kg^{-1}] | | | | | | | | | |
|------------------|--|------------------|------------------|------|------|------|--|--|------|------|------|------|------|------|-----|------|----|
| | Al | Fe ²⁺ | Fe ³⁺ | Sr | Mn | B | | Cd | Co | Cr | Cu | Ni | Pb | Zn | V | Ti | Mo |
| LOQ ¹ | 0.28 | 0.1 | 0.1 | 0.01 | 0.1 | 0.9 | | 0.17 | 0.3 | 0.8 | 0.6 | 0.05 | 5.0 | 2.0 | 6.0 | 0.11 | |
| 1* | 0.93 | | | 0.62 | 9.4 | 7.9 | | 0.24 | 107 | 1.4 | 13.5 | 41.1 | 73 | 17 | 482 | 0.31 | |
| 2* | 0.99 | | | 0.81 | 58.6 | 3.3 | | <LOQ | 1.3 | <LOQ | <LOQ | 1.7 | <LOQ | <LOQ | 490 | <LOQ | |
| 3* | 1.25 | | | 0.52 | 38.1 | 3.9 | | <LOQ | 31.8 | <LOQ | <LOQ | 13.0 | <LOQ | <LOQ | 328 | 0.17 | |
| 4* | 2.81 | | | 0.91 | 57.0 | 8.0 | | <LOQ | 1.0 | 5.8 | 8.0 | 12.5 | <LOQ | <LOQ | 598 | 0.26 | |
| 1a | <LOQ | <LOQ | 0.7 | 0.57 | <LOQ | <LOQ | | <LOQ | 18.8 | 20.1 | 16.8 | 29.4 | 27.5 | 35 | 452 | 0.41 | |
| 2a | 2.18 | 371 | 10.2 | 0.58 | 38.1 | 5.7 | | <LOQ | 29.3 | 4.6 | <LOQ | 11.5 | 130 | 6 | 375 | 0.24 | |
| 3a | 2.64 | 460 | 12.1 | 0.73 | 52.5 | 6.2 | | <LOQ | 1.1 | 4.2 | <LOQ | 2.2 | 81 | 14 | 432 | <LOQ | |
| 4a | 2.57 | 562 | 24.9 | 0.94 | 59.8 | 7.7 | | <LOQ | 0.8 | 3.6 | <LOQ | 1.6 | 102 | 3 | 599 | <LOQ | |
| 1b | <LOQ | <LOQ | 0.7 | 0.60 | 0.0 | <LOQ | | <LOQ | 3.0 | 6.5 | 20.6 | 31.2 | 2362 | 77 | 439 | 0.38 | |
| 2b | 2.63 | 415 | 25.7 | 0.70 | 41.2 | 6.4 | | <LOQ | 29.1 | 4.7 | <LOQ | 14.1 | 242 | 35 | 450 | 0.28 | |
| 3b | 2.62 | 388** | 86.4** | 0.76 | 51.9 | 6.8 | | <LOQ | 0.9 | 4.3 | <LOQ | 3.4 | 375 | 37 | 450 | <LOQ | |
| 4b | 2.63 | 464 | 93.9 | 0.92 | 57.0 | 7.0 | | <LOQ | 1.0 | 3.8 | 0.9 | 6.4 | 431 | 32 | 587 | 0.30 | |
| 1c | 1.70 | 0.4 | 0.9 | 0.63 | <LOQ | <LOQ | | <LOQ | 2.4 | 13.4 | 20.9 | 25.4 | 268 | 41 | 449 | 0.30 | |
| 2c | 2.96 | 412 | 78.5 | 0.79 | 46.8 | 7.3 | | <LOQ | 28.1 | 6.6 | <LOQ | 11.8 | 62 | 8 | 498 | 0.24 | |
| 3c | 2.55 | 391 | 74.5 | 0.78 | 52.3 | 7.0 | | <LOQ | 0.6 | 8.8 | <LOQ | <LOQ | 46 | 14 | 452 | <LOQ | |
| 4c | 2.64 | 451 | 86.0 | 0.91 | 56.1 | 7.1 | | <LOQ | 0.5 | 6.2 | <LOQ | <LOQ | 39 | 4 | 568 | <LOQ | |
| 1d | <LOQ | <LOQ | 0.8 | 0.49 | 6.7 | <LOQ | | 0.20 | 73.9 | 4.0 | 23.2 | 23.6 | 305 | 28 | 373 | 0.34 | |
| 2d | 2.13 | 364 | 12.0 | 0.59 | 34.2 | 5.4 | | <LOQ | 20.8 | 5.3 | 1.2 | 9.7 | 246 | 9 | 389 | 0.14 | |
| 3d | 2.33 | 465 | 9.8 | 0.77 | 51.4 | 6.1 | | <LOQ | 0.5 | 4.8 | <LOQ | <LOQ | 186 | 14 | 442 | <LOQ | |
| 4d | 2.47 | 535 | 24.5 | 0.91 | 56.2 | 6.8 | | <LOQ | 0.5 | 3.6 | <LOQ | 1.0 | 289 | 3 | 576 | <LOQ | |
| 1e | 1.54 | <LOQ | 0.6 | 0.53 | 4.6 | <LOQ | | 0.28 | 37.8 | 6.8 | 31.2 | 31.2 | 318 | 27 | 412 | 0.31 | |
| 2e | 2.11 | 246 | 12.5 | 0.43 | 24.9 | <LOQ | | <LOQ | 17.4 | 7.5 | 6.0 | 26.6 | 321 | 9 | 303 | 0.29 | |
| 3e | 2.76 | 438 | 13.6 | 0.73 | 47.9 | 6.3 | | <LOQ | 0.6 | 8.0 | 1.2 | 2.4 | 153 | 13 | 435 | <LOQ | |
| 4e | 2.53 | 506 | 20.7 | 0.88 | 51.2 | 6.4 | | <LOQ | 0.4 | 8.6 | <LOQ | <LOQ | 113 | 3 | 533 | <LOQ | |

¹ LOQ = Limit of Quantification

** sample not used for modelling due to missing analysis

** Fe species calculated from Fe_{tot} and measured Eh

S2: Additions to the minteq.v4.dat (Allison et al., 1991; U.S. Environmental Protection Agency, 1998) thermodynamic database used for the geochemical modelling calculations performed in the present study.

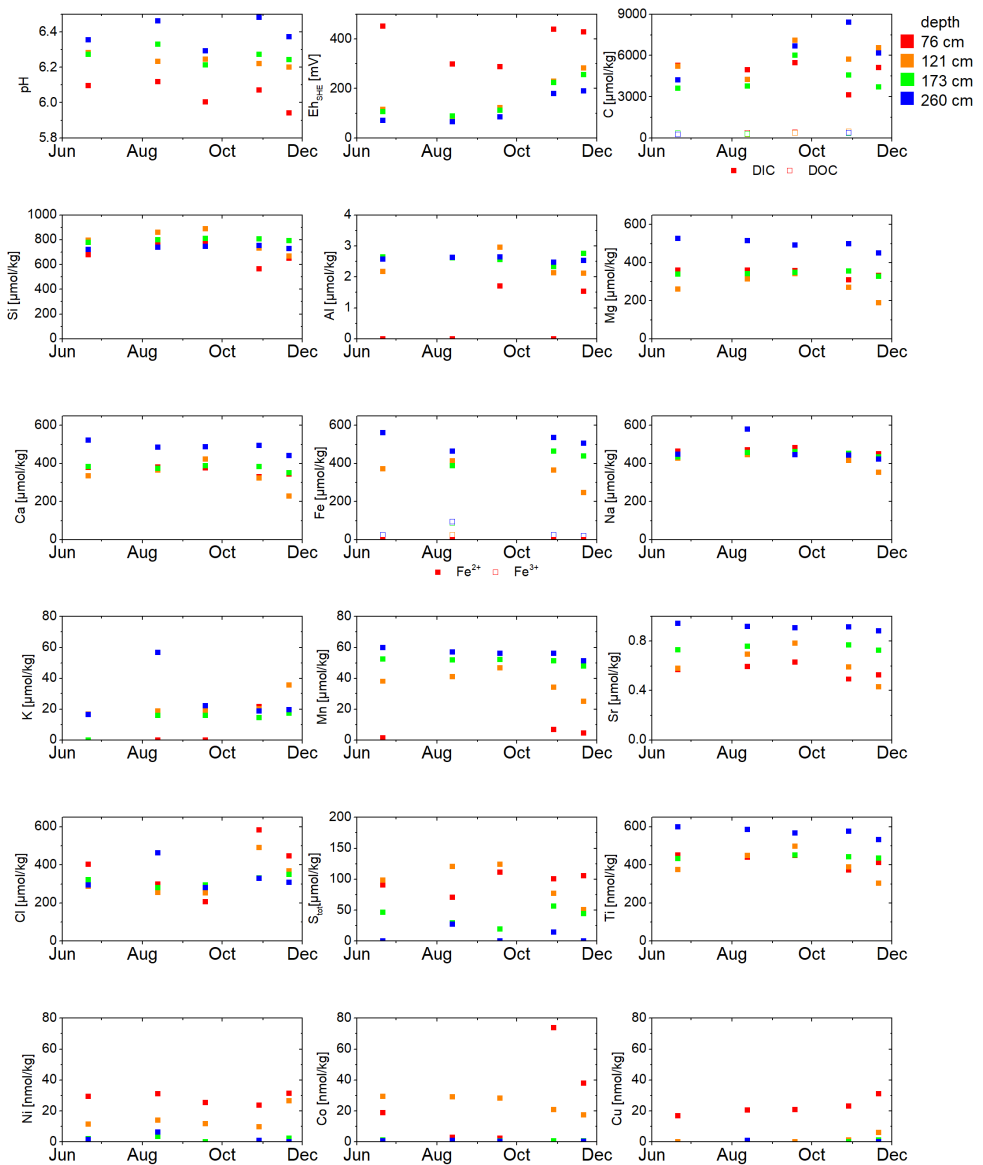
| Phase | Reaction | Log K | Ref |
|--------------------------|--|---------|--|
| Allophane Al/Si=2.02 | $(Al_2O_3SiO_2)(H_2O)_{2.53} + 4.47H_2O = 2Al(OH)_4^- + 2H^+ + H_4SiO_4$ | -32.16 | Stefanson and Gislason 2001 |
| Allophane Al/Si=1.64 | $(Al_2O_3(SiO_2)_{1.22})(H_2O)_{2.5} + 4.94H_2O = 2Al(OH)_4^- + 2H^+ + 1.22H_4SiO_4$ | -33.47 | Stefanson and Gislason 2001 |
| Allophane Al/Si=1.26 | $(Al_2O_3(SiO_2)_{1.59})(H_2O)_{2.63} + 5.55H_2O = 2Al(OH)_4^- + 2H^+ + 1.59H_4SiO_4$ | -35.04 | Stefanson and Gislason 2001 |
| Imogolite Natural Gel | $(Al_2SiO_3)((OH)_4) + 5H_2O = 2Al(OH)_4^- + 2H^+ + H_4SiO_4$ | -33.79 | Stefanson and Gislason 2001 |
| Moganite | $SiO_2 + 2H_2O = H_4SiO_4$ | -3.025 | Gislason et al. 1997 |
| Albite | $NaAlSi_3O_8 + 8H_2O = Na^+ + Al(OH)_4^- + 3H_4SiO_4$ | -18.002 | Parkhurst and Appelo 1999 |
| Anorthite | $CaAl_2Si_2O_8 + 8H_2O = Ca^{2+} + 2 Al(OH)_4^- + 2H_4SiO_4$ | -19.714 | Parkhurst and Appelo 1999 |
| K-feldspar | $KAlSi_3O_8 + 8H_2O = K^+ + Al(OH)_4^- + 3H_4SiO_4$ | -20.573 | Parkhurst and Appelo 1999 |
| Diopside | $CaMgSi_2O_6 + 4H^+ = Ca^{2+} + Mg^{2+} + 2H_2O + 2SiO_2$ | 20.9643 | Voigt et al. 2018 |
| Fayalite | $Fe_2SiO_4 + 4H^+ = SiO_2 + 2Fe^{2+} + 2H_2O$ | 19.1113 | Voigt et al. 2018 |
| Forsterite | $Mg_2SiO_4 + 4H^+ = SiO_2 + 2 H_2O + 2Mg^{2+}$ | 27.8626 | Voigt et al. 2018 |
| On-Site Basaltic Glass | $SiAl_{0.335}Fe_{0.265}Mg_{0.165}Ca_{0.22}Na_{0.12}K_{0.019}O_{3.222} + 1.104H^+ + 2.118H_2O = H_4SiO_4 + 0.335Al(OH)_4^- + 0.265Fe^{2+} + 0.165Mg^{2+} + 0.22Ca^{2+} + 0.12Na^+ + 0.019K^+$ | 0.75* | Oelkers and Gislason 2001 |
| Al-Oxalate+ | $Al^{3+} + Oxalate^{2-} = AlOxalate^+$ | 6.1 | IUPAC stability constant database, Version 5.84* |
| Al-Oxalate2- | $Al^{3+} + 2Oxalate^{2-} = Al(Oxalate)_2^-$ | 12.38 | IUPAC stability constant database, Version 5.84* |
| Al-Oxalate3-3 | $Al^{3+} + 3Oxalate^{2-} = Al(Oxalate)_3^{3-}$ | 15.12 | IUPAC stability constant database, Version 5.84* |

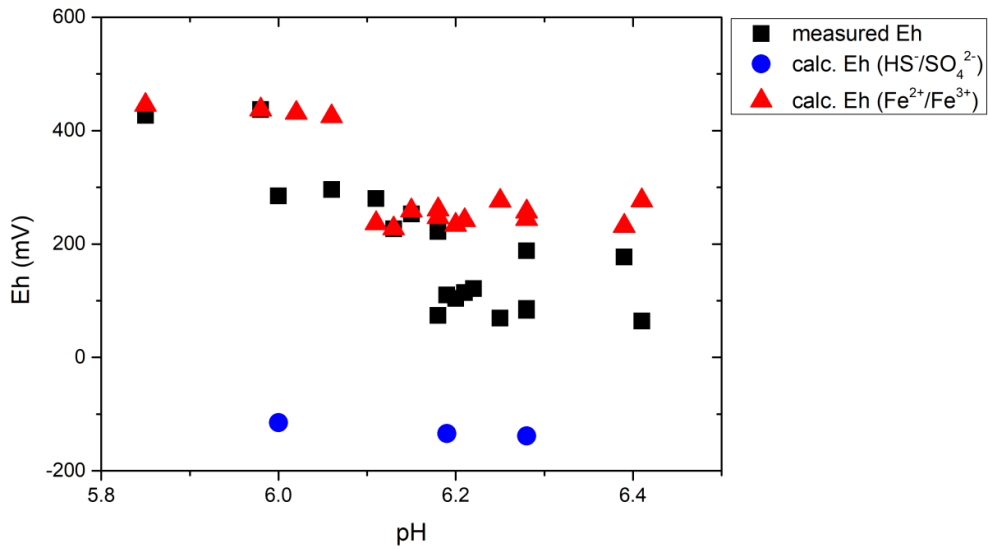
* ScQuery v.5.84, 2005 The IUPAC Stability Constant Database, Academic Software, (2005)

Table S3: Average rainwater composition from Mjóanes (southern Iceland) as reported by Eiriksdottir et al. (2014)

| Constituent | Concentration |
|------------------|--|
| pH | 5.6 |
| Ca ²⁺ | 10 $\mu\text{mol kg}_{\text{water}}^{-1}$ |
| Cl ⁻ | 225 $\mu\text{mol kg}_{\text{water}}^{-1}$ |
| K ⁺ | 4 $\mu\text{mol kg}_{\text{water}}^{-1}$ |
| Mg ²⁺ | 25 $\mu\text{mol kg}_{\text{water}}^{-1}$ |
| Na ⁺ | 261 $\mu\text{mol kg}_{\text{water}}^{-1}$ |
| S ⁶⁺ | 5 $\mu\text{mol kg}_{\text{water}}^{-1}$ |

S4: Elemental concentrations, pH and Eh of measured water samples as a function of time during the present study. The color of the symbols indicates the depth of the sample as indicated in the figure.





S5: Variation of sampled soil water Eh as a function of the corresponding fluid pH. The Eh measured using a redox electrode are shown as black squares. The Eh calculated from the measured Fe²⁺/Fe³⁺ concentration ratio are shown as blue circles. The Eh calculated from the measured HS⁻/SO₄²⁻ concentration ratios are shown as blue circles. The close correspondence between measured Eh values and those calculated using measured iron speciation suggests that iron speciation is controlling the oxidation potential in this system.

Dissolution rate calculations

| | | | |
|--------------------------|-----------------------------------|--------------------------------|------------------------------|
| Average Size calculation | μm | $d_{\text{eff}} (\mu\text{m})$ | $d_{\text{eff}} (\text{cm})$ |
| size | min 10 | 28.50 | 0.00285 |
| | max 62 | | |
| Surface area | 779.7 $\text{cm}^2 \text{g}^{-1}$ | | |

| | |
|------------------------------|---|
| Observed Basalt dissolution | $2.60 \times 10^{-3} \text{ mol kgw}^{-1}$ |
| Total rain per cm^2 | 925 mm |
| Annual Water Flux | 0.925 $\text{kgw cm}^{-2} \text{ surface}$ |
| Annual Basalt dissolution | $2.41 \times 10^{-3} \text{ mol cm}^{-2} \text{ surface}$ |

| | |
|---------------------------------------|---------------------------------------|
| Percent of remaining basalt each year | |
| Maximum mass of basalt added | 800 $\text{g yr}^{-1} \text{ m}^{-2}$ |
| Mass of basalt dissolved | 310 g kgw^{-1} |
| Mass of basalt dissolved annually | 286.75 g yr^{-1} |

| | |
|-----------------------------------|------------------------|
| Estimate of basalt in soil column | |
| mass of soil column calculation | |
| soil column height | 2.7 m |
| density of basalt | 2.7 g cm^{-3} |
| volume of basalt in 2.7 m | 40.5 cm^3 |
| mass of basalt in column | 109.35 g |

| | |
|-----------------------------|---|
| Estimation of reaction rate | |
| total surface area | 85263 cm^2 |
| rate | $2.82 \times 10^{-8} \text{ mol yr}^{-1}$ |
| surface normalized rate | $9.17 \times 10^{-16} \text{ mol cm}^{-2} \text{ s}^{-1}$ |

kgw = kilogram water

Appendix B: Supplementary Material Paper II

Direct evidence of CO₂ drawdown through enhanced weathering in soils

T. Linke, E.H. Oelkers, S.C. Möckel, S.R. Gislason

Supplementary Information

The Supplementary Information includes:

- Soil Classification and Soil Evolution in Iceland
- Detailed Field Site Description
- Details of Field Sampling
- Analytical Methods
- Elemental Analysis
- Calculation of Alkalinity Creation and Export in Our Studied Soil
- Estimated Organic Carbon Storage Within the Studied Soil
- Effect of Basalt on Organic Carbon
- Tables S-1 to S-4
- Supplementary Information References

Soil Classification and Soil Evolution in Iceland

Iceland is built of volcanic rocks, which are predominantly (80–85 %) of basaltic composition, the remainder being intermediate and silicic volcanics and clastic sediments that are mostly of basaltic composition (Saemundsson, 1979). The oldest exposed rocks are about 15 Myr (McDougall *et al.*, 1984). Iceland was fully covered with glaciers at the Last Glacial Maximum (~20 kyr BP). The ice sheet retreated close to the present coastline around 10.3 kyr BP, and at about 8.0 kyr BP Icelandic glaciers were of similar, or little lesser extent, than at the present (Norðdahl *et al.*, 2008). Hence, all Icelandic soils are of Holocene age younger than ~10 kyr BP (Arnalds, 2008).

Andosols are the dominant soils in Iceland, Vitrisols are present in desert areas and organic-rich Histosols are found in some wetland areas (Arnalds, 2008). Andosols are not common in Europe, but they are widespread in the active volcanic areas of the world (Arnalds, 2008). Two main factors are commonly used to classify Icelandic soils: deposition of aeolian (volcanic) material and drainage (Arnalds, 2004). Aeolian material mostly originates from the sandy desert areas located near active volcanic zones or from glaciofluvial outwash plains. After the settlement in Iceland, around 1076 yr BP, the extent of barren areas that are a source for aeolian material significantly increased (Gísladóttir *et al.*,

2008, Dugmore *et al.*, 2009). Andosols are often found in the wetland areas of Iceland where substantial aeolian input is present, lowering the relative organic content, or where some drainage is present, whereas organic-rich Histosols are found in wetlands with little aeolian input. The progression of soil types with improving drainage conditions from wet to dry follows: Histosols (>20 % C), Histic Andosols (12–20 % C), Gleyic Andosols (>1 to < 12 % C, poorly drained), and Brown Andosols (>1 to < 12 % C, freely drained) and Vitrisols with <1 % organic carbon (Arnalds, 2008). This order also reflects the decreasing distance from the volcanic zones and the source of aeolian materials. The transition between these soil types is fluent, and changes in drainage or aeolian input can lead to a change of the soil type. It is postulated that in absence of the volcanic influences, Icelandic wetland soils would largely be organic Histosols, typical of the arctic environments (Arnalds, 2015, 2008). This suggests that applying enhanced weathering EW by the addition of basaltic dust to an organic-rich Histosol can lead to its transition to a more mineral-rich soil such as an Andosol, as found in our study area.

Histosols or peatlands are classified further as *ombrotrophic* or *minerotrophic*, based on the origin and mineral content of the waters feeding them (Rydin and Jeglum, 2013). While *minerotrophic* soils receive mostly ground water that has interacted with the bedrock upstream, leading to an enrichment of the mineral content in the water, *ombrotrophic* soils are dominantly fed by rainwater, and are therefore nearly free of rock derived dissolved constituents (Rydin and Jeglum, 2013). Our studied field site receives mostly rainwater. Therefore, all dissolved constituents in our soil water are assumed to originate from the interaction of rainwater with the embedded dust of our soil, and the decay of organic matter. Based on this assumption, we compare our data (see Fig. 3) with data from other sites reported in the literature as mostly *ombrotrophic*, implying limited interaction with the underlying bedrocks.

Detailed Field Site Description

The field site is located above the source of the Rauðalækur (“Red creek”) river at 63° 53' 42.5" N 20° 21' 15.9" W, 7 km north of the town of Hella, South Iceland. This field site has not been used for agriculture or fertilized for at least the past 10 years prior to this study, hence limited anthropogenic contamination is therefore expected. Based on data from the Icelandic Meteorological Office, the average soil temperature is ~7 °C during the summer (Petersen and Berber, 2018). At 100 cm soil depth, the annual maximum temperature is 9 °C and the annual minimum temperature is 1 °C. The soil can, however, temporarily freeze down to a depth of 50 cm (Petersen and Berber, 2018). The annual rainfall in this area is 1250 ± 200 mm. The average storm yields an average of 15 mm of rain with a maximum duration of 20 hours (www.en.vedur.is/climatology/data). The surface of the studied soil is hummocky, and the vegetation is characterized by graminoids with a clear predominance of Poaceae. The direction of the groundwater flow, estimated based on the surrounding drainage channels, is towards S/SE. Based on field observations, the groundwater table fluctuates near a depth of 50 cm.

The field site is adjacent to a natural escarpment allowing for the characterization of the subsurface soil profile. Several tephra layers were identified within a cleared vertical face of the escarpment. Layers of organic-rich soil

admixed with air-borne basaltic dust separate the tephra layers. The dust in these layers is finer grained than the basalt in the tephra layers. The tephra layers can be assigned to specific volcanic eruptions, as each volcanic eruption in Iceland has its own chemical fingerprint (Dugmore *et al.*, 2009; Grönvold *et al.*, 1995). These allow determination of the soil accumulation rates. As can be seen in Figure 1b, over the last 3300 years about 220 cm of soil has accumulated, averaging to a soil thickening rate of 0.067 cm yr^{-1} . The ‘Settlement layer’, a tephra layer from an eruption of the Vatnaöldur volcanic system at $1079 \pm 2 \text{ BP}$ (Grönvold *et al.*, 1995), which approximately coincides with the initial settlement (Landnám) of Iceland, was barely discernible in the soil profile. Although the exact depth of this Settlement tephra at around 96 cm depth is somewhat uncertain, its location suggests an average soil accumulation rate of 0.086 cm yr^{-1} during the last 1120 years. This is consistent with Gísladóttir *et al.* (2011) who reported that the dust flux over South-Central Iceland increased following the emplacement of the Settlement layer. A detailed description of the soil profile is provided in Table S-1 of the Supplementary Information following the guidelines provided in Schoeneberger *et al.* (2012).

Details of Field Sampling

In situ soil waters were sampled 10 m North from the escarpment in the field with suction cup samplers obtained from Prenart, Denmark. Four suction cup samplers were installed into holes drilled at an angle of 60° at depths of 76, 121, 173, 260 cm on 8 November 2017, following the method of Sigfusson *et al.* (2006). The samplers were left in the field over the winter to allow settling of the soil around the samplers and tubing. The first samples from these suction cup samplers were collected during May 2018 and the last were collected November 2018. The suction cup samplers, which are 95 mm long and 21 mm in outer diameter, consist of a 48/52 % mixture of Polytetrafluorethylene (PTFE) and quartz with an average pore size of $2 \mu\text{m}$. These samplers were connected by 1.8 mm inner diameter Teflon (Fluorinated ethylene propylene) tubing to the surface. Four 60-mL syringes located at the surface were connected *via* 3-way valves and 100 cm long connection polyethylene tubing to the Teflon tubing of the subsurface samplers. The first 30–50 mL of extracted soil water during any sampling was discarded to avoid contamination. It took about 6–8 hours to fill the 60 mL sampling syringes. During the sampling the syringes were kept in a closed cooling box to prevent heating and exposure to sunlight. This approach was adapted to avoid any degassing of the soil solutions and oxidation of the samples. No colour change of the soil solutions due to iron oxidation was observed during the sampling.

Initial sample analysis was performed in the field including sample pH, temperature and Eh measurements, conductivity determination and H_2S titration. Subsamples for major and trace element analysis *via* ICP-OES and ICP-MS as well as for ion chromatography to determine $\text{Fe}^{2+}/\text{Fe}^{3+}$, DOC analysis and alkalinity titration were collected and stabilized on site and analysed later in the lab.



Analytical Methods

The redox potentials (E_{meas}) of the collected fluids were measured directly in the sample syringes in the field using a Microelectrodes Inc MI-800 Micro-ORP Ag/AgCl micro combination redox electrode with a ± 10 mV uncertainty. These values were converted to equivalent potentials for a standard hydrogen electrode (E_{SHE}) using a +199 mV reference potential, E° , for the Ag/AgCl electrode (Sawyer *et al.*, 1995). This calculation was performed using the Nernst equation:

$$E_{\text{SHE}} = E_{\text{meas}} + \ln(10) \cdot (R \cdot T) / F \cdot \text{pH} + E^\circ_{\text{Ag/AgCl}},$$

where R refers to the gas constant, F designates the Faraday's constant, and T symbolizes the temperature in kelvin. Subsequently, ~ 5 mL of each sampled fluid was transferred into 10 mL polypropylene vials for pH temperature, dissolved oxygen, and conductivity measurement. The pH was measured using a Eutech pH 6+ electrode with an uncertainty of ± 0.01 pH units. The dissolved oxygen and conductivity of the samples were measured using a Micro electrodes MI-730 Micro-Oxygen Electrode with an uncertainty of ± 0.5 % and a Eutech COND 6+ with an uncertainty of ± 10 μS , respectively. For major and trace element analysis, 10 mL of each fluid sample was first filtered through 0.2 μm cellulose acetate in-line filters then transferred into acid washed polypropylene bottles. A small quantity of 65 % Merck suprapure HNO_3 was added to acidify these samples to 0.5 % HNO_3 . Samples for iron speciation measurement were first filtered through 0.2 μm cellulose acetate in-line filters then placed into acid cleaned polypropylene bottles. Merck HCl was added to these samples to attain a final acid concentration of 0.5 %. Samples for dissolved organic carbon analysis were collected in acid washed polycarbonate bottles and acidified with 0.5 M suprapure, Merck HCl to a final acid concentration of 3.3 %.

Dissolved hydrogen sulphide, H_2S , was determined in the field by precipitation titration immediately after sampling with an uncertainty of ± 0.7 $\mu\text{mol kg}^{-1}$, using mercury acetate solution $\text{Hg}(\text{CH}_3\text{COO})_2$ of a known concentration as described by Arnórsson (2000). Alkalinity titrations were performed immediately after returning the samples to the laboratory. For each titration, ~ 5 mL of fluid was transferred in a 10 mL vial and titrated to pH 3.3 by addition of 0.1 M HCl while constantly stirring the fluid. The pH of the fluid was recorded using a glass pH electrode together with a pH 110, Eutech instruments millivolt meter. The alkalinity was calculated by the Gran method using the inflection points (Gran, 1952). The final measured alkalinity values are given in meq kg^{-1} with an uncertainty of ± 5 % or less.

Elemental Analysis

Major element compositions of all fluid samples were determined using a Ciroso Vision, Spectro Inductively Coupled Plasma Optical Emission Spectrometer (ICP-OES). The instrument was calibrated using the SEL-11 in-house standard, which was referenced to the SPEX CertiPrep commercial standard material. All standards and measured samples were acidified to 0.5 % using suprapure HNO_3 prior to analysis. All measurements were run in duplicate. Blank solutions were measured after every 5 samples and uncertainties were below ± 5 % for each element.



Iron species were determined using a Dionex 3000 ion chromatography system equipped with a Variable Wavelength Detector using the method described by Kaasalainen *et al.* (2016). This method separates Fe^{2+} and Fe^{3+} using pyridine-2,6-dicarboxylic acid (PDCA) as a chelating agent. It detects the distinct Fe cations by post-column derivatization using 4-(2-pyridylazo)resorcinol with a peak absorbance at 530 nm, a detection limit of $\sim 2 \mu\text{g L}^{-1}$ and an uncertainty of $\pm 2\%$ or less for Fe^{2+} and $\pm 10\%$ for Fe^{3+} for 200–1000 μL samples.

Dissolved organic carbon concentrations were determined by size exclusion chromatography using a Liquid Chromatography – Organic Carbon Detection system (LC-OCD) obtained from DOC Labor in Karlsruhe, Germany, following the method of Huber *et al.* (2011). The system was calibrated for the molecular masses of humic and fulvic acids using standard material from the Suwannee River, provided by the International Humic Substances Society (IHSS). All DOC measurements have an uncertainty of 5 % or less.

Calculation of Alkalinity Creation and Export in Our Studied Soil

Alkalinity export in our field site was determined by multiplying the mass of water passing through the soil by the alkalinity generated in the soil, taking account the loss of alkalinity as the soil solution interacted with the atmosphere. Any effect of eventual changes in this alkalinity after the fluids arrive in the oceans is not taken into account. The alkalinity of the soil solution after its equilibration with the atmosphere was calculated using the PHREEQC software version 3.4.0 (Parkhurst and Appelo, 1999) together with the minteq.v4 thermodynamic database (Allison *et al.*, 1991; US Environmental Protection Agency, 1998). This alkalinity was determined from the average of all measured major element concentrations, pH and alkalinity in the deepest soil water samplers (see Table S-2). This fluid was equilibrated with atmospheric O_2 concentration. Ferrihydrite is allowed to precipitate at local equilibrium as the fluid oxidized. The resulting fluid was then equilibrated with the 400 ppm CO_2 concentration of the atmosphere to account for fluid degassing.

The mass of fluid passing through the soil was estimated to be equal to the difference between the mean precipitation for the field site minus the evapotranspiration and the direct runoff. The mean precipitation is equal to $1250 \pm 200 \text{ mm yr}^{-1}$, based on the records from the measurement station in Hella located ~ 7 km away from the field site operated by the Icelandic Metrological Office Veðurstofa Íslands (<https://en.vedur.is/climatology/data>). The evapotranspiration at the field site was estimated based on Jóhannesson *et al.* (2007) to be equal to 16 % of the precipitation corresponding to 200 mm yr^{-1} . The direct surface runoff is estimated to be 10 %, based on data published by Sigurðsson *et al.* (2004). After subtracting the evapotranspiration and direct surface runoff, approximately $925 \pm 150 \text{ kg m}^{-2} \text{ yr}^{-1}$ of water are estimated to pass through the studied soil annually.

The soil water alkalinity in the deep soil was $2.59 \pm 0.34 \text{ meq kg}^{-1}$ based on the average of the measurements at 260 cm depth. The average alkalinity for the surface waters after oxidation and the precipitation of ferrihydrite calculated with PHREEQC is $1.53 \pm 0.2 \text{ meq kg}^{-1}$. Note that the oxidation from Fe^{2+} to Fe^{3+} releases H^+ . The consequential formation of ferrihydrite from the Fe^{3+} releases additional H^+ , decreasing the pH and alkalinity as well as decreasing

CO₂ solubility. Multiplying this 1.53 ± 0.2 meq kg⁻¹ average alkalinity value by the estimated annual water flux through the soil yields an annual alkalinity export *via* surface waters of 1.45 ± 0.3 eq m⁻² yr⁻¹. Multiplying this number by the atomic weight of carbon yields an annual carbon flux of 17 ± 3.6 g m⁻² yr⁻¹ or 0.17 ± 3.6 t ha⁻¹ yr⁻¹ of C. Note the long-term fate of this captured carbon may evolve once the river water transporting this carbon arrives in the oceans. It should be emphasized that the alkalinity drawn down by the increasing alkalinity could include some contribution from decaying organic material in the soil column. This carbon was originally removed from the atmosphere by photosynthesis, so contributes to the carbon drawdown from the atmosphere as does the direct dissolution of CO₂ from the atmosphere.

To extrapolate the annual mass of carbon drawdown to the gigaton scale, we divided one gigaton of CO₂, which is equal to 2.73×10^8 tons of C by the 0.17 t ha⁻¹ yr⁻¹ of C drawdown in rivers provoked by the addition of basaltic dust to our field site. This yielded a surface area of 1.6×10^9 ha. This surface area is equal to 1.6×10^7 km². This is larger than the surface area of the United States, which is equal to 9.8×10^6 km². The mass of dust needed to be added to 1.6×10^7 km² annually to attain the same $500\text{--}800$ g m⁻² yr⁻¹ of dust added to our study site is obtained by multiplying this flux and surface area. This calculation yields 8 to 13×10^9 t yr⁻¹, which equals 8 to 13 Gt yr⁻¹.

One additional caveat to applying alkalinity generation from enhanced weathering of soils on the continents to global carbon drawdown from the atmosphere is the fate of soil generated alkalinity after its transport in rivers to the oceans. The exact mass of CO₂ removed from the oceans due to alkalinity input is currently debated, but is likely attenuated by carbonate mineral precipitation (Renforth and Henderson, 2017; Moras *et al.*, 2022; Hartmann *et al.*, 2023). Recent estimates suggest a CO₂ uptake efficiency of only 0.6 to 0.8 mol of CO₂ for each mole of alkalinity added to the oceans (He and Tyka, 2023). Such observations suggest that the total carbon drawdown from the atmosphere by alkalinity generation on the continents will depend on the eventual fate of this alkalinity and it is likely decreased by marine processes.

Estimated Organic Carbon Storage Within the Studied Soil

A substantial mass of carbon is stored by soils in organic material. The rate of organic carbon buildup in our studied soil can be estimated by taking account of the rate of soil formation and the organic content of this soil. The average soil formation rate at our study site is estimated to be 0.067 cm yr⁻¹. This estimate is made by dividing the current 2.2 m soil thickness by 3300 years, the time the soil developed (see Fig. 1). The organic carbon content of the studied Histic/Gleyic Andosol is between $\sim 12\%$ and 20% of the dry mass and it has a porosity between 50% and 75% (Snæbjörnsson, 1982; Orradóttir *et al.*, 2008). The mass of organic carbon in our studied soil was estimated by considering it is comprised of two parts, an upper part formed after the settlement (1076 yr BP) and a lower part formed from 1076 down to 3300 yr BP (Fig. 1). This separation is based on the report of an increase in dust flux after this time (Gísladóttir *et al.*, 2008; Dugmore *et al.*, 2009). These parts are divided based on the position of tephra layers that allow the direct determination of the net rates of soil accumulation, including the effects of soil erosion, over time. The upper part is a Gleyic Andosol containing

<12 % C by dry weight extending down to ~90 cm, while the lower part is a Histic Andosol containing 12–20 % C by dry weight from ~90 to 218 cm. These maximum soil carbon values of 12 and 20 % were multiplied by the height of each soil section, assuming a porosity between 50 and 75 % (Snæbjörnsson, 1982; Orradottir *et al.*, 2008) to estimate the total carbon present in the studied soil. The combination of this range of carbon content and porosity values yield an estimated total mass of organic carbon stored in this soil equal to 86–172 kg C m⁻². The total mass of carbon estimated in our study area compares well with corresponding estimates of Óskarsson *et al.* (2004), who estimate the C stocks of Histosols in Iceland to be on average 197 kg C m⁻², and the more mineral-rich Histic Andosols in Iceland to be 89 kg C m⁻². Further details of this calculation are provided in Table S-4. Dividing this mass by the 3300-year age of the soil column yields an average organic carbon production rate of 26–52 gC m⁻² yr⁻¹. Note that the mass of carbon in organic material, reported in units of mass of C can be converted to the equivalent mass CO₂ by multiplying the former by the ratios of their respective molar masses: 44/12.

Effect of Basalt on Organic Carbon

The degree to which the addition of basalt increases or decreases the total mass of organic carbon in a soil is currently poorly constrained. Vicca *et al.* (2022) argued that the efficiency of enhanced weathering effort is governed by biologic processes. These authors noted that nutrients released by the addition of ground rocks to soils could enhance plant growth and promote organic carbon storage in soils. They also postulated that the addition of this material could accelerate organic material decay in the subsurface. Goll *et al.* (2021) suggested that the addition of basalt to soils would improve the fertility potentially, enhancing organic carbon storage in soils. Some supporting evidence was reported by Angst *et al.* (2018), who observed that soils derived from a basaltic rock stored more organic carbon than soils derived from sandstone or from loess. This was interpreted by these authors to be due to a combination of a higher clay content and greater availability of nutrients in the basalt derived soils. Similarly, da Silva *et al.* (2016) concluded that the organic carbon content of soils derived from granitic rocks increased with increasing mafic content of the parent rock due to increased clay mineral content. Möckel *et al.* (2021a, 2021b) provided evidence that volcanic mineral dust, and soil and tephra layers hamper organic carbon decomposition in Histosols of natural peatlands in Iceland. In contrast, other studies found that soil parent material and mineral oxide compositions have little effect on the mass of organic carbon in soils (Araujo *et al.*, 2017). One factor that is clearly detrimental to the preservation of soil organic carbon is tilling. Soil tilling has been shown to accelerate greatly soil organic carbon degradation (Wang *et al.*, 2020; Shakoor *et al.*, 2021; Li *et al.*, 2023). Such observations suggest that the way that basaltic dust is added to soil during enhanced weathering efforts may be critical for increasing the net carbon drawdown in these soils. In either case, consideration of the relative rates of carbon drawdown through inorganic compared to organic processes presented in this study suggests that the latter may dominate the net carbon storage in soils due to enhanced weathering. This makes the quantification of the role of basaltic dust on productivity and organic preservation a critical factor in optimizing enhanced weathering efforts.

Supplementary Tables

Table S-1 Description of the soil profile depicted in Figure 1a and 1b. Profile description following Schoeneberger *et al.* (2012). Note that O horizons are here defined as layers with an estimated carbon content $\geq 12\%$.

| Horizon | Depth (cm) | Roots (quantity and size) ¹ | Boundary (distinctness, topography) ² | Structure (grade, size, type) ³ | Mottles (quantity and size) ⁴ | Soil colour (moist; Munsell colour code) | Comments |
|---------|--|--|--|--|--|--|--|
| A (O) | 0–23 | 3 vf, 2 f, 2 m | G, S | 3, f, sbk | f 1 | 2.5YR 3/4 7.5YR 2.5/2; colour change towards 2.5YR 4/3 in the lower half of the horizon | |
| 2O1 | 23–35 | 3 vf, 2 f, 1 m | C, W | 2, f, abk | f 1 | Gradual downwards colour change from 10YR 3/3 to 7.5YR 2.5/3 | |
| 2O2 | 35–58 | 3 vf, 1 f, 1 m | C, W | 2, tn, pl | – | 7.5YR 2.5/2 (main horizon colour); 7.5YR 4/6 (mottles) | 41–41.5 cm: dark basaltic tephra At the top 0.5–1 cm: intermixing of dark basaltic tephra |
| 2O3 | 58–71 | 1 vf, very few f, very few co | G, B | t, m, sbk | m 5 | | |
| 2O4 | 71–96 | very few vf, 1 co | A, W | 1, m, abk | m 5 | 7.5 YR 4/6 | 100.5–101.5 cm: coarse grey beige coloured tephra |
| 2O5 | 96–114.5 | 2 vf, 1 f, 1 co | A, W | 2, f, sbk | c 2, c 3 | 7.5YR 2.5/1 | |
| 2O6 | 116.5–133 | 3 vf, very few f, 1 co | A, W | 2, m, pl | f 1 | 7.5YR 2.5/1 | 124.5–125 cm: dark basaltic tephra Layer of rather coarse material; might for instance be from a flooding event |
| 2O7 | 133–137 | 3 vf | A, W | 2, m, gr | f 2 | 7.5YR 2.5/2 | dark basaltic tephra |
| 3C – T | 137–139.5 | | | | | | wood remains in the lower half of the horizon (σ : c. 1.5–4 cm) |
| 4O | 139.5–162 | 3 vf, 1 f, f co | A, W | 2, tk, pl | – | 7.5YR 2.5/1 | |
| 5C – T | 162–164.5 | | | | | | very coarse dark-light tephra |
| 6O | 164.5–182 | 3 vf | A, W | 1, m, pl | – | 7.5YR 2.5/1 | wood remains (quite evenly distributed); σ : c. 1.5 cm |
| 7C – T | 182–187.5 187.5–2018 (bottom of the ditch) | 3 vf, 1 f | not applicable, bottom of the ditch | 2 tk pl | – | 7.5YR 2/2 | dark basaltic tephra |
| 8O | | | | | | | Wood remains ($\sigma \leq$ c. 2 cm) |

¹ vf=very fine, f=fine, m=medium, co=coarse; ² A=abrupt, C=clear, G=gradual, S=smooth, W=wavy, B=broken; ³ f=fine, tn=fine, m=medium, tk=coarse, sbk=subangular blocky, abk-angular blocky, pl=platy, gr=granular; ⁴ f=few, m=many, c=common.



Table S-2 Soil water compositions measured in the present study.

| Sample | Date | Depth (cm) | T (°C) | pH | E _h SHE (mV) | Alk (meq kg ⁻¹) | DIC (mmol kg ⁻¹) | DOC (µmol kg ⁻¹) | Major element concentrations (µmol kg ⁻¹) | | | | | | | | | |
|------------------|------|------------|--------|------|-------------------------|-----------------------------|------------------------------|------------------------------|---|-----|------|-----|-----|---------------------|-----|------|------------------|------------------|
| | | | | | | | | | Si | Na | K | Ca | Mg | S(tot) ⁻ | Cl | Al | Fe ²⁺ | Fe ³⁺ |
| LOQ ¹ | | | | | | | | | 4.0 | 11 | 3.0 | 1.0 | 0.2 | 6.0 | 28 | 0.28 | 0.1 | 0.1 |
| 1* | 23 | 76 | 9 | 5.84 | 233 | 1.48 | | | 678 | 449 | 7 | 420 | 402 | 97 | 402 | 0.93 | | |
| 2* | May | 121 | 9 | 6.27 | -9 | | | | 716 | 435 | 13 | 427 | 379 | 102 | 357 | 0.99 | | |
| 3* | 2018 | 173 | 8.9 | 6.35 | -8 | | | | 717 | 390 | 14 | 293 | 233 | 79 | 350 | 1.25 | | |
| 4* | | 260 | 10.1 | 6.37 | -57 | 2.3 | | | 644 | 441 | 20 | 513 | 535 | 7 | 284 | 2.81 | | |
| 1a | 21 | 76 | 19.7 | 6.02 | 451 | 1.41 | 4.45 | 247 | 678 | 464 | <LOQ | 380 | 359 | 90 | 404 | <LOQ | <LOQ | 0.7 |
| 2a | June | 121 | 19 | 6.21 | 116 | 1.56 | 3.72 | 252 | 797 | 427 | 17 | 334 | 261 | 99 | 287 | 2.18 | 371 | 10.2 |
| 3a | 2018 | 173 | 19.2 | 6.2 | 106 | 1.53 | 3.67 | 344 | 778 | 435 | <LOQ | 384 | 340 | 47 | 322 | 2.64 | 460 | 12.1 |
| 4a | | 260 | 24.8 | 6.25 | 71 | 2.21 | 4.75 | 233 | 722 | 448 | 16 | 522 | 527 | <LOQ | 295 | 2.57 | 562 | 24.9 |
| 1b | 14 | 76 | 16.8 | 6.06 | 298 | 1.5 | 4.57 | 381 | 761 | 471 | 0 | 381 | 361 | 71 | 300 | <LOQ | <LOQ | 0.7 |
| 2b | Aug | 121 | 15.9 | 6.18 | 76 | 1.38 | 3.50 | 258 | 860 | 446 | 19 | 365 | 314 | 120 | 255 | 2.63 | 415 | 25.7 |
| 3b | 2018 | 173 | 15.2 | 6.28 | 88 | 1.59 | 3.55 | 265 | 802 | 456 | 16 | 374 | 341 | 29 | 280 | 2.62 | 388** | 86.4** |
| 4b | | 260 | 15.4 | 6.41 | 66 | 2.13 | 4.05 | | 740 | 581 | 57 | 486 | 515 | 27 | 462 | 2.63 | 464 | 93.9 |
| 1c | 18 | 76 | 7.6 | 6 | 287 | 1.5 | 5.47 | 418 | 772 | 482 | <LOQ | 378 | 358 | 111 | 206 | 1.70 | 0.4 | 0.9 |
| 2c | Sep | 121 | 8.9 | 6.22 | 123 | 2.34 | 5.85 | 339 | 887 | 450 | 19 | 422 | 342 | 124 | 254 | 2.96 | 412 | 78.5 |
| 3c | 2018 | 173 | 8.2 | 6.19 | 112 | 2.5 | 6.53 | 344 | 810 | 463 | 16 | 387 | 348 | 20 | 293 | 2.55 | 391 | 74.5 |
| 4c | | 260 | 7.5 | 6.28 | 85 | 3.02 | 7.04 | 331 | 747 | 446 | 22 | 487 | 493 | <LOQ | 282 | 2.64 | 451 | 86.0 |
| 1d | 29 | 76 | 22.5 | 5.98 | 439 | 0.83 | 2.73 | 382 | 566 | 449 | 22 | 330 | 310 | 101 | 583 | <LOQ | <LOQ | 0.8 |
| 2d | Oct | 121 | 22.5 | 6.13 | 229 | 1.56 | 4.04 | 488 | 732 | 416 | 20 | 323 | 269 | 77 | 492 | 2.13 | 364 | 12.0 |
| 3d | 2018 | 173 | 22.5 | 6.18 | 224 | 2.16 | 5.20 | 329 | 807 | 453 | 14 | 383 | 354 | 57 | 332 | 2.33 | 465 | 9.8 |
| 4d | | 260 | 22.5 | 6.39 | 179 | 2.8 | 5.20 | 366 | 755 | 444 | 19 | 494 | 499 | 14 | 328 | 2.47 | 535 | 24.5 |
| 1e | 21 | 76 | 22.6 | 5.85 | 429 | 1.08 | 4.40 | | 650 | 450 | 17 | 343 | 333 | 106 | 446 | 1.54 | <LOQ | 0.6 |
| 2e | Nov | 121 | 22.6 | 6.11 | 282 | 1.21 | 3.24 | | 668 | 354 | 36 | 229 | 190 | 50 | 368 | 2.11 | 246 | 12.5 |
| 3e | 2018 | 173 | 22.6 | 6.15 | 255 | 2.17 | 5.45 | | 794 | 435 | 17 | 351 | 327 | 44 | 349 | 2.76 | 438 | 13.6 |
| 4e | | 260 | 22.6 | 6.28 | 190 | 2.78 | 5.88 | | 730 | 423 | 20 | 442 | 451 | <LOQ | 309 | 2.53 | 506 | 20.7 |

¹ Limit of Quantification.

* Sample not used for modelling due to missing analysis.

** Fe species calculated from Fe_{tot} and measured Eh.

Table S-3 Literature data included in Figure 3.

| pH | Alkalinity (meq kg ⁻¹) | Classification | Reference | Location |
|--|--|--|-------------------------------|--|
| 3.96 3.93 5.38 5.44 6.28 6.21 6.00 5.93 | 0 0 0.198 0.371 0.764 0.743 0.623 0.695 | Bog Poor fen Forested moderately rich fen Open moderately rich fen | Vitt <i>et al.</i> (1995) | Central Alberta, Canada |
| 5.17 5.33 | 0.055 0.01 | Not specified | Dawson <i>et al.</i> (2002) | NE Scotland, United Kingdom Mid Wales, United Kingdom |
| 5.46 4.68 4.74 4.52 | 0.5 0.2 0 0 | Minerotrophic lawns Ombrotrophic carpets Ombrotrophic lawns Ombrotrophic hummocks | Bragazza <i>et al.</i> (2005) | Wöfl Moor, South Tyrol, Italy |
| 5.04 3.76 3.75 3.68 | 0.7 0 0 0 | Minerotrophic lawns Ombrotrophic carpets Ombrotrophic lawns Ombrotrophic hummocks | Bragazza <i>et al.</i> (2005) | Ryggmossen, Uppsala, Sweden |
| 4.2 4.17 4.66 | 0.02 0.02 0.076 | Bog water | Kulzer <i>et al.</i> (2001) | Western Washington, King County, USA |
| 3.6 6.5 | 0 1.082 | Ombrotrophic bog Groundwater fen | Verry (1975) | Minnesota, USA |

Table S-4 Estimates of the carbon stock of the field site and annual accumulation rates with varying porosity.

| Depth | 75 % porosity | | 50 % porosity | |
|------------------------------------|---|---|---|---|
| | 0–90 cm soil | 90–218 cm soil | 0–90 cm soil | 90–218 cm soil |
| cm of tephra (zero organic carbon) | – | 10 cm | – | 10 cm |
| C content | 12 % | 20 % | 12 % | 20 % |
| Soil height | 90 cm | 118 cm | 90 cm | 118 cm |
| Soil mass | 225 kg m ⁻² | 295 kg m ⁻² | 450 kg m ⁻² | 590 kg m ⁻² |
| mass organic carbon | 27 kg C m ⁻² | 59 kg C m ⁻² | 54 kg C m ⁻² | 118 kg C m ⁻² |
| Total C stored | 86 kg C m⁻² | | 172 kg C m⁻² | |
| Timespan | 1140 years | 2180 years | 1140 years | 2180 years |
| C accumulation rate | 0.024 kg C m ⁻² yr ⁻¹ | 0.027 kg C m ⁻² yr ⁻¹ | 0.047 kg C m ⁻² yr ⁻¹ | 0.054 kg C m ⁻² yr ⁻¹ |

Supplementary Information References

- Allison, J.D., Brown, D.S., Novo-Gradac, K.J. (1991) MINTEQA2/PRODEFA2, *A geochemical assessment model for environmental systems: version 3.0 user's manual*. Environmental Research Laboratory Office of Research and Development U.S. Environmental Protection Agency, Athens, Georgia.
- Angst, G., Messinger, J., Greiner, M., Häusler, W., Hertel, D., Kirfel, K., Kögel-Knabner, I., Leuschner, C., Rethemeyer, J., Mueller, C.W. (2018) Soil organic carbon stocks in topsoil and subsoil controlled by parent material, carbon input in the rhizosphere, and microbial-derived compounds. *Soil Biology and Biochemistry* 122, 19–30. <https://doi.org/10.1016/j.soilbio.2018.03.026>
- Araujo, M.A., Zinn, Y.L., Lal, R. (2017) Soil parent material, texture and oxide contents have little effect on soil organic carbon retention in tropical highlands. *Geoderma* 300, 1–10. <https://doi.org/10.1016/j.geoderma.2017.04.006>
- Arnalds, O. (2004) Volcanic soils of Iceland. *Catena* 56, 3–20. <https://doi.org/10.1016/j.catena.2003.10.002>
- Arnalds, O. (2008) Soils of Iceland. *Jökull* 58, 409–421. <https://doi.org/10.33799/jokull2008.58.409>
- Arnalds, O. (2015) *The Soils of Iceland*. World Soils Book Series, Springer, Dordrecht. <https://doi.org/10.1007/978-94-017-9621-7>
- Arnórsson, S. (2000) *Isotopic and Chemical Techniques in Geothermal Exploration, Development and Use*. International Atomic Energy Agency, Vienna.
- Bragazza, L., Rydin, H., Gerdol, R. (2005) Multiple gradients in mire vegetation: A comparison of a Swedish and an Italian bog. *Plant Ecology* 177, 223–236. <https://www.jstor.org/stable/20146727>
- Da Silva, Y.J.A.B., do Nascimento, C.W.A., Biondi, C.M., van Straaten, P., de Souza Jr., V.S., Ferreira, T.O. (2016) Weathering rates and carbon storage along a climosequence of soils developed from contrasting granites in northeast Brazil. *Geoderma* 284, 1–12. <https://doi.org/10.1016/j.geoderma.2016.08.009>
- Dawson, J.J.C., Billett, M.F., Neal, C., Hill, S. (2002) A comparison of particulate, dissolved and gaseous carbon in two contrasting upland streams in the UK. *Journal of Hydrology* 257, 226–246. [https://doi.org/10.1016/S0022-1694\(01\)00545-5](https://doi.org/10.1016/S0022-1694(01)00545-5)
- Dugmore, A.J., Gísladóttir, G., Simpson, I.A., Newton, A. (2009) Conceptual Models of 1200 Years of Icelandic Soil Erosion Reconstructed Using Tephrochronology. *Journal of the North Atlantic* 2, 1–18. <https://doi.org/10.3721/037.002.0103>
- Gísladóttir, G., Erlendsson, E., Lal, R., Bigham, J. (2008) Erosional effects on terrestrial resources over the last millennium in Reykjanes, southwest Iceland. *Quaternary Research* 73, 20–32. <https://doi.org/10.1016/j.yqres.2009.09.007>
- Gísladóttir, G., Erlendsson, E., Lal, R. (2011) Soil evidence for historical human-induced land degradation in West Iceland. *Applied Geochemistry* 26, 2009–2012. <https://doi.org/10.1016/j.apgeochem.2011.03.021>
- Goll, D.S., Ciais, P., Amann, T., Buermann, W., Chang, J., Eker, S., Hartmann, J., Janssens, I., Li, W., Obersteiner, M., Penuelas, J., Tanaka, K., Vicca, S. (2021) Potential CO₂ removal from enhanced weathering by ecosystem

- responses to powdered rock. *Nature Geoscience* 14, 545–549. <https://doi.org/10.1038/s41561-021-00798-x>
- Gran, G. (1952) Determination of the equivalence point in potentiometric Titrations. Part II. *Analyst* 77, 661–671. <https://doi.org/10.1039/AN9527700661>
- Grönvold, K., Óskarsson, N., Johnsen, S.J., Clausen, H.B., Hammer, C.U., Bond, G., Bard, E. (1995) Ash layers from Iceland in the Greenland GRIP ice core correlated with oceanic and land sediments. *Earth and Planetary Science Letters* 135, 149–155. [https://doi.org/10.1016/0012-821X\(95\)00145-3](https://doi.org/10.1016/0012-821X(95)00145-3)
- Hartmann, J., Suitner, N., Lim, C., Schneider, J., Marín-Samper, L., Aristegui, J., Renforth, P., Taucher, J., Riebsell, U. (2023) Stability of alkalinity in ocean alkalinity enhancement (OAE) approaches-consequences for durability of CO₂ storage. *Biogeosciences* 20, 781–802. <https://doi.org/10.5194/bg-20-781-2023>
- He, J., Tyka, M.D. (2023) Limits and CO₂ equilibration of near-coast alkalinity enhancement. *Biogeosciences* 20, 27–43. <https://doi.org/10.5194/bg-20-27-2023>
- Huber, S.A., Balz, A., Abert, M., Pronk, W. (2011) Characterisation of aquatic humic and non-humic matter with size-exclusion chromatography – organic carbon detection – organic nitrogen detection (LC-OCD-OND). *Water Research* 45, 879–885. <https://doi.org/10.1016/j.watres.2010.09.023>
- Jóhannesson, T., Aðalgeirsdóttir, G., Björnsson, H., Crochet, P., Elíasson, E.B., Sverrir Guðmundsson, S., Jónsdóttir, J.F., Ólafsson, H., Pálsson, F., Rögnvaldsson, O., Sigurðsson, O., Snorrason, A., Sveinsson, O.G.B., Thorsteinsson, T. (2007) *Effect of climate change on hydrology and hydro-resources in Iceland*. National Energy Authority - Hydrological Service Technical Report OS-2007/011, 91.
- Kaasalainen, H., Stefánsson, A., Druschel, G.K. (2016) Determination of Fe(II), Fe(III) and Fe_{total} in thermal water by ion chromatography spectrophotometry (IC-Vis). *International Journal of Environmental Analytical Chemistry* 96, 1074–1090. <https://doi.org/10.1080/03067319.2016.1232717>
- Kulzer, L., Luchessa, S., Cooke, S., Errington, R., Weinmann, F. (2001) *Characteristics of the Low-Elevation Sphagnum-Dominated Peatlands of Western Washington: A Community Profile Part I: Physical, Chemical and Vegetation Characteristics*. Report to U.S. Environmental Protection Agency. King County Department of Natural Resources, Seattle.
- Li, Z., Zhang, Q., Li, Z., Qiao, Y., Du, K., Yue, Z., Tian, C., Leng, P., Cheng, H., Chen, G., Li, F. (2023) Responses of soil greenhouse gas emissions to no-tillage: A global meta-analysis. *Sustainable Production and Consumption* 36, 479–492. <https://doi.org/10.1016/j.spc.2023.02.003>
- McDougall, I., Kristjánsson, L., Saemundsson, K. (1984) Magnetostratigraphy and Geochronology of Northwest Iceland. *Journal of Geophysical Research: Solid Earth* 89, 7029–7060. <https://doi.org/10.1029/JB089iB08p07029>
- Möckel, S.C., Erlendsson, E., Gísladóttir, G. (2021a) Andic Soil Properties and Tephra Layers Hamper C Turnover in Icelandic Peatlands. *Journal of Geophysical Research: Biogeosciences* 126, e2021JG006433. <https://doi.org/10.1029/2021JG006433>
- Möckel, S.C., Erlendsson, E., Prater, I., Gísladóttir, G. (2021b) Tephra deposits and carbon dynamics in peatlands of a

- volcanic region: Lessons from the Hekla 4 eruption. *Land Degradation and Development* 32, 654–669. <https://doi.org/10.1002/ldr.3733>
- Moras, C.A., Bach, L.T., Cyronak, T., Joannes-Boyau, R., Schulz, K.G. (2022) Ocean alkalinity enhancement-avoiding runaway CaCO₃ precipitation during quick and hydrated lime dissolution. *Biogeosciences* 19, 3537–3557. <https://doi.org/10.5194/bg-19-3537-2022>
- Norðdahl, H., Ingólfsson, Ó., Pétursson, H.G., Hallsdóttir, M. (2008) Late Weichselian and Holocene environmental history of Iceland. *Jökull* 58, 343–364. <http://dx.doi.org/10.33799/jokull2008.58.343>
- Orradottir, B., Archer, S.R., Arnalds, O., Wilding, L.P., Thurow, T.L. (2008) Infiltration in Icelandic Andisols: The Role of Vegetation and Soil Frost. *Arctic, Antarctic and Alpine Research* 40, 412–421. [https://doi.org/10.1657/1523-0430\(06-076\)\[ORRADOTTIR\]2.0.CO;2](https://doi.org/10.1657/1523-0430(06-076)[ORRADOTTIR]2.0.CO;2)
- Óskarsson, H., Arnalds, Ó., Gudmundsson, J., Gudbergsson, G. (2004) Organic carbon in Icelandic Andosols: Geographical variation and impact of erosion. *Catena* 56, 225–238. <https://doi.org/10.1016/j.catena.2003.10.013>
- Parkhurst, D.L., Appelo, C.A.J. (1999) *User's guide to PHREEQC (Version 2): A computer program for speciation, batch-reaction, one-dimensional transport, and inverse geochemical calculations*. Water-Resources Investigations Report 99-4259, US Geological Survey, Denver. <https://doi.org/10.3133/wri994259>
- Petersen, G.N., Berber, D. (2018) Soil temperature measurements in Iceland, status and future outlook (in Icelandic: *Jarðvegshitamælingar á Íslandi. Staða núverandi kerfis og framtíðarsýn*). Report of the Icelandic Meteorological Office (*Skýrsla Veðurstofu Íslands*), VÍ 2018-009, Reykjavík, Iceland. https://www.vedur.is/media/vedurstofan-utgafa-2018/VI_2018_009_rs.pdf
- Renforth, P., Henderson, G. (2017) Assessing ocean alkalinity for carbon sequestration. *Reviews of Geophysics* 55, 636–674. <https://doi.org/10.1002/2016RG000533>
- Rydin, H., Jeglum, J.K. (2013) *The Biology of Peatlands*. Second Edition, Biology of Habitats Series, Oxford University Press, Oxford. <https://doi.org/10.1093/acprof:osobl/9780199602995.001.0001>
- Saemundsson, K. (1979) Outline of the geology of Iceland. *Jökull* 29, 7–28. <https://doi.org/10.33799/jokull1979.29.007>
- Sawyer, D.T., Roberts, J.L., Sobkowiak, A. (1995) *Electrochemistry for chemists*. Second Edition, Wiley, New York.
- Schoeneberger, P.J., Wysocki, D.A., Benham, E.C., Soil Survey Staff (2012) *Field Book for Describing and Sampling Soils*, version 3.0. Natural Resources Conservation Service, U.S. Department of Agriculture, National Soil Survey Center, Lincoln, NE.
- Shakoor, A., Shahbaz, M., Farooq, T.H., Sahar, N.E., Shahzad, S.H., Altaf, M.M., Ashraf, M. (2021) A global meta-analysis of greenhouse gases emission and crop yield under no-tillage as compared to conventional tillage. *Science of the Total Environment* 750, 142299. <https://doi.org/10.1016/j.scitotenv.2020.142299>
- Sigfusson, B., Paton, G.I., Gislason, S.R. (2006) The impact of sampling techniques on soil pore water carbon measurements of an Icelandic Histic Andosol. *Science of the Total Environment* 369, 203–219. <https://doi.org/10.1016/j.scitotenv.2006.01.012>
- Sigurðsson, B.D., Bjarnadóttir, B., Strachan, I., Palmason, F. (2004) The experimental forest in Gunnarsholt II - Water

- in the forest (in Icelandic: *Tilraunaskógurinn í Gunnarsholti II – Vatnið í skóginum*). *The Forestry Journal (In Icelandic: Skógræktarritið)* 1, 55–64.
- Snæbjörnsson, Á. (1982) *Review of soil hydraulic conductivity measurements in Borgarfjörður, Iceland* (in Icelandic: *Um Vatnsleiðnimælingar í Jarðvegi á nokkrum stöðum í Borgarfirði*), Report number 45-1982. <https://vatnsidnadur.net/wp-content/uploads/2017/05/45.-Um-vatnsleiðnimælingar-á-nokkrum-stöðum-í-Borgarfirði.-BÁH.pdf>
- U.S. Environmental Protection Agency (1998) MINTEQA2/PRODEFA2, A Geochemical Assessment Model for Environmental Systems: User Manual Supplement for Version 4.0. vol. 1998.
- Verry, E. (1975) Streamflow Chemistry and Nutrient Yields from Upland-Peatland Watersheds in Minnesota. *Ecology* 56, 1149–1157. <https://doi.org/10.2307/1936154>
- Vicca, S., Goll, D.S., Hagens, M., Hartmann, J., Janssens, I.A., Neubeck, A., Peñuelas, J., Poblador, S., Rijnders, J., Sardans, J., Struyf, E., Swoboda, P., van Groenigen, J.W., Vienne, A., Verbruggen, E. (2022) Is the climate change mitigation effect of enhanced silicate weathering governed by biological processes? *Global Change Biology* 28, 711–726. <https://doi.org/10.1111/gcb.15993>
- Vitt, D.H., Bayley, S.E., Jin, T.-L. (1995) Seasonal variation in water chemistry over a bog-rich fen gradient in Continental Western Canada. *Canadian Journal of Fisheries and Aquatic Sciences* 52, 587–606. <https://doi.org/10.1139/f95-059>
- Wang, H., Wang, S., Yu, Q., Zhang, Y., Wang, R., Li, J., Wang, X. (2020) No tillage increases soil organic carbon storage and decreases carbon dioxide emission in the crop residue-returned farming system. *Journal of Environmental Management* 261, 110261. <https://doi.org/10.1016/j.jenvman.2020.110261>

Appendix C: Supplementary Material Paper III

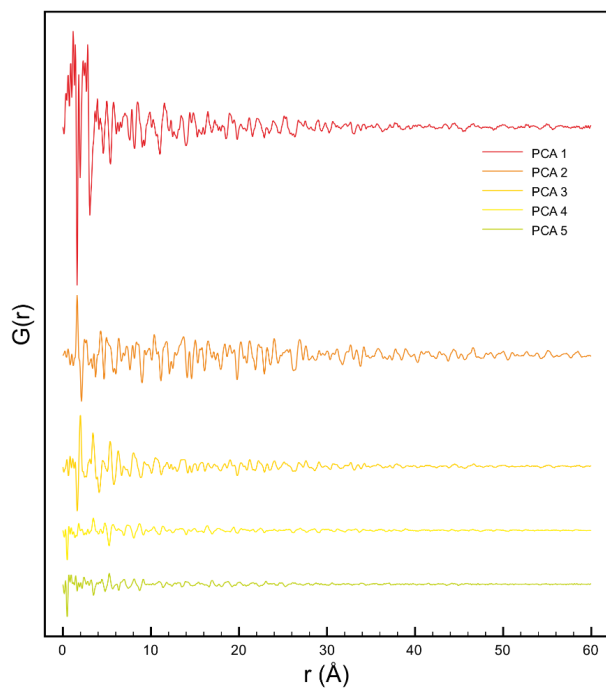


Figure ES1: The PC. The principal components derived from the PCA

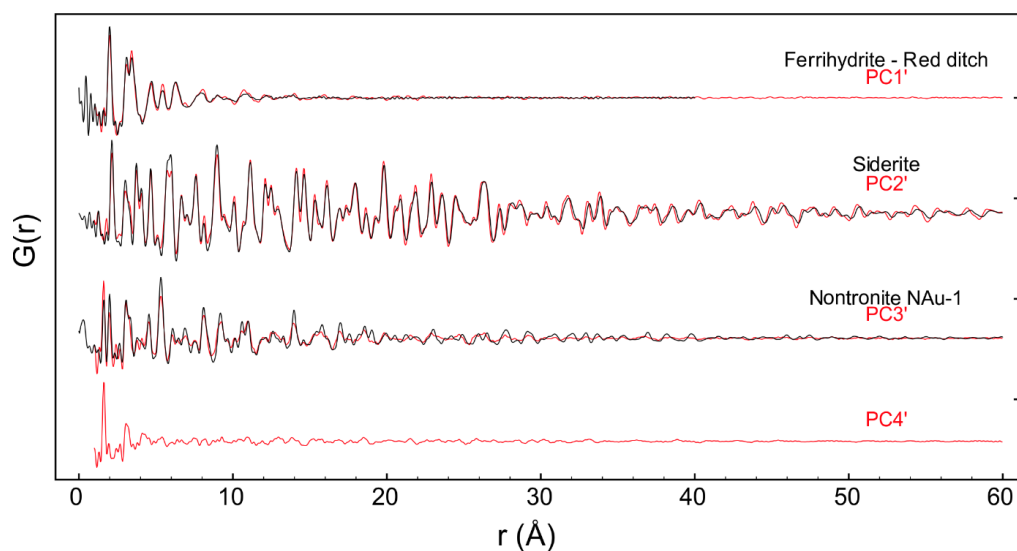


Figure ES2: The deconvoluted PC' (red) and the patterns measured for ferrihydrite, siderite and nontronite Nau-1. The siderite pattern is based on reproduction of the data in Dideriksen et al., 2015 using $Q_{max} = 24$. PC4' resembles a short range ordered SiO_2 phase, presumably basaltic glass, nanocrystalline silica or a mixture of these phases

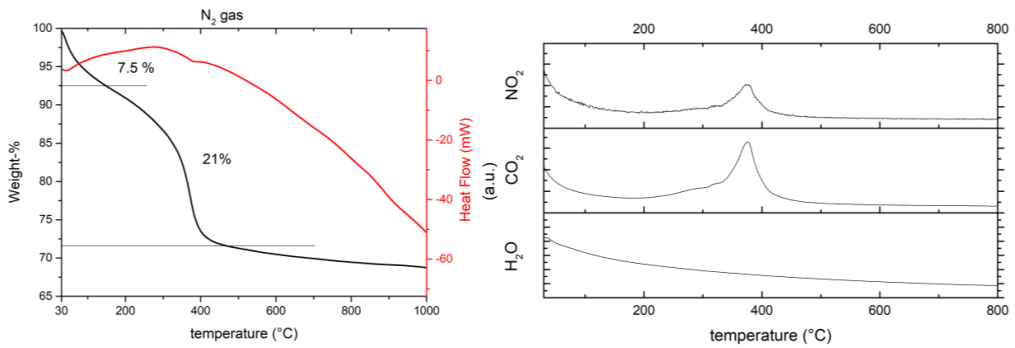


Figure ES3: exemplary results of the thermal analysis of the greyish nodules under N_2 gas flow, **left:** mass loss (black) and heat flow (red) during heating of the samples, **right:** different gases that are released during the continuous heating

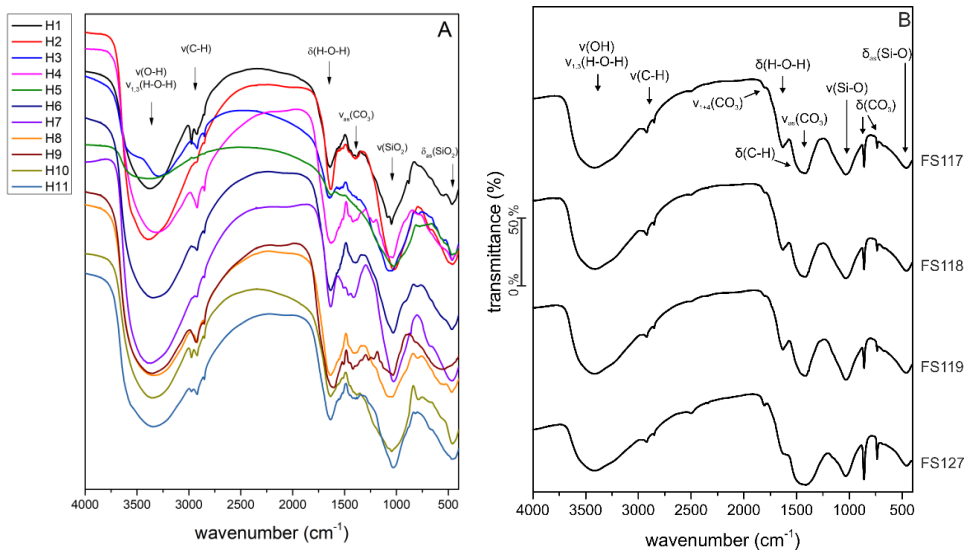


Figure ES4 A: FT-IR spectra of dried material from the different soil horizons and **B:** the greyish inclusions and assigned main features

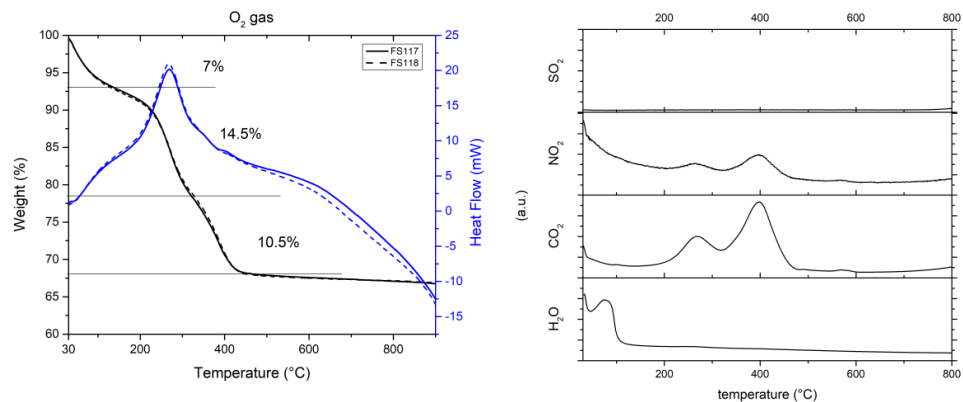


Figure ES5: exemplary results of the thermal analysis of the greyish nodules under O₂ gas flow, **left:** mass loss (black) and heat flow (blue) during heating of the samples, **right:** different gases that are released during the continuous heating

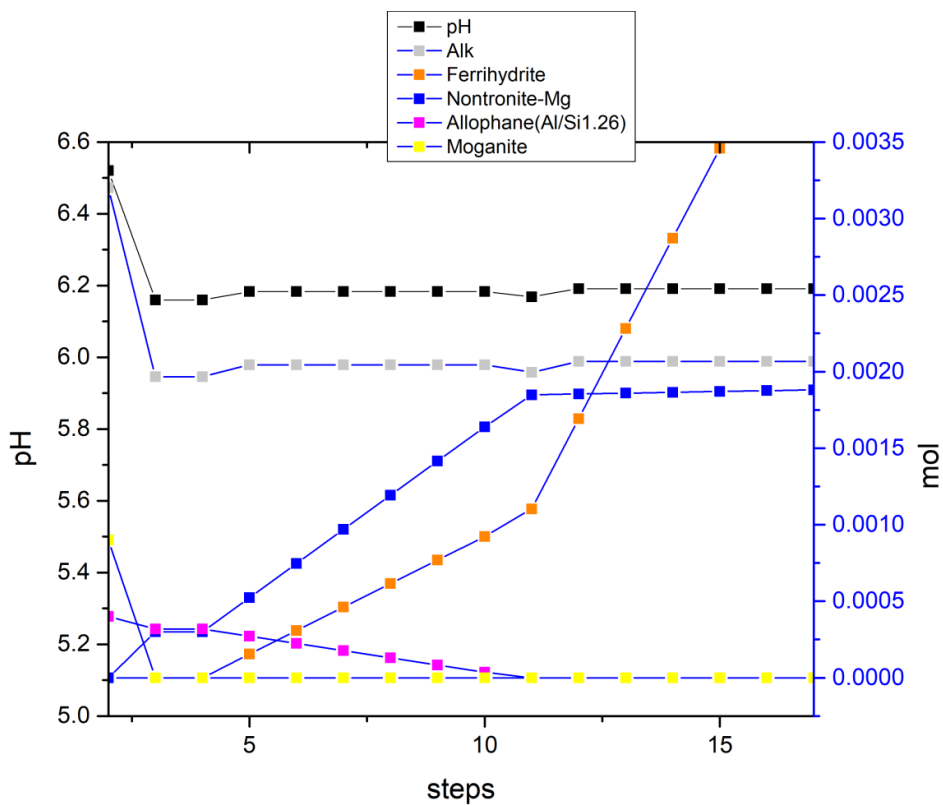


Figure ES6: Modelled reaction path and phase transformation of previously formed allophane and moganite under the presence of oxygen and continuous inflow of reduced iron-rich soil waters

Supplementary information: ES FT-IR band positions and assignments for siderite samples

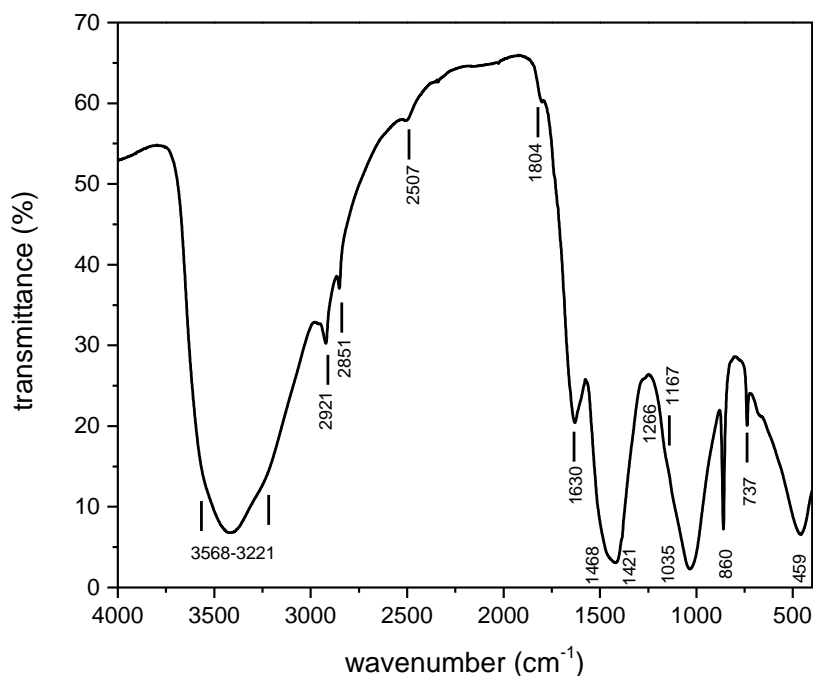


Figure ES7: FT-IR spectra of the dried **sample FS117** from 4000 to 400 cm^{-1} with band positions.

Table ES1: Band positions of the FT-IR spectra of FS117 with corresponding assignments and literature references.

| band position [cm^{-1}] | assignment | literature |
|------------------------------------|--|--|
| 3568-3221 | $\nu(\text{OH})$ (O-H) stretching vibration of hydroxyl groups from main layer $\nu_1, \nu_3(\text{H}_2\text{O})$ (H-O-H) stretching vibration of interlayer water; broadening due to hydrogen bridge bonds | Hernandez-Moreno et al. (1978); Kloprogge & Frost (2004); Labajos et al. (1992); Richardson & Braterman (2006) |
| 2921 | $\nu_{\text{as}}(\text{CH}_2)$ antisymmetric (C-H) stretching mode of the CH_2 -groups | Pretsch et al. (2010); Zhang et al. (2017) |
| 2851 | $\nu_{\text{s}}(\text{CH}_2, \text{CH}_3)$ symmetric (C-H) stretching vibration of CH_2 - and CH_3 -groups | Pretsch et al. (2010); Zhang et al. (2017) |
| 2507 | | |
| 1805 sh | $\nu_1 + \nu_4$ (CO_3) symmetric vibration in poorly crystalline polymorphs | Huang & Kerr 1960, Rodriguez-Blanco et al. 2010 |
| 1630 | $\delta(\text{H}_2\text{O})$ bending vibration of hydroxyl groups from the interlayer water | Hernandez-Moreno et al. (1978); Kloprogge & Frost (2004); Labajos et al. (1992); Richardson & Braterman (2006) |
| 1468 (sh) | $\delta(\text{CH}_2), \delta_{\text{as}}(\text{CH}_3)$ (C-H) bending vibration of the CH_2 - and CH_3 -groups | Pretsch et al. (2010); Zhang et al. (2017) |

| | | |
|------|--|---|
| | ($\nu_{as/s}(\text{COO}^-)$ antisymmetric/ symmetric stretching vibration of the carboxyl-groups) | (Naymbo et al. (2008); Pretsch et al. (2010)) |
| 1421 | $\nu_3(\text{CO}_3)$ antisymmetric stretching vibration of carbonate | Dubrawski & Channon 1989 |
| 1267 | Stretching vibration in G-bands of lignin | Bock & Gierlinger 2019 |
| 1167 | Si-O stretching vibration | Lippincott et al. 1958, Viana et al. (2012) |
| 1040 | Si-O stretching vibration | Lippincott et al. 1958 |
| 860 | $\delta(\text{CO}_3)$ out-of-plane bending vibration (ν_2) | Dubrawski & Channon 1989 |
| 737 | $\delta(\text{CO}_3)$ in-plane bending vibration (ν_4) | Dubrawski & Channon 1989 |
| 459 | (O-Me-O) vibration/ $\delta_{as}(\text{Si-O})$ antisymmetric bending vibration | Hernandez-Moreno et al. (1978); Kloprogge & Frost (2004); Labajos et al. (1992); Richardson & Braterman (2006)/ Saikia et al. 2008, Lippincott et al. 1958 |

Supplementary information: FT-IR Band position and assignments of selected soil samples

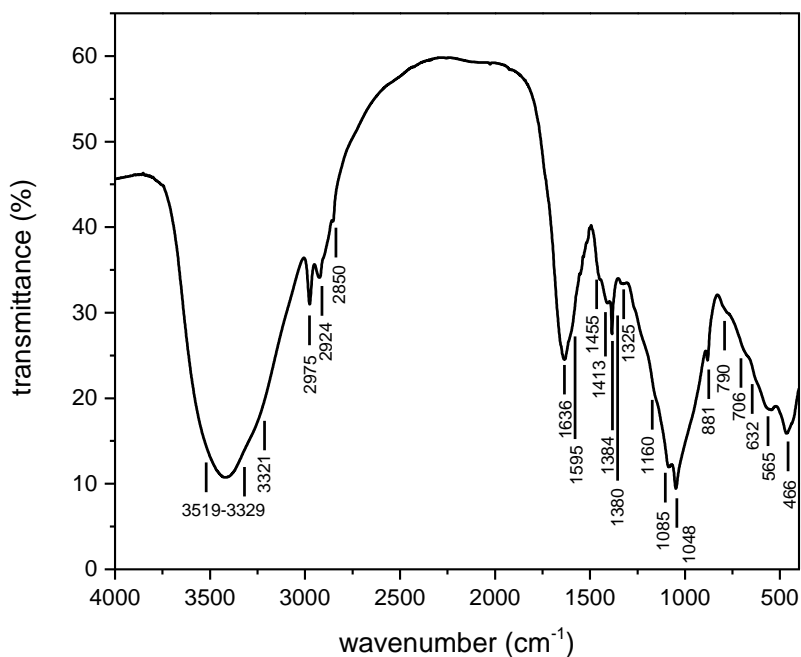


Figure ES8: FT-IR spectra of the dried **sample H1** from 4000 to 400 cm⁻¹ with band positions.

Table ES2: Band positions of the FT-IR spectra of H1 with corresponding assignments and literature references.

| band position [cm ⁻¹] | assignment | literature |
|-----------------------------------|--|---|
| 3519-3329 | v(O-H) stretching vibration of hydroxyl groups from main layer/ v ₁ ,v ₃ (H-O-H) stretching vibration of interlayer water; broadening due to hydrogen bridge bonds/ | Hernandez-Moreno et al. (1978); Klopogge & Frost (2004); Labajos et al. (1992); Richardson & Braterman (2006) |
| 3215 | v _s (N-H) symmetric vibrations in N-H groups | Battacharya et al. 2018; Pretsch et al. (2010) |
| 2975 | v _{as} (CH ₃) antisymmetric (C-H) stretching vibration of CH ₃ -groups | Pretsch et al. (2010); Zhang et al. (2017) |
| 2924 | v _{as} (CH ₂) antisymmetric (C-H) stretching mode of CH ₂ -groups | Pretsch et al. (2010); Zhang et al. (2017) |
| 2850 | v _s (CH ₂ ,CH ₃) symmetric (C-H) stretching vibration of CH ₂ - and CH ₃ -groups | Pretsch et al. (2010); Zhang et al. (2017) |
| 1763 | v(C=O) stretching vibration | Naymbo et al. (2008); Pretsch et al. (2010); Zhang et al. (2017) |
| 1636 | δ(H ₂ O) bending vibration of hydroxyl groups from the interlayer water | Hernandez-Moreno et al. (1978); Klopogge & Frost (2004); Labajos et al. (1992); Richardson & Braterman (2006) |

| | | |
|----------|---|---|
| | | al. (1992); Richardson & Braterman (2006) |
| 1595 | $\nu_{as/s}(\text{COO}^-)$ antisymmetric/symmetric stretching vibration of carboxyl-groups; $\delta(\text{CH}_2)$, $\delta_{as}(\text{CH}_3)$ (C-H) bending vibration of CH_2 - and CH_3 - groups; $\nu(\text{C}=\text{N})$ aromatic $\text{C}=\text{N}$; ($\text{C}=\text{C}$) stretching vibration | Naymbo et al. (2008); Pretsch et al. (2010); Zhang et al. (2017) Battacharya et al. 2018; Bock & Gierlinger 2019 |
| 1455 | $\delta(\text{C-H})$ Bending vibration in Aliphatic C-H/ $\delta(\text{CH}_2)$, $\delta_{as}(\text{CH}_3)$ (C-H) bending vibration of the CH_2 - and CH_3 -groups | Battacharya et al. 2018/ Hernandez-Moreno et al. (1978); Kloprogge & Frost (2004); Labajos et al. (1992) ; Richardson & Braterman (2006); Pretsch et al. (2010); Zhang et al. (2017) |
| 1413 | $\nu_3(\text{CO}_3)$ antisymmetric stretching vibration of carbonate | |
| 1384 | $\delta_s(\text{CH}_3)$ symmetric (C-H) bending vibration of the CH_3 -groups | Hernandez-Moreno et al. (1978); Kloprogge & Frost (2004); Labajos et al. (1992) ; Richardson & Braterman (2006); Pretsch et al. (2010); Zhang et al. (2017) |
| 1380 | $\nu_3(\text{COO})$ symmetric stretching vibration in carboxylates | Battacharya et al. 2018 |
| 1325 | $\delta_s(\text{CH}_3)$ symmetric (C-H) bending vibration of the CH_3 -groups | Hernandez-Moreno et al. (1978); Kloprogge & Frost (2004) ; Richardson & Braterman (2006) |
| 1160 | $\delta_{as}(\text{CH}_3)$ antisymmetric (C-H) bending vibration of the CH_3 -groups/ $\nu(\text{Si-O})$ stretching | Pretsch et al. (2010); Zhang et al. (2017)/ Viana et al. (2012) |
| 1085 | $\nu_3(\text{Si-O})$ asymm. Stretching vibration/ (C-C) stretching vibration in aliphatic chains | Saikia et al. 2008/ Bock & Gierlinger 2019 |
| 1048 | $\nu_s(\text{SO}_2)$ symmetric (S-O) stretching vibration | Pretsch et al. (2010); Viana et al. (2012) Zhang et al. (2017) |
| *881 | | |
| 790 (sh) | $\delta(\text{Si-OH})$ bending vibration/ $\nu(\text{C-S})$ stretching vibrations | Bishop et al. 2013 Pretsch et al. (2010)/ |
| 706 | $\rho(\text{CH}_2)$ rocking vibrations of the CH_2 -groups, $\delta(\text{Me-OH})$ (Me-OH) bending vibrations/ $\delta(\text{Al-OH})$ bending vibration | Pretsch et al. (2010); Hernandez-Moreno et al. (1978); Kloprogge & Frost (2004; Richardson & Braterman (2006)/ Bishop et al. 2013 |
| 632 | (Me-OH), metal-hydroxyl-translation motions | Hernandez-Moreno et al. (1978); Kloprogge & Frost (2004); Labajos et al. (1992); Richardson & Braterman (2006) |
| 565 | Si-O-Al bending | Bishop et al. 2013 |

| | | |
|-----|---|--|
| 466 | (O-Me-O) vibration/ δ_{as} (Si-O) asymmetrical bending vibration | Hernandez-Moreno et al. (1978); Kloprogge & Frost (2004); Labajos et al. (1992); Richardson & Braterman (2006)/ Saikia et al. 2008 |
|-----|---|--|

Supplementary information: FT-IR Band position and assignments of selected soil samples

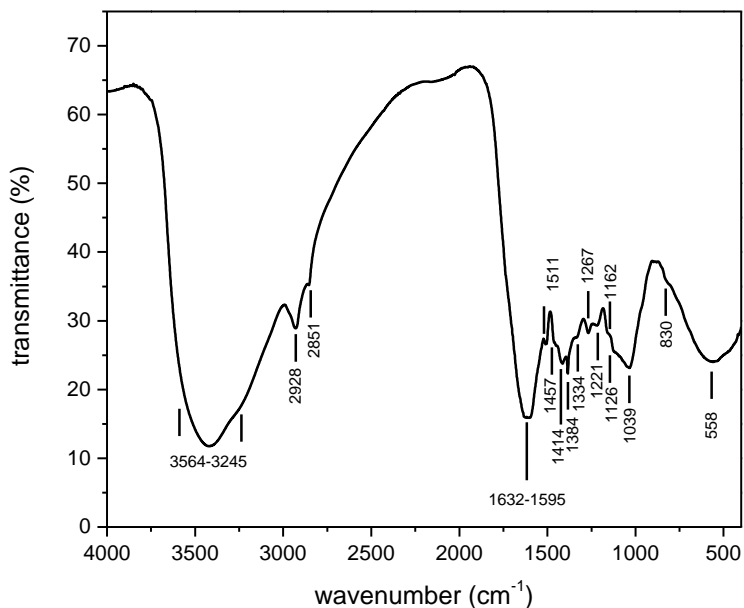


Figure ES9: FT-IR spectra of the dried sample H9 from 4000 to 400 cm^{-1} with band positions.

Table ES3: Band positions of the FT-IR spectra of H9 with corresponding assignments and literature references.

| band position [cm^{-1}] | assignment | literature |
|------------------------------------|--|--|
| 3564-3245 | $\nu(\text{OH})$ (O-H) stretching vibration of hydroxyl groups from main layer/ $\nu_1, \nu_3(\text{H}_2\text{O})$ (H-O-H) stretching vibration of interlayer water; broadening due to hydrogen bridge bonds | Hernandez-Moreno et al. (1978); Klopogge & Frost (2004); Labajos et al. (1992); Richardson & Braterman (2006) |
| 2928 | $\nu_{\text{as}}(\text{CH}_2)$ asymmetric (C-H) stretching mode of the CH_2 -groups | Pretsch et al. (2010); Zhang et al. (2017) |
| 2851 | $\nu_{\text{s}}(\text{CH}_2, \text{CH}_3)$ symmetric (C-H) stretching vibration of CH_2 - and CH_3 -groups | Pretsch et al. (2010); Zhang et al. (2017) |
| 1632 | $\delta(\text{H}_2\text{O})$ bending vibration of hydroxyl groups from the interlayer water | Hernandez-Moreno et al. (1978); Klopogge & Frost (2004); Labajos et al. (1992); Richardson & Braterman (2006) |
| 1595 | $\nu_{\text{as/s}}(\text{COO}^-)$ asymmetric/symmetric stretching vibration of carboxyl-groups; $\delta(\text{CH}_2)$, $\delta_{\text{as}}(\text{CH}_3)$ (C-H) bending vibration of CH_2 - and CH_3 - groups; ν (C=N) aromatic C=N; (C=C) stretching vibration | Naymbo et al. (2008); Pretsch et al. (2010); Zhang et al. (2017) Battacharya et al. 2018; Bock & Gierlinger 2019 |

| | | |
|------|--|--|
| 1511 | | |
| 1457 | | |
| 1414 | | |
| 1384 | $\delta_s(\text{CH}_3)$ symmetric (C-H) bending vibration of the CH_3 -groups | Hernandez-Moreno et al. (1978); Kloprogge & Frost (2004); Labajos et al. (1992); Richardson & Braterman (2006); Pretsch et al. (2010); Zhang et al. (2017) |
| 1334 | $\delta_s(\text{CH}_3)$ symmetric (C-H) bending vibration of the CH_3 -groups | Hernandez-Moreno et al. (1978); Kloprogge & Frost (2004); Richardson & Braterman (2006) |
| 1267 | Stretching vibration in G-bands of lignin | Bock & Gierlinger 2019 |
| 1221 | Stretching vibration in G-bands of lignin | Bock & Gierlinger 2019 |
| 1162 | $\delta_{as}(\text{CH}_3)$ asymmetric (C-H) bending vibration of the CH_3 -groups/ $\nu(\text{Si-O})$ stretching/ $\nu_{as}(\text{SO}_3^-)$ antisymmetric (S-O) stretching vibration of the SO_3^- -groups | Pretsch et al. (2010); Zhang et al. (2017)/ Viana et al. (2012)/ |
| 1126 | (C-H) bending associated to ring structures | Bock & Gierlinger 2019 |
| 1040 | $\nu_s(\text{SO}_2)$ symmetric (S-O) stretching vibration | Pretsch et al. (2010); Viana et al. (2012) Zhang et al. (2017) |
| 830 | | |
| 558 | Si-O-Al bending | Bishop et al. 2013 |

Supplementary information: FT-IR Band position and assignments of selected soil samples

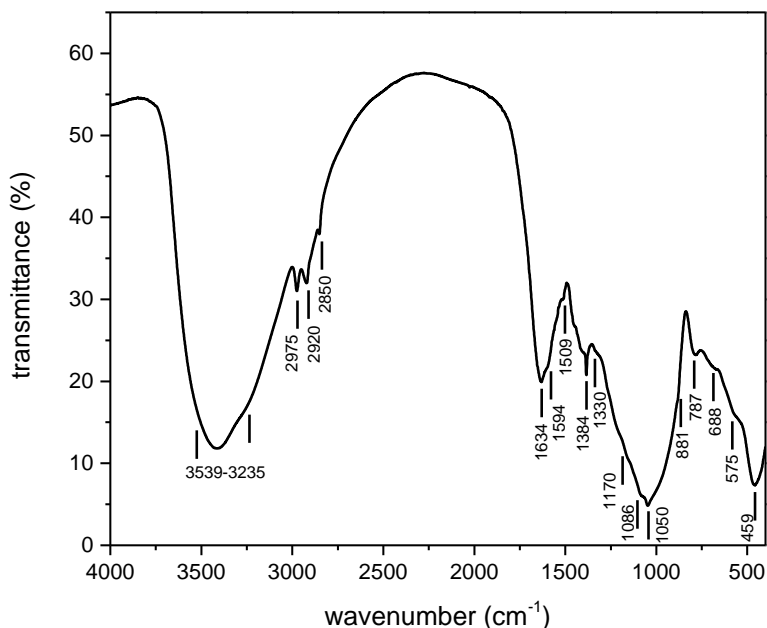


Figure ES10: FT-IR spectra of the dried sample H10 from 4000 to 400 cm^{-1} with band positions.

Table ES4: Band positions of the FT-IR spectra of H10 with corresponding assignments and literature references.

| band position [cm^{-1}] | assignment | literature |
|------------------------------------|---|---|
| 3539-3235 | $\nu(\text{OH})$ (O-H) stretching vibration of hydroxyl groups from main layer/ $\nu_1, \nu_3(\text{H}_2\text{O})$ (H-O-H) stretching vibration of interlayer water; broadening due to hydrogen bridge bonds | Hernandez-Moreno et al. (1978); Klopogge & Frost (2004); Labajos et al. (1992); Richardson & Braterman (2006) |
| 2975 | $\nu_{\text{as}}(\text{CH}_3)$ asymmetric (C-H) stretching vibration of CH_3 -groups | Pretsch et al. (2010); Zhang et al. (2017) |
| 2920 | $\nu_{\text{as}}(\text{CH}_2)$ asymmetric (C-H) stretching mode of CH_2 -groups | Pretsch et al. (2010); Zhang et al. (2017) |
| 2850 | $\nu_s(\text{CH}_2, \text{CH}_3)$ symmetric (C-H) stretching vibration of CH_2 - and CH_3 -groups | Pretsch et al. (2010); Zhang et al. (2017) |
| 1634 | $\delta(\text{H}_2\text{O})$ bending vibration of hydroxyl groups from the interlayer water | Hernandez-Moreno et al. (1978); Klopogge & Frost (2004); Labajos et al. (1992); Richardson & Braterman (2006) |
| 1594 | $\nu_{\text{as/s}}(\text{COO}^-)$ asymmetric/symmetric stretching vibration of carboxyl-groups; $\delta(\text{CH}_2)$, $\delta_{\text{as}}(\text{CH}_3)$ (C-H) bending vibration of CH_2 - and CH_3 - groups; | Naymbo et al. (2008); Pretsch et al. (2010); Zhang et al. (2017) Battacharya et al. 2018; |

| | | |
|----------|---|--|
| | v (C=N) aromatic C=N; (C=C) stretching vibration | Bock & Gierlinger 2019 |
| 1509 | | |
| 1384 | $\delta_s(\text{CH}_3)$ symmetric (C-H) bending vibration of the CH_3 -groups | Richardson & Braterman (2006); Pretsch et al. (2010); Zhang et al. (2017) |
| 1330 | $\delta_s(\text{CH}_3)$ symmetric (C-H) bending vibration of the CH_3 -groups | Hernandez-Moreno et al. (1978); Klopogge & Frost (2004) ; Richardson & Braterman (2006) |
| 1170 | $\delta_{as}(\text{CH}_3)$ asymmetric (C-H) bending vibration of the CH_3 -groups/ v(Si-O) stretching/ $\nu_{as}(\text{SO}_3^-)$ asymmetric (S-O) stretching vibration of the SO_3^- groups | Pretsch et al. (2010); Zhang et al. (2017)/ Viana et al. (2012)/ |
| 1086 | ν_3 (Si-O) asymm. Stretching vibration/ (C-C) stretching vibration in aliphatic chains | Saikia et al. 2008/ Bock & Gierlinger 2019 |
| 1050 | $\nu_s(\text{SO}_2)$ symmetric (S-O) stretching vibration | Pretsch et al. (2010); Viana et al. (2012) Zhang et al. (2017) |
| *881 | $\delta(\text{CO}_3)$ out-of-plane bending vibration | Dubrawski & Channon 1989 |
| 787 (sh) | $\delta(\text{Si-OH})$ bending vibration/ v(C-S) stretching vibrations | Bishop et al. 2013 Pretsch et al. (2010)/ |
| 688 | Hindered rotation of H-bonded OH-groups | Bock & Gierlinger 2019 |
| 575 | Si-O-Al bending | Bishop et al. 2013 |
| 459 | (O-Me-O) vibration/ δ_{as} (Si-O) asymmetrical bending vibration | Hernandez-Moreno et al. (1978); Klopogge & Frost (2004); Labajos et al. (1992); Richardson & Braterman (2006)/ Saikia et al. 2008 |

Supplementary information: FT-IR Band position and assignments of selected soil samples

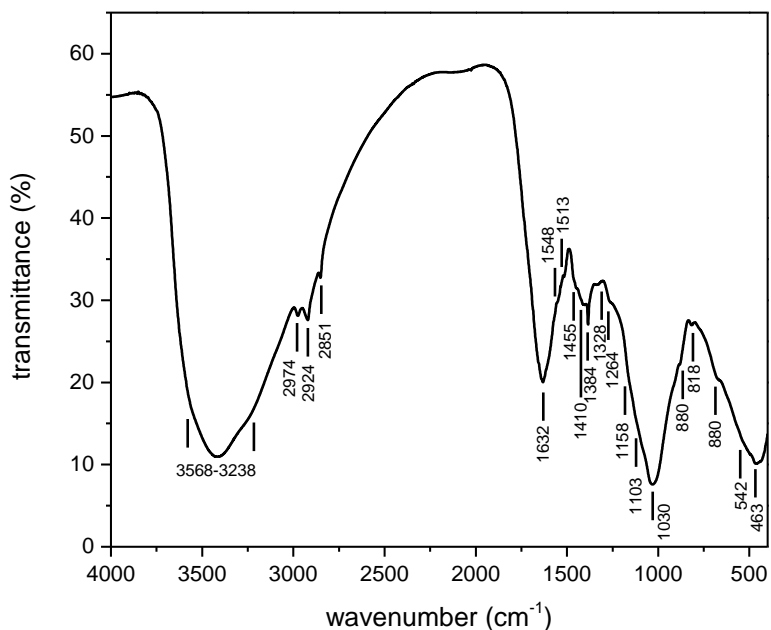


Figure ES11: FT-IR spectra of the dried sample H11 from 4000 to 400 cm^{-1} with band positions.

Table ES5: Band positions of the FT-IR spectra of H11 with corresponding assignments and literature references.

| band position [cm^{-1}] | assignment | literature | Possible Mineral |
|------------------------------------|---|---|------------------|
| 3568-3228 | $\nu(\text{OH})$ (O-H) stretching vibration of hydroxyl groups from main layer/ $\nu_1, \nu_3(\text{H}_2\text{O})$ (H-O-H) stretching vibration of interlayer water; broadening due to hydrogen bridge bonds | Hernandez-Moreno et al. (1978); Klopogge & Frost (2004); Labajos et al. (1992); Richardson & Braterman (2006) | |
| 2974 | $\nu_{\text{as}}(\text{CH}_3)$ asymmetric (C-H) stretching vibration of CH_3 -groups | Pretsch et al. (2010); Zhang et al. (2017) | |
| 2924 | $\nu_{\text{as}}(\text{CH}_2)$ asymmetric (C-H) stretching mode of CH_2 -groups | Pretsch et al. (2010); Zhang et al. (2017) | |
| 2851 | $\nu_s(\text{CH}_2, \text{CH}_3)$ symmetric (C-H) stretching vibration of CH_2 - and CH_3 -groups | Pretsch et al. (2010); Zhang et al. (2017) | |
| 1632 | $\delta(\text{H}_2\text{O})$ bending vibration of hydroxyl groups from the interlayer water | Hernandez-Moreno et al. (1978); Klopogge & Frost (2004); Labajos et al. (1992); Richardson & Braterman (2006) | |
| 1548 | $\nu_{\text{as/s}}(\text{COO}^-)$ asymmetric/symmetric stretching vibration of carboxyl-groups; $\delta(\text{CH}_2)$, $\delta_{\text{as}}(\text{CH}_3)$ (C-H) bending vibration of CH_2 - and CH_3 - groups; | Naymbo et al. (2008); Pretsch et al. (2010); Zhang et al. (2017) Battacharya et al. 2018; | |

| | | | |
|----------|---|--|-----------------|
| | ν (C=N) aromatic C=N; (C=C) stretching vibration | Bock & Gierlinger 2019 | |
| 1513 | | | |
| 1455 | δ (C-H) Bending vibration in Aliphatic C-H/ δ (CH) (C-H) bending vibration of the CH ₂ - and CH ₃ -groups | Battacharya et al. 2018/ Hernandez-Moreno et al. (1978); Kloprogge & Frost (2004); Labajos et al. (1992); Richardson & Braterman (2006); Pretsch et al. (2010); Zhang et al. (2017) | |
| 1410 | ν_3 (CO ₃) asymmetric stretching vibration of carbonate | Dubrawski & Channon 1989 | Sid |
| 1384 | δ_s (CH ₃) symmetric (C-H) bending vibration of the CH ₃ -groups | Richardson & Braterman (2006); Pretsch et al. (2010); Zhang et al. (2017) | |
| 1328 | δ_s (CH ₃) symmetric (C-H) bending vibration of the CH ₃ -groups | Hernandez-Moreno et al. (1978); Kloprogge & Frost (2004); Richardson & Braterman (2006) | |
| 1264 | Stretching vibration lignin | Bock & Gierlinger 2019 | |
| 1158 | δ_{as} (CH ₃) asymmetric (C-H) bending vibration of the CH ₃ -groups/ ν (Si-O) stretching/ ν_{as} (SO ₃) asymmetric (S-O) stretching vibration of the SO ₃ -groups | Pretsch et al. (2010); Zhang et al. (2017)/ Viana et al. (2012)/ | All, <i>Mac</i> |
| 1085 | ν_3 (Si-O) asymm. Stretching vibration/ (C-C) stretching vibration in aliphatic chains | Saikia et al. 2008/ Bock & Gierlinger 2019 | |
| 1048 | ν_s (SO ₂) symmetric (S-O) stretching vibration | Pretsch et al. (2010); Viana et al. (2012) Zhang et al. (2017) | |
| 881* | δ (CO ₃) out-of-plane bending vibration | Dubrawski & Channon 1989 | Sid |
| 790 (sh) | δ (Si-OH) bending vibration/ ν (C-S) stretching vibrations | Bishop et al. 2013 Pretsch et al. (2010)/ | All/Imo |
| 706 | ρ (CH ₂) rocking vibrations of the CH ₂ - groups in the alkyl chain; δ (Me-OH) (Me- OH) bending vibrations/ δ (Al-OH) bending vibration | Pretsch et al. (2010); Hernandez- Moreno et al. (1978); Kloprogge & Frost (2004); Richardson & Braterman (2006)/ Bishop et al. 2013 | All/Imo |
| 632 | (Me-OH), metal-hydroxyl-translation motions | Hernandez-Moreno et al. (1978); Kloprogge & Frost (2004); Labajos et al. (1992); Richardson & Braterman (2006) | |
| 565 | Si-O-Al bending | Bishop et al. 2013 | All |
| 466 | (O-Me-O) vibration/ δ_{as} (Si-O) asymmetrical bending vibration | Hernandez-Moreno et al. (1978); Kloprogge & Frost (2004); Labajos et al. (1992); Richardson & Braterman (2006), Saikia et al. 2008 | All |

References

- Hernandez-Moreno, M.J., Ulibarri, M.A.; Rendon, J.L. and Serna, C.J. (1985) IR Characteristics of Hydrotalcite-like Compounds. *Physics and Chemistry of Minerals*, 12, 34–38
- Labajos, F.M., Rives, V. and Ulibarri, M.A. (1992) Effect of hydrothermal and thermal treatments on the physicochemical properties of Mg-Al hydrotalcite-like materials. *Journal of Materials Science*, 27, 1546–1552
- Kloppogge, J.T. and Frost, R.L. (2004) FT-Raman and FT-IR spectroscopic study of synthetic Mg/Zn/Al-hydrotalcites. *Journal of Raman Spectroscopy*, 2004, 35, 967–974
- Richardson, M.C.; Braterman, P.S. Infrared Spectra of Oriented and Nonoriented Layered Double Hydroxides in the Range from 4000 to 250 cm⁻¹, with Evidence for Regular Short-Range Order in a Synthetic Magnesium-Aluminum LDH with Mg:Al = 2:1 but not with Mg:Al = 3:1. *The Journal of Physical Chemistry C*, 2007, 111, 4209–4215
- Huang, C.K. and Kerr, P.F. (1960) Infrared Study of the carbonate minerals. *The American Mineralogist*, 45
- Pretsch, E., Bühlmann, P., Affolter, C. and Badertscher, M. (2010) *Spektroskopische Daten zur Strukturaufklärung organischer Verbindungen*. Springer-Verlag, Berlin, pp. 419
- Zhang, B., Dong, Z., Sun, D. and Wu, T. (2017) Enhanced adsorption capacity of dyes by surfactant-modified layered double hydroxides from aqueous solution. *Journal of Industrial and Engineering Chemistry*, 49, 208-218
- Rodriguez-Blanco, J.D., Shaw, S., Benning, L.G. (2011) The kinetics and mechanisms of amorphous calcium carbonate (ACC) crystallization to calcite, via vaterite. *Nanoscale*, 3, 265-271
- Nyambo, C., Songtipya, P., Manias, E., Jimenez-Gasco, M.M. and Wilkie, C.A. (2008) Effect of MgAl-layered double hydroxide exchanged with linear alkyl carboxylates on fire-retardancy of PMMA and PS. *Journal of Materials Chemistry*, 18, 4827-4838
- Dubrawski, J.V. and Channon, S.S.J. (1958) Examination of the siderite-magnesite mineral series by Fourier transform infrared spectroscopy. *The American Mineralogist*, 74 (1-2), 187–190
- RB Viana, ABF da Silva, AS Pimentel (2012): *Infrared Spectroscopy of Anionic, Cationic, and Zwitterionic Surfactants – Advances in Physical Chemistry*, Vol. 2012
- Bishop, J. L., Ethbrampe, E. B., Bish, D. L., Abidin, Z. L., Baker, L. L., Matsue, N., and Henmi, T. (2013). Spectral and Hydration Properties of Allophane and Imogolite. *Clays and Clay Minerals*, 61(1), 57–74. doi:10.1346/ccmn.2013.0610105
- Bock, P. and Gierlinger, N. (2019) Infrared and Raman spectra of lignin substructures: Coniferyl alcohol, abietin, and coniferyl aldehyde. *Journal of Raman Spectroscopy*, 50 (6), 778-792
- Saikia, B.J., Parthasarathy, G. and Sarmah, N.C. (2008) Fourier transform infrared spectroscopic estimation of crystallinity in SiO₂ based rocks. *Bulletin of Materials Science*, 31, 775-779
- Lippincott, E.R., Van Valkenburg, A., Weir, C.E. and Bunting, E.N. (1958) Infrared Studies on Polymorphs of Silicon Dioxide and Germanium Dioxide. *Journal of Research of the National Bureau of Standards*, 61 (1), 2885
- Bishop, J.L., Rampe, E.B., Bish, D.L., Abidin, Z., Baker, L.L., Matsue, N. and Henmi, T. (2013) Spectral and Hydration Properties of Allophane and Imogolite. *Clays and Clay Minerals*, 61, 57–74

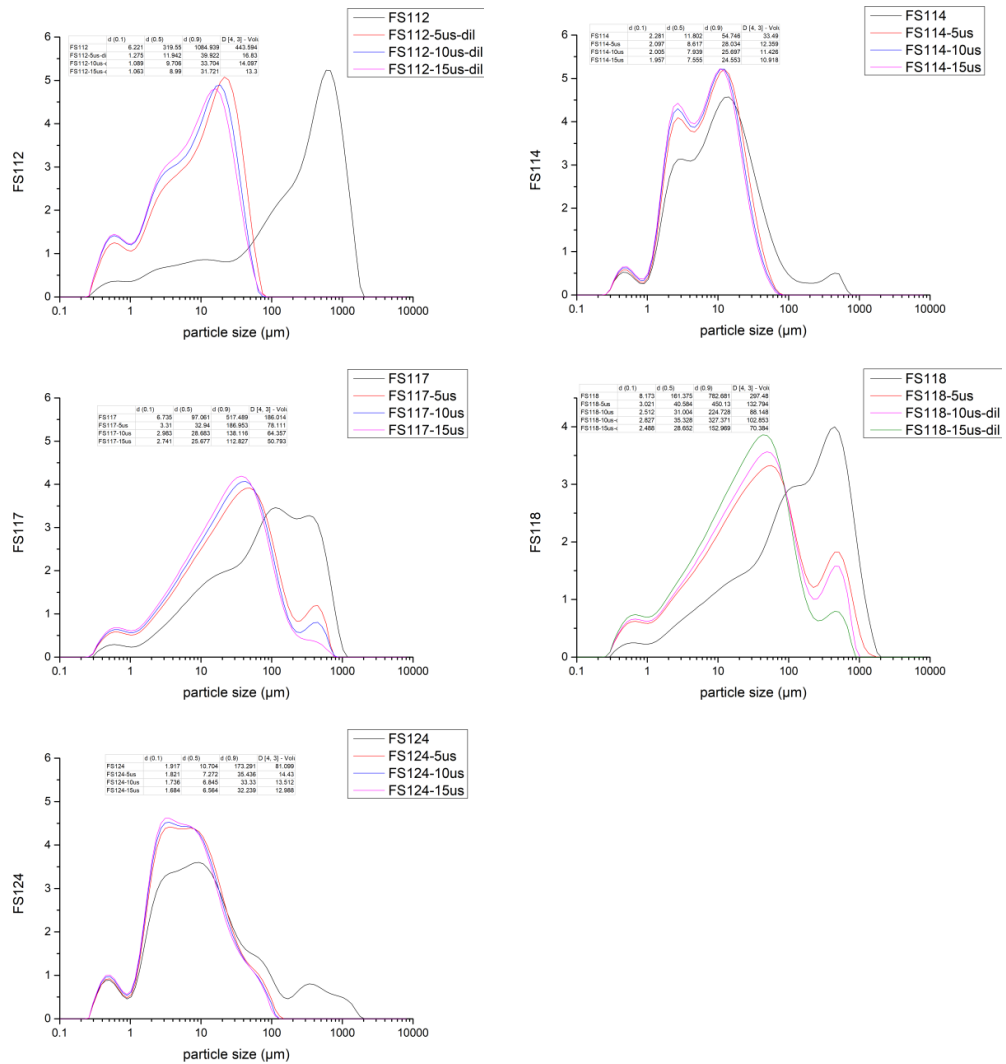


Figure ES12: PSD analysis via laser diffraction of different siderite containing samples including d(0.1), d(0.5) d(0.9) and D(4,3) values after different durations of ultrasonic treatment

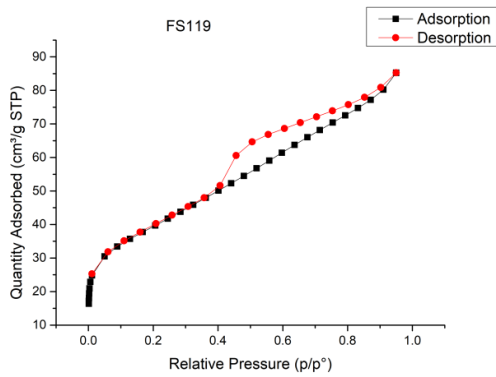
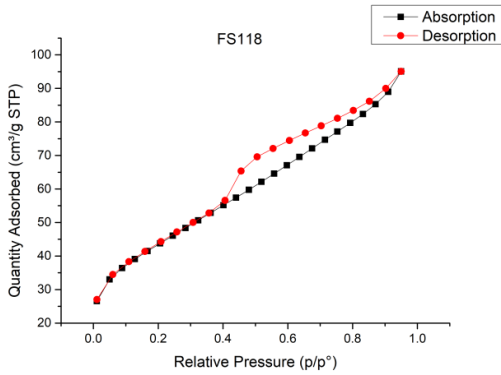
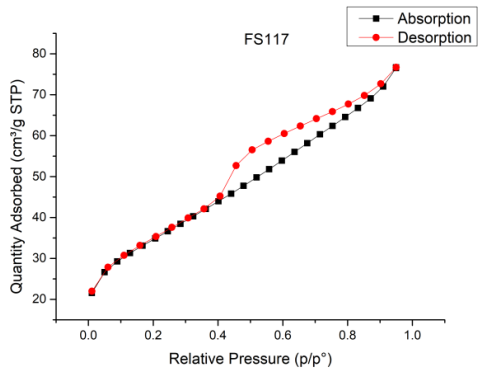


Figure ES13: Isotherm linear plots from the surface area analysis after the BET method via N₂ infiltration for selected siderite containing samples

Appendix D: Supplementary Material Paper V

Appendix 1:

Figure A1: Probable water levels in Háslón Reservoir

Figure A2: Relationship of the surface area and the usable volume of the Háslón reservoir to the reservoir fill level shown as elevation above sea level

Figure A3: Map including the 3 sampling locations of the temperature profiles

Figure A4: The temperature profiles H1, H2 and H3 (19th May 2018)

Figure A5: Temperature profiles of the Háslón reservoir (August 2018, September 2011/2012/2013)

Appendix 2:

The appendix 2 contains the chemical compositions including temperature, pH, alkalinity and major elements of the Jökulsá á Dal river at Hjardarhagi before (Tab A1) and after (Tab A2) the damming at Kárahnjúkar, Jökulsá á Dal at Brú before damming (Tab A3), the Lagarfljót reservoir at Lagarfoss before (Tab A4) and after (Tab A5) damming. Additional data from Háslón reservoir collected at various depths and times (tab A6), and Kárahnjúkar power plant outlet (Tab A7) are included. Much of this data has been previously reported by Eiriksdottir et al., 2015, 2017. Here, we have added the composition of the Lagarfljót reservoir waters and particles before the installation of the Kárahnjúkar dam (Table A4). Furthermore, to all tables we have added the mass percent of organic carbon in the suspended organic and inorganic particle, the C/N molar ratio of the organic particles, the *in-situ* pH, the *in-situ* pCO_{2w} and CO_{2(aq)} the *in-situ* concentration of dissolved CO₂ in the water. *In-situ* refers to the calculated value at the measured water temperature at the time of sampling. Temperature and wind speed data presented in figure 3 are provided (Tab. A8).

Table A1. Jökulsá á Dal at Hjardarhagi 18 November 1998 - 27 November 2003

Table A2. Jökulsá á Dal at Hjardarhagi 28 November 2007 - 10 December 2013

Table A3. Jökulsá á Dal at Brú 21 November 2000 - 27 November 2003

Table A4. Lagarfljót at Lagarfoss 1998-2003

Table A5. Lagarfljót at Lagarfoss Dam 28 November 2007 - 10 December 2013

Table A6. Háslón reservoir 19 June 2008 - 10 September 2013

Table A7. Outlet from Kárahnjúkar Power Plant 28.11.2007-10.12.2013

Table A8. Wind speed and temperature data accompanying Figure 3

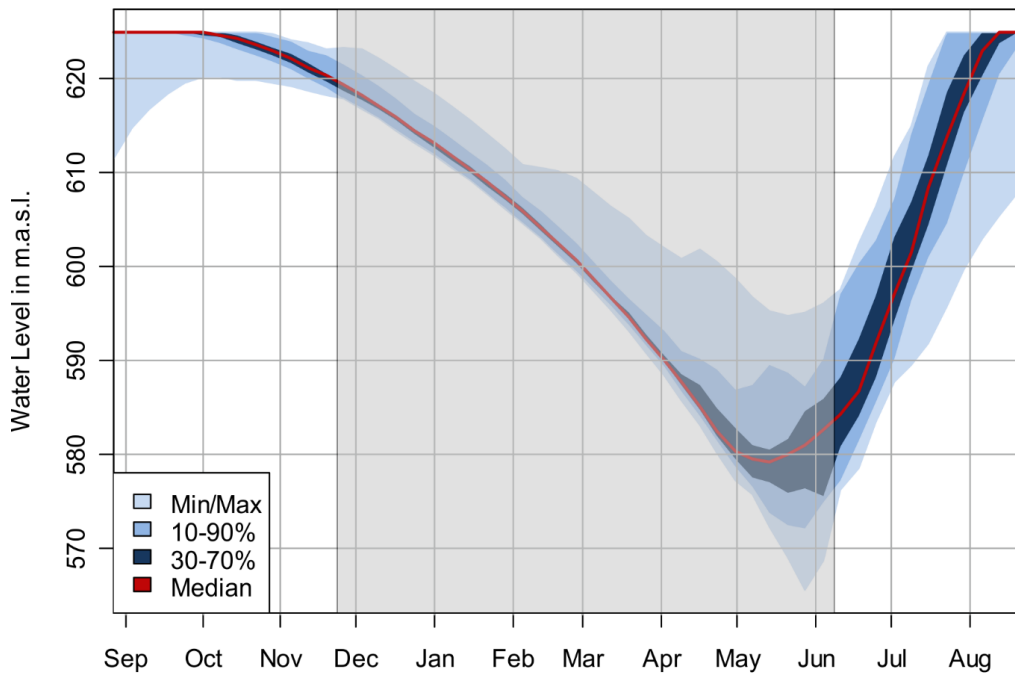


Figure A1. Probable water levels in Hálslón Reservoir according to simulation results of Landsvirkjun energy operations over 20 years, from 1 Sept. 1985 to 31 August 2005 (modified from Leifsson et al. 2009, with permission from Landsvirkjun). The grey shaded area shows the approximate time of ice cover.

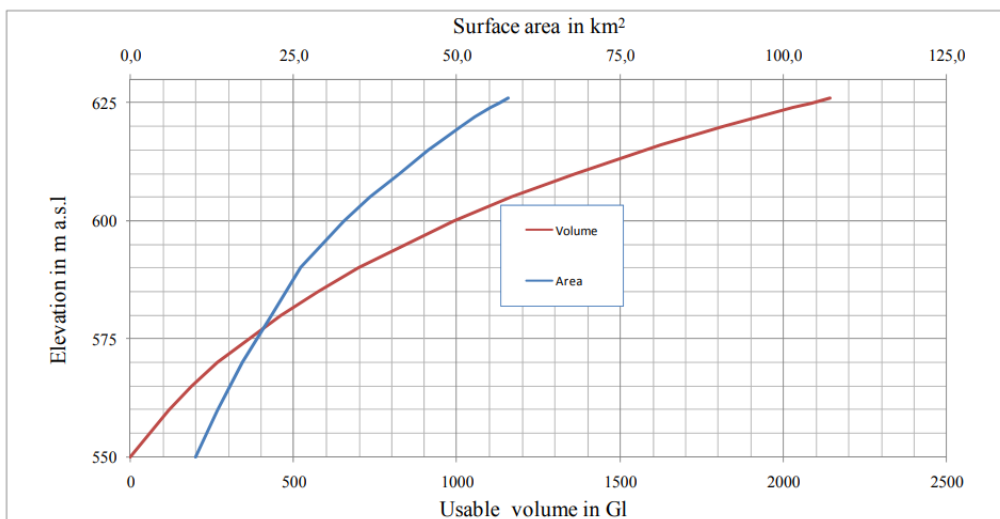


Figure A2. Relationship of the surface area and the usable volume of the Hálslón reservoir to the reservoir fill level shown as elevation above sea level (from Leifsson et al. 2009, with permission from Landsvirkjun)

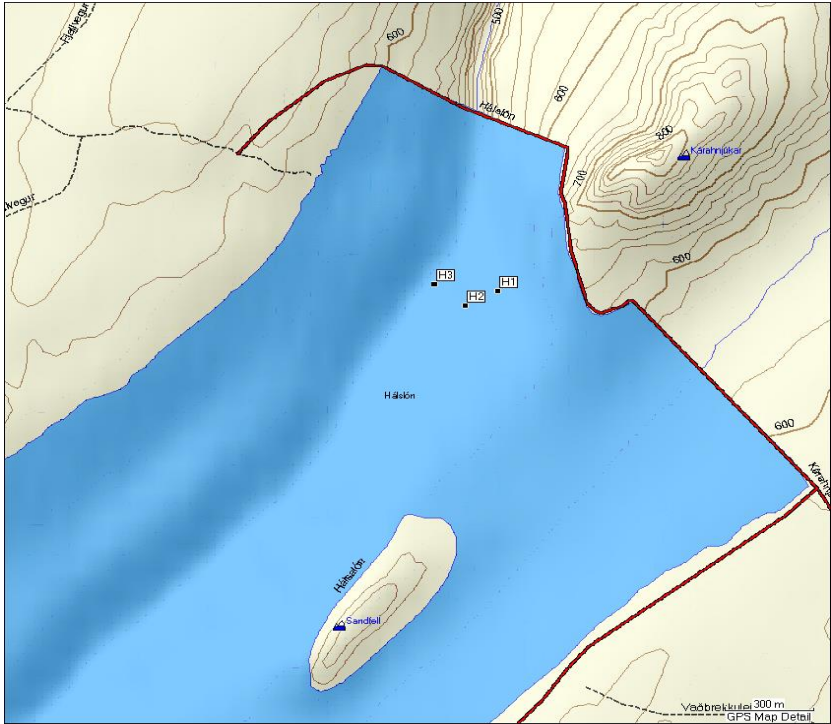


Figure A3. Map including the 3 sampling locations of the temperature profiles.

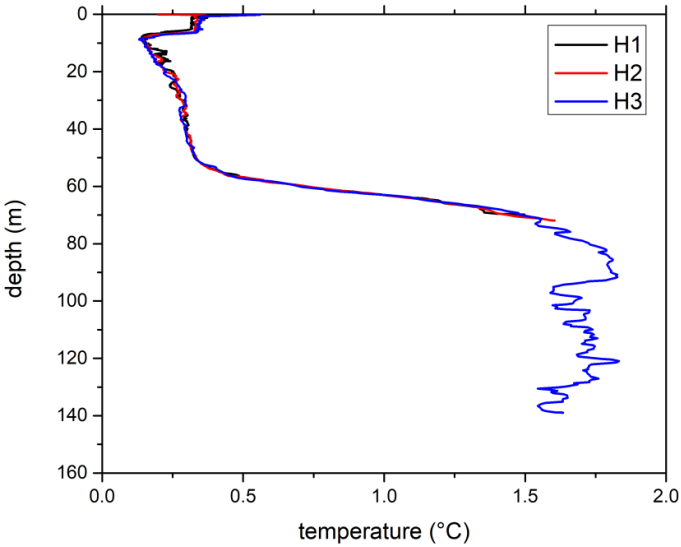


Figure A4. The temperature profiles H1, H2 and H3 measured at 3 locations (see Fig. A3) through snow covered ice 19 May 2008 down to a depth of 70, 72 and 139 m respectively. H3 is at the deepest part of the Háslón Reservoir.

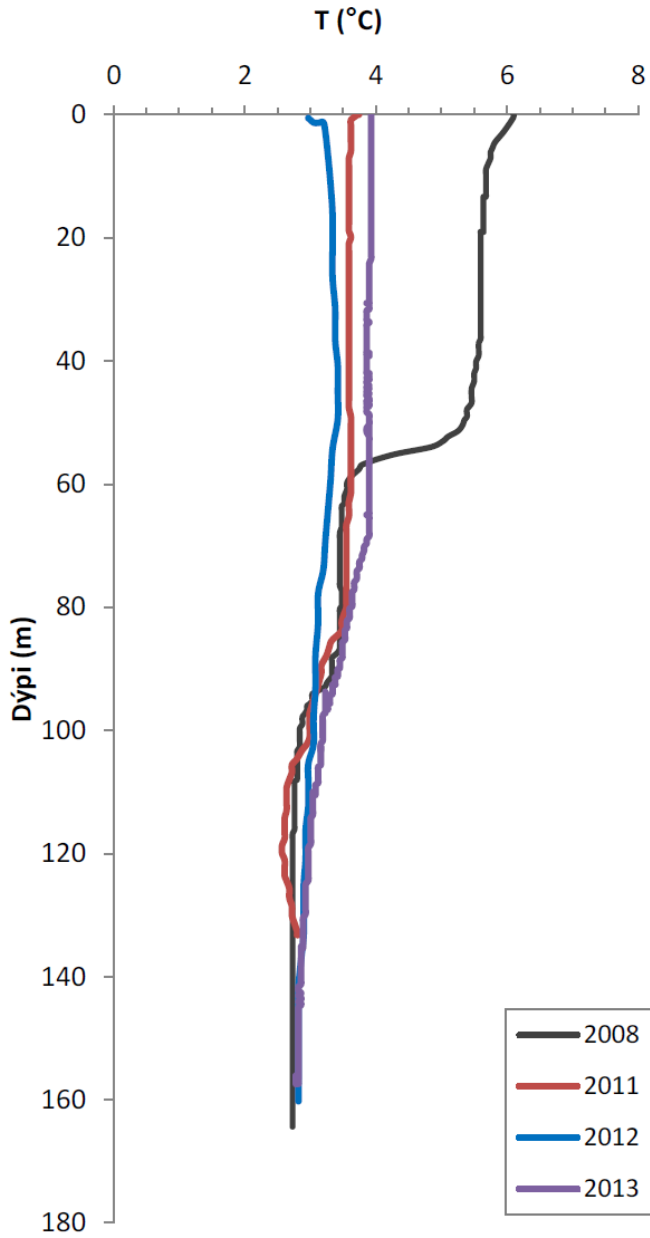


Figure A5. Temperature profiles of the Háslón reservoir from August 2008, and September 2011, 2012 and 2013 from the deepest part of the reservoir, shown by the white filled circle in Figure 1.

Table A1. Jökulsá á Dal at Hjarðarhagi 18 November 1998 – 27 November 2003

| Sample number | Date | Time | Discharge m ³ /s | T _{water} °C | T _{air} °C | pH | T _{ref} °C | SIM mg/L | POC µg/L | PON µg/kg | POC µg/kg | C/N | Alkalinity µeq/L | SiO ₂ µM | DOC µM | DOC % | Na µM | K µM | Ca µM | Mg µM | SO ₄ µM | Cl µM | F µM | Al µM | Fe µM | pH _{ln-atu} | log(pCO _{2w}) µatm | pCO _{2w} µatm | CO _{2aq} µM | charge balance % | |
|----------------|------------|-------|--------------------------------|--------------------------|------------------------|-------------|------------------------|-------------|-------------|--------------|--------------|--------------|---------------------|------------------------|-----------|----------|----------|---------|----------|----------|-----------------------|----------|---------|----------|----------|----------------------|---------------------------------|---------------------------|-------------------------|---------------------|-------|
| 98-A002 | 18.11.1998 | 15:30 | 61 | 0.1 | 6.5 | 7.69 | 16.2 | 19 | 201 | | 1.05 | | 816 | 859 | 41.7 | 4.6 | 242 | 338 | 11.2 | 187 | 115 | 26 | 52 | 4.41 | 0.68 | 0.06 | 7.80 | -3.04 | 913 | 39.8 | 1.49 |
| 99-A001 | 12.01.1999 | 13:00 | 20 | 0.0 | -0.1 | 7.67 | 15.7 | 15 | 156 | <1.5 | 1.03 | 243 | 940 | 993 | 33.3 | 3.2 | 278 | 391 | 9.1 | 216 | 116 | 32 | 57 | 5.45 | 1.58 | 0.92 | 7.79 | -2.96 | 1087 | 48.0 | -0.07 |
| 99-A009 | 01.03.1999 | 16:00 | 15 | 0.1 | -0.6 | 7.25 | 20.2 | 10 | 109 | <1.5 | 1.08 | 169 | 1025 | 1164 | 33.3 | 2.8 | 294 | 425 | 10.0 | 233 | 129 | 36 | 60 | 6.28 | 0.49 | 0.08 | 7.37 | -2.47 | 3357 | 130.7 | -0.38 |
| 99-A016 | 12.04.1999 | 16:00 | 11 | 0.1 | -4.3 | 8.21 | 17.4 | 2 | 174 | 11.5 | 7.98 | 270 | 1029 | 1047 | 25.0 | 2.3 | 302 | 448 | 14.4 | 239 | 130 | 40 | 64 | 6.32 | 0.52 | 0.16 | 8.38 | -3.46 | 736 | 14.6 | 0.96 |
| 99-A027 | 10.05.1999 | 18:45 | 145 | 2.2 | 5.9 | 7.53 | 22.7 | 97 | 398 | 43.4 | 0.41 | 21 | 408 | 436 | 75.0 | 14.7 | 130 | 151 | 8.5 | 111 | 69 | 8 | 56 | 1.85 | 0.25 | 0.32 | 7.66 | -3.13 | 736 | 26.8 | 3.88 |
| 99-A030 | 10.06.1999 | 13:15 | 220 | 4.6 | 18.4 | 7.41 | 23.0 | 162 | 304 | 32.5 | 0.11 | 22 | 336 | 366 | 66.7 | 15.4 | 125 | 104 | 5.9 | 87 | 50 | 2 | 24 | 2.04 | 0.28 | 0.09 | 7.53 | -3.09 | 806 | 29.1 | 2.35 |
| 99-A037 | 19.07.1999 | 14:15 | 343 | 3.1 | 11.0 | 7.66 | 20.2 | 887 | 1017 | <0.5 | 0.11 | 59 | 312 | 328 | 16.7 | 4.8 | 86 | 138 | <1.0 | 85 | 17 | 13 | 26 | 2.07 | 1.38 | 0.18 | 7.80 | -3.40 | 498 | 15.5 | -3.30 |
| 99-A044 | 23.08.1999 | 16:00 | 285 | 4.6 | 18.9 | 7.54 | 21.5 | 1031 | 431 | 15.4 | 0.04 | 65 | 281 | 300 | 33.3 | 10.0 | 70 | 115 | 3.5 | 78 | 13 | 9 | 18 | 1.68 | 0.70 | 0.05 | 7.66 | -3.31 | 388 | 18.3 | -3.10 |
| 99-A051 | 28.09.1999 | 19:35 | | 1.3 | -0.6 | 7.49 | 21.2 | 287 | 340 | 26.5 | 0.12 | 30 | 369 | 397 | <1.7 | 4.1 | 110 | 163 | 3.8 | 99 | 32 | 28 | 2.56 | 0.47 | 0.08 | 7.62 | -3.15 | 715 | 27.1 | -0.88 | |
| 99-A058 | 03.11.1999 | 14:30 | 52 | 0.1 | 5.1 | 7.60 | 19.2 | 57 | 488 | 20.2 | 0.85 | 56 | 629 | 668 | 25.0 | 3.6 | 196 | 293 | 6.6 | 151 | 79 | 25 | 49 | 4.16 | 0.90 | 0.13 | 7.71 | -3.04 | 909 | 36.4 | 1.78 |
| 99-A064 | 08.12.1999 | 13:00 | 39 | 0.1 | -1.7 | 7.56 | 19.4 | 50 | 445 | 13.0 | 0.88 | 80 | 731 | 780 | 25.0 | 3.1 | 218 | 313 | 7.1 | 173 | 91 | 27 | 54 | 4.39 | 0.70 | 0.04 | 7.66 | -2.94 | 1161 | 46.2 | 0.14 |
| 00-A011 | 03.01.2000 | 13:22 | 29 | -0.1 | -8.2 | 7.69 | 17.7 | 17 | 198 | <1.5 | 1.15 | 308 | 844 | 884 | 16.7 | 1.9 | 246 | 405 | 8.6 | 189 | 86 | 38 | 56 | 5.76 | 0.83 | 0.04 | 8.00 | -3.02 | 960 | 40.1 | -0.75 |
| 00-A016 | 03.03.2000 | 19:10 | 23 | 0.0 | -13.7 | 7.85 | 19.2 | 13 | 243 | <1.5 | 1.90 | 377 | 955 | 989 | 16.7 | 1.7 | 275 | 431 | 9.6 | 209 | 106 | 39 | 60 | 6.76 | 0.59 | 0.04 | 8.00 | -3.11 | 769 | 30.8 | -1.42 |
| 00-A026 | 11.04.2000 | 18:20 | 19 | -0.1 | -5.3 | 7.54 | 21.9 | 21 | 330 | 17.7 | 1.52 | 44 | 489 | 523 | 41.7 | 7.4 | 140 | 181 | 8.9 | 115 | 72 | 12 | 64 | 3.16 | 0.71 | 0.54 | 7.69 | -3.07 | 847 | 31.5 | -1.31 |
| 00-A028 | 08.05.2000 | 13:20 | 288 | 2.7 | 11.5 | 7.59 | 22.5 | | 386 | 38.2 | | 24 | 292 | 309 | 33.3 | 9.7 | 83 | 89 | 7.0 | 70 | 48 | 5 | 39 | 1.63 | 0.28 | 0.18 | 7.73 | -3.34 | 458 | 16.8 | -1.67 |
| 00-A050 | 12.07.2000 | 10:00 | 293 | 2.4 | 12.8 | 7.62 | 20.7 | 922 | 477 | 95.1 | 0.05 | 12 | 236 | 250 | <1.7 | 6.4 | 53 | 103 | 1.9 | 69 | 11 | 6 | 17 | 0.97 | 0.57 | 0.07 | 7.72 | -3.47 | 336 | 12.9 | -0.03 |
| 00-A059 | 09.08.2000 | 10:00 | 466 | 2.2 | 17.5 | 7.76 | 23.2 | 1771 | 449 | 69.5 | 0.03 | 15 | 240 | 250 | 16.7 | 6.3 | 44 | 95 | 1.6 | 70 | 8 | 4 | 13 | 0.84 | 1.69 | 0.09 | 7.97 | -3.60 | 251 | 9.0 | -1.17 |
| 00-A068 | 14.09.2000 | 11:00 | 196 | 2.6 | 7.6 | 7.52 | 21.5 | 575 | 286 | 31.8 | 0.05 | 21 | 286 | 306 | 16.7 | 5.2 | 68 | 117 | 3.2 | 77 | 16 | 7 | 16 | 0.95 | 0.46 | 0.07 | 7.65 | -3.28 | 520 | 19.6 | -1.87 |
| 00-A077 | 17.10.2000 | 07:30 | 71 | 0.6 | -1.6 | 7.66 | 22.8 | 72 | 165 | | | | 618 | 649 | 25.0 | 3.7 | 177 | 246 | 6.5 | 144 | 75 | 24 | 44 | 2.92 | 0.60 | 0.03 | 7.81 | -3.09 | 820 | 29.8 | -1.67 |
| 00-A082 | 20.11.2000 | 12:20 | 19 | 0.1 | 2.2 | 7.88 | 20.5 | 16 | 122 | 24.1 | 0.76 | 12 | 845 | 873 | 30.8 | 3.4 | 235 | 330 | 7.8 | 195 | 103 | 27 | 52 | 4.32 | 0.59 | 0.03 | 8.04 | -3.19 | 648 | 25.0 | -1.26 |
| 01-A009 | 06.01.2001 | 20:05 | 15 | 0.0 | 0.8 | 7.89 | 19.0 | 9 | 82 | 11.0 | 0.90 | 17 | 1016 | 1049 | 17.5 | 1.6 | 291 | 409 | 14.0 | 230 | 130 | 38 | 59 | 5.71 | 0.66 | 0.09 | 8.03 | -3.13 | 741 | 29.8 | -0.62 |
| 01-A018 | 03.03.2001 | 16:00 | 12 | 0.0 | -6.8 | 7.98 | 20.6 | | 280 | 35.7 | | 18 | 1135 | 1165 | 45.8 | 3.8 | 321 | 439 | 10.3 | 267 | 149 | 36 | 70 | 6.18 | 0.46 | 0.05 | 8.15 | -3.16 | 685 | 26.4 | -0.24 |
| 01-A028 | 09.05.2001 | 18:50 | 174 | 2.9 | 10.2 | 7.64 | 23.0 | 219 | 310 | 31.7 | 0.14 | 23 | 386 | 407 | 46.7 | 10.3 | 138 | 182 | 8.7 | 122 | 75 | 12 | 84 | 2.21 | 0.29 | 0.31 | 7.75 | -3.27 | 540 | 19.5 | 8.17 |
| 01-A035 | 25.06.2001 | 19:30 | 298 | 6.1 | 10.4 | 7.60 | 20.9 | 538 | 342 | 30.8 | 0.06 | 26 | 339 | 359 | 19.2 | 5.1 | 135 | 147 | 3.8 | 90 | 35 | 8 | 39 | 2.08 | 0.57 | 0.06 | 7.66 | -3.30 | 506 | 19.3 | 0.73 |
| 01-A042 | 16.08.2001 | 09:20 | 297 | 2.0 | 11.0 | 7.56 | 22.1 | 540 | 200 | 10.6 | 0.04 | 44 | 224 | 239 | 9.2 | 3.7 | 57 | 92 | 2.1 | 62 | 14 | 6 | 20 | 1.03 | 0.38 | 0.05 | 7.70 | -3.43 | 376 | 13.9 | -2.29 |
| 01-A049 | 08.10.2001 | 18:45 | 192 | 3.4 | 7.6 | 7.69 | 19.5 | 350 | 143 | 15.7 | 0.04 | 21 | 420 | 441 | 30.8 | 6.5 | 128 | 169 | 3.9 | 117 | 46 | 12 | 32 | 2.16 | 0.64 | 0.14 | 7.80 | -3.30 | 498 | 19.8 | 2.28 |
| 01-A056 | 10.12.2001 | 19:30 | 45 | 0.4 | 8.5 | 7.76 | 22.2 | 64 | 206 | 25.3 | 0.32 | 19 | 717 | 746 | 16.7 | 2.2 | 213 | 326 | 7.5 | 170 | 89 | 29 | 74 | 4.53 | 0.64 | 0.17 | 7.90 | -3.13 | 745 | 27.5 | -0.24 |
| 02-A002 | 18.03.2002 | 14:20 | 13 | 0.0 | -7.2 | 7.74 | 23.0 | 35 | 152 | 12.3 | 0.43 | 29 | 915 | 954 | 26.6 | 2.7 | 283 | 448 | 7.2 | 205 | 96 | 36 | 73 | 6.40 | 0.51 | 0.03 | 7.90 | -3.00 | 1005 | 36.3 | -0.29 |
| 02-A008 | 22.04.2002 | 13:25 | 254 | 1.5 | 5.0 | 7.30 | 24.9 | 285 | 171 | 66.3 | 0.27 | 27 | 233 | 259 | 81.6 | 23.9 | 76 | 88 | 5.5 | 72 | 41 | <6 | 68 | 1.16 | 0.97 | 1.58 | 7.45 | -3.14 | 732 | 25.1 | 3.67 |
| 02-A014 | 04.06.2002 | 11:40 | 159 | 2.9 | 2.9 | 7.58 | 26.2 | 108 | 374 | 52.4 | 0.35 | 17 | 366 | 387 | 33.3 | 7.9 | 129 | 130 | 4.6 | 89 | 48 | <6 | 35 | 1.95 | 0.34 | 0.12 | 7.72 | -3.21 | 619 | 20.5 | 0.94 |
| 02-A020 | 25.06.2002 | 11:40 | 225 | 4.2 | 10.2 | 7.67 | 25.7 | 516 | 311 | 44.1 | 0.06 | 16 | 368 | 386 | 15.0 | 3.7 | 118 | 164 | 3.5 | 96 | 26 | 6 | 31 | 2.13 | 0.75 | 0.12 | 7.79 | -3.30 | 499 | 16.8 | -0.15 |
| 02-A026 | 13.08.2002 | 12:40 | 347 | 3.8 | 7.9 | 7.55 | 21.1 | 686 | 213 | 18.9 | 0.03 | 26 | 284 | 303 | 69.1 | 18.6 | 68 | 108 | 2.6 | 77 | 17 | 5 | 27 | 1.34 | 0.45 | 0.13 | 7.67 | -3.32 | 480 | 18.2 | -3.93 |
| 02-A032 | 18.09.2002 | 12:39 | 287 | 2.4 | 6.6 | 7.63 | 20.9 | 838 | 401 | 15.8 | 0.05 | 6 | 281 | 297 | 26.6 | 8.2 | 70 | 121 | 2.7 | 82 | 13 | 5 | 22 | 1.32 | 0.71 | 0.17 | 7.77 | -3.41 | 392 | 15.0 | -0.17 |
| 02-A038 | 22.10.2002 | 14:40 | 137 | 0.4 | 0.7 | 7.29 | 21.0 | 327 | 412 | 62.5 | 0.13 | 15 | 396 | 445 | 18.3 | 4.0 | 107 | 189 | 3.7 | 109 | 27 | 15 | 38 | 2.50 | 0.37 | 0.20 | 7.40 | -2.92 | 1215 | 46.3 | -0.43 |
| 03-A008 | 14.01.2003 | 14:55 | 22 | 0.0 | -6.7 | 7.76 | 17.1 | 33 | 507 | 15.1 | 0.23 | 33 | 920 | 961 | 26.2 | 2.7 | 266 | 366 | 7.1 | 203 | 96 | 29 | 69 | 5.84 | 0.51 | 0.06 | 7.86 | -3.05 | 887 | 37.7 | -4.33 |
| 03-A008 | 14.04.2003 | 15:10 | 52 | 1.6 | 2.9 | 7.73 | 26.5 | 16 | 191 | 28.7 | 1.18 | 15 | 588 | 612 | 34.2 | 5.3 | 189 | 215 | 6.4 | 133 | 72 | 16 | 63 | 3.42 | 0.36 | 0.11 | 7.91 | -3.15 | 700 | 23.0 | -4.35 |
| 03-A014 | 20.05.2003 | 14:30 | 56 | 4.7 | 3.3 | 7.70 | 18.3 | 44 | 262 | 26.1 | 0.59 | 23 | 638 | 669 | 31.7 | 4.5 | 218 | 258 | 6.0 | 151 | 76 | 21 | 60 | 4.05 | 0.72 | 0.28 | 7.80 | -3.14 | 722 | 29.7 | -1.85 |
| 03-A020 | 19.07.2003 | 13:50 | 158 | | 7.24 | 24.4 | 369 | 346 | 48.6 | 0.09 | 17 | 338 | 382 | 15.0 | 3.8 | 115 | 177 | 3.2 | 92 | 27 | 10 | 36 | 2.05 | 0.69 | 0.17 | 7.39 | -2.91 | 1219 | 42.3 | 2.44 | |
| 03-A026 | 19.07.2003 | 12:40 | 343 | 5.7 | 17.7 | 7.46 | 22.5 | 1436 | 612 | 57.3 | 0.04 | 25 | 263 | 284 | 10.8 | 3.7 | 68 | 120 | 2.5 | 84 | 14 | 6 | 23 | 1.13 | 1.49 | 0.84 | 7.55 | -3.26 | 549 | 20.1 | 3.54 |
| 03-A035 | 27.08.2003 | 11:45 | 511 | 2.2 | 8.6 | 7.48 | 22.3 | 1342 | 1091 | 101 | 0.08 | 25 | 213 | 229 | <1.7 | 6.9 | 48 | 105 | 2.1 | 67 | 13 | 5 | 14 | 0.79 | 0.37 | 0.10 | 7.62 | -3.37 | 430 | 15.8 | 5.29 |
| 03-A038 | 26.09.2003 | 14:05 | 78 | 0.2 | 5.2 | 7.23 | 23.4 | 153 | 105 | 12.0 | 0.07 | 20 | 362 | 411 | 88.3 | 17.7 | 108 | 204 | 3.6 | 97 | 32 | 16 | 41 | 2.29 | 0.60 | 0.27 | 7.35 | -2.88 | 1316 | 47.0 | 4.53 |
| 03-A044 | 27.11.2003 | 15:15 | 62 | 0.3 | 0.0 | 7.62 | 19.0 | 65 | 232 | 16.0 | 0.35 | 34 | 625 | 662 | 16.7 | 2.5 | 198 | 317 | 5.2 | 157 | 67 | 25 | 55 | 4.24 | 0.82 | 0.23 | 7.75 | -3.07 | 859 | 34.6 | 2.72 |
| Average | | | 154 | 1.7 | 4.4 | 7.61 | 21.2 | 350 | 340 | 34.8 | 0.65 | 58 </ | | | | | | | | | | | | | | | | | | | |

Table A2. Jökulsá á Dal at Hjarðarfjazi 28 November 2007 -10 December 2013

| Sample number | Date | Time | Discharge m ³ /s | T _{water} °C | T _{air} °C | pH | T _{ref} °C | SIM mg/l | POC µg/kg | PON µg/kg | POC %wt. mole | C/N | Alk µeq/kg | DIC µM | DOC µM | DOC %mol | SiO ₂ µM | Na µM | K µM | Ca µM | Mg µM | SO ₄ µM | Cl µM | F µM | Al µM | Fe µM | pH _{free-stu} | log(pCO _{2w}) | pCO _{2w} µatm | CO _{2(aq)} µM | charge balance % |
|---------------|------------|-------|-----------------------------|-----------------------|---------------------|------|---------------------|----------|-----------|-----------|---------------|------|------------|--------|--------|----------|---------------------|-------|------|-------|-------|--------------------|-------|------|-------|-------|------------------------|-------------------------|------------------------|------------------------|------------------|
| 07A002 | 27.11.2007 | 16:55 | 16.8 | 0.0 | -2.8 | 7.82 | 19.7 | 18.1 | 2425 | 89.9 | 11.8 | 63 | 1113 | 1154 | 30.8 | 2.6 | 353 | 402 | 11.7 | 259 | 154 | 26.3 | 63.4 | 5.35 | 0.31 | 0.08 | 7.96 | -3.29 | 509 | 36.0 | -0.07 |
| 08A004 | 20.05.2008 | 12:14 | 167 | 3.5 | 10.2 | 7.32 | 24.3 | 35.5 | 932 | 251.1 | 2.55 | 23 | 356 | 395 | 56.6 | 12.5 | 107 | 107 | 10.7 | 89 | 68 | 10.1 | 54.0 | 1.57 | 0.49 | 2.44 | 7.45 | -2.97 | 1066 | 37.1 | 1.58 |
| 08A014 | 28.08.2008 | 14:15 | 217 | 7.1 | 11.2 | 7.42 | 22.0 | 159 | 344 | 54.5 | 0.22 | 15 | 345 | 376 | 14.2 | 3.6 | 107 | 161 | 6.4 | 104 | 27 | 12.3 | 33.6 | 1.82 | 1.08 | 0.46 | 7.51 | -3.10 | 789 | 29.3 | 3.37 |
| 09A001 | 04.02.2009 | 09:45 | 10.8 | 0.0 | -8.5 | 7.86 | 19.3 | 11.9 | 807 | 52.2 | 6.33 | 36 | 1244 | 1241 | 159 | 11.4 | 388 | 500 | 12.6 | 282 | 184 | 31.7 | 73.6 | 5.50 | 0.62 | 0.78 | 7.89 | -3.01 | 972 | 36.8 | 1.46 |
| 09A007 | 02.04.2009 | 17:30 | 10.2 | 0.0 | 0.7 | 7.91 | 20.5 | 5.8 | 279 | 17.0 | 4.58 | 38 | 1100 | 1087 | 177 | 13.9 | 354 | 483 | 12.3 | 262 | 164 | 27.7 | 70.0 | 5.12 | 0.72 | 1.05 | 8.06 | -3.11 | 779 | 30.1 | 3.00 |
| 09A011 | 02.06.2009 | 12:50 | 130 | 4.7 | 12.1 | 7.47 | 20.3 | 24.4 | 488 | 47.1 | 1.96 | 24 | 384 | 363 | 55.8 | 12.7 | 152 | 112 | 7.4 | 89 | 68 | 4.8 | 30.6 | 1.54 | 0.53 | 2.51 | 7.57 | -3.11 | 768 | 29.8 | 2.56 |
| 09A017 | 30.06.2009 | 09:10 | 43.5 | 13.4 | 15.7 | 7.84 | 21.8 | 9.3 | 174 | 15.3 | 1.84 | 27 | 598 | 586 | 50.0 | 7.7 | 256 | 218 | 11.7 | 129 | 87 | 9.2 | 40.0 | 3.61 | 0.63 | 1.38 | 7.90 | -3.29 | 514 | 19.2 | 0.38 |
| 09A024 | 12.08.2009 | 09:20 | 37.3 | 11.5 | 12.2 | 8.04 | 20.8 | 1.3 | 139 | 6.9 | 9.62 | 47 | 1059 | 1055 | 71.6 | 6.4 | 352 | 314 | 10.2 | 244 | 181 | 14.6 | 56.6 | 3.76 | 1.19 | 2.58 | 8.00 | -3.25 | 557 | 21.1 | 0.87 |
| 09A034 | 23.09.2009 | 15:30 | 30.2 | 10.3 | 5.2 | 7.55 | 21.3 | 177 | 334 | <24.7 | 0.19 | 32 | 463 | 463 | 14.2 | 3.0 | 155 | 197 | 5.3 | 125 | 45 | 10.5 | 30.3 | 2.05 | 1.25 | 0.60 | 7.60 | -3.11 | 774 | 29.3 | 2.23 |
| 09A039 | 04.11.2009 | 09:40 | 30.2 | 1.5 | 4.2 | 7.86 | 20.2 | 1.00 | 159 | <8.1 | 13.6 | 46 | 1036 | 1033 | 94.1 | 8.3 | 360 | 314 | 10.2 | 244 | 181 | 14.6 | 56.6 | 3.76 | 1.19 | 2.58 | 8.00 | -3.09 | 820 | 32.0 | 1.94 |
| 09A044 | 08.12.2009 | 17:10 | 25.7 | 1.3 | 7.88 | 22.1 | 1.2 | 229 | <10.1 | 15.9 | 5.3 | 1113 | 1133 | 101.1 | 51.6 | 4.4 | 352 | 368 | 10.8 | 155 | 112 | 8.7 | 55.8 | 2.41 | 0.34 | 3.38 | 7.68 | -2.96 | 1086 | 40.6 | 2.13 |
| 10A004 | 02.03.2010 | 19:10 | 15.3 | 0.0 | -8.1 | 7.92 | 21.9 | 4.7 | 167 | <8.2 | 3.42 | 47 | 1182 | 1178 | 90.8 | 7.2 | 370 | 461 | 12.6 | 272 | 167 | 28.8 | 73.8 | 4.76 | 0.73 | 1.10 | 8.07 | -3.08 | 833 | 31.0 | 0.96 |
| 10A010 | 14.04.2010 | 17:15 | 61.0 | 3.0 | 10.3 | 7.67 | 22.2 | 17.7 | 751 | 92.6 | 4.05 | 19 | 564 | 563 | 115 | 17.0 | 191 | 206 | 10.5 | 140 | 99 | 11.5 | 87.5 | 1.98 | 0.53 | 2.24 | 7.80 | -3.14 | 724 | 26.7 | 1.31 |
| 10A012 | 27.05.2010 | 09:05 | 60.3 | 2.4 | 5.3 | 7.55 | 21.7 | 6.9 | 270 | 19.8 | 3.75 | 32 | 645 | 644 | 72.4 | 10.1 | 237 | 206 | 10.8 | 155 | 112 | 8.7 | 55.8 | 2.41 | 0.34 | 3.38 | 7.68 | -2.96 | 1086 | 40.6 | 2.13 |
| 10A018 | 14.07.2010 | 10:25 | 25.9 | 12.2 | 13.1 | 8.10 | 22.9 | 4.7 | 196 | 21.2 | 3.99 | 22 | 1002 | 997 | 80.8 | 7.5 | 330 | 332 | 13.1 | 229 | 155 | 13.7 | 51.7 | 4.18 | 0.35 | 1.18 | 8.20 | -3.33 | 472 | 17.1 | 1.00 |
| 10A029 | 26.08.2010 | 10:30 | 240 | 5.2 | 8.0 | 7.63 | 23.0 | 244 | 373 | <24.1 | 0.15 | 36 | 363 | 362 | 35.0 | 8.8 | 119 | 144 | 4.0 | 102 | 31 | 6.9 | 19.1 | 1.15 | 1.10 | 0.40 | 7.74 | -3.29 | 517 | 18.7 | 1.51 |
| 10A031 | 13.10.2010 | 09:10 | 76.0 | 4.8 | 6.2 | 7.67 | 19.8 | 145 | 307 | <18.4 | 0.21 | 39 | 516 | 515 | 0.0 | 0.0 | 164 | 187 | 5.2 | 136 | 59 | 9.2 | 26.4 | 1.71 | 1.10 | 0.47 | 7.76 | -3.19 | 640 | 25.2 | 3.67 |
| 10A035 | 02.11.2010 | 10:30 | 10.1 | 0.2 | 1.1 | 7.87 | 22.5 | 26.6 | 317 | 47.6 | 1.17 | 16 | 1142 | 1139 | 69.1 | 5.7 | 349 | 404 | 10.9 | 269 | 181 | 25.4 | 82.8 | 4.05 | 1.20 | 1.18 | 8.03 | -3.04 | 912 | 33.3 | 3.54 |
| 10A040 | 08.12.2010 | 10:35 | 9.9 | -0.1 | -9.5 | 7.87 | 21.8 | 4.3 | 183 | 21.5 | 4.06 | 20 | 1247 | 1244 | 55.8 | 4.3 | 385 | 439 | 12.1 | 287 | 197 | 27.0 | 74.6 | 4.42 | 0.90 | 1.00 | 8.04 | -3.01 | 985 | 36.7 | 3.54 |
| 11A004 | 08.03.2011 | 15:45 | 9.5 | 0.2 | -3.1 | 7.93 | 20.1 | 11.2 | 225 | 25.2 | 1.97 | 21 | 598 | 597 | 123 | 17.1 | 189 | 184 | 11.0 | 140 | 113 | 8.7 | 92.3 | 2.63 | 0.30 | 4.32 | 7.86 | -3.17 | 676 | 25.5 | -0.17 |
| 11A009 | 28.04.2011 | 16:00 | 80.9 | 3.0 | 8.5 | 7.72 | 21.4 | 33.4 | 436 | 48.4 | 1.29 | 21 | 598 | 597 | 123 | 17.1 | 189 | 184 | 11.0 | 140 | 113 | 8.7 | 92.3 | 2.63 | 0.30 | 4.32 | 7.86 | -3.17 | 676 | 25.5 | -0.17 |
| 11A013 | 16.05.2011 | 13:50 | 72.2 | 4.0 | 11.2 | 7.69 | 19.5 | 30 | 331 | 35.7 | 1.09 | 22 | 590 | 529 | 69.1 | 11.6 | 205 | 164 | 8.5 | 123 | 98 | 7.2 | 64.4 | 2.63 | 0.27 | 2.99 | 7.79 | -3.20 | 627 | 24.9 | 0.52 |
| 11A017 | 23.06.2011 | 15:00 | 43.3 | 6.9 | 11.7 | 7.79 | 20.7 | 24.3 | 332 | 27.7 | 0.94 | 19 | 643 | 641 | 42.5 | 6.2 | 266 | 214 | 8.9 | 143 | 107 | 10.3 | 57.7 | 3.72 | 0.28 | 1.93 | 7.89 | -3.21 | 612 | 23.5 | 0.05 |
| 11A019 | 28.07.2011 | 10:30 | 22.7 | 12.1 | 17.2 | 7.76 | 23.5 | 28.7 | 840 | 838 | 62.4 | 6.9 | 315 | 288 | 11.6 | 170 | 123 | 288 | 4.4 | 244 | 194 | 13.4 | 68.5 | 4.15 | 0.71 | 1.40 | 8.08 | -3.15 | 715 | 27.6 | 0.48 |
| 11A028 | 15.09.2011 | 20:20 | 23.5 | 5.2 | 9.6 | 7.98 | 22.1 | 38.4 | 282 | 23.4 | 0.73 | 28 | 973 | 970 | 97.4 | 9.1 | 322 | 341 | 11.1 | 203 | 143 | 22.3 | 70.8 | 4.90 | 0.65 | 0.35 | 8.12 | -3.22 | 601 | 22.2 | -2.20 |
| 11A031 | 01.11.2011 | 10:25 | 38.4 | 1.0 | 2.5 | 7.93 | 20.5 | 22.7 | 187 | 12.5 | 0.82 | 35 | 1057 | 1054 | 91.6 | 8.0 | 350 | 288 | 4.4 | 244 | 194 | 13.4 | 68.5 | 4.15 | 0.71 | 1.40 | 8.08 | -3.15 | 715 | 27.6 | 0.48 |
| 11A037 | 07.12.2011 | 15:25 | 14.9 | 0.0 | -8.8 | 7.86 | 21.0 | 6.4 | 107 | <7.9 | 1.64 | 32 | 1102 | 1099 | 54.1 | 4.7 | 395 | 386 | 4.1 | 255 | 175 | 25.3 | 70.3 | 5.46 | 1.35 | 1.55 | 8.03 | -3.05 | 882 | 33.6 | 1.18 |
| 12A004 | 08.03.2012 | 16:00 | 18.4 | 0.1 | 1.9 | 7.95 | 19.2 | 9.9 | 210 | <8.9 | 2.07 | 55 | 955 | 952 | 106 | 10.0 | 318 | 311 | 10.2 | 234 | 168 | 16.7 | 81.7 | 3.97 | 0.79 | 3.28 | 8.10 | -3.22 | 605 | 24.2 | 2.42 |
| 12A005 | 17.04.2012 | 10:00 | 20.8 | 1.9 | 0.2 | 7.86 | 21.9 | 19.6 | 253 | 18.7 | 1.27 | 32 | 939 | 936 | 85.8 | 8.4 | 335 | 329 | 11.2 | 222 | 159 | 18.7 | 62.0 | 4.44 | 0.58 | 2.67 | 8.01 | -3.12 | 765 | 28.4 | 2.99 |
| 12A009 | 06.06.2012 | 14:30 | 17.9 | 6.2 | 7.2 | 7.88 | 20.2 | 15.2 | 193 | 15.8 | 1.25 | 28 | 847 | 845 | 51.6 | 5.8 | 318 | 331 | 10.4 | 194 | 129 | 18.6 | 53.9 | 5.02 | 0.62 | 2.02 | 7.99 | -3.19 | 645 | 25.1 | 2.54 |
| 12A013 | 04.07.2012 | 10:15 | 11.5 | 12.3 | 17.3 | 8.14 | 22.3 | 37.4 | 240 | 19.5 | 0.64 | 29 | 1008 | 1002 | 70.8 | 6.6 | 346 | 403 | 13.0 | 229 | 151 | 22.9 | 58.0 | 5.95 | 0.59 | 1.20 | 8.24 | -3.37 | 428 | 15.7 | 2.61 |
| 12A023 | 05.09.2012 | 17:30 | 141 | 5.2 | 11.8 | 7.60 | 20.5 | 229 | 351 | <18.5 | 0.15 | 44 | 386 | 385 | 33.3 | 4.3 | 115 | 159 | 3.5 | 105 | 33 | 9.3 | 23.4 | 1.66 | 0.73 | 0.15 | 7.69 | -3.24 | 572 | 22.1 | 0.95 |
| 12A027 | 25.09.2012 | 14:10 | 32.3 | 5.1 | 5.9 | 7.78 | 20.3 | 20.1 | 310 | 25.9 | 1.52 | 28 | 981 | 979 | 72.4 | 6.9 | 327 | 289 | 9.5 | 216 | 165 | 13.6 | 53.1 | 3.95 | 1.36 | 3.87 | 7.90 | -3.03 | 939 | 36.5 | 0.29 |
| 12A031 | 30.10.2012 | 14:15 | 38.3 | 0.3 | -0.4 | 7.80 | 21.0 | 12.5 | 1125 | 1122 | 53.3 | 4.5 | 355 | 408 | 9.4 | 274 | 183 | 26.5 | 58.9 | 4.93 | 0.51 | 0.91 | 0.78 | 7.95 | 2.98 | -2.98 | 1037 | 39.5 | 3.48 | | |
| 12A033 | 05.12.2012 | 10:00 | 19.0 | 0.0 | -10.3 | 7.81 | 19.9 | 16.6 | 1201 | 1199 | 47.5 | 3.8 | 367 | 439 | 10.9 | 287 | 188 | 30.9 | 68.4 | 5.05 | 0.83 | 1.02 | 7.94 | 2.97 | -2.97 | 1063 | 41.7 | 2.43 | | | |
| 13A003 | 18.03.2013 | 15:25 | 14.4 | 0.0 | -2.4 | 7.85 | 21.0 | 8.5 | 132 | 14.8 | 1.53 | 21 | 1258 | 1255 | 20.0 | 1.6 | 349 | 441 | 11.4 | 262 | 209 | 20.5 | 97.7 | 3.74 | 0.46 | 1.48 | 8.00 | -2.99 | 1032 | 39.3 | -1.66 |
| 13A005 | 23.04.2013 | 10:15 | 12.2 | 1.3 | 3.0 | 7.71 | 19.9 | 14.7 | 184 | 18.8 | 1.62 | 23 | 1200 | 1198 | 63.3 | 5.0 | 329 | 448 | 11.4 | 243 | 174 | 27.2 | 76.5 | 4.42 | 0.34 | 0.72 | 7.83 | -2.87 | 1346 | 52.8 | -1.55 |
| 13A009 | 28.05.2013 | 10:15 | 13.7 | 2.6 | 5.6 | 7.44 | 19.2 | 33.1 | 547 | 32.0 | 1.23 | 40 | 544 | 543 | 64.9 | 10.7 | 163 | 163 | 10.0 | 118 | 99 | 6.8 | 65.2 | 1.63 | 0.56 | 4.26 | 7.55 | -2.94 | 1143 | 45.7 | -1.00 |
| 13A013 | 02.07.2013 | 10:25 | 47.8 | 7.0 | 8.8 | 7.68 | 19.9 | 9.1 | 140 | 20.0 | 1.51 | 16 | 661 | 660 | 45.0 | 6.4 | 255 | 221 | 9.4 | 137 | 106 | 9.0 | 51.1 | 2.66 | 0.33 | 2.69 | 7.77 | -3.10 | 803 | 31.6 | -0.98 |
| 13A017 | 18.07.2013 | 10:30 | 30.7 | 10.3 | 13.3 | 7.59 | 22.0 | 15.9 | 242 | 26.1 | 1.50 | 22 | 797 | 796 | 88.6 | 10.0 | 267 | 278 | 10.6 | 146 | 113 | 10.9 | 49.4 | 3.38 | 0.33 | 1.41 | 7.66 | -2.91 | 1229 | 45.6 | -1.92 |
| 13A021 | 09.09.2013 | 10:15 | 64.5 | 6.4 | 8.4 | 7.97 | 21.1 | 153 | 895 | 61.3 | 0.58 | 34 | 416 | 414 | 35.4 | 7.2 | 125 | 204 | 5.3 | 91 | 32 | 11.3 | 26.5 | 1.83 | 0.71 | 0.25 | 8.10 | -3.58 | 263 | 10.0 | -3.46 |
| 13A029 | 24.10.2013 | 10:10 | 30.4 | 1.8 | 2.2 | 7.69 | 2 | | | | | | | | | | | | | | | | | | | | | | | | |

Table A3. Jökulsá á Dal at Brú 21 November 2000 - 27 November 2003

| Sample Date | Time | Discharge | T _{water} | T _{air} | pH | T _{ref} * | SIM | POC | PON | POC | %wt. mole | C/N | Alkalinity | DIC | DOC | DOC | SiO ₂ | Na | K | Ca | Mg | SO ₄ | Cl | F | Al | Fe | pH _{in-situ} | log(pCO _{2w}) | pCO _{2w} | CO _{2w} | charge/balance | |
|----------------|------------|-------------------|--------------------|------------------|------------|--------------------|-------------|------------|------------|-------------|-------------|-------------|------------|------------|-------------|------------|------------------|------------|-------------|-------------|------------|-----------------|-------------|-------------|-------------|-------------|-----------------------|-------------------------|-------------------|------------------|----------------|-------------|
| number | | m ³ /s | °C | °C | | °C | mg/l | µg/kg | µg/kg | µg/kg | | | µeq/l | µM | µM | %mol | µM | µM | µM | µM | µM | µM | µM | µM | µM | µM | µM | µatm | µM | µM | % | |
| 00-A086 | 21.11.2000 | 10:00 | 14.0 | 0.1 | 10 | 7.87 | 20.5 | 45 | 177 | 19.7 | 0.39 | 21.0 | 664 | 686 | 18.3 | 2.6 | 190 | 362 | 6.64 | 157 | 46 | 37.4 | 46.5 | 5.29 | 0.32 | 8.01 | -3.28 | 522 | 522 | -1.17 | | |
| 01-A008 | 06.01.2001 | 16:15 | 11.0 | 0.0 | -2.4 | 8.25 | 19.6 | 12 | 107 | 15.4 | 0.89 | 16.3 | 828 | 841 | 17.0 | 2.0 | 246 | 461 | 7.71 | 188 | 56 | 47.1 | 53.7 | 6.68 | 0.95 | 0.04 | 8.44 | -3.58 | 263 | 263 | -1.51 | |
| 01-A017 | 03.03.2001 | 14:15 | 9.0 | 0.0 | -12.8 | 8.21 | 20.0 | 441 | 37.3 | 27.5 | | | 974 | 990 | 15.8 | 1.6 | 285 | 518 | 8.57 | 234 | 77 | 52.4 | 63.5 | 7.29 | 0.73 | 0.04 | 8.40 | -3.47 | 340 | 340 | -0.27 | |
| 01-A020 | 06.04.2001 | 16:50 | 6.0 | 0.0 | -0.3 | 8.30 | 25.0 | 9 | 154 | <1.5 | 1.69 | | 959 | 972 | <1.7 | 1.7 | 273 | 539 | 8.63 | 211 | 69 | 48.0 | 56.7 | 7.87 | 0.66 | 0.03 | 8.54 | -3.54 | 290 | 290 | -0.59 | |
| 01-A027 | 09.05.2001 | 16:10 | 67.7 | 2.5 | 10.7 | 7.53 | 23.1 | 304 | 504 | 52.2 | 0.17 | 22.6 | 380 | 406 | 27.5 | 6.3 | 120 | 189 | 5.53 | 105 | 41 | 14.8 | 57.2 | 2.42 | 0.33 | 0.07 | 7.65 | -3.16 | 690 | 690 | 1.58 | |
| 01-A034 | 25.06.2001 | 18:00 | 205 | 4.5 | 12.3 | 7.78 | 20.7 | 849 | 661 | 54.1 | 0.08 | 28.5 | 301 | 314 | 15.0 | 4.6 | 111 | 159 | 3.26 | 80 | 19 | 9.82 | 35.5 | 1.87 | 0.83 | 0.04 | 7.90 | -3.53 | 294 | 294 | 0.38 | |
| 01-A041 | 15.08.2001 | 21:20 | 322 | 8.0 | 8.2 | 7.50 | 22.0 | 621 | 157 | 8.6 | 0.03 | 42.8 | 179 | 193 | <1.7 | 8.1 | 43 | 81 | 1.74 | 49 | 7 | 5.80 | 16.7 | 0.87 | 0.36 | 0.05 | 7.57 | -3.46 | 344 | 344 | -3.60 | |
| 01-A048 | 08.10.2001 | 16:50 | 152 | 2.1 | 7.0 | 7.63 | 19.5 | 351 | 130 | 14.2 | 0.04 | 21.3 | 289 | 305 | 21.7 | 6.6 | 88 | 157 | 2.93 | 82 | 18 | 11.7 | 25.2 | 1.95 | 0.61 | 0.08 | 7.72 | -3.40 | 395 | 395 | 2.42 | |
| 01-A055 | 10.12.2001 | 17:20 | 25.4 | 1.1 | 6.0 | 7.79 | 22.2 | 103 | 131 | 16.8 | 0.13 | 18.3 | 556 | 577 | 14.2 | 2.4 | 172 | 350 | 5.22 | 128 | 40 | 31.5 | 61.8 | 4.82 | 0.83 | 0.08 | 7.92 | -3.27 | 541 | 541 | 0.20 | |
| 02-A001 | 18.03.2002 | 12:20 | 8.8 | 0.0 | -8.7 | 8.04 | 23.0 | 15 | 120 | 8.2 | 0.79 | 34.0 | 788 | 807 | 27.5 | 3.3 | 257 | 500 | 6.21 | 171 | 48 | 48.0 | 68.6 | 7.37 | 0.89 | 0.04 | 8.26 | -3.37 | 430 | 430 | -0.57 | |
| 02-A007 | 22.04.2002 | 11:30 | 131 | 1.3 | 3.8 | 7.16 | 24.9 | 181 | 517 | 48.4 | 0.28 | 24.9 | 215 | 249 | 35.8 | 12.6 | 68 | 92 | 3.67 | 65 | 26 | 5.80 | 58.6 | 1.24 | 0.34 | 0.49 | 7.29 | -3.02 | 945 | 945 | -1.47 | |
| 02-A013 | 04.06.2002 | 09:00 | 73.8 | 2.1 | 5.2 | 7.42 | 25.9 | 149 | 408 | 48.4 | 0.27 | 19.6 | 297 | 322 | 13.3 | 4.0 | 107 | 147 | 3.52 | 75 | 24 | 8.89 | 27.5 | 2.13 | 0.44 | 0.08 | 7.56 | -3.14 | 724 | 724 | 0.70 | |
| 02-A019 | 25.06.2002 | 09:20 | 171 | 2.5 | 6.5 | 7.57 | 25.1 | 492 | 297 | 7.4 | 0.03 | 61.3 | 204 | 217 | 55.8 | 20.4 | 52 | 102 | 2.12 | 60 | 8 | 5.24 | 26.6 | 1.16 | 0.48 | 0.10 | 7.70 | -3.30 | 502 | 502 | 0.23 | |
| 02-A025 | 13.08.2002 | 10:00 | 291 | 1.8 | 5.3 | 7.56 | 20.6 | 622 | 194 | 7.4 | 0.03 | 61.3 | 204 | 217 | 55.8 | 20.4 | 52 | 102 | 2.12 | 60 | 8 | 5.24 | 26.6 | 1.16 | 0.48 | 0.10 | 7.70 | -3.48 | 334 | 334 | -0.63 | |
| 02-A031 | 18.09.2002 | 10:33 | 254 | 1.7 | 9.0 | 7.61 | 21.6 | 812 | 358 | 45.1 | 0.04 | 18.5 | 219 | 232 | 17.5 | 7.0 | 59 | 113 | 2.33 | 64 | 8 | <6 | 19.6 | 1.21 | 1.30 | 0.27 | 7.79 | -3.50 | 319 | 319 | 4.11 | |
| 02-A037 | 22.10.2002 | 12:00 | 125 | 0.0 | 0.3 | 7.50 | 21.7 | 343 | 437 | 56.6 | 0.13 | 18.0 | 330 | 355 | 19.2 | 5.1 | 85 | 177 | 3.18 | 87 | 13 | 14.3 | 34.7 | 2.37 | 0.25 | 0.15 | 7.62 | -3.20 | 632 | 632 | -2.52 | |
| 03-A004 | 21.01.2003 | 10:30 | 12.5 | 0.0 | -10.5 | 7.99 | 16.7 | 24 | 98 | 11.0 | 0.40 | 20.7 | 753 | 774 | 13.3 | 1.7 | 243 | 435 | 5.90 | 171 | 47 | 40.5 | 60.5 | 6.76 | 0.82 | 0.08 | 8.10 | -3.37 | 423 | 423 | -1.60 | |
| 03-A007 | 14.04.2003 | 11:30 | 25.8 | 0.9 | 1.4 | 7.65 | 26.2 | 21 | 409 | 24.0 | 1.91 | 39.7 | 465 | 488 | 24.2 | 4.7 | 164 | 263 | 5.09 | 112 | 33 | 22.8 | 64.2 | 4.03 | 0.54 | 0.05 | 7.82 | -3.18 | 665 | 665 | -2.28 | |
| 03-A013 | 20.05.2003 | 12:20 | 25.6 | 4.4 | 3.3 | 7.76 | 18.2 | 58 | 229 | 30.7 | 0.39 | 17.4 | 581 | 606 | 24.2 | 3.8 | 189 | 308 | 5.23 | 142 | 42 | 29.9 | 57.4 | 4.55 | 1.02 | 0.28 | 7.87 | -3.24 | 571 | 571 | -1.68 | |
| 03-A019 | 19.06.2003 | 11:30 | 140 | 7.8 | 3.4 | 7.39 | 24.6 | 408 | 238 | 35.1 | 0.06 | 15.8 | 267 | 292 | 11.7 | 3.8 | 91 | 178 | 2.61 | 74 | 12 | 9.98 | 36.6 | 1.71 | 0.70 | 0.18 | 7.50 | -3.17 | 683 | 683 | 3.44 | |
| 03-A034 | 27.08.2003 | 08:50 | 506 | 1.4 | 5.3 | 7.32 | 22.3 | 1306 | 925 | 69.7 | 0.07 | 31.0 | 181 | 201 | <1.7 | 7.8 | 42 | 100 | 1.90 | 54 | 8 | 5.55 | 13.3 | 0.87 | 0.56 | 0.15 | 7.45 | -3.28 | 527 | 527 | 4.38 | |
| 03-A037 | 26.09.2003 | 12:00 | 69.3 | 0.2 | -0.8 | 7.68 | 19.3 | 92 | 202 | 18.8 | 0.22 | 25.1 | 447 | 469 | 32.5 | 6.5 | 154 | 314 | 4.89 | 115 | 28 | 28.7 | 53.7 | 4.18 | 0.81 | 0.21 | 7.82 | -2.75 | 1765 | 539 | 3.04 | |
| 03-A043 | 27.11.2003 | 12:30 | 31.9 | 0.2 | -1.9 | 7.68 | 19.3 | 92 | 202 | 18.8 | 0.22 | 25.1 | 447 | 469 | 32.5 | 6.5 | 154 | 314 | 4.89 | 115 | 28 | 28.7 | 53.7 | 4.18 | 0.81 | 0.21 | 7.82 | -3.27 | 539 | 539 | 4.02 | |
| Average | | | 116 | 1.9 | 2.2 | 7.71 | 22.0 | 329 | 309 | 29.5 | 0.38 | 25.8 | 455 | 477 | 17.2 | 4.3 | 111 | 140 | 257 | 4.46 | 112 | 30 | 22.1 | 43.6 | 3.51 | 0.69 | 0.13 | 7.81 | -3.30 | 554 | 499 | 0.29 |
| Median | | | 69.3 | 1.3 | 3.4 | 7.64 | 22.0 | 243 | 215 | 24.7 | 0.17 | 21.3 | 330 | 355 | 17.2 | 4.3 | 111 | 189 | 3.67 | 87 | 26 | 14.8 | 46.5 | 2.37 | 0.70 | 0.08 | 7.79 | -3.28 | 522 | 512 | -0.27 | |

Table A4. Lagartijot at Lagarfoss 1998-2003

| Sample number | Date | Time | Discharge m ³ /s | T _{water} °C | T _{air} °C | pH | T _{ref} °C | SIM | POC µg/kg | PON µg/kg | POC % wt. mole | C/N | Alk µeq/kg | DIC | DOC µM | DOC % mol | SiO ₂ µM | Na | K | Ca | Mg | SO ₄ | Cl | F | Al | Fe | pH _{in-situ} | log(pCO _{2w}) | pCO _{2w} µatm | CO _{2aq} µM | charge balance % |
|---------------|------------|-------|--------------------------------|--------------------------|------------------------|------|------------------------|------|--------------|--------------|-------------------|------|---------------|------|-----------|--------------|------------------------|------|------|------|------|-----------------|------|------|------|------|-----------------------|-------------------------|---------------------------|-------------------------|---------------------|
| 98-A005 | 19.11.1998 | 17:00 | 58.8 | 0.3 | 4.1 | 7.42 | 17.7 | 36 | 291 | 0.80 | 0.80 | 439 | 481 | 35.3 | 6.5 | 160 | 159 | 6.21 | 133 | 69.1 | 21.5 | 75.2 | 1.87 | 0.21 | 0.17 | 7.53 | -3.25 | 564 | 40 | 0.48 | |
| 99-A002 | 12.01.1999 | 17:30 | 40.3 | 0.0 | -0.8 | 7.36 | 15.2 | 19 | 137 | 8.7 | 0.72 | 37.0 | 465 | 518 | 33.3 | 6.0 | 172 | 166 | 6.09 | 143 | 80.2 | 21.7 | 84.2 | 2.03 | 0.14 | 0.20 | 7.45 | -3.15 | 710 | 50 | 1.49 |
| 99-A010 | 01.03.1999 | 17:45 | 28.1 | 0.0 | -0.2 | | 20.2 | 23 | | | | 501 | 609 | 33.3 | 5.2 | 183 | 177 | 6.74 | 160 | 81.7 | 25.2 | 98.3 | 1.92 | 0.22 | 0.21 | 7.17 | -2.84 | 102 | 30 | 1.94 | |
| 99-A017 | 12.04.1999 | 18:15 | 32.5 | 0.1 | -4.6 | 7.61 | 17.7 | 14 | 182 | 22.9 | 1.28 | 18.5 | 511 | 543 | 33.3 | 5.8 | 174 | 172 | 7.05 | 160 | 91.8 | 25.0 | 102 | 2.14 | 0.16 | 0.20 | 7.72 | -3.38 | 420 | 30 | 1.33 |
| 99-A028 | 10.05.1999 | 22:30 | 216 | 2.2 | 1.4 | 7.51 | 22.5 | 16 | 290 | 26.6 | 1.78 | 25.4 | 460 | 493 | 41.7 | 7.8 | 159 | 144 | 6.94 | 139 | 75.3 | 20.4 | 80.6 | 1.64 | 0.19 | 0.17 | 7.64 | -3.33 | 468 | 31 | -0.20 |
| 99-A031 | 10.06.1999 | 16:15 | 310 | 8.8 | 19.4 | 7.55 | 23.4 | 14 | 204 | 24.4 | 1.43 | 19.5 | 398 | 424 | 25.0 | 5.6 | 153 | 135 | 5.91 | 135 | 67.1 | 19.2 | 64.6 | 1.85 | 0.17 | 0.08 | 7.64 | -3.35 | 447 | 24 | 4.11 |
| 99-A038 | 19.07.1999 | 16:00 | 289 | 9.4 | 10.1 | 7.46 | 20.5 | 16 | 242 | 24.4 | 1.48 | 21.7 | 376 | 407 | 25.0 | 5.8 | 135 | 104 | 6.09 | 112 | 57.6 | 16.6 | 45.7 | 1.89 | 0.41 | 0.19 | 7.53 | -3.26 | 554 | 29 | -1.32 |
| 99-A043 | 23.08.1999 | 12:10 | 59.0 | 11.2 | 21.0 | 7.57 | 20.8 | 29 | 462 | 68.3 | 1.56 | 15.8 | 400 | 425 | 33.3 | 7.3 | 131 | 109 | 5.61 | 117 | 58.0 | 18.4 | 50.4 | 1.91 | 0.22 | 0.08 | 7.63 | -3.32 | 480 | 24 | -2.60 |
| 99-A055 | 29.09.1999 | 15:40 | 58.0 | 5.6 | 5.0 | 7.53 | 21.2 | 34 | 338 | 28.2 | 0.98 | 28.0 | 391 | 418 | 25.0 | 5.6 | 142 | 114 | 5.44 | 126 | 57.2 | 19.6 | 51.1 | 2.06 | 0.22 | 0.08 | 7.63 | -3.37 | 430 | 26 | -0.02 |
| 99-A057 | 03.11.1999 | 11:30 | 57.7 | 2.0 | 1.7 | 7.43 | 19.2 | 44 | 375 | 23.0 | 0.84 | 38.0 | 405 | 441 | 25.0 | 5.4 | 155 | 147 | 5.60 | 130 | 61.3 | 20.1 | 68.1 | 1.87 | 0.31 | 0.21 | 7.54 | -3.29 | 518 | 34 | 2.03 |
| 99-A067 | 09.12.1999 | 14:00 | 27.9 | 0.5 | -1.5 | 7.31 | 19.4 | 28 | 324 | 40.2 | 1.14 | 38.8 | 470 | 526 | 25.0 | 4.5 | 162 | 151 | 5.75 | 147 | 70.4 | 23.1 | 64.2 | 2.05 | 0.15 | 0.05 | 7.42 | -3.11 | 774 | 54 | 0.40 |
| 00-A001 | 04.01.2000 | 21:05 | 30.7 | 0.1 | -1.6 | 7.31 | 18.6 | 27.5 | 511 | 35.1 | 1.82 | 34.0 | 501 | 561 | 16.7 | 2.9 | 165 | 148 | 6.35 | 147 | 72.0 | 25.1 | 75.8 | 2.45 | 0.13 | 0.08 | 7.40 | -3.07 | 845 | 60 | -2.92 |
| 00-A009 | 02.03.2000 | 12:00 | 28.7 | 0.0 | -3.0 | 7.35 | 19.1 | 23.5 | 96 | <1.5 | | 471 | 522 | 25.0 | 4.6 | 162 | 149 | 6.26 | 146 | 62.6 | 14.9 | 73.3 | 2.23 | 0.13 | 0.07 | 7.46 | -3.16 | 698 | 49 | -0.98 | |
| 00-A022 | 10.04.2000 | 19:00 | 128 | 0.0 | -0.2 | 7.42 | 21.9 | 14.1 | 523 | 41.9 | 3.56 | 29.1 | 418 | 455 | 33.3 | 6.8 | 141 | 139 | 7.02 | 125 | 72.0 | 20.2 | 98.1 | 2.47 | 0.15 | 0.23 | 7.56 | -3.30 | 496 | 35 | -1.93 |
| 00-A027 | 08.05.2000 | 10:30 | 244 | 5.2 | 13.2 | 7.70 | 22.6 | 27.4 | 765 | 53.5 | 2.71 | 33.4 | 452 | 473 | 25.0 | 5.0 | 140 | 136 | 6.30 | 127 | 67.5 | 20.4 | 90.0 | 1.58 | 0.30 | 0.08 | 7.82 | -3.50 | 317 | 19 | -4.88 |
| 00-A036 | 06.06.2000 | 16:00 | 106 | 9.7 | 14.0 | 7.74 | 23.8 | 33.1 | 310 | 30.0 | 0.93 | 24.1 | 428 | 446 | 25.0 | 5.3 | 134 | 124 | 5.85 | 125 | 64.2 | 20.1 | 70.0 | 1.82 | 0.27 | 0.05 | 7.84 | -3.51 | 309 | 16 | -3.19 |
| 00-A045 | 11.07.2000 | 11:50 | 142 | 10.3 | 13.0 | 7.47 | 21.4 | 27.7 | 212 | 30.5 | 0.76 | 16.2 | 376 | 406 | 25.0 | 5.8 | 117 | 116 | 4.42 | 117 | 53.9 | 18.4 | 53.9 | 1.79 | 0.29 | 0.05 | 7.54 | -3.26 | 549 | 28 | 1.25 |
| 00-A054 | 08.08.2000 | 11:30 | 53.4 | 12.0 | 16.3 | 7.64 | 21.9 | 9 | 341 | 38.6 | 3.64 | 20.6 | 398 | 419 | 33.3 | 7.4 | 114 | 118 | 4.89 | 123 | 54.3 | 19.1 | 52.8 | 1.53 | 0.32 | 0.05 | 7.71 | -3.39 | 407 | 20 | -1.03 |
| 00-A063 | 13.09.2000 | 10:45 | 56.6 | 8.4 | 12.6 | 7.58 | 20 | 29.2 | 132 | 22.1 | 0.45 | 14.0 | 374 | 398 | 25.0 | 5.9 | 117 | 117 | 3.52 | 115 | 56.0 | 20.5 | 61.1 | 1.61 | 0.22 | 0.04 | 7.66 | -3.39 | 406 | 22 | -1.36 |
| 00-A072 | 16.10.2000 | 10:15 | 58.1 | 3.9 | 9.4 | 7.62 | 22.6 | 34.2 | 319 | 30.0 | 0.93 | 24.1 | 428 | 446 | 25.0 | 5.3 | 134 | 124 | 5.85 | 125 | 64.2 | 20.1 | 70.0 | 1.82 | 0.27 | 0.05 | 7.84 | -3.48 | 329 | 21 | -1.35 |
| 00-A081 | 20.11.2000 | 11:30 | 55.8 | 0.3 | 1.9 | 7.62 | 20.7 | 18.8 | 182 | 30.5 | 0.96 | 13.9 | 434 | 459 | 35.8 | 7.2 | 154 | 147 | 5.61 | 134 | 67.5 | 22.3 | 83.6 | 1.53 | 0.17 | 0.10 | 7.73 | -3.46 | 347 | 24 | -0.85 |
| 01-A001 | 05.01.2001 | 11:00 | 55.8 | 0.0 | -2.0 | 7.56 | 19.5 | 18.8 | 148 | 26.3 | 0.78 | 13.2 | 477 | 509 | 26.7 | 5.0 | 175 | 151 | 6.11 | 145 | 75.7 | 23.0 | 86.5 | 2.21 | 0.25 | 0.12 | 7.68 | -3.37 | 424 | 30 | -1.57 |
| 01-A010 | 02.03.2001 | 11:30 | 12.0 | 0.0 | -3.5 | 7.55 | 21.7 | - | 202 | 34.8 | | 13.5 | 482 | 513 | 40.0 | 7.2 | 173 | 149 | 6.01 | 141 | 79.4 | 23.3 | 101 | 1.71 | 0.18 | 0.12 | 7.68 | -3.37 | 427 | 30 | -3.35 |
| 01-A022 | 07.04.2001 | 08:45 | 60.0 | 0.0 | 1.5 | 7.59 | 24 | 24 | 168 | 17.2 | 0.70 | 22.8 | 504 | 533 | 24.2 | 4.3 | 170 | 187 | 6.69 | 159 | 86.0 | 23.9 | 127 | 2.08 | 0.13 | 0.07 | 7.73 | -3.40 | 396 | 28 | 0.43 |
| 01-A029 | 10.05.2001 | 08:00 | 146 | 6.5 | 13.0 | 7.62 | 23.3 | 13 | 223 | 26.4 | 1.69 | 19.7 | 407 | 434 | 40.0 | 8.5 | 157 | 165 | 6.39 | 141 | 74.5 | 19.0 | 131 | 1.76 | 0.27 | 0.28 | 7.72 | -3.44 | 365 | 21 | 2.31 |
| 01-A036 | 26.06.2001 | 09:30 | 378 | 8.2 | 14.8 | 7.58 | 21.3 | 24 | 190 | 20.9 | 0.78 | 21.1 | 373 | 396 | 23.3 | 5.6 | 142 | 126 | 4.25 | 118 | 60.5 | 18.3 | 83.2 | 1.37 | 0.25 | 0.19 | 7.67 | -3.40 | 394 | 22 | -0.77 |
| 01-A043 | 16.08.2001 | 11:15 | 205 | 9.2 | 13.4 | 7.71 | 22.1 | 28 | 222 | 18.7 | 0.79 | 27.8 | 380 | 397 | 20.8 | 5.0 | 133 | 121 | 4.41 | 121 | 58.4 | 19.2 | 66.8 | 1.39 | 0.20 | 0.06 | 7.80 | -3.52 | 300 | 16 | -0.09 |
| 01-A050 | 09.10.2001 | 08:50 | 149 | 5.8 | 7.4 | 7.61 | 19.1 | 38 | 155 | 21.0 | 0.41 | 17.3 | 379 | 402 | 37.5 | 8.5 | 146 | 130 | 4.80 | 123 | 59.7 | 18.3 | 71.3 | 1.34 | 0.26 | 0.11 | 7.70 | -3.45 | 357 | 21 | 1.06 |
| 01-A057 | 11.12.2001 | 09:30 | 285 | 0.0 | 7.8 | 7.57 | 22.1 | 35 | 226 | 33.0 | 0.64 | 16.0 | 476 | 506 | 14.2 | 2.7 | 154 | 140 | 4.94 | 148 | 70.0 | 22.1 | 82.9 | 1.74 | 0.12 | 0.07 | 7.69 | -3.49 | 416 | 29 | -1.63 |
| 02-A003 | 18.03.2002 | 16:00 | 29.5 | 0.0 | -4.0 | 7.37 | 23.2 | 70 | 141 | 18.1 | 0.20 | 18.1 | 511 | 562 | 29.1 | 4.9 | 181 | 152 | 5.16 | 163 | 82.3 | 24.7 | 104 | 1.82 | 0.10 | 0.08 | 7.51 | -3.17 | 670 | 47 | -0.78 |
| 02-A009 | 22.04.2002 | 15:00 | 377 | 3.7 | 5.9 | 7.47 | 24.2 | 17 | 197 | 23.8 | 1.15 | 19.4 | 370 | 398 | 30.8 | 7.2 | 151 | 127 | 4.85 | 129 | 63.8 | 21.2 | 99.0 | 1.50 | 0.13 | 0.16 | 7.58 | -3.35 | 445 | 28 | 1.15 |
| 02-A015 | 04.06.2002 | 12:20 | 412 | 0.0 | 7.2 | 7.38 | 17.2 | 36 | 207 | 25.6 | 0.97 | 18.9 | 368 | 392 | 24.1 | 5.8 | 139 | 123 | 4.50 | 118 | 57.2 | 18.6 | 76.4 | 1.47 | 0.17 | 0.18 | 7.63 | -3.36 | 433 | 23 | 0.15 |
| 02-A021 | 25.06.2002 | 13:40 | 216 | 8.8 | 8.1 | 7.56 | 25.8 | 17 | 251 | 33.1 | 1.45 | 17.7 | 378 | 401 | 25.0 | 5.9 | 138 | 120 | 4.40 | 118 | 56.8 | 17.5 | 69.2 | 1.58 | 0.19 | 0.10 | 7.66 | -3.38 | 412 | 22 | -0.35 |
| 02-A027 | 13.08.2002 | 14:45 | 92.3 | 9.8 | 10.4 | 7.64 | 21.2 | 22 | 272 | 25.2 | 1.22 | 25.2 | 389 | 411 | 62.4 | 13.2 | 126 | 110 | 4.23 | 121 | 53.5 | 18.1 | 58.4 | 1.63 | 0.23 | 0.07 | 7.72 | -3.42 | 376 | 20 | -1.73 |
| 02-A033 | 18.09.2002 | 15:15 | 90.6 | 9.4 | 8.5 | 7.60 | 21 | 24 | 426 | 42.8 | 1.74 | 23.2 | 394 | 418 | 32.5 | 7.2 | 131 | 116 | 4.32 | 126 | 53.5 | 19.7 | 56.5 | 1.63 | 0.24 | 0.07 | 7.68 | -3.38 | 415 | 22 | -0.47 |
| 02-A039 | 22.10.2002 | 16:50 | 53.9 | 2.8 | 1.0 | 7.28 | 20.8 | 88 | 577 | 60.5 | 0.65 | 22.3 | 413 | 464 | 23.3 | 4.8 | 141 | 122 | 4.37 | 136 | 55.1 | 20.2 | 62.2 | 1.63 | 0.16 | 0.07 | 7.39 | -3.12 | 767 | 50 | 0.10 |
| 03-A006 | 21.01.2003 | 16:40 | 34.9 | 0.0 | -7.2 | 7.38 | 17.2 | 36 | 207 | 25.6 | 0.97 | 18.9 | 368 | 392 | 24.1 | 5.8 | 139 | 123 | 4.50 | 118 | 57.2 | 18.6 | 76.4 | 1.47 | 0.17 | 0.18 | 7.63 | -3.36 | 433 | 23 | 0.15 |
| 03-A009 | 14.04.2003 | 16:25 | 102 | 3.6 | 3.9 | 7.64 | 22.6 | 25 | 259 | 29.6 | 1.02 | 20.4 | 390 | 411 | 25.8 | 5.9 | 147 | 125 | 4.29 | 135 | 60.1 | 21.6 | 72.2 | 1.76 | 0.15 | 0.11 | 7.47 | -3.20 | 635 | 45 | -3.22 |
| 03-A015 | 20.05.2003 | 16:30 | 106 | 4.0 | 6.2 | 7.52 | 18.2 | 29 | 403 | 36.4 | 1.37 | 25.9 | 402 | 432 | 40.8 | 8.6 | 142 | 128 | 4.42 | 128 | 58.4 | 18.6 | 89.9 | 1.74 | 0.20 | 0.07 | 7.61 | -3.35 | 451 | 28 | -2.00 |
| 03-A021 | 19.06.2003 | 16:05 | 181 | 8.4 | 8.2 | 7.46 | 24.6 | 17 | 305 | 38.6 | 1.76 | 24.6 | 379 | 409 | 27.5 | 6.3 | 132 | 137 | 3.82 | 124 | 59.2 | 18.8 | 72.2 | 1.58 | 0.31 | 0.10 | 7.56 | -3.29 | 511 | 28 | 1.89 |
| 03-A027 | 19.07.2003 | 14:15 | 123 | 13.2 | 16.1 | 7.56 | 22.7 | 26 | 277 | 36.0 | 1.05 | 17.9 | 407 | 433 | 23.3 | 5.1 | 135 | 135 | 4.08 | 127 | 56.0 | 18.9 | 65.2 | 1.66 | 0.53 | 0.20 | 7.61 | -3.28 | 530 | 25 | -0.27 |
| 03-A036 | 27.08.2003 | 13:20 | 123 | 9.2 | 11.4 | 7.38 | 22.5 | 32 | 313 | <1.5 | | 397 | 435 | 16.7 | 3.7 | 139 | 132 | | | | | | | | | | | | | | |

Table A5. Lagarfljót at Lagarfoss Dam 28 November 2007 - 10 December 2013

| Sample number | Date | Time | Discharge m ³ /s | T _{water} °C | T _{air} °C | pH | T _{ref} °C | SIM mg/l | POC µg/kg | PON µg/kg | POC % wt. mole | C/N | Alk µeq/kg | DIC µM | DOC µM | DOC % mol | SiO ₂ µM | Na µM | K µM | Ca µM | Mg µM | SO ₄ µM | Cl µM | F µM | Al µM | Fe µM | pH _{ln-stu} | log(pCO _{2(aq)}) | pCO _{2(aq)} µatm | CO _{2(aq)} µM | charge balance % |
|---------------|------------|-------|-----------------------------|-----------------------|---------------------|------|---------------------|----------|-----------|-----------|----------------|------|------------|--------|--------|-----------|---------------------|-------|------|-------|-------|--------------------|-------|------|-------|-------|----------------------|----------------------------|---------------------------|------------------------|------------------|
| 07A006 | 28.11.2007 | 17:40 | 108 | 0.1 | 0.8 | 7.45 | 20.6 | 58 | 452 | 60.2 | 0.78 | 17.5 | 545 | 592 | 32.5 | 5.2 | 177 | 160 | 10.1 | 186 | 71.2 | 138 | 53.4 | 6.25 | 0.37 | 0.24 | 7.58 | -3.21 | 611 | 43 | 1.95 |
| 08A008 | 21.05.2008 | 17:00 | 354 | 6.2 | 7.0 | 7.53 | 22.0 | 116 | 309 | 43.6 | 0.27 | 16.6 | 442 | 473 | 26.6 | 5.3 | 154 | 148 | 7.5 | 147 | 55.5 | 20.2 | 72.8 | 1.83 | 0.25 | 0.24 | 7.62 | -3.30 | 506 | 30 | 0.25 |
| 08A018 | 29.08.2008 | 13:45 | 195 | 10.5 | 10.5 | 6.7 | 23.7 | 100 | 444 | 63.6 | 0.44 | 16.3 | 399 | 419 | 22.5 | 5.1 | 131 | 148 | 7.0 | 141 | 44.0 | 17.3 | 45.9 | 1.86 | 0.88 | 0.33 | 7.75 | -3.44 | 361 | 19 | 4.15 |
| 09A005 | 04.02.2009 | 18:15 | 159 | 0.0 | 4.3 | 7.41 | 19.8 | 122 | 134 | 32.8 | 0.11 | 24.4 | 433 | 433 | 101.6 | 19.0 | 147 | 167 | <10 | 146 | 51.0 | 16.7 | 72.5 | 1.83 | 0.25 | 0.10 | 7.52 | -3.25 | 559 | 40 | 0.86 |
| 09A006 | 02.04.2009 | 14:45 | 130 | 0.1 | 0.7 | 7.41 | 19.8 | 122 | 134 | 32.8 | 0.11 | 24.4 | 433 | 433 | 101.6 | 19.0 | 147 | 167 | <10 | 146 | 49.0 | 14.9 | 58.1 | 1.47 | 0.24 | 0.24 | 7.60 | -3.33 | 468 | 33 | 1.86 |
| 09A012 | 02.06.2009 | 17:30 | 413 | 7.0 | 7.5 | 7.46 | 18.8 | 102 | 312 | 34.8 | 0.30 | 20.9 | 350 | 350 | 44.1 | 11.2 | 131 | 130 | 4.9 | 111 | 40.0 | 12.1 | 52.6 | 1.22 | 0.64 | 0.48 | 7.52 | -3.30 | 506 | 29 | 0.77 |
| 09A016 | 29.06.2009 | 19:00 | 346 | 10.1 | 17.0 | 7.45 | 22.3 | 78 | 287 | 45.9 | 0.37 | 14.6 | 345 | 345 | 25.0 | 6.8 | 128 | 127 | 5.0 | 109 | 37.9 | 11.6 | 45.6 | 1.30 | 1.32 | 0.81 | 7.51 | -3.28 | 530 | 28 | 1.66 |
| 09A023 | 11.08.2009 | 19:25 | 363 | 13.2 | 11.7 | 7.58 | 20.8 | 87 | 267 | 23.5 | 0.31 | 26.5 | 360 | 360 | 19.1 | 5.1 | 158 | 127 | 4.9 | 113 | 41.1 | 14.3 | 41.5 | 1.38 | 1.04 | 0.50 | 7.61 | -3.34 | 460 | 22 | 1.20 |
| 09A035 | 23.09.2009 | 18:15 | 148 | 7.4 | 7.71 | 7.17 | 13.4 | 362 | 211 | 11.0 | 0.27 | 40.0 | 405 | 405 | 15.0 | 3.6 | 142 | 139 | 5.0 | 131 | 44.0 | 14.1 | 41.3 | 1.47 | 1.93 | 1.27 | 7.81 | -3.53 | 296 | 17 | 2.01 |
| 09A040 | 04.11.2009 | 11:35 | 266 | 4.2 | 5.2 | 7.49 | 20.2 | 107 | 445 | 60.0 | 0.41 | 17.3 | 398 | 398 | 54.1 | 12.0 | 139 | 140 | 5.0 | 132 | 47.3 | 14.2 | 47.2 | 1.34 | 0.46 | 0.22 | 7.58 | -3.31 | 485 | 30 | 2.06 |
| 09A045 | 02.03.2010 | 21:45 | 180 | 0.0 | -6.2 | 7.62 | 21.9 | 125 | 566 | 63.8 | 0.45 | 20.7 | 454 | 453 | 80.8 | 15.1 | 153 | 160 | 5.8 | 146 | 52.7 | 16.7 | 58.3 | 1.29 | 0.36 | 0.19 | 7.75 | -3.46 | 344 | 24 | 1.28 |
| 10A009 | 14.04.2010 | 15:10 | 269 | 3.6 | 11.0 | 7.49 | 21.6 | 140 | 651 | 29.6 | 0.46 | 51.3 | 461 | 461 | 70.8 | 13.3 | 152 | 165 | 5.4 | 135 | 49.8 | 15.6 | 78.4 | 1.18 | 0.38 | 0.06 | 7.58 | -3.26 | 544 | 34 | -3.34 |
| 10A011 | 26.05.2010 | 21:30 | 148 | 3.5 | 3.0 | 7.34 | 22.0 | 112 | 456 | 78.4 | 0.40 | 13.6 | 394 | 394 | 47.5 | 9.6 | 151 | 135 | 4.8 | 134 | 47.3 | 18.6 | 46.0 | 1.15 | 0.96 | 0.53 | 7.72 | -3.18 | 465 | 42 | 0.97 |
| 10A016 | 13.07.2010 | 21:00 | 236 | 9.0 | 9.1 | 7.28 | 23.4 | 93 | 425 | 53.5 | 0.45 | 18.6 | 370 | 370 | 54.1 | 12.8 | 137 | 140 | 5.1 | 122 | 40.1 | 14.5 | 43.2 | 1.17 | 0.35 | 0.06 | 7.36 | -3.09 | 809 | 43 | 2.75 |
| 10A025 | 24.08.2010 | 19:40 | 263 | 8.6 | 6.9 | 7.66 | 23.3 | 112 | 261 | 17.6 | 0.23 | 34.5 | 385 | 384 | 41.6 | 9.8 | 131 | 142 | 4.4 | 126 | 39.3 | 14.1 | 42.3 | 1.23 | 0.77 | 0.36 | 7.74 | -3.46 | 345 | 19 | 1.74 |
| 10A030 | 13.10.2010 | 21:20 | 180 | 6.4 | 6.5 | 7.64 | 20.1 | 121 | 274 | 20 | 0.23 | 32.1 | 411 | 410 | 76.6 | 15.7 | 150 | 151 | 4.8 | 130 | 49.4 | 16.4 | 82.8 | 2.05 | 1.01 | 0.91 | 7.78 | -3.44 | 362 | 21 | 6.07 |
| 10A039 | 02.11.2010 | 18:15 | 155 | 2.0 | 2.3 | 7.49 | 22.3 | 167 | 876 | 143 | 0.52 | 14.3 | 424 | 423 | 66.6 | 13.6 | 154 | 167 | 5.4 | 142 | 55.5 | 17.3 | 92.3 | 1.10 | 1.42 | 1.20 | 7.62 | -3.35 | 443 | 29 | 5.17 |
| 10A044 | 08.12.2010 | 18:40 | 181 | 0.0 | -8.4 | 7.53 | 21.1 | 129 | 287 | 31.9 | 0.22 | 21.0 | 423 | 422 | 18.3 | 4.2 | 142 | 143 | 4.5 | 139 | 48.1 | 17.2 | 53.5 | 1.19 | 0.27 | 0.10 | 7.67 | -3.41 | 389 | 28 | 4.55 |
| 11A005 | 08.03.2011 | 17:35 | 185 | 0.1 | -3.1 | 7.64 | 20.6 | 113 | 448 | 56.8 | 0.39 | 18.4 | 411 | 410 | 76.6 | 15.7 | 150 | 151 | 4.8 | 130 | 49.4 | 16.4 | 82.8 | 2.05 | 1.01 | 0.91 | 7.78 | -3.53 | 293 | 21 | -0.84 |
| 11A010 | 28.04.2011 | 17:45 | 182 | 4.2 | 8.0 | 7.51 | 21.7 | 119 | 330 | 58.3 | 0.28 | 13.2 | 368 | 367 | 51.6 | 12.3 | 142 | 142 | 4.6 | 120 | 41.6 | 15.0 | 65.1 | 2.02 | 0.58 | 0.35 | 7.61 | -3.38 | 417 | 26 | 0.82 |
| 11A014 | 16.05.2011 | 15:45 | 296 | 5.5 | 9.4 | 7.55 | 19.9 | 103 | 364 | 51.2 | 0.35 | 16.6 | 364 | 363 | 55.8 | 13.3 | 140 | 140 | 4.8 | 116 | 41.6 | 14.4 | 69.9 | 1.95 | 1.07 | 0.79 | 7.65 | -3.42 | 384 | 23 | 0.25 |
| 11A022 | 28.07.2011 | 16:30 | 226 | 6.7 | 8.3 | 7.59 | 20.6 | 89 | 2460 | 72.0 | 2.70 | 79.7 | 359 | 358 | 64.9 | 15.4 | 138 | 124 | 5.1 | 105 | 39.0 | 15.5 | 48.3 | 2.05 | 0.73 | 0.23 | 7.60 | -3.34 | 462 | 23 | -2.47 |
| 11A023 | 14.09.2011 | 19:15 | 183 | 6.5 | 4.9 | 7.66 | 22.5 | 74 | 450 | 54.7 | 0.60 | 19.2 | 386 | 386 | 62.4 | 13.9 | 143 | 133 | 4.9 | 115 | 41.6 | 15.5 | 49.7 | 2.13 | 1.32 | 0.93 | 7.78 | -3.52 | 305 | 18 | -1.40 |
| 11A032 | 01.11.2011 | 12:25 | 292 | 4.2 | 4.2 | 7.67 | 19.8 | 63 | 431 | 47.4 | 0.68 | 21.2 | 398 | 397 | 51.6 | 11.5 | 156 | 140 | 3.3 | 132 | 51.4 | 16.8 | 57.1 | 2.15 | 0.35 | 0.09 | 7.75 | -3.49 | 322 | 20 | 1.60 |
| 11A038 | 07.12.2011 | 17:45 | 166 | 0.1 | -9.7 | 7.53 | 20.9 | 78 | 249 | 15.5 | 0.32 | 37.4 | 416 | 415 | 35.8 | 7.9 | 153 | 139 | 0.0 | 138 | 51.0 | 18.5 | 49.8 | 2.22 | 0.22 | 0.03 | 7.67 | -3.41 | 385 | 27 | 1.10 |
| 12A003 | 08.03.2012 | 13:10 | 90 | 0.1 | 1.9 | 7.63 | 18.3 | 79 | 401 | 39.0 | 0.50 | 24.0 | 375 | 375 | 242.3 | 39.3 | 155 | 373 | 3.7 | 108 | 63.4 | 15.3 | 62.3 | 1.80 | 0.35 | 0.24 | 7.71 | -3.51 | 309 | 22 | 19.0 |
| 12A006 | 17.04.2012 | 12:00 | 198 | 1.8 | 1.7 | 7.56 | 21.9 | 138 | 530 | 69.3 | 0.38 | 17.8 | 398 | 397 | 59.9 | 13.1 | 150 | 152 | 3.4 | 135 | 48.5 | 15.8 | 52.5 | 1.87 | 0.68 | 0.59 | 7.67 | -3.43 | 371 | 25 | 4.07 |
| 12A010 | 06.06.2012 | 16:20 | 247 | 5.6 | 4.8 | 7.57 | 20.1 | 94 | 572 | 55.6 | 0.60 | 24.0 | 386 | 386 | 29.1 | 7.0 | 143 | 144 | 3.5 | 128 | 47.7 | 15.4 | 48.4 | 1.85 | 0.80 | 0.52 | 7.66 | -3.40 | 396 | 24 | 3.65 |
| 12A014 | 04.07.2012 | 12:30 | 207 | 11.1 | 18.5 | 7.74 | 22.1 | 91 | 311 | 32.3 | 0.34 | 22.5 | 361 | 360 | 46.6 | 11.5 | 135 | 143 | 4.2 | 123 | 42.4 | 15.5 | 42.0 | 1.96 | 1.06 | 0.51 | 7.80 | -3.54 | 287 | 14 | 4.83 |
| 12A024 | 06.09.2012 | 09:20 | 164 | 6.2 | 7.8 | 7.51 | 20.5 | 120 | 271 | 26.9 | 0.23 | 23.5 | 384 | 384 | 21.6 | 5.3 | 126 | 138 | 3.6 | 127 | 36.7 | 16.1 | 32.6 | 1.58 | 0.45 | 0.05 | 7.59 | -3.33 | 464 | 27 | 1.93 |
| 12A028 | 25.09.2012 | 15:45 | 294 | 9.4 | 7.52 | 20.2 | 95 | 280 | 25.3 | 0.29 | 25.7 | 79.7 | 403 | 403 | 25.0 | 5.8 | 130 | 131 | 4.0 | 108 | 35.1 | 15.2 | 39.0 | 1.36 | 0.30 | 0.09 | 7.60 | -3.33 | 469 | 28 | -5.49 |
| 12A032 | 30.10.2012 | 16:05 | 134 | 0.8 | -8.0 | 7.48 | 20.7 | 128 | 412 | 412 | 22.5 | 5.2 | 396 | 412 | 22.5 | 5.2 | 139 | 147 | 3.7 | 146 | 44.8 | 18.7 | 38.7 | 1.56 | 0.53 | 0.30 | 7.59 | -3.34 | 453 | 31 | 3.85 |
| 12A034 | 05.12.2012 | 12:15 | 135 | 0.1 | -6.1 | 7.46 | 20.0 | 90 | 435 | 435 | 39.1 | 8.3 | 435 | 435 | 39.1 | 8.3 | 145 | 167 | 4.3 | 155 | 56.4 | 19.7 | 60.1 | 1.57 | 0.20 | 0.08 | 7.58 | -3.31 | 490 | 35 | 4.63 |
| 13A004 | 18.03.2013 | 17:30 | 182 | 0.0 | -2.5 | 7.53 | 21.1 | 92 | 327 | 34.0 | 0.35 | 22.5 | 416 | 416 | 52.5 | 11.0 | 138 | 158 | 4.6 | 121 | 47.3 | 15.6 | 62.8 | 1.35 | 0.37 | 0.29 | 7.66 | -3.41 | 387 | 27 | -1.50 |
| 13A006 | 23.04.2013 | 12:00 | 139 | 2.9 | 3.5 | 7.50 | 19.2 | 110 | 475 | 41.9 | 0.43 | 26.4 | 417 | 416 | 17.5 | 4.0 | 126 | 153 | 4.9 | 116 | 42.4 | 14.9 | 54.5 | 1.37 | 0.44 | 0.30 | 7.60 | -3.32 | 475 | 31 | -3.04 |
| 13A010 | 28.05.2013 | 12:00 | 348 | 5.6 | 9.8 | 7.39 | 19.5 | 74 | 689 | 31.8 | 0.93 | 50.5 | 404 | 404 | 20.5 | 5.8 | 141 | 157 | 5.3 | 113 | 49.0 | 15.0 | 80.5 | 1.31 | 0.51 | 0.41 | 7.47 | -3.19 | 641 | 38 | -3.00 |
| 13A014 | 02.07.2013 | 12:15 | 338 | 7.9 | 16.0 | 7.49 | 19.5 | 67 | 461 | 50.1 | 0.69 | 21.5 | 344 | 344 | <8 | 2.3 | 127 | 131 | 4.6 | 97 | 41.1 | 12.5 | 52.2 | 1.19 | 0.80 | 0.55 | 7.56 | -3.34 | 458 | 25 | -1.36 |
| 13A018 | 18.07.2013 | 12:40 | 294 | 10.4 | 17.8 | 7.38 | 21.7 | 55 | 825 | 49.0 | 1.48 | 39.3 | 423 | 423 | 62.7 | 12.9 | 130 | 143 | 5.5 | 95 | 42.8 | 13.2 | 45.8 | 1.19 | 0.67 | 0.33 | 7.45 | -3.11 | 771 | 40 | -8.05 |
| 13A022 | 09.09.2013 | 12:15 | 180 | 3.9 | 7.75 | 20.9 | 85 | 719 | 72.6 | 0.84 | 23.1 | 365 | 364 | 46.2 | 11.3 | 124 | 139 | 5.0 | 106 | 39.4 | 14.6 | 39.0 | 1.31 | 1.85 | 1.34 | 7.88 | -3.64 | 229 | 13 | 0.42 | |
| 13A030 | 24.10.2013 | 12:10 | 160 | 3.9 | 3.5 | 7.50 | 20.5 | 120 | 291 | 25.8 | 0.24 | 26.3 | 380 | 379 | 36.4 | 8.8 | 130 | 154 | 4.8 | 115 | 43.6 | 14.5 | 45.6 | 1.28 | 0.72 | 0.47 | 7.60 | -3.36 | 435 | 27 | 1.93 |
| 13A034 | 10.12.2013 | 13:15 | 153 | -0.1 | -2.8 | 7.38 | 20.5 | 107 | 396 | 395 | 34.2 | 8.0 | 396 | 395 | 34.2 | 8.0 | 135 | 165 | 4.8 | 119 | 46.1 | 15.7 | 45.3 | 1.31 | 0.59 | 0.38 | 7.51 | -3.28 | 525 | 37 | 2.38 |
| Average | | | 223 | 4.5 | 4.9 | 7.54 | 21.1 | 103 | 473 | 45.8 | 0.50 | 25.7 | 401 | 403 | 48.4 | 10.3</ | | | | | | | | | | | | | | | |

Table A6. Hälslösn reservoir 19 June 2008 - 10 September 2013

| Sample number | Date | Time | Depth | Discharge | T _{water} | T _{air} | pH | T _{ref} | SIM* | POC | PON | POC | C/N | Alk | DIC | DOC | DOC | SiO ₂ | Na | K | Ca | Mg | SO ₄ | Cl | F | Al | Fe | pH _{11-stu} | log(pCO _{2w}) | pCO _{2w} | CO _{2-req} | charge balance |
|----------------|------------|------------|-------------|-------------------|--------------------|------------------|-------------|------------------|-------------|------------|------------|-------------|------------|-----------|------------|------------|-------------|------------------|-------------|-------------|-------------|-------------|-----------------|-------------|-------------|--------------|------------|----------------------|-------------------------|-------------------|---------------------|----------------|
| | | | m | m ³ /s | °C | °C | | °C | mg/l | µg/kg | µg/kg | % wt. | mole | µeq./kg | µM | % mol | µM | µM | µM | µM | µM | µM | µM | µM | µM | µM | µM | | µatm | µM | % | |
| 08A001 | 19.05.2008 | 15:00 | 18 | N/A | 0.2 | 5.0 | 7.46 | 22.9 | 52.9 | 389 | 59.8 | 0.73 | 15 | 334 | 361 | 23.3 | 6.1 | 110 | 137 | 4.9 | 99.6 | 20.4 | 12.4 | 28.7 | 1.83 | 0.73 | 0.42 | 7.60 | -3.44 | 361 | 25 | -0.21 |
| 08A002 | 19.05.2008 | 15:30 | 40 | N/A | 0.2 | 5.0 | 7.48 | 23.0 | 52.4 | 322 | 346 | 15.0 | 4.1 | 322 | 346 | 15.0 | 4.1 | 105 | 132 | 5.2 | 99.3 | 18.2 | 12.4 | 28.8 | 1.79 | 0.49 | 0.16 | 7.61 | -3.47 | 337 | 24 | -0.30 |
| 08A009 | 27.08.2008 | 13:00 | 70 | N/A | 3.5 | 7.79 | 22.3 | 328 | 1193 | 101 | 28 | 235 | 244 | 8.3 | 3.3 | 77 | 130 | 5.7 | 76.6 | 12.1 | 11.5 | 32.5 | 1.37 | 2.76 | 0.29 | 7.98 | -3.97 | 107 | 7 | 5.46 | | |
| 08A010 | 27.08.2008 | 15:00 | 130 | N/A | 2.7 | 7.41 | 22.4 | 328 | 258 | 281 | 14.2 | 4.8 | 258 | 281 | 14.2 | 4.8 | 82 | 124 | 5.5 | 82.8 | 13.8 | 11.3 | 30.7 | 1.44 | 0.85 | 0.08 | 7.54 | -3.47 | 335 | 22 | 2.45 | |
| 08A011 | 27.08.2008 | 16:00 | 20 | N/A | 5.6 | 7.37 | 22.3 | 328 | 257 | 283 | 17.5 | 5.8 | 257 | 283 | 17.5 | 5.8 | 82 | 124 | 5.5 | 81.3 | 14.6 | 11.3 | 30.6 | 1.46 | 1.37 | 0.47 | 7.47 | -3.39 | 405 | 24 | 2.80 | |
| 08A012 | 27.08.2008 | 16:30 | 40 | N/A | 5.5 | 7.63 | 22.8 | 328 | 263 | 277 | 16.7 | 5.7 | 263 | 277 | 16.7 | 5.7 | 83 | 124 | 3.6 | 81.8 | 13.8 | 11.0 | 30.7 | 1.47 | 1.50 | 0.55 | 7.75 | -3.67 | 216 | 13 | 1.60 | |
| 09A021 | 11.08.2009 | 12:00 | 5 | N/A | 7.1 | 8.0 | 7.83 | 20.9 | 191 | 355 | <22.9 | 0.18 | 36 | 281 | 280 | 19.1 | 6.4 | 94 | 130 | 3.7 | 85.6 | 18.1 | 8.43 | 28.0 | 1.32 | 3.39 | 2.44 | 7.97 | -3.86 | 138 | 8 | 3.54 |
| 09A031 | 22.09.2009 | 16:15 | 5 | N/A | 0.4 | 4.6 | 7.63 | 21.5 | 181 | 279 | <25.0 | 0.15 | 26 | 270 | 269 | <8 | 2.9 | 85 | 124 | 3.4 | 80.3 | 13.4 | 7.97 | 23.5 | 1.19 | 1.11 | 0.45 | 7.74 | -3.68 | 209 | 15 | 0.55 |
| 10A026 | 25.08.2010 | 11:00 | 5 | N/A | 3.5 | 3.3 | 8.25 | 23.0 | 245 | 357 | <22.8 | 0.15 | 37 | 215 | 214 | 46.6 | 17.9 | 65 | 105 | 2.3 | 63.9 | 8.1 | 5.77 | 13.4 | 0.61 | 2.24 | 0.06 | 8.49 | -4.53 | 30 | 2 | 3.36 |
| 11A024 | 15.09.2011 | 12:09 | 20 | N/A | 3.6 | 8.4 | 7.89 | 22.9 | 179 | 406 | <34.4 | 0.23 | 28 | 259 | 259 | 50.0 | 16.2 | 79 | 120 | 3.7 | 74.6 | 12.3 | 8.33 | 25.2 | 1.81 | 2.36 | 0.83 | 8.08 | -4.02 | 95 | 6 | -0.01 |
| 11A025 | 15.09.2011 | 13:33 | 40 | N/A | 3.5 | 8.4 | 7.76 | 22.9 | 261 | 258 | 257 | 60.8 | 19.1 | 258 | 257 | 60.8 | 19.1 | 82 | 122 | 3.3 | 74.6 | 11.9 | 8.44 | 25.4 | 1.83 | 1.72 | 0.38 | 7.89 | -3.84 | 146 | 9 | -0.19 |
| 11A026 | 15.09.2011 | 13:48 | 80 | N/A | 3.2 | 8.4 | 8.00 | 22.0 | 204 | 450 | <36.5 | 0.22 | 29 | 263 | 263 | 64.9 | 19.8 | 81 | 122 | 3.5 | 73.6 | 11.6 | 8.09 | 24.5 | 1.79 | 2.47 | 0.41 | 8.17 | -4.12 | 77 | 5 | -0.12 |
| 11A027 | 15.09.2011 | 14:10 | 130 | N/A | 2.8 | 8.4 | 8.82 | 22.0 | 560 | 633 | 62.4 | 224 | 224 | 224 | 224 | 17.5 | 7.2 | 66 | 109 | 2.1 | 69.6 | 10.0 | 7.07 | 15.0 | 1.01 | 1.52 | 0.04 | 7.65 | -3.64 | 228 | 14 | 3.48 |
| 12A017 | 04.09.2012 | 17:35 | 93 | N/A | | | 7.50 | 20.7 | 289 | 226 | 226 | 19.1 | 7.8 | 226 | 226 | 19.1 | 7.8 | 68 | 112 | 2.7 | 70.9 | 9.7 | 6.73 | 15.0 | 0.98 | 2.36 | 0.30 | 7.97 | -3.97 | 106 | 7 | 4.68 |
| 12A018 | 04.09.2012 | 18:25 | 158 | N/A | 2.9 | 7.81 | 20.7 | 486 | 222 | 221 | 19.1 | 8.0 | 69 | 109 | 29 | 72.1 | 10.0 | 64.2 | 14.2 | 0.95 | 1.26 | 0.14 | 7.90 | 7.43 | 0.09 | 7.43 | -3.90 | 125 | 8 | 5.17 | | |
| 12A019 | 04.09.2012 | 18:55 | 149 | N/A | 3.3 | 7.77 | 20.1 | 267 | 231 | 231 | 25.8 | 10.0 | 83 | 111 | 20 | 76.1 | 10.7 | 6.94 | 14.8 | 0.98 | 0.46 | 0.09 | 7.43 | 0.09 | 7.43 | -3.41 | 388 | 25 | 4.50 | | | |
| 12A020 | 04.09.2012 | 19:45 | 37 | N/A | 3.6 | 7.35 | 20.1 | 267 | 231 | 231 | 25.8 | 10.0 | 83 | 111 | 20 | 76.1 | 10.7 | 6.94 | 14.8 | 0.98 | 0.46 | 0.09 | 7.43 | 0.09 | 7.43 | -3.41 | 388 | 25 | 4.50 | | | |
| 13A025 | 10.09.2013 | 12:42 | 40 | N/A | | | 11.0 | 7.66 | 20.6 | 372 | 43.3 | 0.18 | 20 | 237 | 237 | 32.6 | 12.1 | 71 | 128 | 3.3 | 63.9 | 11.3 | 6.66 | 18.4 | 1.00 | 2.33 | 1.43 | 7.85 | -3.83 | 149 | 9 | 2.78 |
| 13A026 | 10.09.2013 | 12:54 | 80 | N/A | | | 11.0 | 7.79 | 20.0 | 594 | 27.7 | 0.17 | 50 | 246 | 246 | 32.5 | 11.7 | 75 | 141 | 3.2 | 66.6 | 10.3 | 6.33 | 18.7 | 1.01 | 2.54 | 0.49 | 7.96 | -3.92 | 119 | 8 | 3.92 |
| 13A027 | 10.09.2013 | 13:08 | 120 | N/A | | | 11.0 | 7.98 | 20.2 | 685 | 61.5 | 0.18 | 26 | 254 | 254 | 30.7 | 10.8 | 76 | 150 | 3.1 | 67.6 | 9.9 | 6.13 | 17.3 | 0.95 | 3.49 | 0.74 | 8.19 | -4.15 | 71 | 5 | 5.20 |
| 13A028 | 10.09.2013 | 13:25 | 160 | N/A | | | 11.0 | 8.70 | 20.5 | 595 | 1303 | 109 | 0.22 | 28 | 258 | 255 | 32.7 | 11.4 | 76 | 139 | 3.1 | 64.9 | 9.9 | 5.82 | 16.0 | 0.92 | 6.89 | -4.97 | 11 | 1 | 4.38 | |
| Average | 3.2 | 8.0 | 7.80 | 21.6 | 290 | 585 | 50.5 | 0.24 | 29.2 | 258 | 263 | 29.2 | 9.9 | 81 | 125 | 3.6 | 76.7 | 12.6 | 8.50 | 22.8 | 1.32 | 2.48 | 0.89 | 0.89 | 7.96 | -3.92 | 174 | 11 | 2.81 | | | |
| Median | 3.4 | 8.4 | 7.77 | 22.0 | 278 | 428 | 39.9 | 0.18 | 27.6 | 258 | 257 | 25.3 | 8.0 | 81 | 124 | 3.4 | 74.6 | 11.9 | 8.09 | 24.5 | 1.32 | 2.24 | 0.42 | 0.42 | 7.90 | -3.86 | 138 | 8 | 3.36 | | | |

Table A7. Outlet from Kárahjúkar Power Plant 28.11.2007-10.12.2013

| Sample number | Date | Time | Discharge m ³ /s | T _{water} °C | T _{air} °C | pH | T _{ref} °C | SIM mg/l | POC µg/kg | PON µg/kg | POC %wt. | C/N | Alk µeq/kg | DIC µM | DOC µM | DOC %mol | SiO ₂ µM | Na µM | K µM | Ca µM | Mg µM | SO ₄ µM | Cl µM | F µM | Al µM | Fe µM | pH _{in-situ} | log(pCO _{2w}) µatm | pCO _{2w} µatm | CO _{2aq} µM | charge balance % | |
|---------------|------------|-------|-----------------------------|-----------------------|---------------------|------|---------------------|----------|-----------|-----------|----------|------|------------|--------|--------|----------|---------------------|-------|------|-------|-------|--------------------|-------|-------|-------|-------|-----------------------|------------------------------|------------------------|----------------------|------------------|-----|
| 07A005 | 28.11.2007 | 13:40 | 54.8 | 1.4 | -0.4 | 7.79 | 20.5 | 242 | 789 | 71.3 | 0.33 | 25.8 | 348 | 362 | 15.8 | 4.2 | 99 | 154 | 6.7 | 101 | 18.4 | 25.6 | 71.6 | 2.33 | 0.89 | 0.16 | 7.95 | -3.77 | 170 | 12 | -5.6 | |
| 08A006 | 20.05.2008 | 17:20 | 121 | 0.7 | 7.3 | 7.43 | 22.8 | 190 | 115 | 16.5 | 0.06 | 16.2 | 345 | 375 | 10.8 | 2.8 | 117 | 147 | 5.6 | 100 | 20.8 | 13.0 | 29.1 | 1.89 | 0.84 | 0.43 | 7.56 | -3.39 | 411 | 28 | -0.7 | |
| 08A015 | 28.08.2008 | 17:30 | 118 | 3.7 | 11.5 | 8.08 | 22.4 | 317 | 377 | 37.7 | 0.12 | 23.3 | 258 | 263 | 20.8 | 7.3 | 80 | 141 | 4.1 | 76 | 13.5 | 12.1 | 34.1 | 1.62 | 2.44 | 0.15 | 8.26 | -4.21 | 62 | 4 | 2.3 | |
| 09A003 | 04.02.2009 | 14:00 | 114 | 0.4 | -6.1 | 7.63 | 19.3 | 203 | 206 | 25.3 | 0.10 | 18.9 | 327 | 326 | 57.4 | 63.7 | 96 | 144 | <10 | 98 | 17.3 | 10.0 | 26.4 | 1.67 | 0.54 | 0.32 | 7.73 | -3.58 | 264 | 18 | -0.5 | |
| 09A008 | 03.04.2009 | 09:30 | 104 | 0.6 | 1.9 | 7.64 | 22.1 | 529 | 308 | 44.4 | 0.06 | 16.2 | 334 | 334 | 59.1 | 15.0 | 152 | 154 | 3.5 | 104 | 20.2 | 10.5 | 27.4 | 1.39 | 0.89 | 0.52 | 7.77 | -3.62 | 242 | 17 | 2.0 | |
| 09A013 | 03.06.2009 | 08:25 | 119 | 1.5 | 11.3 | 7.68 | 19.8 | 116 | 298 | 30.5 | 0.26 | 22.8 | 394 | 393 | 46.6 | 10.6 | 101 | 138 | 4.0 | 136 | 25.8 | 19.0 | 36.3 | 1.72 | 0.59 | 0.29 | 7.80 | -3.56 | 274 | 19 | -0.9 | |
| 09A018 | 30.06.2009 | 11:50 | 123 | 5.5 | 15.0 | 7.94 | 21.8 | 186 | 397 | 34.4 | 0.21 | 26.9 | 407 | 406 | 25.8 | 6.0 | 108 | 141 | 4.3 | 140 | 24.9 | 15.2 | 29.5 | 1.87 | 2.49 | 1.31 | 8.06 | -3.79 | 163 | 10 | 0.8 | |
| 09A025 | 09.08.2009 | 12:45 | 112 | 4.9 | 15.2 | 8.89 | 20.9 | 683 | 617 | 22.3 | 0.09 | 64.5 | 370 | 364 | 84.1 | 18.8 | 105 | 131 | 4.0 | 133 | 27.7 | 17.9 | 22.5 | 1.34 | 4.71 | 2.17 | 9.10 | -4.94 | 11 | 1 | 1.8 | |
| 09A030 | 22.09.2009 | 13:45 | 122 | 6.3 | 3.6 | 8.90 | 21.6 | 479 | 364 | 23.4 | 0.08 | 36.3 | 316 | 309 | <8 | 2.5 | 89 | 149 | 3.6 | 95 | 12.8 | 11.4 | 23.1 | 1.26 | 3.40 | 0.67 | 9.11 | -5.01 | 10 | 1 | 1.4 | |
| 09A036 | 03.11.2009 | 13:35 | 104 | 1.4 | 2.9 | 8.11 | 20.5 | 307 | 608 | 82.1 | 0.20 | 17.3 | 408 | 406 | 35.0 | 7.9 | 115 | 157 | 3.6 | 147 | 24.3 | 23.3 | 25.3 | 1.85 | 5.00 | 3.51 | 8.33 | -4.10 | 79 | 5 | 3.1 | |
| 09A041 | 02.03.2010 | 11:30 | 109 | 1.1 | -1.0 | 7.66 | 22.1 | 219 | 408 | 67.6 | 0.19 | 14.1 | 350 | 349 | 40.0 | 10.3 | 149 | 3.9 | 111 | 22.1 | 19.3 | 26.1 | 1.53 | 0.36 | 0.10 | 7.77 | -3.59 | 260 | 18 | 0.9 | | |
| 10A001 | 02.03.2010 | 12:00 | 128 | 0.9 | -13.1 | 7.55 | 22.5 | 230 | 436 | 41.6 | 0.19 | 24.4 | 344 | 344 | 74.9 | 17.9 | 108 | 157 | 3.8 | 108 | 20.2 | 12.0 | 26.4 | 1.37 | 0.43 | 0.11 | 7.67 | -3.49 | 323 | 22 | 1.8 | |
| 10A006 | 14.04.2010 | 10:15 | 116 | 1.0 | 9.8 | 7.19 | 21.4 | 196 | 1405 | 97.2 | 0.71 | 33.7 | 375 | 375 | 76.6 | 17.0 | 110 | 161 | 5.8 | 120 | 20.2 | 19.0 | 32.9 | 1.71 | 0.54 | 0.02 | 7.30 | -3.09 | 814 | 56 | 0.6 | |
| 10A013 | 27.05.2010 | 11:50 | 112 | 1.1 | 6.7 | 7.53 | 21.5 | 225 | 423 | 57.3 | 0.19 | 17.2 | 392 | 391 | 30.8 | 7.3 | 110 | 167 | 3.9 | 135 | 26.4 | 19.8 | 32.7 | 1.75 | 0.53 | 0.16 | 7.63 | -3.40 | 395 | 27 | 2.3 | |
| 10A019 | 14.07.2010 | 14:00 | 120 | 4.2 | 16.9 | 8.26 | 22.9 | 261 | 408 | 40.8 | 0.16 | 23.3 | 338 | 336 | 13.3 | 3.8 | 100 | 161 | 4.7 | 106 | 17.7 | 13.5 | 24.9 | 1.31 | 2.66 | 0.92 | 8.46 | -4.30 | 50 | 3 | 3.5 | |
| 10A022 | 24.08.2010 | 14:25 | 110 | 3.3 | 8.0 | 8.03 | 23.3 | 267 | 393 | 22.1 | 0.15 | 41.5 | 220 | 220 | 56.6 | 20.5 | 63 | 112 | 2.8 | 62 | 8.4 | 6.3 | 13.7 | 0.79 | 3.05 | 0.13 | 8.26 | -4.29 | 52 | 3 | 2.0 | |
| 10A032 | 13.10.2010 | 13:40 | 107 | 3.2 | 12.3 | 8.26 | 19.8 | 390 | 304 | 31 | 0.08 | 23.0 | 312 | 311 | 0 | 0.0 | 84 | 134 | 3.0 | 104 | 14.5 | 17.0 | 16.8 | 0.88 | 2.45 | 0.30 | 8.43 | -4.30 | 50 | 3 | 7.1 | |
| 10A036 | 02.11.2010 | 13:00 | 115 | 2.3 | 1.4 | 7.83 | 22.2 | 225 | 444 | 58.7 | 0.20 | 17.6 | 290 | 290 | 45.8 | 13.6 | 85 | 124 | 3.1 | 88 | 15.2 | 10.5 | 16.8 | 0.91 | 1.71 | 0.66 | 7.98 | -3.88 | 132 | 9 | 4.7 | |
| 10A041 | 08.12.2010 | 13:30 | 127 | 1.2 | -5.8 | 7.70 | 20.9 | 214 | 235 | 23.9 | 0.11 | 23.0 | 299 | 299 | 226 | 43.1 | 89 | 133 | 3.4 | 92 | 16.4 | 9.6 | 19.3 | 0.86 | 0.97 | 0.42 | 7.86 | -3.75 | 179 | 12 | 5.3 | |
| 11A001 | 08.03.2011 | 10:20 | 129 | 0.7 | -3.8 | 7.79 | 18.6 | 183 | 270 | 65.2 | 0.15 | 9.7 | 335 | 334 | 75.8 | 18.5 | 96 | 135 | 3.5 | 102 | 17.6 | 14.0 | 25.2 | 1.84 | 0.97 | 0.56 | 7.90 | -3.74 | 180 | 12 | -0.9 | |
| 11A006 | 28.04.2011 | 10:30 | 124 | 1.0 | 9.8 | 7.79 | 21.6 | 150 | 332 | 62.7 | 0.22 | 12.3 | 357 | 356 | 41.6 | 10.5 | 106 | 149 | 3.8 | 116 | 22.5 | 17.7 | 31.9 | 2.26 | 0.52 | 0.15 | 7.90 | -3.71 | 193 | 13 | 0.4 | |
| 11A011 | 16.05.2011 | 10:00 | 121 | 1.9 | 10.0 | 7.64 | 20.0 | 143 | 324 | 73.0 | 0.23 | 10.3 | 382 | 382 | 54.9 | 12.6 | 116 | 150 | 4.0 | 132 | 24.6 | 20.9 | 33.8 | 2.40 | 0.85 | 0.40 | 7.75 | -3.53 | 298 | 20 | 0.5 | |
| 11A015 | 23.06.2011 | 10:30 | 116 | 2.9 | 10.9 | 7.82 | 20.8 | 144 | 341 | 59.2 | 0.24 | 13.5 | 414 | 413 | 31.6 | 7.1 | 126 | 169 | 4.7 | 128 | 27.9 | 21.0 | 31.3 | 2.66 | 0.99 | 0.38 | 7.92 | -3.66 | 220 | 14 | 0.0 | |
| 11A020 | 28.07.2011 | 13:15 | 96.5 | 5.5 | 18.6 | 8.00 | 23.4 | 453 | 366 | 395 | 0.50 | 11.2 | 74 | 116 | 34 | 143 | 20.6 | 19.8 | 21.6 | 20.7 | 2.20 | 0.37 | 8.19 | -3.93 | 116 | 7 | -0.3 | 116 | 7 | -0.3 | | |
| 11A029 | 16.09.2011 | 09:10 | 109 | 4.0 | 13.3 | 7.83 | 22.0 | 209 | 310 | 44.3 | 0.15 | 16.3 | 269 | 268 | 64.1 | 19.3 | 84 | 136 | 3.7 | 75 | 13.6 | 9.4 | 30.7 | 1.93 | 2.02 | 0.52 | 7.95 | -3.88 | 133 | 8 | 0.4 | |
| 11A033 | 01.11.2011 | 17:00 | 106 | 2.2 | 2.4 | 7.62 | 19.8 | 170 | 343 | 31.6 | 0.20 | 25.3 | 303 | 303 | 31.6 | 9.5 | 96 | 135 | 3.6 | 105 | 19.7 | 14.6 | 27.0 | 2.10 | 0.69 | 0.28 | 7.73 | -3.60 | 250 | 16 | 2.8 | |
| 11A035 | 07.12.2011 | 10:10 | 116 | 1.1 | -6.0 | 7.49 | 21.2 | 139 | 295 | 14.3 | 0.21 | 48.2 | 311 | 311 | 15.0 | 4.6 | 102 | 140 | 3.4 | 104 | 21.7 | 17.3 | 28.0 | 2.18 | 0.44 | 0.15 | 7.58 | -3.45 | 352 | 24 | 1.7 | |
| 12A001 | 08.03.2012 | 09:50 | 119 | 1.0 | -0.4 | 7.81 | 20.1 | 123 | 613 | 59.7 | 0.50 | 24.0 | 327 | 327 | 84.1 | 20.5 | 103 | 150 | 2.4 | 113 | 21.5 | 15.3 | 33.0 | 1.83 | 0.71 | 0.35 | 7.90 | -3.75 | 176 | 12 | 3.5 | |
| 12A011 | 17.04.2012 | 14:30 | 115 | 1.1 | 1.5 | 7.62 | 21.8 | 138 | 353 | 35.7 | 0.26 | 23.0 | 325 | 324 | 51.6 | 13.7 | 110 | 153 | 2.7 | 109 | 21.8 | 13.8 | 28.9 | 1.87 | 0.79 | 0.43 | 7.74 | -3.59 | 258 | 18 | 4.3 | |
| 12A015 | 06.06.2012 | 18:40 | 118 | 3.8 | 18.5 | 8.52 | 21.9 | 274 | 366 | 31.8 | 0.13 | 26.8 | 293 | 289 | 38.3 | 11.7 | 100 | 165 | 2.2 | 92 | 15.8 | 12.5 | 23.3 | 1.90 | 2.73 | 0.69 | 8.75 | -4.66 | 22 | 1 | 5.8 | |
| 12A021 | 05.09.2012 | 13:00 | 117 | 3.8 | 12.7 | 7.52 | 20.2 | 233 | 775 | 126 | 0.33 | 14.4 | 239 | 239 | 133.3 | 5.3 | 72 | 121 | 2.5 | 71.5 | 7.8 | 18.9 | 11.4 | 2.84 | 0.52 | 7.65 | -3.63 | 234 | 15 | 3.9 | | |
| 12A025 | 25.09.2012 | 10:15 | 111 | 3.4 | 4.8 | 7.50 | 20.8 | 237 | 207 | 18.2 | 0.09 | 26.5 | 260 | 259 | 12.5 | 4.6 | 77 | 125 | 2.1 | 78 | 12.9 | 5.4 | 19.9 | 1.18 | 1.16 | 0.72 | 7.63 | -3.56 | 278 | 18 | 2.7 | |
| 12A029 | 30.10.2012 | 10:00 | 104 | 2.3 | -2.1 | 7.33 | 21.3 | 180 | 294 | 294 | 0.23 | 26.5 | 284 | 294 | 18.3 | 5.9 | 90 | 125 | 2.2 | 99 | 18.7 | 14.7 | 17.2 | 1.37 | 0.37 | 0.11 | 7.44 | -3.32 | 474 | 31 | 2.6 | |
| 12A036 | 05.12.2012 | 10:00 | 107 | -3.3 | 7.38 | 20.0 | 139 | 298 | 297 | 32.5 | 9.8 | 89 | 134 | 2.4 | 102 | 20.4 | 102 | 20.4 | 102 | 20.4 | 102 | 20.4 | 102 | 20.4 | 102 | 20.4 | 0.06 | 7.46 | -3.33 | 463 | 30 | 4.7 |
| 13A001 | 18.03.2013 | 10:40 | 124 | 0.5 | -2.5 | 7.23 | 21.0 | 149 | 438 | 27.9 | 0.29 | 36.7 | 325 | 325 | 37.5 | 10.3 | 103 | 143 | 3.5 | 94 | 21.5 | 13.8 | 25.4 | 1.25 | 2.36 | 2.01 | 7.37 | -3.23 | 589 | 41 | 0.2 | |
| 13A007 | 23.04.2013 | 14:10 | 128 | 0.7 | 3.6 | 7.47 | 19.4 | 139 | 638 | 34.4 | 0.46 | 43.3 | 340 | 339 | <8 | 2.3 | 98 | 153 | 3.6 | 88 | 18.7 | 10.9 | 19.8 | 1.49 | 0.31 | 0.12 | 7.58 | -3.41 | 386 | 27 | -2.1 | |
| 13A011 | 28.05.2013 | 13:45 | 104 | 0.9 | 10.0 | 7.47 | 19.5 | 170 | 435 | 34.2 | 0.26 | 29.6 | 446 | 446 | <8 | 1.8 | 110 | 174 | 4.4 | 139 | 30.0 | 29.4 | 33.5 | 1.73 | 0.73 | 0.32 | 7.59 | -3.30 | 499 | 34 | -2.2 | |
| 13A015 | 02.07.2013 | 15:15 | 121 | 3.9 | 15.4 | 7.65 | 20.1 | 167 | 648 | 52.9 | 0.39 | 28.6 | 349 | 349 | <8 | 2.2 | 102 | 136 | 4.0 | 108 | 25.8 | 16.9 | 33.6 | 1.45 | 0.75 | 0.28 | 7.76 | -3.56 | 276 | 17 | -1.3 | |
| 13A019 | 18.07.2013 | 15:30 | 127 | 5.5 | 12.6 | 7.53 | 21.5 | 285 | 1427 | 103 | 0.50 | 32.5 | 388 | 388 | 48.4 | 11.1 | 87 | 140 | 3.9 | 108 | 21.7 | 15.5 | 27.9 | 1.38 | 1.50 | 0.45 | 7.64 | -3.38 | 413 | 25 | -5.2 | |
| 13A023 | 09.09.2013 | 15:15 | 110 | 5.3 | 13.7 | 7.74 | 20.6 | 203 | 307 | 26.5 | 0.15 | 27.0 | 250 | 249 | 29.2 | 10.5 | 74 | 136 | 3.3 | 66 | 11.7 | 7.0 | 18.9 | 1.08 | 1.84 | 0.96 | 7.90 | -3.84 | 145 | 9 | 2.0 | |
| 13A031 | 24.10.2013 | 14:45 | 126 | 3.0 | 3.4 | 7.40 | 20.5 | 213 | 336 | 33.4 | 0.16 | 23.5 | 268 | 268 | 29.7 | 10.0 | 82 | 148 | 3.4 | 74 | 14.1 | 9.8 | 19.1 | 1.19 | 0.72 | 0.17 | 7.50 | -3.42 | 378 | 24 | 2.5 | |
| 13A036 | 10.12.2013 | 16:50 | 126 | 1.2 | -5.2 | 7.41 | 20.5 | 161 | 291 | 291 | 25.4 | 8.3 | 97 | 143 | <10 | 8.9 | 18.4 | <10 | 8.9 | 18.4 | <10 | 20.3 | 1.31 | 0.52 | | | | | | | | |

Table A8. Wind speed and temperature data accompanying Figure 3

| Karahnjukar weather station | | | | | | | | | | | | | |
|-----------------------------|--------|-------|-------|-------|------|------|------|------|------|------|-------|-------|-------|
| Temperature | Month | 1 | 2 | 3 | 4 | 5 | 6 | 7 | 8 | 9 | 10 | 11 | 12 |
| | min | -18.4 | -20.9 | -18.5 | -16 | -8.2 | -4 | -0.6 | -1.1 | -6.6 | -12.6 | -15.3 | -20.8 |
| | q25 | -7.3 | -8.7 | -7.9 | -6 | -1.2 | 2.8 | 5.7 | 4.5 | 0.8 | -4.1 | -6.2 | -9.6 |
| | median | -3.2 | -3.9 | -4.4 | -2.7 | 1.2 | 5.1 | 7.8 | 6.8 | 4 | -1 | -3.1 | -5.9 |
| | q75 | 0.1 | -0.5 | -0.8 | 0.4 | 3.5 | 7.7 | 10.5 | 8.9 | 6.8 | 1.7 | 0.2 | -2.1 |
| | max | 7 | 7.1 | 7.7 | 9.2 | 10.5 | 15 | 17.6 | 15.4 | 15.5 | 10.4 | 8.3 | 6.5 |
| Windspeed | Month | 1 | 2 | 3 | 4 | 5 | 6 | 7 | 8 | 9 | 10 | 11 | 12 |
| | min | 0.0 | 0.0 | 0.0 | 0.0 | 0.0 | 0.0 | 0.0 | 0.0 | 0.0 | 0.0 | 0.0 | 0.0 |
| | q25 | 4.2 | 3.3 | 4.1 | 3.3 | 3.1 | 2.1 | 2.6 | 3 | 3.3 | 3.3 | 3.5 | 3.8 |
| | median | 7.2 | 6.1 | 6.9 | 5.8 | 5.3 | 4.2 | 4.6 | 5 | 6 | 5.7 | 6.6 | 6.4 |
| | q75 | 11.2 | 10.1 | 10.4 | 8.9 | 8 | 6.5 | 6.9 | 7.2 | 9.3 | 8.9 | 9.7 | 9.7 |
| | max | 21.6 | 20 | 19.8 | 17.2 | 15.3 | 13 | 13.3 | 13.4 | 18.3 | 17.2 | 18.9 | 18.5 |
| Egilsstadir 1998-2003 | | | | | | | | | | | | | |
| Temperature | Month | 1 | 2 | 3 | 4 | 5 | 6 | 7 | 8 | 9 | 10 | 11 | 12 |
| | min | -15.4 | -16.6 | -15.7 | -12 | -6 | -1.8 | 0.5 | 0.6 | -1 | -8 | -12.4 | -14.6 |
| | q25 | -4.7 | -5.3 | -5 | -1.9 | 2.6 | 5.8 | 8.1 | 8.2 | 5.9 | 1 | -2.2 | -4 |
| | median | -0.7 | -1.7 | -1.5 | 1.3 | 5.2 | 8.1 | 10.3 | 10.5 | 8.1 | 4 | 1.6 | -0.2 |
| | q75 | 2.5 | 2.3 | 2.3 | 5.2 | 8.5 | 11.2 | 13.5 | 13.3 | 10.6 | 7 | 4.6 | 3.1 |
| | max | 13.2 | 10.1 | 13.2 | 15.8 | 17.3 | 19.3 | 21.4 | 20.9 | 17.6 | 15.6 | 14.4 | 11.8 |
| Windspeed | Month | 1 | 2 | 3 | 4 | 5 | 6 | 7 | 8 | 9 | 10 | 11 | 12 |
| | min | 0.0 | 0.0 | 0.0 | 0.0 | 0.0 | 0.0 | 0.0 | 0.0 | 0.0 | 0.0 | 0.0 | 0.0 |
| | q25 | 2.00 | 2.80 | 2.10 | 2.4 | 2.80 | 2.80 | 2.20 | 1.80 | 1.90 | 2.10 | 1.90 | 2.00 |
| | median | 4.30 | 5.30 | 4.30 | 4.7 | 4.80 | 4.90 | 4.20 | 3.60 | 3.60 | 4.20 | 3.80 | 4.10 |
| | q75 | 7.80 | 8.20 | 6.90 | 7.5 | 7.00 | 6.70 | 6.20 | 5.90 | 5.90 | 6.50 | 6.10 | 6.70 |
| | max | 16.5 | 16.3 | 14.1 | 15.1 | 13.1 | 12.3 | 11.8 | 11.8 | 11.9 | 12.9 | 12.4 | 13.7 |
| Egilstadir 2007-2013 | | | | | | | | | | | | | |
| Temperature | Month | 1 | 2 | 3 | 4 | 5 | 6 | 7 | 8 | 9 | 10 | 11 | 12 |
| | min | -18.4 | -20.9 | -18.5 | -16 | -8.2 | -4 | -0.6 | -1.1 | -6.6 | -12.6 | -15.3 | -20.8 |
| | q25 | -7.3 | -8.7 | -7.9 | -6 | -1.2 | 2.8 | 5.7 | 4.5 | 0.8 | -4.1 | -6.2 | -9.6 |
| | median | -3.2 | -3.9 | -4.4 | -2.7 | 1.2 | 5.1 | 7.8 | 6.8 | 4 | -1 | -3.1 | -5.9 |
| | q75 | 0.1 | -0.5 | -0.8 | 0.4 | 3.5 | 7.7 | 10.5 | 8.9 | 6.8 | 1.7 | 0.2 | -2.1 |
| | max | 7 | 7.1 | 7.7 | 9.2 | 10.5 | 15 | 17.6 | 15.4 | 15.5 | 10.4 | 8.3 | 6.5 |
| Windspeed | Month | 1 | 2 | 3 | 4 | 5 | 6 | 7 | 8 | 9 | 10 | 11 | 12 |
| | min | 0.0 | 0.0 | 0.0 | 0.0 | 0.0 | 0.0 | 0.0 | 0.0 | 0.0 | 0.0 | 0.0 | 0.0 |
| | q25 | 1.8 | 1.6 | 2.2 | 2.1 | 2.5 | 2.3 | 2.1 | 1.9 | 1.8 | 1.6 | 1.8 | 1.7 |
| | median | 4 | 3.6 | 4.4 | 4.2 | 4.6 | 4.4 | 4 | 3.8 | 3.8 | 3.3 | 3.9 | 3.7 |
| | q75 | 6.8 | 6.5 | 6.9 | 6.5 | 6.6 | 6.2 | 5.9 | 5.8 | 6.1 | 5.5 | 6.6 | 6.6 |
| | max | 14.3 | 13.8 | 13.9 | 13 | 12.7 | 12 | 11.5 | 11.6 | 12.5 | 11.3 | 13.7 | 13.9 |

Table A9: Average water level and surface area of the Háslón reservoir during ice-free months.

| Month | Water level (m a.s.l.) [m] | Surface area [km ²] |
|-----------|-------------------------------|------------------------------------|
| May | 580 | 17 |
| June | 585-595 | 24-29 |
| July | 595-615 | 29-45 |
| August | 615-625 | 45-58 |
| September | 625 | 58 |
| October | 625 | 58 |
| November | 623-625 | 54-58 |

Table A10: Observed ice-free periods of the Háslón reservoir.

| year | melted | frozen |
|------|---------|-----------|
| 2009 | 4. Jun | 30. Nov |
| 2010 | 11. Jun | 25. Nov |
| 2011 | 9. Jun | 21. Nov |
| 2012 | 1. Jun | 22. Nov |
| 2013 | 12. Jun | 17. Nov |
| 2014 | 8. Jun | 10. Dec |
| 2015 | 20. Jun | 28. Nov |
| 2016 | >3. Jun | > 21. Nov |
| 2017 | 20. May | 22. Nov |
| 2018 | 31. May | 26. Nov |
| 2019 | 18. May | 5. Nov |
| 2020 | 3. Jun | 22. Nov |
| 2021 | 13. Jun | 18. Nov |
| 2022 | 7. Jun | 5. Dec |
| 2023 | 24. May | 24. Nov |

Appendix E: Unpublished Material

Table ES1: Measured data from different surface water sampling spots

| Date | sample No | water T °C | pH | T lab °C | pH lab | cond µS | OZ % | EN(SHE) mV | Alkalinity meq/kg | ICP-OES Si as SiO2 mg/kg | ICP-OES Na mg/kg | ICP-OES K mg/kg | ICP-OES Ca mg/kg | ICP-OES Mg mg/kg | ICP-OES SO4 mg/kg | ICP-OES Cl mg/kg | titration H2S mg/kg | IC 2000 SO4 mg/kg | IC 2000 Cl mg/kg | IC 2000 F mg/kg |
|------------|-------------------|------------|------|----------|--------|---------|------|------------|-------------------|--------------------------|------------------|-----------------|------------------|------------------|-------------------|------------------|---------------------|-------------------|------------------|-----------------|
| 04.04.17 | S1 source | 4.4 | 6.69 | | | 265 | | | | 31.8 | 0.3 | 0.10 | 0.0 | 0.20 | 2.03 | 1.0 | | | | |
| | S2 | 4.7 | 6.83 | | | 255 | | | | 19.0 | 1.50 | 34.2 | 21.0 | | 1.27 | 11.7 | | | | |
| | S3 | 5.4 | 6.88 | | | 257 | | | | 31.4 | 19.9 | 1.67 | 37.0 | 23.1 | 1.13 | | | | | |
| | S4 Raude | 5.3 | 7.00 | | | 197 | | | | | | | | | | | | | | |
| | S5 | 5.4 | 6.99 | | 6.22 | 250 | | | 2.35 | | | | | | | | | | | |
| 03.05.17 | S6 puddle | 7.0 | 6.77 | | 7.52 | 417 | | | 1.72 | | | | | | | | | | | |
| | S11 river | 10.8 | 6.43 | | 7.52 | 209 | | | | 32.1 | 15.2 | 1.63 | 17.2 | 9.7 | 2.47 | 11.7 | | | | |
| | S12 | 9.9 | 6.32 | | 7.35 | 246 | | | 2.14 | 29.7 | 19.8 | 1.87 | 19.1 | 10.5 | 1.90 | 12.2 | | | | |
| | S13 | 9.2 | 6.47 | | 6.85 | 240 | | | 2.62 | 32.7 | 20.9 | 1.53 | 20.1 | 10.9 | 1.32 | 12.3 | | | | |
| | S14 source | 6.4 | 6.18 | | 6.52 | 325 | | | 2.99 | 37.0 | 12.3 | 1.77 | 17.7 | 15.0 | 6.25 | 12.5 | | | | |
| 09.05.17 | S21 river | 10.9 | 6.67 | | 7.76 | 225 | | | 2.26 | 32.9 | 16.8 | 1.70 | 15.6 | 10.8 | 2.72 | 2.37 | 2.37 | | | 0.19 |
| | S22 far from soil | 8.7 | 6.77 | | 7.07 | 302 | | | 2.78 | 32.7 | 21.8 | 1.59 | 22.6 | 12.3 | 1.16 | 1.02 | 1.02 | | | 0.19 |
| | S23 | 6.9 | 6.65 | | 6.65 | 338 | | | 2.72 | 35.2 | 22.1 | 1.58 | 22.5 | 12.4 | 0.88 | 0.88 | | | | |
| | S24 source | 7.8 | 6.52 | | 6.54 | 192 | | | 1.14 | 35.7 | 11.2 | 1.93 | 12.5 | 7.5 | 8.77 | 8.75 | | | | |
| | S31 river | 7.8 | 7.11 | | 7.68 | 224 | | | 2.28 | 30.7 | 16.8 | 1.63 | 21.2 | 11.4 | 2.74 | 11.1 | | | | |
| 04.06.17 | S32 | 9.1 | 6.71 | | 6.74 | 374 | | | 3.47 | 33.7 | 21.3 | 0.97 | 30.0 | 16.9 | 1.38 | 11.3 | | | | |
| | S33 | 6.8 | 6.53 | | 6.59 | 306 | | | 2.80 | 36.2 | 22.5 | 1.26 | 21.8 | 11.3 | 0.67 | 11.6 | | | | |
| | S34 source | 7.2 | 6.37 | | 6.32 | 282 | | | 2.42 | 30.8 | 14.1 | 0.60 | 17.1 | 10.0 | 0.62 | 10.1 | | | | |
| | S35 Raude | 13.6 | 7.78 | | 7.97 | 237 | | | 2.31 | 33.3 | 14.8 | 1.34 | 20.9 | 12.5 | 4.22 | 10.7 | | | | |
| | S41 source | 8.6 | 6.86 | | 6.32 | 270 | | | 2.45 | 38.8 | 14.6 | 0.69 | 16.7 | 10.3 | 0.39 | 10.3 | | | | |
| 18.12.1917 | S42 | 6.5 | 7.14 | | 6.46 | 340 | | | 2.88 | 36.3 | 22.9 | 1.52 | 22.8 | 11.7 | 0.61 | 12.1 | | | | |
| | S43 | 7.3 | 6.72 | | 6.59 | 343 | | | 2.83 | 36.6 | 23.3 | 1.52 | 22.3 | 12.2 | 1.14 | 12.6 | | | | |
| | S44 river | 9.5 | 6.87 | | 7.31 | 259 | | | 2.52 | 31.7 | 18.8 | 1.75 | 21.9 | 12.0 | 2.86 | 12.0 | | | | |
| | S52 | 2.9 | 7.20 | | 6.65 | 250 | | | 1.82 | 29.6 | 19.1 | 1.63 | 18.7 | 9.6 | 2.38 | 11.9 | | | | |
| | S51 source | 8.0 | 6.22 | | 21.6 | 638 | 169 | 67+5 | 1.02 | 28.4 | 11.3 | 1.68 | 11.5 | 6.9 | 8.98 | 13.5 | | | | |
| 23.05.1918 | S62 | 7.9 | 6.57 | | 21.6 | 660 | 255 | 53.9 | 2.31 | 28.9 | 19.4 | 1.40 | 19.0 | 8.6 | 1.85 | 12.6 | | | | |
| | S63 | 9.3 | 7.00 | | 21.6 | 703 | 237 | 78.8 | 2.11 | 24.1 | 23.0 | 1.42 | 21.8 | 11.3 | 1.27 | 12.1 | | | | |
| | S64 | 10.4 | 7.12 | | 21.6 | 734 | 188 | 83.2 | 3.91 | 17.7 | 27.8 | 1.39 | 19.5 | 8.6 | 2.41 | 12.4 | | | | |
| | S65 Raude | 10.9 | 7.50 | | 21.6 | 748 | 188 | 100.6 | 4.47 | 1.73 | 31.2 | 1.28 | 1.30 | 15.1 | 9.3 | 5.36 | 12.5 | | | |
| | S66 | 12.3 | 7.50 | | 21.6 | 763 | 185 | 92.0 | 4.23 | 1.28 | 24.7 | 1.36 | 1.40 | 11.9 | 7.3 | 3.89 | 15.3 | | | |
| 07.06.18 | S71 source | 10.1 | 6.15 | | 6.49 | 168 | | | 1.36 | 29.7 | 11.6 | 1.37 | 12.7 | 7.6 | 10.3 | 9.3 | | | | |
| | S72 | 6.9 | 6.56 | | 21.1 | 665 | 171 | 9-1 | 119 | 2.67 | 34.2 | 21.9 | 1.41 | 22.1 | 11.3 | 1.07 | 12.1 | | | |
| | S73 | 8.8 | 6.93 | | 21.1 | 705 | 286 | 76.1 | 138 | 2.69 | 29.9 | 21.3 | 1.42 | 21.8 | 11.3 | 1.27 | 12.1 | | | |
| | S74 | 9.0 | 7.43 | | 21.1 | 744 | 229 | 83.6 | 139 | 2.35 | 31.5 | 1.62 | 20.4 | 10.7 | 2.79 | 11.2 | 11.2 | | | |
| | S75 Raude | 12.4 | 7.92 | | 21.1 | 789 | 223 | 101.5 | 144 | 2.21 | 32.7 | 14.5 | 1.33 | 19.4 | 11.5 | 4.83 | 11.5 | | | |
| 20.06.18 | S76 | 13.9 | 7.22 | | 7.48 | 185 | | | 1.76 | 25.2 | 14.6 | 1.46 | 15.2 | 9.0 | 3.84 | 13.9 | | | | |
| | S81 source | 10.5 | 6.22 | | 22.3 | 624 | 185 | 23.1 | 259 | 1.71 | 28.9 | 11.9 | 0.39 | 12.3 | 7.7 | 4.70 | 4.70 | | | |
| | S82 | 6.5 | 6.54 | | 22.3 | 664 | 336 | 16.5 | 107 | 2.89 | 35.4 | 22.1 | 1.17 | 22.2 | 11.3 | 0.89 | 11.9 | | | |
| | S83 | 10.6 | 6.72 | | 22.3 | 700 | 272 | 67.2 | 111 | 2.69 | 31.3 | 2.22 | 1.17 | 22.5 | 11.2 | 0.96 | 11.2 | | | |
| | S84 | 11.6 | 7.17 | | 22.3 | 747 | 232 | 88.0 | 113 | 2.31 | 31.8 | 1.76 | 1.70 | 20.7 | 11.1 | 2.80 | 11.4 | | | |
| 13.06.18 | S85 Raude | 18.8 | 8.17 | | 22.3 | 803 | 223 | 98.2 | 438 | 2.26 | 32.3 | 1.52 | 1.32 | 20.3 | 12.1 | 4.20 | 11.3 | | | |
| | S86 | 16.0 | 7.97 | | 22.3 | 773 | 214 | 101.0 | 460 | 1.98 | 27.4 | 1.68 | 1.42 | 18.0 | 10.7 | 3.39 | 14.3 | | | |
| | S82 room 1 | 12.1 | 7.93 | | 22.5 | 817 | 244 | 102.0 | 306 | 2.46 | 29.8 | 1.44 | 21.3 | 11.5 | 4.38 | 10.8 | | | | |
| | S101 | 4.9 | 6.04 | | 22.3 | 632 | 152 | 75+5 | 3.24 | 0.93 | 24.2 | 12.9 | 6.32 | 7.3 | 4.8 | 17.2 | 17.2 | | | |
| | S102 | 6.1 | 6.41 | | 22.3 | 633 | 332 | 21.0 | 149 | 2.95 | 35.2 | 22.7 | 1.43 | 21.7 | 11.2 | 0.85 | 12.3 | | | |
| 28.10.18 | S103 | 6.9 | 6.53 | | 22.3 | 668 | 268 | 53.0 | 194 | 2.70 | 26.8 | 2.26 | 1.74 | 21.5 | 1.11 | 1.15 | 13.0 | | | |
| | S104 | 8.6 | 7.33 | | 22.3 | 744 | 244 | 100.0 | 10.0 | 2.53 | 32.1 | 1.79 | 1.82 | 21.8 | 11.9 | 2.89 | 11.6 | | | |
| | S111 source | 3.9 | 5.93 | | 6.46 | 181 | | | 1.47 | 32.8 | 12.8 | 1.85 | 15.9 | 9.6 | 13.22 | 12.4 | | | | |
| | S112 | 4.2 | 7.42 | | 22.5 | 687 | 224 | 35.0 | 312 | 2.06 | 26.9 | 18.8 | 2.50 | 18.5 | 9.9 | 13.1 | | | | |
| | S113 | 3.0 | 7.36 | | 22.5 | 739 | 197 | 84.0 | 209 | 1.74 | 24.5 | 16.3 | 2.47 | 16.3 | 8.6 | 5.23 | 12.7 | | | |
| 21.11.18 | S114 | 3.0 | 7.41 | | 22.5 | 745 | 169 | 92.0 | 229 | 1.52 | 27.0 | 1.95 | 14.8 | 8.2 | 2.77 | 11.3 | | | | |
| | S115 | 2.3 | 7.42 | | 22.5 | 719 | 128 | 98+1 | 254 | 1.39 | 29.1 | 10.5 | 11.9 | 7.2 | 4.76 | 11.1 | | | | |
| | S116 | 1.5 | 8.07 | | 22.5 | 605 | 341 | 93.0 | 341 | 0.93 | 19.8 | 10.3 | 1.99 | 9.4 | 5.7 | 3.08 | 12.6 | | | |
| | S121 source | 4.0 | 6.45 | | 22.6 | 618 | 184 | 52.2 | 339 | 1.39 | 33.1 | 12.1 | 2.15 | 15.1 | 9.4 | 13.40 | 10.3 | | | |
| | S122 | 3.9 | 7.06 | | 22.6 | 710 | 189 | 40.9 | 264 | 1.71 | 24.4 | 15.2 | 1.38 | 15.8 | 8.8 | 4.04 | 11.0 | | | |
| 21.11.18 | S123 | 4.5 | 7.32 | | 22.6 | 740 | 224 | 60.0 | 169 | 2.07 | 26.2 | 18.3 | 1.47 | 18.0 | 9.8 | 11.8 | | | | |
| | S124 | 4.2 | 7.46 | | 22.6 | 744 | 219 | 144 | 2.03 | 31.5 | 15.1 | 1.52 | 18.4 | 10.3 | 2.72 | 10.3 | | | | |
| | S125 | 2.7 | 7.36 | | 22.6 | 740 | 184 | 98.5 | 139 | 1.57 | 33.2 | 11.8 | 1.25 | 14.8 | 9.2 | 5.21 | 9.8 | | | |
| | S126 | 4.9 | 7.62 | | 22.6 | 718 | 112 | 93.8 | 376 | 0.87 | 20.6 | 9.3 | 1.44 | 8.1 | 5.1 | 2.64 | 9.7 | | | |

| Date | sample No | ICP-OES P | ICP-OES Al | ICP-OES Fe | IC 3000 Fe 2+ | IC 3000 Fe 3+ | ICP-OES Sr | ICP-OES Mn | IC 3000 Mn 2+ | ICP-OES Ti | ICP-OES Li | ICP-OES Mo | ICP-OES B | ICP-OES Br | DOC µgCl |
|------------|-------------------|--------------|---------------|---------------|------------------|------------------|---------------|---------------|------------------|---------------|---------------|---------------|--------------|---------------|-------------|
| 04.04.17 | S1 source | <0.0175 | 0.04 | 14.25 | 12.44 | 1.59 | 0.08 | 0.99 | 0.01 | <0.0025 | <0.005 | <0.005 | 0.04 | 0.11 | |
| | S2 | 0.03 | 0.04 | 14.50 | 14.42 | 1.02 | 0.08 | 0.98 | 0.01 | <0.0025 | <0.005 | <0.005 | 0.04 | 0.11 | |
| | S3 | | | | | | | | | | | | | | |
| | S4 Raude | | | | | | | | | | | | | | |
| | S5 | | | | | | | | | | | | | | |
| | S6 puddle | | | | | | | | | | | | | | |
| 03.05.17 | S11 river | <0.0175 | 0.03 | 2.23 | 0.71 | 0.53 | 0.06 | 0.17 | 0.01 | <0.005 | <0.005 | <0.005 | 0.02 | 0.08 | |
| | S12 | <0.0175 | 0.01 | 2.96 | | | 0.06 | 0.57 | | <0.0025 | <0.005 | <0.005 | 0.02 | 0.12 | |
| | S13 | <0.0175 | 0.04 | 13.77 | | | 0.06 | 1.10 | | <0.0025 | <0.005 | <0.005 | 0.04 | 0.11 | |
| | S14 source | <0.0175 | 0.06 | 15.19 | | | 0.06 | 1.53 | | <0.0025 | <0.005 | <0.005 | 0.04 | 0.07 | |
| 09.05.17 | S21 river | <0.0175 | 0.01 | 1.06 | 0.51 | 0.46 | 0.06 | 0.18 | 0.01 | <0.0025 | <0.005 | <0.005 | 0.02 | 0.09 | |
| | S22 far from soil | <0.0175 | 0.03 | 10.91 | 8.87 | 1.42 | 0.07 | 1.25 | 0.07 | <0.0025 | <0.005 | <0.005 | 0.04 | 0.10 | |
| | S23 | <0.0175 | 0.06 | 23.69 | 20.27 | 1.40 | 0.07 | 1.69 | 0.07 | <0.0025 | <0.005 | <0.005 | 0.06 | 0.12 | |
| | S24 source | <0.0175 | 0.01 | 1.38 | 1.32 | 0.23 | 0.05 | 0.58 | 0.01 | <0.0025 | <0.005 | <0.005 | 0.01 | 0.10 | |
| 20.06.17 | S31 river | <0.0175 | 0.01 | 1.03 | | | 0.07 | 0.23 | | <0.0025 | <0.005 | <0.005 | 0.02 | 0.10 | |
| | S32 | <0.0175 | 0.05 | 24.01 | | | 0.10 | 2.01 | | <0.0025 | <0.005 | <0.005 | 0.05 | 0.10 | |
| | S33 | <0.0175 | 0.06 | 24.00 | | | 0.07 | 1.56 | | <0.0025 | <0.005 | <0.005 | 0.06 | 0.08 | |
| | S34 source | <0.0175 | 0.09 | 31.16 | | | 0.07 | 3.03 | | <0.0025 | <0.005 | <0.005 | 0.07 | 0.11 | |
| | S35 Raude | <0.0175 | 0.00 | 0.02 | | | 0.08 | 0.42 | | <0.0025 | <0.005 | <0.005 | 0.01 | <0.075 | |
| 04.06.17 | S41 source | <0.0175 | 0.07 | 25.50 | | | 0.07 | 2.94 | | <0.0025 | <0.005 | <0.005 | 0.05 | 0.11 | |
| | S42 | <0.0175 | 0.06 | 24.70 | | | 0.07 | 1.54 | | <0.0025 | <0.005 | <0.005 | 0.06 | 0.11 | |
| | S43 | <0.0175 | 0.07 | 26.54 | | | 0.07 | 1.64 | | <0.0025 | <0.005 | <0.005 | 0.07 | 0.12 | |
| | S44 river | <0.0175 | 0.01 | 1.89 | | | 0.07 | 0.21 | | <0.0025 | <0.005 | <0.005 | 0.02 | 0.11 | |
| 19.12.1917 | S52 | 0.29 | 0.02 | 6.82 | | | 0.05 | 1.69 | | <0.0025 | <0.005 | <0.005 | 0.03 | <0.075 | 1069 |
| 23.05.1918 | S51 source | <0.0175 | <0.0075 | 1.59 | 0.92 | 0.51 | 0.05 | 0.43 | 0.45 | <0.0025 | <0.005 | <0.005 | 0.01 | <0.075 | 3181 |
| | S52 | <0.0175 | 0.02 | 9.81 | 9.93 | 0.93 | 0.06 | 0.91 | 0.86 | <0.0025 | <0.005 | <0.005 | 0.04 | <0.075 | 1826 |
| | S53 | <0.0175 | 0.01 | 3.32 | 3.30 | 0.44 | 0.06 | 0.57 | 0.56 | <0.0025 | <0.005 | <0.005 | 0.02 | 0.09 | 3223 |
| | S54 | <0.0175 | 0.01 | 1.30 | 0.67 | 0.30 | 0.05 | 0.16 | 0.17 | <0.0025 | <0.005 | <0.005 | 0.02 | <0.075 | 3070 |
| | S55 Raude | <0.0175 | <0.0075 | 0.33 | 0.24 | 0.08 | 0.06 | 0.40 | 0.42 | <0.0025 | <0.005 | <0.005 | <0.01 | <0.075 | 2388 |
| | S56 | <0.0175 | 0.01 | 0.08 | <LOD | <LOD | 0.05 | 0.16 | 0.17 | <0.0025 | <0.005 | <0.005 | 0.01 | <0.075 | 2626 |
| 07.06.18 | S71 source | <0.0175 | 0.02 | 0.16 | 0.20 | 0.08 | 0.05 | 0.38 | 0.40 | <0.0025 | <0.005 | <0.005 | <0.01 | <0.075 | 2865 |
| | S72 | <0.0175 | 0.06 | 25.46 | 28.89 | 1.48 | 0.07 | 2.05 | 1.90 | <0.0025 | <0.005 | <0.005 | 0.07 | 0.09 | 1612 |
| | S73 | <0.0175 | 0.01 | 5.72 | 5.47 | 0.34 | 0.07 | 0.84 | 0.81 | <0.0025 | <0.005 | <0.005 | 0.03 | 0.09 | 1421 |
| | S74 | <0.0175 | <0.0075 | 0.85 | 0.99 | 0.17 | 0.06 | 0.20 | 0.20 | <0.0025 | <0.005 | <0.005 | 0.02 | <0.075 | 1737 |
| | S75 Raude | <0.0175 | <0.0075 | 0.13 | <LOD | 0.00 | 0.07 | 0.45 | 0.49 | <0.0025 | <0.005 | <0.005 | <0.01 | <0.075 | 2141 |
| | S76 | <0.0175 | <0.0075 | 0.11 | 0.25 | 0.28 | 0.07 | 0.28 | 0.29 | <0.0025 | <0.005 | <0.005 | <0.01 | <0.075 | 2626 |
| 20.06.18 | S81 source | <0.0175 | <0.0075 | 2.30 | 6.23 | 0.99 | 0.05 | 0.77 | 1.24 | <0.0025 | <0.005 | <0.005 | 0.01 | 0.10 | 2450 |
| | S82 | <0.0175 | 0.07 | 29.55 | 36.50 | 1.26 | 0.07 | 1.93 | 1.76 | <0.0025 | <0.005 | <0.005 | 0.08 | 0.10 | 1976 |
| | S83 | <0.0175 | 0.02 | 7.49 | 7.40 | 0.46 | 0.07 | 0.96 | 0.94 | <0.0025 | <0.005 | <0.005 | 0.03 | <0.075 | 1901 |
| | S84 | <0.0175 | <0.0075 | 0.60 | 0.69 | 0.34 | 0.07 | 0.20 | 0.20 | <0.0025 | <0.005 | <0.005 | 0.02 | 0.12 | 1746 |
| | S85 Raude | <0.0175 | <0.0075 | 0.08 | 0.20 | 0.04 | 0.08 | 0.40 | 0.42 | <0.0025 | <0.005 | <0.005 | 0.01 | <0.075 | 2162 |
| | S86 | <0.0175 | <0.0075 | 0.04 | <LOD | <LOD | 0.02 | 0.08 | 0.19 | <0.0025 | <0.005 | <0.005 | 0.01 | 0.09 | 2812 |
| 13.06.18 | S87 read 1 | <0.0175 | <0.0075 | 0.08 | 0.20 | 0.16 | 0.03 | 0.43 | 0.45 | <0.0025 | <0.005 | <0.005 | 0.01 | 0.09 | 1913 |
| 18.09.18 | S101 | <0.0175 | <0.0075 | 0.13 | 0.29 | 0.14 | 0.03 | 0.10 | 0.10 | <0.0025 | <0.005 | <0.005 | <0.01 | 0.10 | 3838 |
| | S102 | <0.0175 | 0.06 | 23.46 | 25.01 | 1.25 | 0.06 | 1.46 | 1.34 | <0.0025 | <0.005 | <0.005 | 0.07 | 0.08 | 1740 |
| | S103 | <0.0175 | 0.01 | 2.51 | 2.06 | 0.12 | 0.07 | 0.92 | 0.95 | <0.0025 | <0.005 | <0.005 | 0.02 | <0.075 | 1558 |
| | S104 | <0.0175 | 0.01 | 1.56 | 0.85 | 0.24 | 0.07 | 0.23 | 0.23 | <0.0025 | <0.005 | <0.005 | 0.02 | 0.10 | |
| 28.10.18 | S111 source | <0.0175 | 0.02 | 8.18 | 4.91 | 0.71 | 0.06 | 1.15 | 0.78 | <0.0025 | <0.005 | <0.005 | 0.02 | <0.075 | 3452 |
| | S112 | <0.0175 | 0.01 | 4.69 | 4.50 | 0.43 | 0.05 | 0.59 | 0.59 | <0.0025 | <0.005 | <0.005 | 0.02 | <0.075 | 1983 |
| | S113 | <0.0175 | <0.0075 | 0.85 | 0.67 | 0.17 | 0.05 | 0.35 | 0.36 | <0.0025 | <0.005 | <0.005 | 0.01 | <0.075 | 1969 |
| | S114 | <0.0175 | 0.01 | 1.46 | 1.08 | 0.46 | 0.05 | 0.16 | 0.16 | <0.0025 | <0.005 | <0.005 | 0.01 | <0.075 | 2413 |
| | S115 | <0.0175 | 0.01 | 2.51 | 1.43 | 0.34 | 0.05 | 0.29 | 0.28 | <0.0025 | <0.005 | <0.005 | 0.01 | <0.075 | 2741 |
| | S116 | <0.0175 | <0.0075 | 0.17 | <LOD | <LOD | 0.05 | 0.04 | 0.25 | <0.0025 | <0.005 | <0.005 | <0.01 | <0.075 | 4250 |
| 21.11.18 | S121 source | <0.0175 | 0.02 | 4.00 | 3.48 | 0.68 | 0.06 | 0.66 | 0.73 | <0.0025 | <0.005 | <0.005 | 0.02 | <0.075 | 2935 |
| | S122 | <0.0175 | <0.0075 | 0.06 | 0.18 | 0.02 | 0.05 | 0.11 | 0.17 | <0.0025 | <0.005 | <0.005 | 0.01 | <0.075 | 1951 |
| | S123 | <0.0175 | <0.0075 | 0.13 | 0.20 | 0.14 | 0.06 | 0.15 | 0.43 | <0.0025 | <0.005 | <0.005 | 0.01 | <0.075 | 1606 |
| | S124 | <0.0175 | 0.01 | 1.80 | 1.32 | 0.67 | 0.06 | 0.20 | 0.20 | <0.0025 | <0.005 | <0.005 | 0.02 | <0.075 | 1891 |
| | S125 | <0.0175 | 0.01 | 2.51 | 1.97 | 0.34 | 0.06 | 0.42 | 0.42 | <0.0025 | <0.005 | <0.005 | 0.01 | <0.075 | 6121 |
| | S126 | <0.0175 | <0.0075 | 0.12 | 0.18 | 0.03 | 0.04 | 0.14 | 0.15 | <0.0025 | <0.005 | <0.005 | <0.01 | <0.075 | 5663 |

| Date | sample No | ICP-MS As | ICP-MS Cd | ICP-MS Co | ICP-MS Cr | ICP-MS Cu | ICP-MS Ni | ICP-MS Pb | ICP-MS Se | ICP-MS Zn | ICP-MS V | ICP-MS 48Ti | ICP-MS 99Mo | ICP-MS 118Sn |
|------------|-------------------|-----------|-----------|-----------|-----------|-----------|-----------|-----------|-----------|-----------|----------|-------------|-------------|--------------|
| | | ppt | ppt | ppt | ppt | ppt |
| 04.04.17 | S1 source | <LOD | <LOD | 687 | 431 | 579 | 356 | 47 | <LOD | 1308 | 49658 | 214 | <LOD | |
| | S2 | <LOD | <LOD | 477 | 384 | 403 | 410 | 35 | <LOD | 2872 | 1532 | 54614 | 255 | <LOD |
| | S3 | - | - | - | - | - | - | - | - | - | - | - | - | - |
| | S4 Raude | - | - | - | - | - | - | - | - | - | - | - | - | - |
| | S5 | - | - | - | - | - | - | - | - | - | - | - | - | - |
| | S6 puddle | - | - | - | - | - | - | - | - | - | - | - | - | - |
| 03.05.17 | S11 river | <LOD | <LOD | 404 | 239 | 462 | 526 | 14 | <LOD | 1785 | 1754 | 23008 | 312 | <LOD |
| | S12 | <LOD | <LOD | 570 | 52 | 615 | 489 | <LOD | <LOD | 3251 | <LOD | 27147 | 175 | <LOD |
| | S13 | <LOD | <LOD | 705 | 114 | 262 | 297 | <LOD | <LOD | 1983 | 470 | 28589 | 285 | <LOD |
| | S14 source | <LOD | <LOD | 671 | 92 | 760 | 578 | <LOD | <LOD | 5303 | 702 | 22727 | 13 | <LOD |
| 09.05.17 | S21 river | <LOD | <LOD | 377 | 74 | 312 | 346 | <LOD | <LOD | 2183 | 725 | 27718 | 362 | <LOD |
| | S22 far from soil | <LOD | <LOD | 1068 | 138 | 74 | 368 | <LOD | <LOD | 1340 | 149 | 32215 | 236 | <LOD |
| | S23 | <LOD | <LOD | 1071 | 123 | 176 | 468 | 19 | <LOD | 2981 | 623 | 34489 | 329 | <LOD |
| | S24 source | <LOD | <LOD | 639 | 74 | 838 | 633 | <LOD | <LOD | 3419 | 351 | 17936 | 13 | <LOD |
| 20.06.17 | S31 river | <LOD | <LOD | 414 | 263 | 117 | 332 | 32 | <LOD | 1471 | 643 | 29701 | 402 | <LOD |
| | S32 | <LOD | <LOD | 2737 | 169 | <LOD | 839 | <LOD | <LOD | 3552 | 261 | 42318 | 207 | <LOD |
| | S33 | <LOD | <LOD | 933 | 269 | <LOD | 367 | <LOD | <LOD | 2646 | 1013 | 31539 | 313 | <LOD |
| | S34 source | <LOD | <LOD | 612 | 388 | 1470 | 543 | 84 | <LOD | 6137 | 1372 | 24543 | <LOD | <LOD |
| | S35 Raude | <LOD | <LOD | 654 | 210 | 217 | 695 | <LOD | <LOD | 1804 | <LOD | 29278 | 140 | <LOD |
| 04.08.17 | S41 source | <LOD | 51.4 | 224 | 4023 | 1708 | 4293 | 34 | <LOD | 18000 | 688 | 24289 | 44 | <LOD |
| | S42 | <LOD | <LOD | 669 | 468 | <LOD | 423 | <LOD | <LOD | 2188 | 1210 | 32985 | 380 | <LOD |
| | S43 | <LOD | <LOD | 1178 | 368 | 238 | 1102 | <LOD | <LOD | 4617 | 831 | 33577 | 431 | <LOD |
| | S44 river | <LOD | <LOD | 326 | 327 | 322 | 537 | <LOD | <LOD | 2793 | 660 | 32168 | 505 | <LOD |
| 19.12.1917 | S52 | <LOD | <LOD | 1103 | 62 | 139 | 269 | <LOD | <LOD | 6492 | 174 | 26297 | 2750 | <LOD |
| 23.05.1918 | S51 source | <LOD | <LOD | 156 | <LOD | 693 | 298 | <LOD | <LOD | 6423 | <LOD | 16939 | 11 | <LOD |
| | S52 | <LOD | <LOD | 693 | <LOD | 95 | 211 | <LOD | <LOD | 1442 | 279 | 26623 | 180 | <LOD |
| | S53 | <LOD | <LOD | 472 | <LOD | <LOD | 170 | <LOD | <LOD | 1274 | <LOD | 26623 | 166 | <LOD |
| | S54 | <LOD | <LOD | 489 | <LOD | 388 | 389 | <LOD | <LOD | 2584 | 743 | 21433 | 240 | <LOD |
| | S55 Raude | <LOD | <LOD | 989 | 95 | 1112 | 966 | <LOD | <LOD | 4631 | <LOD | 20676 | 68 | <LOD |
| | S56 | <LOD | <LOD | 223 | <LOD | 693 | 473 | <LOD | <LOD | 1057 | 273 | 16541 | 78 | <LOD |
| 07.06.18 | S71 source | <LOD | <LOD | 198 | 256 | 518 | 422 | <LOD | <LOD | 2353 | <LOD | 17659 | <LOD | <LOD |
| | S72 | <LOD | <LOD | 1229 | 175 | <LOD | 411 | <LOD | <LOD | 2406 | 674 | 31453 | 385 | <LOD |
| | S73 | <LOD | <LOD | 611 | 91 | <LOD | 187 | <LOD | <LOD | 1228 | <LOD | 30188 | 195 | <LOD |
| | S74 | <LOD | <LOD | 410 | 495 | 92 | 373 | <LOD | <LOD | 766 | 390 | 27659 | 379 | <LOD |
| | S75 Raude | <LOD | <LOD | 964 | 183 | 239 | 899 | <LOD | <LOD | 1519 | <LOD | 27117 | 112 | <LOD |
| | S76 | <LOD | <LOD | 277 | 127 | 502 | 445 | 18 | <LOD | 762 | 171 | 20875 | 95 | <LOD |
| 20.06.18 | S81 source | <LOD | <LOD | 352 | 886 | 382 | 650 | <LOD | <LOD | 2599 | <LOD | 16080 | 12 | <LOD |
| | S82 | <LOD | <LOD | 1147 | 226 | <LOD | 376 | <LOD | <LOD | 1319 | 873 | 30751 | 405 | <LOD |
| | S83 | <LOD | <LOD | 606 | 99 | <LOD | 208 | <LOD | <LOD | 907 | 108 | 30405 | 221 | <LOD |
| | S84 | <LOD | <LOD | 357 | 156 | 138 | 324 | <LOD | <LOD | 1361 | 345 | 27379 | 406 | <LOD |
| | S85 Raude | <LOD | <LOD | 696 | 118 | 245 | 638 | <LOD | <LOD | 758 | <LOD | 27059 | 125 | <LOD |
| | S86 | <LOD | <LOD | 202 | 161 | 470 | 465 | <LOD | <LOD | <LOD | 279 | 24249 | 140 | <LOD |
| 13.08.18 | S92 read 1 | <LOD | <LOD | 698 | 230 | 275 | 706 | <LOD | <LOD | 1519 | <LOD | 29519 | 157 | <LOD |
| 18.09.18 | S101 | <LOD | <LOD | 131 | 1348 | 254 | 926 | <LOD | <LOD | 2388 | <LOD | 10011 | 20 | <LOD |
| | S102 | <LOD | <LOD | 520 | 282 | <LOD | 146 | <LOD | <LOD | 1795 | 1285 | 30841 | 414 | <LOD |
| | S103 | <LOD | <LOD | 932 | 175 | <LOD | 422 | <LOD | <LOD | 4084 | <LOD | 30260 | 120 | <LOD |
| | S104 | <LOD | <LOD | 438 | 70 | 67 | 308 | <LOD | <LOD | 3449 | 558 | 29738 | 423 | <LOD |
| 28.10.18 | S111 source | <LOD | <LOD | 260 | 180 | 506 | 239 | <LOD | <LOD | 3517 | 224 | 20903 | <LOD | <LOD |
| | S112 | <LOD | <LOD | 245 | <LOD | 107 | <LOD | <LOD | <LOD | 1764 | <LOD | 23908 | 161 | <LOD |
| | S113 | <LOD | <LOD | 233 | 71 | 100 | 62 | 203 | <LOD | 892 | 328 | 20627 | 93 | <LOD |
| | S114 | - | - | - | - | - | - | - | - | - | - | - | - | - |
| | S115 | <LOD | <LOD | 922 | 103 | 574 | 846 | <LOD | <LOD | 2399 | 290 | 11811 | 85 | <LOD |
| | S116 | <LOD | <LOD | 456 | 76 | 537 | 483 | <LOD | <LOD | 1426 | 115 | 12300 | 46 | <LOD |
| 21.11.18 | S121 source | <LOD | <LOD | 272 | 55 | 344 | 169 | <LOD | <LOD | 2262 | 170 | 20381 | <LOD | <LOD |
| | S122 | <LOD | <LOD | 93 | <LOD | 131 | 161 | <LOD | <LOD | 1172 | <LOD | 20767 | 49 | <LOD |
| | S123 | <LOD | <LOD | 114 | 42 | <LOD | 64 | <LOD | <LOD | 842 | <LOD | 23915 | 101 | <LOD |
| | S124 | <LOD | <LOD | 477 | <LOD | 124 | 258 | <LOD | <LOD | 1051 | 417 | 24640 | 296 | <LOD |
| | S125 | <LOD | <LOD | 1160 | 64 | 466 | 976 | <LOD | <LOD | 1646 | <LOD | 19406 | 63 | <LOD |
| | S126 | <LOD | <LOD | 261 | 132 | 663 | 434 | <LOD | <LOD | 2136 | <LOD | 10760 | 51 | <LOD |

Table ES2: Measured data from different Rhizon samples installed in the outcrop wall

| Date | sample No | water T | pH | T lab | pH lab | cond | O2 | EN(SHE) | Alkalinity | ICP-OES Si as SiO2 | ICP-OES Na | ICP-OES K | ICP-OES Ca | ICP-OES Mg | ICP-OES SO4 | ICP-OES Cl | ICP-OES P | |
|----------|-------------------|-------------|-------|-------|--------|-------|-------|---------|----------------|-----------------------|---------------|--------------|---------------|---------------|----------------|---------------|--------------|----------|
| | | °C | | °C | | µS | % | mV | meq/kg | mg/kg | mg/kg | mg/kg | mg/kg | mg/kg | mg/kg | mg/kg | mg/kg | |
| LOQ | | | | | | | | | | 0.1 | 0.3 | 0.10 | 0.0 | 0.0 | 0.20 | 1.0 | 0.02 | |
| 20.06.17 | Rhizon samp R1-1 | | | 22.0 | 6.71 | | | | | 0.33 | 18.5 | 5.5 | 3.82 | 1.8 | 1.0 | 0.98 | 4.6 | 0.00 |
| | Rhizon samp R2-1 | | | 22.0 | 6.43 | | | | | 0.26 | 34.7 | 6.4 | 5.73 | 3.9 | 2.1 | 5.63 | 12.8 | 0.15 |
| | Rhizon samp R3-1 | | | 22.0 | 6.37 | | | | | 0.12 | 24.2 | 8.2 | 2.83 | 2.8 | 1.5 | 6.58 | 8.5 | 0.03 |
| | Rhizon samp R4-1 | | | 22.0 | 6.65 | | | | | 0.28 | 22.5 | 7.7 | 3.28 | 5.1 | 3.0 | 3.62 | 10.5 | 0.00 |
| | Rhizon samp R5-1 | | | 22.0 | 6.57 | | | | | 0.43 | 23.2 | 7.5 | 2.63 | 6.8 | 3.3 | 6.64 | 10.9 | 0.01 |
| | Rhizon samp R6-1 | | | 22.0 | 6.44 | | | | | 0.70 | 35.5 | 8.0 | 2.28 | 6.5 | 3.7 | 8.90 | 10.6 | 0.00 |
| | Rhizon samp R7-1 | | | 22.0 | 6.43 | | | | | 0.48 | 32.0 | 7.8 | 2.66 | 6.6 | 3.6 | 7.27 | 10.6 | 0.01 |
| | Rhizon samp R8-1 | | | 22.0 | 6.29 | | | | | 0.44 | 39.0 | 8.4 | 1.69 | 7.3 | 4.2 | 13.81 | 11.0 | 0.09 |
| | Rhizon samp R9-1 | | | 22.0 | 6.32 | | | | | 0.29 | 38.9 | 8.1 | 1.50 | 6.2 | 3.4 | 12.05 | 10.6 | 0.01 |
| | Rhizon samp R10-1 | | | 22.0 | 6.02 | | | | | 0.41 | 39.5 | 8.0 | 1.30 | 8.1 | 4.4 | 16.17 | 10.4 | 0.01 |
| | Rhizon samp R11-1 | | | 22.0 | 6.13 | | | | | 0.62 | 38.1 | 7.8 | 1.48 | 6.1 | 3.5 | 12.74 | 10.9 | 0.00 |
| | Rhizon samp R12-1 | | | 22.0 | 5.94 | | | | | 0.74 | 40.0 | 8.6 | 1.59 | 9.4 | 5.4 | 11.59 | 10.3 | 0.02 |
| | Rhizon samp R13-1 | | | 22.0 | 6.05 | | | | | 0.90 | 39.7 | 9.2 | 1.82 | 11.1 | 6.2 | 10.19 | 10.7 | 0.01 |
| | Rhizon samp R14-1 | | | 22.0 | 6.13 | | | | | 0.62 | 42.3 | 8.9 | 1.57 | 9.3 | 5.7 | 8.66 | 10.8 | 0.00 |
| 04.08.17 | Rhizon samp R1-2 | | | 22.0 | 6.63 | | | | | 19.3 | 4.9 | 3.40 | 1.9 | 0.9 | 1.95 | 0.6 | 0.00 | |
| | Rhizon samp R2-2 | | | 22.0 | 6.48 | | | | | 27.3 | 6.3 | 2.97 | 3.0 | 1.6 | 5.22 | 6.0 | 0.00 | |
| | Rhizon samp R3-2 | empty | empty | empty | empty | empty | empty | empty | empty | empty | empty | empty | empty | empty | empty | empty | empty | |
| | Rhizon samp R4-2 | | | 22.0 | 6.67 | | | | | 23.4 | 7.4 | 3.21 | 5.5 | 3.1 | 4.96 | 8.5 | 0.01 | |
| | Rhizon samp R5-2 | | | 22.0 | 6.73 | | | | | 27.4 | 9.2 | 3.15 | 11.7 | 5.3 | 9.31 | 9.4 | 0.01 | |
| | Rhizon samp R6-2 | | | 22.0 | 6.60 | | | | | 41.6 | 9.4 | 2.50 | 10.1 | 5.6 | 11.80 | 9.0 | 0.00 | |
| | Rhizon samp R7-2 | | | 22.0 | 6.34 | | | | | 40.9 | 9.1 | 1.59 | 9.7 | 5.4 | 16.62 | 10.8 | 0.00 | |
| | Rhizon samp R8-2 | | | 22.0 | 5.94 | | | | | 43.0 | 9.5 | 1.82 | 9.1 | 4.7 | 18.38 | 11.1 | 0.00 | |
| | Rhizon samp R9-2 | | | 22.0 | 6.49 | | | | | 35.1 | 9.2 | 2.70 | 9.9 | 5.3 | 13.15 | 9.6 | 0.00 | |
| | Rhizon samp R10-2 | | | 22.0 | 6.07 | | | | | 43.4 | 9.0 | 1.23 | 11.4 | 5.8 | 28.33 | 9.7 | 0.01 | |
| | Rhizon samp R11-2 | | | 22.0 | 6.06 | | | | | 42.9 | 9.0 | 1.63 | 9.7 | 5.2 | 24.47 | 10.8 | 0.00 | |
| | Rhizon samp R12-2 | | | 22.0 | 6.25 | | | | | 43.8 | 9.8 | 1.70 | 13.3 | 7.3 | 33.76 | 10.0 | 0.00 | |
| | Rhizon samp R13-2 | | | 22.0 | 6.03 | | | | | 42.8 | 9.9 | 1.78 | 11.9 | 6.5 | 22.46 | 10.2 | 0.00 | |
| | Rhizon samp R14-2 | | | 22.0 | 6.16 | | | | | 47.0 | 10.0 | 1.75 | 13.6 | 7.8 | 26.41 | 11.3 | 0.00 | |
| 13.08.18 | H1-1 | empty | empty | empty | empty | empty | empty | empty | empty | empty | empty | empty | empty | empty | empty | empty | empty | |
| | H2-1 | | | 23.0 | 6.04 | 180 | 56.0 | 249 | | 48.7 | 10.9 | 1.72 | 19.9 | 10.8 | 22.68 | 12.5 | < 0.0875 | |
| | H3-1 | x | | 23.0 | 6.05 | 200 | 70 ? | 302 | | 47.6 | 10.3 | 1.26 | 17.6 | 12.3 | 18.33 | 11.0 | < 0.0875 | |
| | H4-1 | x | | 23.0 | 5.72 | 188 | 50.0 | 383 | | 46.0 | 10.3 | 1.35 | 15.3 | 11.1 | 34.94 | 10.5 | < 0.0875 | |
| | H5-1 | x | | 23.0 | 5.40 | 213 | 55.0 | 440 | | 53.8 | 11.6 | 1.80 | 24.2 | 16.8 | 109.37 | 10.1 | < 0.0875 | |
| | H6-1 | x | | 23.0 | 5.72 | 207 | 51.0 | 449 | | 43.7 | 10.9 | 1.60 | 17.5 | 11.4 | 34.15 | 10.4 | < 0.0875 | |
| | H7-1 | | | 23.0 | 6.30 | 217 | 79.0 | 339 | low Volume | - | - | - | - | - | - | - | - | |
| | H8-1 | x | | 23.0 | 6.34 | 261 | 47.0 | 249 | | 36.5 | 10.3 | 1.12 | 16.3 | 12.3 | 1.55 | 10.8 | < 0.0875 | |
| | H9-1 | x | | 23.0 | 6.60 | - | 83.0 | 176 | left over nigh | 34.6 | 12.2 | 1.92 | 15.5 | 11.6 | 1.62 | 12.5 | < 0.0875 | |
| | H10-1 | x | | 23.0 | 6.32 | 255 | 72.0 | 172 | left over nigh | 34.0 | 13.7 | 1.17 | 14.5 | 11.3 | < 1.0 | 11.6 | < 0.0875 | |
| 18.09.18 | H1-2 | not working | empty | empty | empty | empty | empty | empty | empty | empty | empty | empty | empty | empty | empty | empty | empty | |
| | H2-2 | 14.4 | 6.22 | 22.2 | 6.29 | 152 | 31.4 | 283 | | 1.98 | 45.9 | 11.1 | 1.63 | 22.5 | 11.9 | 28.34 | 8.6 | < 0.0875 |
| | H3-2 | 14.4 | 6.10 | 22.2 | 6.20 | 140 | 41.2 | 354 | | 1.74 | 49.3 | 10.7 | 1.24 | 19.5 | 13.2 | 22.88 | 9.7 | < 0.0875 |
| | H4-2 | 15.0 | 5.93 | 22.2 | 5.92 | 222 | 47.1 | 359 | | 0.96 | 50.0 | 11.7 | 1.41 | 23.6 | 15.8 | 78.51 | 9.8 | < 0.0875 |
| | H5-2 | 14.5 | 5.72 | 22.7 | 5.72 | 265 | 3.0 | 389 | | 0.6 | 55.6 | 12.6 | 1.71 | 32.5 | 21.4 | 145.71 | 9.0 | < 0.0875 |
| | H6-2 | 13.4 | 5.88 | 22.7 | 6.34 | 229 | 38.9 | 399 | | 1.27 | 45.0 | 11.3 | 1.20 | 20.5 | 13.2 | 46.91 | 9.2 | < 0.0875 |
| | H7-2 | | empty | empty | empty | empty | empty | empty | empty | empty | empty | empty | empty | empty | empty | empty | empty | |
| | H8-2 | | empty | empty | empty | empty | empty | empty | empty | empty | empty | empty | empty | empty | empty | empty | empty | |
| | H9-2 | 13.6 | 6.26 | 22.7 | 6.5 | 155 | 36.0 | 169 | | 2.78 | 36.3 | 11.4 | 0.90 | 16.1 | 12.3 | < 1 | 11.0 | < 0.0875 |
| | H10-2 | 12.7 | 6.48 | 22.7 | 6.5 | - | - | 152 | | 2.26 | 34.6 | 13.9 | 1.09 | 14.7 | 11.5 | < 1 | 10.7 | < 0.0875 |
| 29.10.18 | H1-3 | not working | empty | empty | empty | empty | empty | empty | empty | empty | empty | empty | empty | empty | empty | empty | empty | |
| | H2-3 | | | 22.5 | 6.14 | | | 264 | | 1.50 | 37.7 | 10.9 | 1.98 | 18.5 | 9.7 | 18.71 | 18.6 | < 0.0875 |
| | H3-3 | | | 22.5 | 6.11 | | | 345 | | 1.86 | 47.6 | 11.0 | 1.22 | 21.0 | 14.4 | 20.45 | 10.0 | < 0.0875 |
| | H4-3 | | | 22.5 | 5.84 | | | 419 | | 1.08 | 47.6 | 10.8 | 1.39 | 19.3 | 13.4 | 51.28 | 11.0 | < 0.0875 |
| | H5-3 | | | 22.5 | 5.57 | | | 379 | | 0.60 | 54.6 | 12.6 | 1.64 | 32.4 | 21.6 | 143.40 | 9.9 | < 0.0875 |
| | H6-3 | | | 22.5 | 5.88 | | | 406 | | 1.35 | 45.8 | 11.5 | 1.16 | 21.3 | 14.1 | 47.78 | 10.0 | < 0.0875 |
| | H7-3 | | | 22.5 | 6.55 | | | 204 | | 2.34 | - | - | - | - | - | - | - | |
| | H8-3 | | | 22.5 | 6.00 | | | 215 | | 2.28 | - | - | - | - | - | - | - | |
| | H9-3 | | | 22.5 | 6.34 | | | 197 | | 2.56 | 37.0 | 11.5 | 0.85 | 16.3 | 12.4 | < 1 | 11.2 | < 0.0875 |
| | H10-3 | | | 22.5 | 6.33 | | | 229 | | 2.18 | 38.6 | 13.9 | 1.30 | 15.2 | 11.8 | < 1 | 11.2 | < 0.0875 |
| 21.11.18 | H1-4 | not working | empty | empty | empty | empty | empty | empty | empty | empty | empty | empty | empty | empty | empty | empty | empty | |
| | H2-4 | | | 22.6 | 6.19 | | | 277 | | 1.92 | 41.2 | 10.6 | 1.77 | 20.7 | 11.1 | 23.18 | 11.6 | < 0.0875 |
| | H3-4 | | | 22.6 | 6.07 | | | 352 | | 2.07 | 46.1 | 11.1 | 1.15 | 21.3 | 14.7 | 17.92 | 9.9 | < 0.0875 |
| | H4-4 | | | 22.6 | | | | 199 | | | | | | | | | | |
| | H5-4 | | | 22.6 | 5.53 | | | 449 | | 0.68 | 52.0 | 11.6 | 1.54 | 26.6 | 18.0 | 108.75 | 10.8 | < 0.0875 |
| | H6-4 | | | 22.6 | 6.28 | | | 449 | | 1.43 | 43.8 | 11.0 | 1.15 | 20.0 | 13.1 | 37.10 | 11.5 | < 0.0875 |
| | H7-4 | | | 22.6 | 6.47 | | | 204 | | 2.82 | 37.6 | 10.5 | 0.88 | 21.7 | 14.0 | 11.24 | 9.5 | < 0.0875 |
| | H8-4 | broken | empty | 22.6 | empty | empty | empty | empty | empty | empty | empty | empty | empty | empty | empty | empty | empty | |
| | H9-4 | | | 22.6 | 6.35 | | | 169 | | 2.88 | 36.2 | 11.3 | 0.87 | 16.5 | 12.4 | < 1 | 10.8 | < 0.0875 |
| | H10-4 | | | 22.6 | 6.51 | | | 239 | | 2.58 | 30.9 | 13.7 | 1.10 | 14.9 | 11.7 | < 1 | 11.1 | < 0.0875 |

| Date | sample No | water T | pH | T lab | pH lab | cond | O2 | Eh | En(SHE) | Alkalinity | ICP-OES | ICP-OES | ICP-OES | ICP-OES | ICP-OES | ICP-OES | ICP-OES | ICP-OES | |
|----------|-----------|-------------|-------|-------|--------|-------|-------|-------|---------|----------------|------------|---------|---------|---------|---------|---------|---------|----------|----------|
| | | °C | | | | µS | % | mV | | meq/kg | Si as SiO2 | Na | K | Ca | Mg | SO4 | Cl | P | |
| LOQ | | | | | | | | | | | 0.1 | 0.3 | 0.10 | 0.0 | 0.0 | 0.20 | 1.0 | 0.02 | |
| 20.06.17 | R1-1 | | | 22.0 | 6.71 | | | | | | 0.33 | 18.5 | 5.5 | 3.82 | 1.8 | 1.0 | 0.98 | 4.6 | 0.00 |
| | R2-1 | | | 22.0 | 6.43 | | | | | | 0.26 | 24.7 | 6.4 | 5.73 | 3.9 | 2.1 | 5.63 | 12.8 | 0.15 |
| | R3-1 | | | 22.0 | 6.37 | | | | | | 0.12 | 24.2 | 6.2 | 2.83 | 2.8 | 1.5 | 6.58 | 8.5 | 0.03 |
| | R4-1 | | | 22.0 | 6.65 | | | | | | 0.28 | 22.5 | 7.7 | 3.28 | 5.1 | 3.0 | 3.62 | 10.5 | 0.00 |
| | R5-1 | | | 22.0 | 6.57 | | | | | | 0.43 | 23.2 | 7.5 | 2.63 | 6.8 | 3.3 | 6.64 | 10.9 | 0.01 |
| | R6-1 | | | 22.0 | 6.44 | | | | | | 0.70 | 35.5 | 8.0 | 2.28 | 6.5 | 3.7 | 8.90 | 10.6 | 0.00 |
| | R7-1 | | | 22.0 | 6.43 | | | | | | 0.48 | 32.0 | 7.8 | 2.86 | 6.6 | 3.6 | 7.27 | 10.6 | 0.01 |
| | R8-1 | | | 22.0 | 6.29 | | | | | | 0.44 | 39.0 | 8.4 | 1.69 | 7.3 | 4.2 | 13.81 | 11.0 | 0.09 |
| | R9-1 | | | 22.0 | 6.32 | | | | | | 0.29 | 39.9 | 8.1 | 1.50 | 6.2 | 3.4 | 12.05 | 10.6 | 0.01 |
| | R10-1 | | | 22.0 | 6.02 | | | | | | 0.41 | 39.5 | 8.0 | 1.30 | 8.1 | 4.4 | 16.17 | 10.4 | 0.01 |
| | R11-1 | | | 22.0 | 6.13 | | | | | | 0.62 | 38.1 | 7.8 | 1.48 | 6.1 | 3.5 | 12.74 | 10.9 | 0.00 |
| | R12-1 | | | 22.0 | 5.94 | | | | | | 0.74 | 40.0 | 8.6 | 1.59 | 9.4 | 5.4 | 11.59 | 10.3 | 0.02 |
| | R13-1 | | | 22.0 | 6.05 | | | | | | 0.90 | 39.7 | 9.2 | 1.82 | 11.1 | 6.2 | 10.19 | 10.7 | 0.01 |
| | R14-1 | | | 22.0 | 6.13 | | | | | | 0.82 | 42.3 | 8.9 | 1.57 | 9.3 | 5.7 | 8.86 | 10.8 | 0.00 |
| 04.08.17 | R1-2 | | | 22.0 | 6.63 | | | | | | 19.3 | 4.9 | 3.40 | 1.0 | 0.9 | 1.95 | 0.6 | 0.00 | |
| | R2-2 | | | 22.0 | 6.48 | | | | | | 27.3 | 6.3 | 2.97 | 3.0 | 1.6 | 5.22 | 6.0 | 0.00 | |
| | R3-2 | empty | empty | empty | empty | empty | empty | empty | empty | empty | empty | empty | empty | empty | empty | empty | empty | empty | empty |
| | R4-2 | | | 22.0 | 6.67 | | | | | | 23.4 | 7.4 | 3.21 | 5.5 | 3.1 | 4.96 | 8.5 | 0.01 | |
| | R5-2 | | | 22.0 | 6.73 | | | | | | 27.4 | 9.2 | 3.15 | 11.7 | 5.3 | 9.31 | 9.4 | 0.01 | |
| | R6-2 | | | 22.0 | 6.60 | | | | | | 41.6 | 9.4 | 2.59 | 10.1 | 5.6 | 11.90 | 6.0 | 0.00 | |
| | R7-2 | | | 22.0 | 6.34 | | | | | | 40.9 | 9.1 | 1.59 | 9.7 | 5.4 | 18.03 | 10.8 | 0.00 | |
| | R8-2 | | | 22.0 | 5.94 | | | | | | 43.0 | 9.5 | 1.82 | 9.1 | 4.7 | 18.38 | 11.1 | 0.00 | |
| | R9-2 | | | 22.0 | 6.49 | | | | | | 35.1 | 9.2 | 2.70 | 9.9 | 5.3 | 13.15 | 9.6 | 0.00 | |
| | R10-2 | | | 22.0 | 6.07 | | | | | | 43.4 | 9.0 | 1.23 | 11.4 | 5.8 | 28.33 | 9.7 | 0.01 | |
| | R11-2 | | | 22.0 | 6.06 | | | | | | 42.9 | 9.0 | 1.63 | 9.7 | 5.2 | 24.47 | 10.8 | 0.00 | |
| | R12-2 | | | 22.0 | 6.25 | | | | | | 42.8 | 9.8 | 1.70 | 13.3 | 7.3 | 23.76 | 10.0 | 0.00 | |
| | R13-2 | | | 22.0 | 6.03 | | | | | | 42.8 | 9.9 | 1.78 | 11.9 | 6.5 | 22.46 | 10.2 | 0.00 | |
| | R14-2 | | | 22.0 | 6.16 | | | | | | 47.0 | 10.0 | 1.75 | 13.6 | 7.8 | 26.41 | 11.3 | 0.00 | |
| 13.08.18 | H1-1 | empty | empty | empty | empty | empty | empty | empty | empty | empty | empty | empty | empty | empty | empty | empty | empty | empty | empty |
| | H2-1 | | | 23.0 | 6.04 | 180 | 56.0 | 50.0 | 249 | empty | 48.7 | 10.9 | 1.72 | 19.9 | 10.8 | 22.68 | 12.5 | < 0.0875 | |
| | H3-1 | x | | 23.0 | 6.05 | 200 | 70.7 | 103.0 | 302 | empty | 47.6 | 10.3 | 1.26 | 17.6 | 12.3 | 18.33 | 11.0 | < 0.0875 | |
| | H4-1 | x | | 23.0 | 5.72 | 188 | 50.0 | 184.0 | 383 | empty | 48.0 | 10.3 | 1.35 | 15.3 | 11.1 | 34.94 | 10.5 | < 0.0875 | |
| | H5-1 | x | | 23.0 | 5.40 | 213 | 55.0 | 241.0 | 440 | empty | 53.8 | 11.6 | 1.80 | 24.2 | 16.8 | 109.37 | 10.1 | < 0.0875 | |
| | H6-1 | x | | 23.0 | 5.72 | 207 | 51.0 | 250.0 | 449 | empty | 43.7 | 10.9 | 1.60 | 17.5 | 11.4 | 34.15 | 10.4 | < 0.0875 | |
| | H7-1 | | | 23.0 | 6.30 | 217 | 79.0 | 140.0 | 339 | low Volume | - | - | - | - | - | - | - | - | - |
| | H8-1 | x | | 23.0 | 6.34 | 261 | 47.0 | 50.0 | 249 | empty | 36.5 | 10.3 | 1.12 | 16.3 | 12.3 | 1.55 | 10.8 | < 0.0875 | |
| | H9-1 | x | | 23.0 | 6.60 | - | 83.0 | -23.0 | 176 | left over nigh | 34.6 | 12.2 | 1.92 | 15.5 | 11.6 | 1.62 | 12.5 | < 0.0875 | |
| | H10-1 | x | | 23.0 | 6.32 | 255 | 72.0 | -27.0 | 172 | left over nigh | 34.0 | 13.7 | 1.17 | 14.5 | 11.3 | < 1.0 | 11.8 | < 0.0875 | |
| 18.09.18 | H1-2 | not working | empty | empty | empty | empty | empty | empty | empty | empty | empty | empty | empty | empty | empty | empty | empty | empty | empty |
| | H2-2 | 14.4 | 6.22 | 22.2 | 6.29 | 152 | 31.4 | 84.0 | 283 | empty | 1.98 | 45.9 | 11.1 | 1.63 | 22.5 | 11.9 | 28.34 | 8.6 | < 0.0875 |
| | H3-2 | 14.4 | 6.10 | 22.2 | 6.20 | 140 | 41.2 | 155.0 | 354 | empty | 1.74 | 49.3 | 10.7 | 1.24 | 19.5 | 13.2 | 22.88 | 9.7 | < 0.0875 |
| | H4-2 | 15.0 | 5.93 | 22.2 | 5.92 | 222 | 47.1 | 160.0 | 359 | empty | 0.96 | 50.0 | 11.7 | 1.41 | 23.6 | 15.8 | 78.51 | 9.8 | < 0.0875 |
| | H5-2 | 14.5 | 5.72 | 22.7 | 5.72 | 265 | 3.0 | 190.0 | 389 | empty | 0.6 | 55.6 | 12.6 | 1.71 | 32.5 | 21.4 | 145.71 | 9.0 | < 0.0875 |
| | H6-2 | 13.4 | 5.88 | 22.7 | 5.91 | 229 | 38.9 | 200.0 | 399 | empty | 1.27 | 45.0 | 11.3 | 1.20 | 20.5 | 13.2 | 46.81 | 9.2 | < 0.0875 |
| | H7-2 | | empty | empty | empty | empty | empty | empty | empty | empty | empty | empty | empty | empty | empty | empty | empty | empty | empty |
| | H8-2 | | empty | empty | empty | empty | empty | empty | empty | empty | empty | empty | empty | empty | empty | empty | empty | empty | empty |
| | H9-2 | 13.6 | 6.26 | 22.7 | 6.5 | 155 | 36.0 | -30.0 | 169 | empty | 2.78 | 36.3 | 11.4 | 0.90 | 16.1 | 12.3 | < 1 | 11.0 | < 0.0875 |
| | H10-2 | 12.7 | 6.48 | 22.7 | 6.5 | - | - | -47.0 | 152 | empty | 2.26 | 34.6 | 13.9 | 1.09 | 14.7 | 11.5 | < 1 | 10.7 | < 0.0875 |
| 29.10.18 | H1-3 | not working | empty | empty | empty | empty | empty | empty | empty | empty | empty | empty | empty | empty | empty | empty | empty | empty | empty |
| | H2-3 | ICP | | 22.5 | 6.14 | | | | 264 | empty | 1.50 | 37.7 | 10.9 | 1.98 | 18.5 | 9.7 | 18.71 | 18.6 | < 0.0875 |
| | H3-3 | ICP | | 22.5 | 6.11 | | | | 345 | empty | 1.86 | 47.6 | 11.0 | 1.22 | 21.0 | 14.4 | 20.45 | 10.0 | < 0.0875 |
| | H4-3 | ICP | | 22.5 | 5.84 | | | | 419 | empty | 1.08 | 47.6 | 10.8 | 1.39 | 19.3 | 13.4 | 51.28 | 11.0 | < 0.0875 |
| | H5-3 | ICP | | 22.5 | 5.57 | | | | 379 | empty | 0.60 | 54.6 | 12.6 | 1.64 | 32.4 | 21.6 | 143.40 | 9.9 | < 0.0875 |
| | H6-3 | ICP | | 22.5 | 5.88 | | | | 406 | empty | 1.35 | 45.8 | 11.5 | 1.16 | 21.3 | 14.1 | 47.78 | 10.0 | < 0.0875 |
| | H7-3 | ICP | | 22.5 | 6.55 | | | | 204 | empty | 2.34 | - | - | - | - | - | - | - | - |
| | H8-3 | ICP | | 22.5 | 6.60 | | | | 215 | empty | 2.28 | - | - | - | - | - | - | - | - |
| | H9-3 | ICP | | 22.5 | 6.34 | | | | 197 | empty | 2.56 | 37.0 | 11.5 | 0.85 | 16.3 | 12.4 | < 1 | 11.2 | < 0.0875 |
| | H10-3 | ICP | | 22.5 | 6.33 | | | | 229 | empty | 2.18 | 38.6 | 13.9 | 1.30 | 15.2 | 11.8 | < 1 | 11.2 | < 0.0875 |
| 21.11.18 | H1-4 | not working | empty | empty | empty | empty | empty | empty | empty | empty | empty | empty | empty | empty | empty | empty | empty | empty | empty |
| | H2-4 | | | 22.6 | 6.19 | | | | 277 | empty | 1.92 | 41.2 | 10.6 | 1.77 | 20.7 | 11.1 | 23.18 | 11.6 | < 0.0875 |
| | H3-4 | | | 22.6 | 6.07 | | | | 352 | empty | 2.07 | 46.1 | 11.1 | 1.15 | 21.3 | 14.7 | 17.92 | 9.9 | < 0.0875 |
| | H4-4 | | | 22.6 | | | | | 199 | empty | | | | | | | | | |
| | H5-4 | | | 22.6 | 5.53 | | | | 449 | empty | 0.68 | 52.0 | 11.6 | 1.54 | 26.6 | 18.0 | 108.75 | 10.8 | < 0.0875 |
| | H6-4 | | | 22.6 | 6.28 | | | | 449 | empty | 1.43 | 43.8 | 11.0 | 1.15 | 20.0 | 13.1 | 37.10 | 11.5 | < 0.0875 |
| | H7-4 | | | 22.6 | 6.47 | | | | 204 | empty | 2.82 | 37.6 | 10.5 | 0.88 | 21.7 | 14.0 | 11.24 | 9.5 | < 0.0875 |
| | H8-4 | broken | empty | 22.6 | empty | empty | empty | empty | empty | empty | empty | empty | empty | empty | empty | empty | empty | empty | empty |
| | H9-4 | | | 22.6 | 6.35 | | | | 169 | empty | 2.88 | 35.2 | 11.3 | 0.87 | 16.5 | 12.4 | < 1 | 10.8 | < 0.0875 |
| | H10-4 | | | 22.6 | 6.51 | | | | 238 | empty | 2.58 | 30.9 | 13.7 | 1.10 | 14.9 | 11.7 | < 1 | 11.1 | < 0.0875 |

| Date | sample No | IC 3000 Fe 2+ mg/kg | IC 3000 Fe 3+ mg/kg | ICP-OES Sr mg/kg | ICP-OES Mn mg/kg | IC 3000 Mn 2+ mg/kg | ICP-OES Ti mg/kg | ICP-OES Li mg/kg | ICP-OES Mo mg/kg | ICP-OES B mg/kg | ICP-OES Br mg/kg | DOC µgC/l |
|----------|-----------|---------------------------|---------------------------|------------------------|------------------------|---------------------------|------------------------|------------------------|------------------------|-----------------------|------------------------|--------------|
| | LOQ | 0.01 | 0.01 | 0.00 | 0.01 | 0.01 | 0.00 | 0.01 | 0.01 | 0.01 | 0.08 | |
| 20.06.17 | R1-1 | | 0.16 | 0.01 | 0.00 | | 0.00 | 0.00 | 0.00 | < 0.05 | 0.08 | |
| | R2-1 | | 0.17 | 0.02 | 0.01 | | 0.00 | 0.00 | 0.00 | < 0.05 | 0.09 | |
| | R3-1 | | 0.09 | 0.01 | 0.01 | | 0.02 | 0.00 | 0.00 | < 0.05 | 0.06 | |
| | R4-1 | | 0.16 | 0.02 | 0.00 | | 0.00 | 0.00 | 0.00 | < 0.05 | 0.04 | |
| | R5-1 | | 0.12 | 0.02 | 0.01 | | 0.01 | 0.00 | 0.00 | < 0.05 | 0.05 | |
| | R6-1 | | 0.09 | 0.02 | 0.01 | | 0.01 | 0.00 | 0.00 | < 0.05 | 0.04 | |
| | R7-1 | | 0.09 | 0.02 | 0.00 | | 0.01 | 0.00 | 0.00 | < 0.05 | 0.04 | |
| | R8-1 | | 0.13 | 0.02 | 0.03 | | 0.02 | 0.00 | 0.00 | < 0.05 | 0.07 | |
| | R9-1 | | 0.08 | 0.02 | 0.01 | | 0.00 | 0.00 | 0.00 | < 0.05 | 0.05 | |
| | R10-1 | | 0.32 | 0.03 | 0.01 | | 0.01 | 0.00 | 0.00 | < 0.05 | 0.05 | |
| | R11-1 | | 0.12 | 0.02 | 0.01 | | 0.01 | 0.00 | 0.00 | < 0.05 | 0.07 | |
| | R12-1 | | 0.11 | 0.03 | 0.04 | | 0.00 | 0.00 | 0.00 | < 0.05 | 0.07 | |
| | R13-1 | | 0.05 | 0.04 | 0.03 | | 0.00 | 0.00 | 0.00 | < 0.05 | 0.06 | |
| | R14-1 | | 0.29 | 0.03 | 0.14 | | 0.00 | 0.00 | < LOD | < 0.05 | 0.07 | |
| 04.08.17 | R1-2 | | 0.03 | 0.01 | 0.00 | | 0.00 | 0.00 | 0.00 | < 0.05 | 0.16 | |
| | R2-2 | | 0.02 | 0.01 | 0.00 | | 0.00 | 0.00 | 0.00 | < 0.05 | 0.14 | |
| | R3-2 | empty | empty | empty | empty | | empty | empty | empty | empty | empty | |
| | R4-2 | | 0.03 | 0.02 | 0.00 | | 0.00 | 0.00 | 0.00 | < 0.05 | 0.04 | |
| | R5-2 | | 0.01 | 0.03 | 0.00 | | 0.00 | 0.00 | 0.00 | < 0.05 | 0.03 | |
| | R6-2 | | 0.02 | 0.03 | 0.00 | | 0.00 | 0.00 | 0.00 | < 0.05 | 0.08 | |
| | R7-2 | | 0.04 | 0.03 | 0.00 | | 0.00 | 0.00 | 0.00 | < 0.05 | 0.07 | |
| | R8-2 | | 0.02 | 0.03 | 0.00 | | 0.00 | 0.00 | 0.00 | < 0.05 | 0.06 | |
| | R9-2 | | 0.03 | 0.03 | 0.00 | | 0.00 | 0.00 | 0.00 | < 0.05 | 0.06 | |
| | R10-2 | | 0.06 | 0.04 | 0.01 | | 0.00 | 0.00 | 0.00 | < 0.05 | 0.04 | |
| | R11-2 | | 0.05 | 0.03 | 0.01 | | 0.00 | 0.00 | 0.00 | < 0.05 | 0.07 | |
| | R12-2 | | 0.24 | 0.04 | 0.07 | | 0.00 | 0.00 | 0.00 | < 0.05 | 0.07 | |
| | R13-2 | | 0.06 | 0.04 | 0.05 | | 0.00 | 0.00 | 0.00 | < 0.05 | 0.04 | |
| | R14-2 | | 0.96 | 0.05 | 0.31 | | 0.00 | 0.00 | 0.00 | < 0.05 | 0.07 | |
| 13.08.18 | H1-1 | empty | empty | empty | empty | | empty | empty | empty | empty | empty | |
| | H2-1 | 9.77 | 3.11 | 0.06 | 0.80 | 0.67 | < 0.0125 | < 0.025 | < 0.025 | < 0.05 | < 0.375 | 4726 |
| | H3-1 | 0.20 | 0.86 | 0.06 | 0.39 | 0.22 | < 0.0125 | < 0.025 | < 0.025 | < 0.05 | < 0.375 | 4140 |
| | H4-1 | | 0.22 | 0.06 | 0.20 | 0.00 | < 0.0125 | < 0.025 | < 0.025 | < 0.05 | < 0.375 | 5656 |
| | H5-1 | | 0.06 | 0.10 | 0.47 | 0.34 | < 0.0125 | < 0.025 | < 0.025 | < 0.05 | < 0.375 | 3636 |
| | H6-1 | | 0.05 | 0.07 | 0.14 | 0.00 | < 0.0125 | < 0.025 | < 0.025 | < 0.05 | < 0.375 | 6059 |
| | H7-1 | | | | | | | | | | | |
| | H8-1 | 21.74 | 3.64 | 0.06 | 1.80 | 1.79 | < 0.0125 | < 0.025 | < 0.025 | 0.06 | < 0.375 | 2941 |
| | H9-1 | 10.29 | 2.14 | 0.06 | 1.64 | 1.60 | < 0.0125 | < 0.025 | < 0.025 | < 0.05 | < 0.375 | 3074 |
| | H10-1 | 21.29 | 1.38 | 0.06 | 1.52 | 1.42 | < 0.0125 | < 0.025 | < 0.025 | 0.06 | < 0.375 | |
| 18.09.18 | H1-2 | empty | empty | empty | empty | | empty | empty | empty | empty | empty | |
| | H2-2 | 6.13 | 1.00 | 0.07 | 1.04 | 0.94 | < 0.0125 | < 0.025 | < 0.025 | < 0.05 | < 0.375 | |
| | H3-2 | 0.45 | 0.64 | 0.06 | 0.39 | 0.22 | < 0.0125 | < 0.025 | < 0.025 | < 0.05 | < 0.375 | |
| | H4-2 | | 0.04 | 0.08 | 0.28 | 0.10 | < 0.0125 | < 0.025 | < 0.025 | < 0.05 | < 0.375 | |
| | H5-2 | | 0.06 | 0.13 | 0.52 | 0.40 | < 0.0125 | < 0.025 | < 0.025 | < 0.05 | < 0.375 | |
| | H6-2 | | 0.04 | 0.08 | 0.15 | 0.00 | < 0.0125 | < 0.025 | < 0.025 | < 0.05 | < 0.375 | |
| | H7-2 | empty | empty | empty | empty | | empty | empty | empty | empty | empty | |
| | H8-2 | empty | empty | empty | empty | | empty | empty | empty | empty | empty | |
| | H9-2 | 29.15 | 1.65 | 0.06 | 1.88 | 1.81 | < 0.0125 | < 0.025 | < 0.025 | 0.07 | < 0.375 | |
| | H10-2 | 13.53 | 15.32 | 0.06 | 1.60 | | < 0.0125 | < 0.025 | < 0.025 | 0.07 | < 0.375 | |
| 29.10.18 | H1-3 | empty | empty | empty | empty | | empty | empty | empty | empty | empty | |
| | H2-3 | 7.13 | 1.03 | 0.06 | 0.83 | 0.66 | < 0.0125 | < 0.025 | < 0.025 | < 0.05 | < 0.375 | |
| | H3-3 | 1.25 | 0.37 | 0.07 | 0.43 | 0.26 | < 0.0125 | < 0.025 | < 0.025 | < 0.05 | < 0.375 | |
| | H4-3 | 0.17 | 0.35 | 0.07 | 0.27 | 0.09 | < 0.0125 | < 0.025 | < 0.025 | < 0.05 | < 0.375 | |
| | H5-3 | 0.38 | 0.60 | 0.12 | 0.79 | 0.75 | < 0.0125 | < 0.025 | < 0.025 | < 0.05 | < 0.375 | |
| | H6-3 | 0.15 | 0.46 | 0.08 | 0.29 | 0.13 | < 0.0125 | < 0.025 | < 0.025 | < 0.05 | < 0.375 | |
| | H7-3 | | | | | | | | | | | |
| | H8-3 | 30.26 | 1.52 | | | 1.97 | | | | | | |
| | H9-3 | 29.81 | 0.93 | 0.07 | 1.92 | 1.80 | 0.22 | < 0.025 | < 0.025 | 0.09 | < 0.375 | |
| | H10-3 | 29.96 | 4.18 | 0.06 | 2.01 | 1.77 | < 0.0125 | < 0.025 | < 0.025 | 0.09 | < 0.375 | |
| 21.11.18 | H1-4 | empty | empty | empty | empty | | empty | empty | empty | empty | empty | |
| | H2-4 | 0.34 | 9.87 | 0.06 | 0.99 | | < 0.0125 | < 0.025 | < 0.025 | < 0.05 | < 0.375 | |
| | H3-4 | 0.01 | 1.87 | 0.07 | 0.43 | | < 0.0125 | < 0.025 | < 0.025 | < 0.05 | < 0.375 | |
| | H4-4 | | | | | | | | | | | |
| | H5-4 | 0.00 | 0.81 | 0.10 | 0.88 | | < 0.0125 | < 0.025 | < 0.025 | < 0.05 | < 0.375 | |
| | H6-4 | 0.00 | 0.09 | 0.07 | 0.38 | | < 0.0125 | < 0.025 | < 0.025 | < 0.05 | < 0.375 | |
| | H7-4 | 0.27 | 2.21 | 0.08 | 1.71 | | < 0.0125 | < 0.025 | < 0.025 | < 0.05 | < 0.375 | |
| | H8-4 | | | empty | empty | | empty | empty | empty | empty | empty | |
| | H9-4 | 11.56 | 16.56 | 0.06 | 1.90 | | < 0.0125 | < 0.025 | < 0.025 | 0.07 | < 0.375 | |
| | H10-4 | 0.26 | 9.56 | 0.06 | 1.60 | | < 0.0125 | < 0.025 | < 0.025 | < 0.05 | < 0.375 | |

| Date | sample No | ICP-MS As ppt | ICP-MS Ba µg/l | ICP-MS Cd ppt | ICP-MS Co ppt | ICP-MS Cr ppt | ICP-MS Cu ppt | ICP-MS Hg ppt | ICP-MS Ni ppt | ICP-MS Pb ppt | ICP-MS Se ppt | ICP-MS Zn ppt | ICP-MS V ppt | ICP-MS 48Ti ppt | ICP-MS 95Mo ppt | ICP-MS 118Sn ppt |
|----------|-----------|---------------------|----------------------|---------------------|---------------------|---------------------|---------------------|---------------------|---------------------|---------------------|---------------------|---------------------|--------------------|-----------------------|-----------------------|------------------------|
| LOQ | | 203 | | 19 | 19 | 40 | 40 | | 53 | 11.2 | 629 | 334 | 102 | 289 | 11 | 29 |
| 20.06.17 | R1-1 | | | | | | | | | | | | | | | |
| | R2-1 | | | | | | | | | | | | | | | |
| | R3-1 | | | | | | | | | | | | | | | |
| | R4-1 | | | | | | | | | | | | | | | |
| | R5-1 | | | | | | | | | | | | | | | |
| | R6-1 | | | | | | | | | | | | | | | |
| | R7-1 | | | | | | | | | | | | | | | |
| | R8-1 | | | | | | | | | | | | | | | |
| | R9-1 | | | | | | | | | | | | | | | |
| | R10-1 | | | | | | | | | | | | | | | |
| | R11-1 | | | | | | | | | | | | | | | |
| | R12-1 | | | | | | | | | | | | | | | |
| | R13-1 | | | | | | | | | | | | | | | |
| | R14-1 | | | | | | | | | | | | | | | |
| 04.08.17 | R1-2 | | | | | | | | | | | | | | | |
| | R2-2 | | | | | | | | | | | | | | | |
| | R3-2 | | | | | | | | | | | | | | | |
| | R4-2 | | | | | | | | | | | | | | | |
| | R5-2 | | | | | | | | | | | | | | | |
| | R6-2 | | | | | | | | | | | | | | | |
| | R7-2 | | | | | | | | | | | | | | | |
| | R8-2 | | | | | | | | | | | | | | | |
| | R9-2 | | | | | | | | | | | | | | | |
| | R10-2 | | | | | | | | | | | | | | | |
| | R11-2 | | | | | | | | | | | | | | | |
| | R12-2 | | | | | | | | | | | | | | | |
| | R13-2 | | | | | | | | | | | | | | | |
| | R14-2 | | | | | | | | | | | | | | | |
| 13.08.18 | H1-1 | <LOD | | <LOD | 886 | 111 | <LOD | | 560 | <LOD | <LOD | 83991 | 777 | 28073 | 14 | 105 |
| | H3-1 | <LOD | | <LOD | 1085 | 102 | 176 | | 638 | <LOD | <LOD | 21557 | 273 | 25051 | 30 | 475 |
| | H4-1 | <LOQ | | <LOD | 193 | 83 | <LOD | | 72 | <LOD | <LOD | 57680 | 1547 | 22173 | 41 | 487 |
| | H5-1 | <LOD | | <LOD | 1522 | 175 | <LOQ | | 489 | <LOD | <LOD | 51877 | 1619 | 34305 | 24 | 159 |
| | H6-1 | <LOD | | 24 | 371 | 103 | 354 | | 437 | 35.6 | <LOD | 74932 | 1847 | 24894 | 77 | 234 |
| | H7-1 | | | | | | | | | | | | | | | |
| | H8-1 | <LOQ | | <LOD | 178 | 78 | <LOD | | 133 | <LOD | <LOD | 48282 | 1943 | 22896 | 50 | 339 |
| | H9-1 | <LOD | | <LOD | 173 | 66 | <LOD | | 388 | <LOD | <LOD | 57900 | <LOD | 21079 | 97 | 577 |
| | H10-1 | <LOQ | | <LOD | 329 | 55 | <LOD | | 164 | <LOD | <LOD | 30239 | 1262 | 20153 | 76 | 82 |
| 18.09.18 | H1-2 | <LOD | | <LOD | 788 | <LOD | <LOD | | 721 | <LOD | <LOD | 29988 | <LOD | 31415 | <LOD | <LOD |
| | H3-2 | <LOD | | <LOD | 473 | <LOD | <LOD | | 158 | <LOD | <LOD | 28013 | 180 | 26967 | 11 | <LOD |
| | H4-2 | <LOD | | <LOD | 636 | <LOQ | <LOD | | 89 | 24.0 | <LOD | 87746 | 2705 | 32688 | 48 | <LOQ |
| | H5-2 | <LOD | | <LOD | 1958 | <LOQ | 55 | | 964 | <LOD | <LOD | 47825 | 2003 | 44520 | 20 | <LOD |
| | H6-2 | <LOD | | <LOQ | 562 | <LOQ | 264 | | 499 | <LOD | <LOD | 70779 | 3157 | 27714 | 113 | <LOD |
| | H7-2 | | | | | | | | | | | | | | | |
| | H8-2 | | | | | | | | | | | | | | | |
| | H9-2 | <LOD | | <LOD | 106 | <LOD | <LOD | | <LOD | <LOD | <LOD | 13223 | 302 | 22733 | <LOQ | <LOD |
| | H10-2 | <LOD | | <LOD | 174 | <LOQ | <LOD | | <LOQ | <LOD | <LOD | 16918 | 3100 | 20744 | <LOQ | <LOD |
| 29.10.18 | H1-3 | <LOD | | <LOD | 704 | 372 | 370 | | 644 | <LOD | <LOD | 18890 | 134 | 26538 | <LOD | <LOD |
| | H3-3 | <LOD | | <LOD | 642 | 216 | <LOD | | 346 | <LOD | <LOD | 15463 | 254 | 29315 | 13 | <LOD |
| | H4-3 | <LOD | | <LOD | 745 | 172 | <LOD | | 139 | <LOD | <LOD | 8121 | 1157 | 28093 | 32 | <LOD |
| | H5-3 | <LOD | | <LOD | 3219 | 178 | <LOQ | | 1321 | <LOD | <LOD | 15036 | 608 | 46146 | 16 | <LOD |
| | H6-3 | <LOD | | <LOQ | 1214 | 186 | 456 | | 704 | <LOD | <LOD | 14150 | 1235 | 33694 | 101 | <LOD |
| | H7-3 | | | | | | | | | | | | | | | |
| | H8-3 | | | | | | | | | | | | | | | |
| | H9-3 | <LOD | | <LOD | 194 | 204 | <LOQ | | 116 | 30.5 | <LOD | 28542 | 650 | 38858 | <LOD | <LOD |
| | H10-3 | <LOD | | <LOD | 2265 | 706 | 1102 | | 848 | 70.8 | <LOD | 23502 | 7721 | 218948 | 11 | <LOD |
| 21.11.18 | H1-4 | | | | | | | | | | | | | | | |
| | H2-4 | <LOD | | 55 | 900 | 137 | 397 | | 718 | 1130.8 | <LOD | 19634 | 189 | 34997 | <LOD | <LOD |
| | H3-4 | <LOD | | <LOD | 611 | 267 | <LOD | | 197 | <LOD | <LOD | 18008 | 261 | 30601 | 12 | <LOD |
| | H4-4 | | | | | | | | | | | | | | | |
| | H5-4 | <LOD | | <LOD | 3464 | 231 | 86 | | 1137 | <LOD | <LOD | 25217 | 668 | 36296 | 13 | <LOD |
| | H6-4 | <LOD | | <LOQ | 1615 | 412 | 664 | | 961 | <LOD | <LOD | 90554 | 1267 | 28846 | 100 | <LOD |
| | H7-4 | <LOD | | <LOD | 2597 | 347 | <LOD | | 2464 | <LOD | <LOD | 43202 | <LOD | 30879 | 44 | <LOD |
| | H8-4 | | | | | | | | | | | | | | | |
| | H9-4 | <LOD | | <LOD | 98 | 474 | <LOD | | 168 | <LOD | <LOD | 17574 | 136 | 23620 | <LOD | <LOD |
| | H10-4 | <LOD | | <LOD | 200 | 248 | 121 | | <LOD | <LOD | <LOD | 19029 | 877 | 24013 | <LOD | <LOD |

